



UNIVERSITÀ DEGLI STUDI DI MILANO

Doctoral School in Pharmaceutical Sciences – XXXVI cycle

DIPARTIMENTO DI SCIENZE FARMACEUTICHE

**Mass spectrometric strategies to identify bioactive components
from natural extracts with anti-inflammatory activities**

CHIM/08

GIULIO FERRARIO

R12827

Tutor: Prof. Giancarlo ALDINI

Coordinator: Prof. Giulio VISTOLI

Academic year 2022-2023

CONTENTS

ABSTRACT	1
GENERAL INTRODUCTION	3
1. Inflammation	3
2. Natural extracts as anti-inflammatory agents	5
2.1. The interconnection between inflammation and oxidative stress	6
3. NRF2 and the antioxidant response.....	7
3.1. NRF2 and inflammation, a crosstalk with NF- κ B.....	9
4. NRF2 activators in natural products	11
5. Metabolomics of natural extracts	14
6. Proteomics and target identification	17
6.1. Phenotypic drug discovery - pharmacological approach	18
6.2. Target identification by proteomics approaches	21
7. References.....	23
AIM OF THIS WORK.....	31
Chapter 1 Characterization of a Red Grape skin by-product.....	33
<i>Study 1 - Effect of extraction solvent and temperature on polyphenol profiles, antioxidant and anti-inflammatory effects of Red Grape Skin By-Product.....</i>	33
1. Abstract.....	33
2. Introduction	34
3. Material and Methods.....	35
4. Results and discussion.....	39
5. Conclusion.....	63
6. References.....	64
7. Supplementary materials.....	68
Chapter 2 Characterization of a Thinned Young Apples polyphenols extract.....	69
<i>Study 1 - Polyphenols from Thinned Young Apples: HPLC-HRMS profile and evaluation of their antioxidant and anti-inflammatory activities by proteomic studies.....</i>	69
1. Abstract.....	69
2. Introduction	70
3. Material and Methods.....	72
4. Results and discussion.....	82
5. Discussion	96
6. Conclusions.....	103
7. References.....	104
8. Supplementary materials.....	110

Study 2 - Thinned apple polyphenols alleviate inflammation in a mouse model of DNBS-induced colitis: label-free quantitative proteomics studies.	115
1. Abstract.....	115
2. Introduction	116
3. Material and Methods.....	118
4. Results and Discussion	125
5. Conclusions.....	148
6. References.....	149
7. Supplementary materials.....	152
Chapter 3 Discovery of biological targets of natural extracts	159
Study 1 - Understanding the biological target of a Polyphenol-Enriched Bergamot Extract: insights from a MS-CETSA proteomic analysis	159
1. Introduction	159
2. Material and methods	160
3. Results and discussion.....	163
4. Conclusions.....	169
GENERAL CONCLUSIONS	173
SCIENTIFIC CONTRIBUTIONS	175

ABSTRACT

Oxidative stress and chronic inflammation are two conditions that can worsen various diseases, spanning metabolic, neurological disorders to tumour formation. In this context, a wide source of bioactive molecules exhibiting anti-inflammatory effects, combined with antioxidant potential, can be found in fruit and vegetables extracts. In particular, it has been reported that certain phytoconstituents are able to target two closely related systems within the cell, namely the NRF2 and NF- κ B pathways. While the NRF2 pathway is responsible for regulating an extensive panel of antioxidant enzymes, NF- κ B is the main effector pathway involved in inflammation. Phytochemicals in general mediate their effects by modulating the DNA-binding capacity of both these transcriptional factors and, in turn, correcting an unbalanced cellular state related to an uncontrolled inflammatory condition. Whereas previously, as a source of these phytochemicals, the focus was on the 'nobler' parts of the plant (i.e. the fruits, leaves and roots), today much more emphasis is placed on the analysis of industrial by-products. Specifically, this strategy aimed at the reuse of industrial by-products could reduce the impact of cultivation on waste production, minimizing disposal problems while obtaining a potential source of bioactive compounds. Even though there is general knowledge on the possible targets of these compounds, newer techniques combining different -omics approaches could better illustrate the biological impact of these extracts while identifying the phytochemical compounds responsible for it. Combining these different approaches to a concept of circular economy to valorise waste products could be a key to obtain useful health care products to prevent or even treat oxidative and inflammatory conditions. In particular, in this thesis, I will explore the antioxidant and anti-inflammatory activities of different extracts obtained from by-products of grape and apple cultivation. This investigation will employ a multifaceted approach, integrating engineered cell cultures for phenotypic screening of bioactive extracts, Mass Spectrometric-based metabolomics to unravel the primary components of these extracts, and Mass Spectrometric-based proteomic studies to comprehensively analyse their impact on the cell proteome. The exploration of potential mechanisms of action will be conducted through both *in-vitro* and *ex-vivo* quantitative proteomic studies. Conclusively, the thesis will showcase the application of a MS-CETSA (Mass Spectrometry – Cellular Thermal Shift Assay) methodology to probe the direct target of a bergamot leaves polyphenols extract.

GENERAL INTRODUCTION

1. Inflammation

Inflammation, both in its acute or chronic forms, constitutes a fundamental biological process that manifests itself as the body's response to external stimuli such as tissue injury either of mechanical origin or due to pathogens, irritants or pathologically altered cells. Although beneficial to the host if short-term and targeted, when inflammation becomes persistent due to repeated stimulation by harmful substances or because of the body's inability to alleviate it, it can transition into a chronic state of inflammation [1]. Continued inflammatory response can lead to the onset of a wide array of pathological conditions, from cardiovascular diseases to cancer, inflammatory bowel diseases and cognitive impairment [2–4]. At cellular and vascular level, the inflammatory phenomenon is associated with a cascade of events, including the vasodilation, the recruitment of plasma proteins and immune cells to the site of inflammation, along with the secretion of inflammatory mediators such as vasoactive amines and peptides, pro-inflammatory cytokines, reactive oxygen species (ROS) and reactive nitrogen species (RNS) [5]. Several inflammatory events occurring in vascular and immune cells are under the control of the transcription factor known as nuclear factor kappa B (NF- κ B), whose crucial role in the modulation, regulation and propagation of inflammation makes it one of the main target investigated for modulating aberrant states of inflammation [6,7].

The NF- κ B transcription factor family consists of structurally related proteins, all of which share a region known as the Rel homology domain (RHD); through this domain, different members of the NF- κ B pathway interact to form homo- and heterodimers, which subsequently bind to κ B sequences located at the promoter region, enhancing the transcription of their respective target genes. This domain also contains at the C-terminus the nuclear-localization sequence (NLS), which is the sequence bound by specific inhibitors known as the I κ B proteins (I κ B- α , I κ B- β , I κ B- γ , I κ B- ϵ); these proteins use an ankyrin domain to bind to the RHD and masking the NLS, sequestering it in the cytoplasm and inhibiting its nuclear translocation and DNA binding.

The NF- κ B family includes RelA, also known as p65, RelB, c-Rel, NF- κ B1 (p50) and NF- κ B2 (p52), which contain transactivation domains necessary for inducing target gene transcription. NF- κ B1 and NF- κ B2 are made of two precursor proteins p105 and p100, which dimerize with different Rel proteins; these two precursors contain both an RHD domain and, at the C-

terminus, an I κ B-like domain making this protein function as a reservoir for mature p50, p52 and for I κ Bs. Normally, p105 undergoes unregulated processing to p50, causing its translocation into the nucleus unless it is sequestered by an I κ B protein; p100, on the other hand, is mostly found in the cytoplasm dimerized with RelB. Given this background, a classical activation of the NF- κ B pathway starts by ubiquitination and degradation of I κ B inhibitory proteins. This process relies on the I κ B kinase complex (IKK) composed of two catalytic subunits, namely IKK α , IKK β , and a regulatory subunit known as NEMO or IKK γ . The IKK kinase responds to various cellular stimuli, pro-inflammatory cytokines such as tumor necrosis factor alpha (TNF α), interleukin-1 beta (IL-1 β), bacterial lipopolysaccharide (LPS) and external agents capable of causing cellular stress. When activated, IKK phosphorylates I κ B α (part of the I κ B family), triggering ubiquitin-dependent degradation, resulting in translocation to the nucleus of canonical NF- κ B members: p50/RelA (p65) and p50/c-Rel (Figure 1).

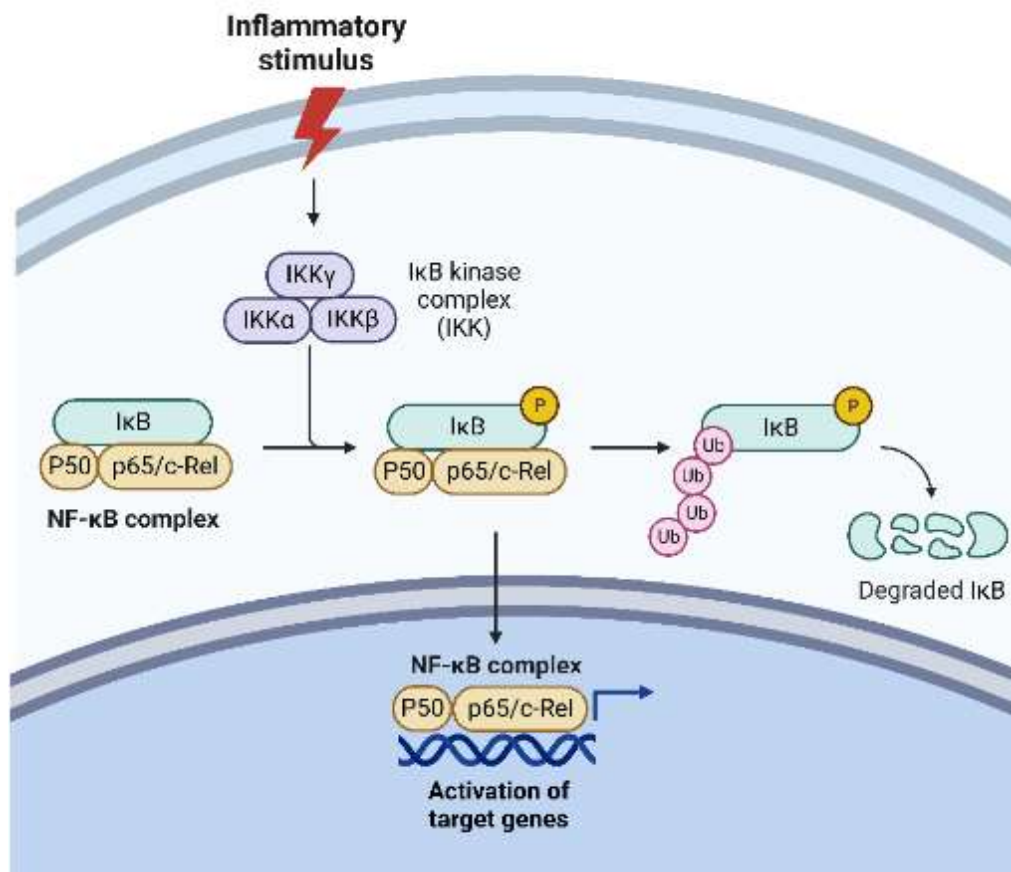


Figure 1 - Schematization of the classical activation of the NF- κ B pathway. This process depends on the IKK complex, which phosphorylates I κ B to induce its degradation and allows the nuclear translocation of the NF- κ B complex.

I κ B α , essential for this signaling pathway, is rapidly resynthesized by NF- κ B through a feedback mechanism [6,8]. If well regulated, this pathway mediates the regulation of the inflammatory

response other than inducing the activation, differentiation of various immune cells. Dysregulation in its activation is considered an hallmark of chronic inflammation, while different strategies have been put in act to strategically modulate this pathway, the most important subunit for the activation of the classical NF- κ B signaling is considered to be IKK β and is also one main target in the strategy for effective NF- κ B inhibitors [6].

2. Natural extracts as anti-inflammatory agents

In the context of inflammatory-based diseases, a significant challenge exists due to the lack of effective treatments and/or preventive strategies. Despite the World Health Organization's (WHO) predicted that the incidence of chronic **vascular** inflammatory diseases will continue to rise in the coming years [7,9], satisfactory solutions remain elusive; to date steroidal and non-steroidal anti-inflammatory drugs (NSAIDs) are the most commonly employed pharmaceuticals for mitigating inflammation. However, their long-term use is associated with severe adverse reactions, gastrointestinal damage, and kidney dysfunction [10]. The search for novel compounds with anti-inflammatory properties, characterized by safer toxicological profiles and robust therapeutic effects, remains an ongoing endeavor. In this scenario, the world of natural products emerges as a truly promising potential source of newly discovered active compounds.

When considering the potential of natural products, it is noteworthy that extracts from medicinal herbs have shown promising anti-inflammatory activity. Some examples are the *Withania somnifera* extract exhibiting the ability to inhibit IKK β kinase activity to reduce NF- κ B translocation and DNA binding, or other crude extracts including *Eurycoma longifolia* and citrus peel [11] for which has been demonstrated inhibitory effects on NF- κ B with evidence of reduced cytokine levels, NO production, COX2 activity, and the modulation of prostaglandins and leukotrienes [12,13].

Many of these extracts contain phenolic and terpenoid compounds, so far associated with NF- κ B inhibition. For instance, flavonoids such as myricetin and resveratrol [6] have been reported to inhibit various signaling key points of NF- κ B, mainly I κ B- α phosphorylation activity and NF- κ B DNA binding activity; compounds like apigenin inhibit both COX2 activity and NF- κ B, leading to reduced cytokine production; epigallocatechin gallate (EGCG) prevents the degradation of I κ B α and subsequent DNA binding of NF- κ B, while quercetin alters the NF- κ B pathway by inhibiting I κ B β phosphorylation; additionally, terpenoids found in different types of plants such as acubin (*Acuba japonica*) has been found to prevent I κ B α dependent degradation and nuclear

translocation of p65; another example is the helenalin A. from *Arnica montana*, which exerts its inhibition via alkylation of the p65 subunit, preventing the DNA binding of NF- κ B[14]; some of these extracts have reached clinical trials due to the established activity of its main bioactive components, such as andrographolide, a terpenoid from *Andrographis paniculate* that can inhibit NF- κ B by binding to the p50 subunit [15,16], for whose extract good efficacy in improving the status of ulcerative colitis was observed in phase three of clinical trials [17,18]. These examples highlight the potential of phytochemical sources, with the added benefit that some of these compounds can be derived from agricultural industry wastes, providing an opportunity for valorization and reuse of raw agricultural products. This topic will be discussed in more detail throughout this chapter.

2.1. The interconnection between inflammation and oxidative stress

As previously mentioned, the activation of the NF- κ B pathway can be caused not only by cytokines, chemokines, and other signaling molecules but also by pivotal mediators of inflammation, namely, radical species originating from oxygen (termed Radical Oxygen Species – ROS) or nitrogen (known as Radical Nitrogen Species – RNS). These radicals may originate either from the immune system's activation or external stimuli and serve as essential mediators for maintaining a redox equilibrium if present in moderate quantities. The line between inflammation and oxidative stress, often indistinct, is so thin that it is challenging to distinguish which process started first. In a physiological context, a primary disorder of inflammation can give rise to a secondary oxidative stress disorder state that is often beneficial and self-resolving. On the other hand, when the primary disorder is oxidative stress-related, it can cause the activation of the inflammatory pathway as a regulatory mechanism. However, in certain scenarios, a prolonged inflammatory state can impair the organism's antioxidant defenses, setting the stage for a prolonged oxidative stress to ensue. Conversely, there are situations where the organism's lack of adequate antioxidant defenses could induce abnormal inflammation via ROS-mediated DNA modifications or increased cytokine production in immune cells [19]. Abnormalities in activation of the inflammatory system, ROS generation and antioxidant depletion can collectively participate in a chronic state of inflammation. In all these cases, an unbalanced redox state is observed, suggesting that some of the pathologies associated with this phenomenon may benefit from restoring a physiological redox state. This could be achieved by direct antioxidants administration or, for more promising results, by

stimulating the cell's antioxidant response which is predominantly controlled by the Nuclear factor-erythroid 2 p45-related factor 2 (NRF2) – Antioxidant Response Elements (ARE) system.

3. NRF2 and the antioxidant response

A first strategy aimed at regulating an imbalanced redox state was the administration of compounds known as non-enzymatic antioxidants, classified into water-soluble (Vitamin C and some phenolic compounds) and lipid-soluble (Vitamin E and carotenoids). The key concept behind these antioxidant compound lies in their ability to exert their effects by preventing or delaying the oxidation of critical biomolecules susceptible to oxidation such as lipids, proteins and nucleic acids [20]. As research progressed over decades, it became more evident that the antioxidant activity of these natural compounds could not be related to their direct efficacy against major oxidative stressors, as their rate constant towards main oxidant species was order of magnitude lower than the enzymatic antioxidant machinery that includes, among others, peroxiredoxines, superoxide dismutases and glutathione peroxidases families, which overall offer a more specific and beneficial approach [21]. In this context, further investigation unveiled that these detoxifying proteins were under the control of a transcriptional factor known as Nuclear factor-erythroid 2 p45-related factor 2 (NRF2); specifically, the NRF2 pathway regulates the transcription of more than two hundred genes that contain an antioxidant response element (ARE) in their promoter region, and these include antioxidant proteins and enzymes of phase I, II and III, enzymes involved in metabolism of lipids, carbohydrates and amino acids and inflammation regulators, constituting a stress-response network to maintain the homeostasis of the microenvironment [22].

NRF2 is regulated by several cellular factors that control its stability and nuclear translocation, and of these, the Kelch-like ECH-associated protein 1 (KEAP1) protein is the most important. Under physiological conditions, NRF2 is bound to KEAP1 and targeted for ubiquitination and proteasomal degradation by the Cul3-E3-ligase, with a $t_{1/2}$ of less than 20 min [23]. Oxidant species, electrophilic by-products of oxidation or electrophilic xenobiotics by covalently binding cysteine residues present in the thiol-rich domain of KEAP1 induce NRF2; in detail, oxidation and covalent adduction to KEAP1 thiols induces a conformational change in the complex, causing NRF2 to adopt an orientation that prevents ubiquitination by the KEAP1-Cul3 complex, and this process leads to the stabilization of NRF2. As a result, NRF2 bypasses proteasomal degradation and accumulates in the cell, translocate to the nucleus, forms a

heterodimer with the small musculoaponeurotic fibrosarcoma (Maf) proteins, binds to ARE region and therefore promotes the transcription of ARE-dependent genes [24]. This process is illustrated in Figure 2.

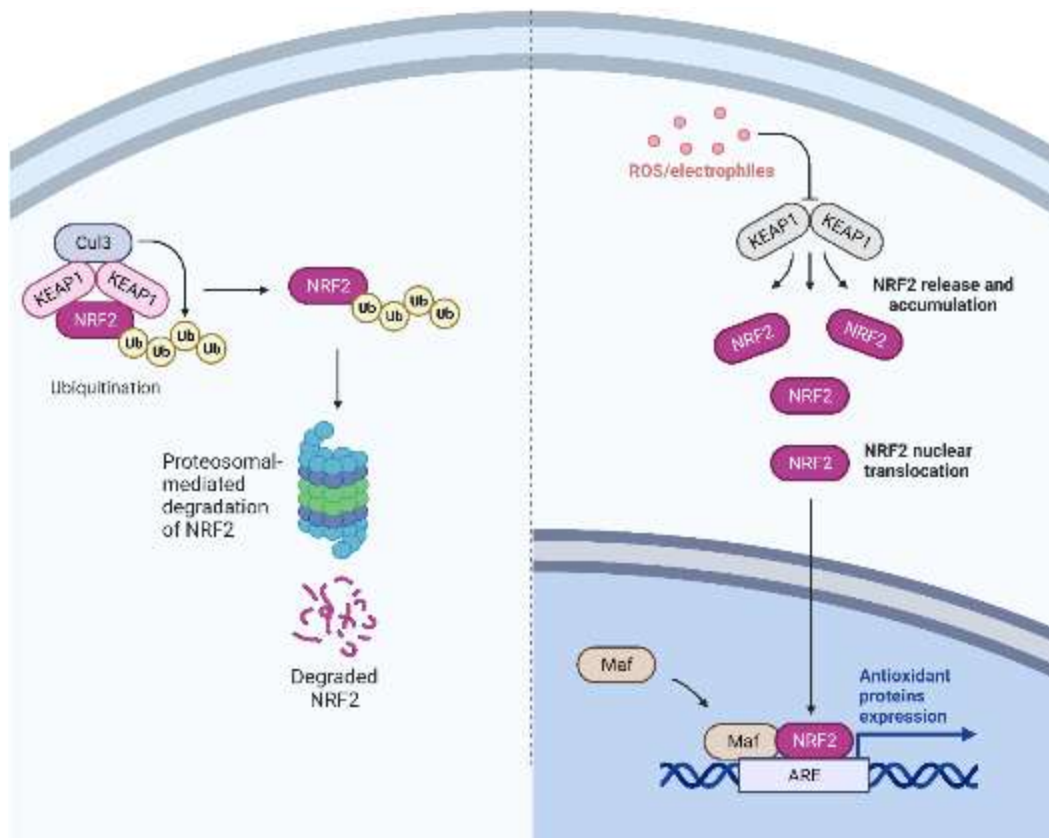


Figure 2 - Schematization of the nuclear translocation of NRF2. On the left the physiological regulation of NRF2 in the cytoplasm by poly-ubiquitination and proteosomal degradation, on the right the conformational change in KEAP1 and subsequent release of NRF2, now free to translocate into the nucleus to bind to the Antioxidant Response Elements (ARE) sequence and activate the transcription of the antioxidant related proteins.

This system is also regulated by additional factors such as phosphorylation and acetylation, while other interacting partners such as p62/SQSTM1 can influence NRF2 abundance [25]. Notably, NRF2 exert a multifaceted control that extends to a wide range of proteins that contribute to different aspect of the antioxidant defenses. For instance, it regulates the expression of the xCT (known as SLC7A11, Solute Carrier Family 7 Member 11) subunit of system xc⁻, responsible for the import of cystine and the export of glutamate into cells, an essential component for maintaining intracellular glutathione equilibrium, one of the major cellular detoxifiers. As part of glutathione metabolism regulation, NRF2 oversees the expression of both the glutamate-cysteine ligase catalytic (GCLC) and modifier (GCLM) subunits which catalyze the rate-limiting step in the biosynthesis of glutathione. Furthermore,

NRF2 governs the expression of glutathione peroxidase (GPX2), which is crucial in the production of oxidized glutathione (GSSG) during the reduction of peroxides. Within the same biological process, it also regulates the expression of glutathione reductase (GSR1), critical for the reduction of GSSG to maintain optimal intracellular levels of reduced glutathione (GSH). NRF2 also maintains the redox balance by regulating cytosolic thioredoxin (TXN1), thioredoxin reductase TXNRD1, and sulfiredoxin (SRXN1), which collectively participate in the reduction of oxidized protein thiols to prevent the formation of oxidized, inactive proteins. As well, what is interesting is NRF2's regulation of a number of NADPH-generating enzymes, including glucose-6-phosphate dehydrogenase (G6PD), 6-phosphogluconate dehydrogenase (PGD), isocitrate dehydrogenase (IDH)1 and malic enzyme (ME)1; this is relevant because a significant number of enzymes that metabolize drugs and antioxidant systems require NADPH as an essential cofactor [25].

Against this background, NRF2 is certainly involved in a complex mechanism of regulating metabolism and oxidative stress. To date, it is speculated that activation of KEAP1-NRF2-ARE signaling may provide protection against various stress and inflammation related diseases, including neurodegenerative diseases, autoimmune diseases, cardiovascular disorders and chronic diseases of the lung, liver, kidney. Likewise, a deficiency of this signalling may also be an important pathological factor for these diseases [26–31]; hence, there is great interest from medicinal chemistry in finding new active molecules that can modulate and restore impaired NRF2.

3.1. NRF2 and inflammation, a crosstalk with NF- κ B

Considering the relationship between inflammation and oxidative stress just described and the central role of NRF2 in regulating the redox state of the cell, a plausible strategy to counter inflammation, particularly chronic inflammation, could be to modulate/contain the concentration of oxidant radical species by reducing the magnitude and extent of oxidative stress induced. This beneficial modulation could be achieved through NRF2 pharmacological activation, a strategy already proven to ameliorate inflammatory states and combat degenerative diseases [32].

The close link between NRF2 and inflammation is further supported by the complex relationship this transcriptional factor has with NF- κ B (illustrated in Figure 3), which is of central importance in the propagation of the inflammatory response. The crosstalk between these two pathways is intricate and finely modulated by direct interactions and specific post-

translational modifications. In more detail, one piece of evidence supporting direct link between these two pathways is the induction of NRF2 by lipopolysaccharide [33], a purely pro-inflammatory stimulus, plausible because NRF2 contains several NF- κ B-like binding sites in its proximal promoter region that can be bound by p65 (canonical RelA subunit of NF- κ B) [34], leading to the initiation of NRF2 transcription. This should be interpreted as a kind of protective mechanism against the consequences of NF- κ B hyperactivation in acute inflammatory settings. In this regard, NRF2 deficiency has been associated with increased dysregulated NF- κ B activity, increased cytokine production, and increased nitrosative / oxidative stress, which, in certain cell types such as astrocytic or microglial cells, results in neuronal death and demyelination; this observation is in line with the neurodegenerative phenotype observed in NRF2 KO mice [35].

Among the enzymes whose expression is under the control of NRF2 particular attention has to be reserved to heme oxygenase 1 (HMOX1), a well-established immunomodulator, which assumes a central role in heme metabolism by catalyzing the cleavage of the porphyrin ring of heme. This enzymatic process gives rise to several components: ferrous iron (Fe²⁺), carbon monoxide (CO), and biliverdin; subsequently, biliverdin is converted into bilirubin, one of the most potent antioxidants, through the action of the enzyme biliverdin reductase (BLVRB). Importantly, this biochemical cascade is connected to the NRF2-mediated inhibition of NF- κ B; in fact, enhanced HMOX1 activity within endothelial cells exerts a suppressive influence on NF- κ B-mediated transcription, particularly impacting the expression of adhesion molecules such as E-Selectin and vascular cell adhesion molecule 1 (VCAM-1). This regulation mechanism may be attributed to the actions of bilirubin and, potentially, a concurrent reduction in free intracellular iron ions [35].

The direct interaction between NRF2 and NF- κ B can be further supported by KEAP1's inhibitory role, via ubiquitination and degradation, of I κ B kinase (IKK- β) and also by reducing the phosphorylation of I κ B, resulting in reduced NF- κ B activity [36,37]. In addition, the overproduction of cytokines and other inflammatory mediators, such as prostaglandins, can activate the NRF2 pathway, as these presenting electrophilic portions can covalently bind KEAP1 reactive cysteines [38].

NRF2 could instead be suppressed by p65 (RelA), which, in addition to amplifying NF- κ B transcription, competes with the binding of NRF2's transcriptional co-activator, CBP-p300 (CREB-binding protein- p300 complex). This competition becomes even more evident when, for various reasons, p65 is overexpressed, favoring its binding to CBP-p300 and consequently enhancing transcription of NF- κ B-dependent genes. This phenomenon can occur during

periods of increased inflammation or NRF2-p300 depletion, further exacerbating the disease state. Conversely, increased translocation of NRF2 into the nucleus will increase its binding to CBP, reducing the expression of NF- κ B target genes [35,39].

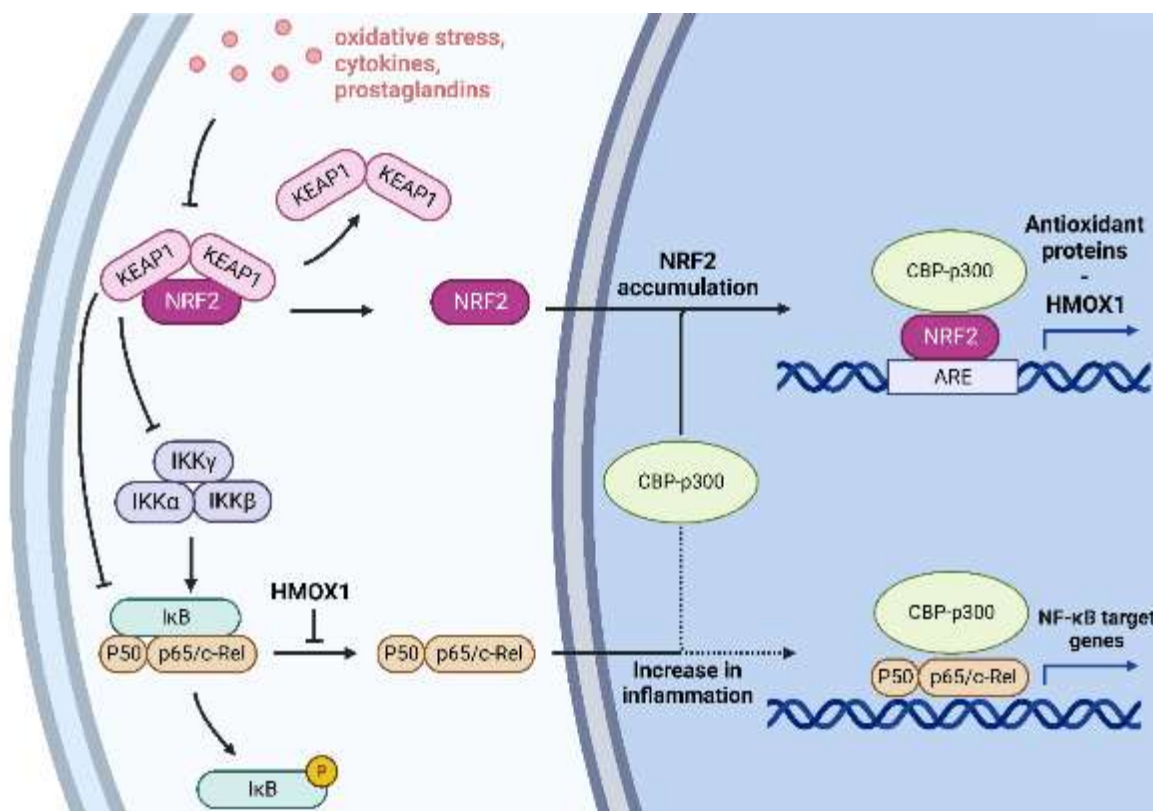


Figure 3 - Diagram illustrating the NRF2 signaling pathway and its interaction with NF- κ B transcriptional factor.

Although more evidence is being gathered, the strong correlation between the NRF2 and NF- κ B pathways suggests the promising and realistic possibility of stimulating NRF2 factor to dampen the inflammatory process, reduce oxidative stress, and potentially attenuate the clinical picture of a range of diseases.

4. NRF2 activators in natural products

Some of the molecular mechanisms behind NRF2 activation target the KEAP1-NRF2 complex based on a noncovalent interaction. Compounds working through this mechanism actually alter KEAP1-NRF2 binding by targeting the concave binding pocket by interacting with different ionized residues. Some small molecules have been found to activate NRF2 translocation through this mechanism including tripeptides such as DKK and DDW [24]; although promising, this class of NRF2 activators is far to become lead compounds.

The main class of compounds that act as "NRF2 activators" should more accurately be termed "KEAP1 inhibitors," since their molecular targets are mainly KEAP1-reactive cysteines and are identified as electrophiles, oxidizable phenols, and Michael acceptors. However, it should be pointed out that most of these NRF2 activators, due to their chemical nature, cannot be highly selective for KEAP1 thiols compared to other ubiquitous cysteines in cells [38], resulting in nonspecific and adverse effects. Moreover, the covalent binding of proteins can induce idiosyncratic reactions. A good example is a well-studied NRF2 activator, namely the bardoxolone methyl (CDDO-methyl ester), a Michael acceptor that was developed for the treatment of chronic kidney disease but was withdrawn from clinical trials because of serious side effects. More recently, omaveloxolone, a second generation and more selective bardoxolone analogue, has been approved for Friedreich's ataxia, a rare, inherited, degenerative disease; its mechanism of action involves the interaction with KEAP1 and the induction of NRF2, aimed at reducing the ROS accumulation deriving from the NRF2 impairment, a typical effect of that disease [40,41].

In addition to synthetically derived compounds, several natural products have been shown to activate NRF2 by acting as moderate non-toxic electrophilic covalent ligands. Sulphoraphane (SFN), a dietary isothiocyanates mainly found in broccoli and Brussel sprouts, has been recognized as one of the most powerful inductors of NAD(P)H Quinone Dehydrogenase 1 (NQO1) via activation of NRF2 through the binding with the cysteine 151 of KEAP1. This class of compounds are activated by the microbiota from the inactive glucosinolate precursors to the more reactive, electrophilic isothiocyanates [42]. Another example is the curcumin, which act as a Micheal acceptor and similarly reacts with KEAP1 cysteines, enhancing NRF2 activity. In addition, epigallocatechin-3-gallate (EGCG) and most of the polyphenol family share the ability to enhance the NRF2 response through oxidation of the di-phenolic moiety and formation of the corresponding quinone reactive as Michel acceptor [42,43]. It should be noted that this is possible only for molecules containing catechol and hydroquinone, since the resorcinol moiety (1, 3-diphenol) is too difficult to oxidize and can be considered inactive. This mechanism of action has been firstly proposed for 5-Aminosalicylic acid which, once oxidized by the inflammatory and pro-oxidant micro-environment typical of the inflammatory bowel diseases, binds to KEAP1 reactive cysteines promoting NRF2 [44].

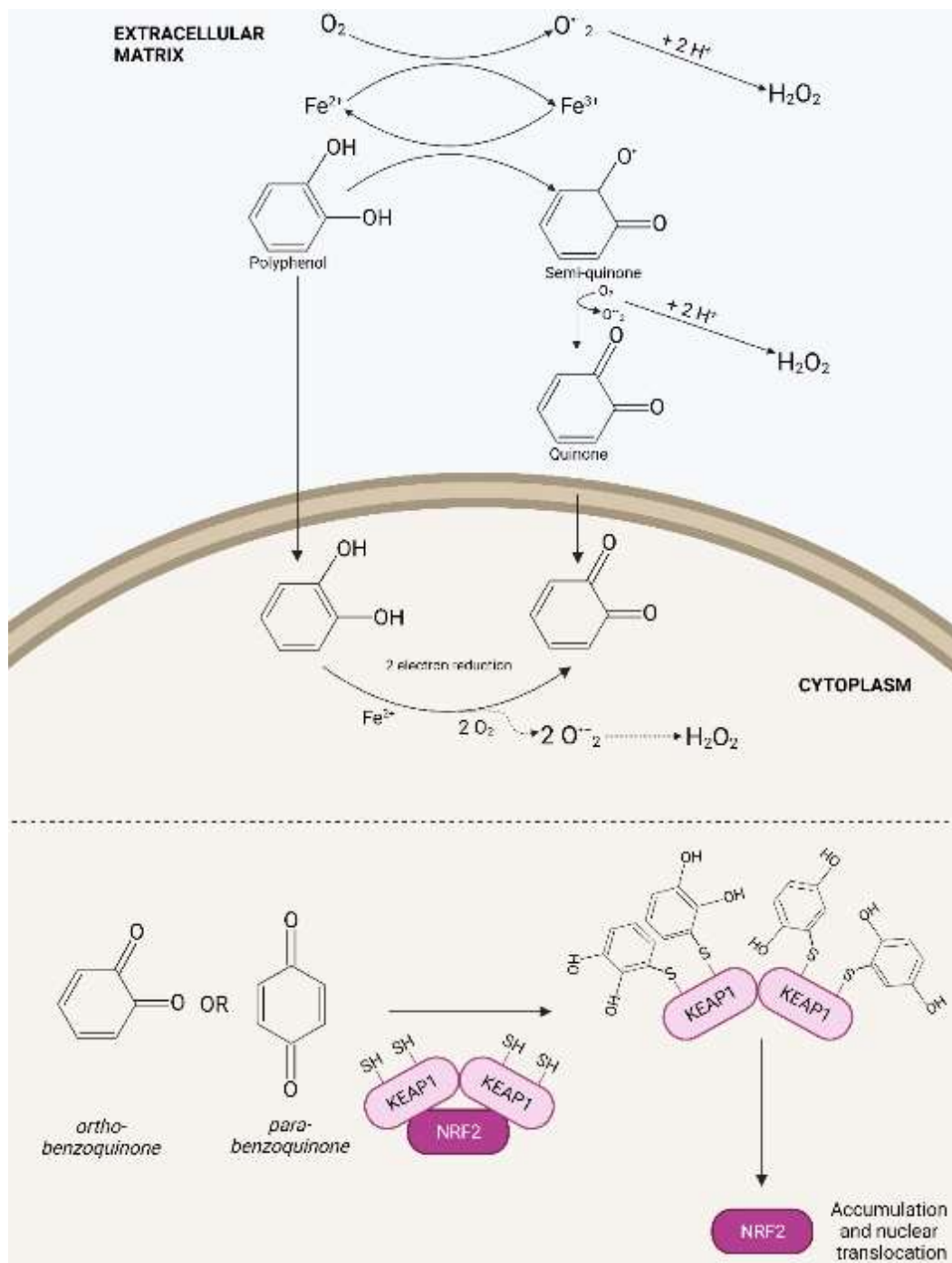


Figure 4 - Mechanism of action for NRF2 activation by polyphenols. Quinones can form both in the extracellular environment or in the cytoplasm after absorption. After quinones formation, KEAP1's cysteines can react with the quinone by Michael addition and NRF2 is free to translocate into the nucleus.

Several experimental evidences proved the potential of some natural products from crude extracts in targeting NRF2 [45,46]. Further effort must be made to investigate the single bioactive moiety responsible for this activity and to implement strategies aimed at reducing the potential adverse reactions often related to the formation of highly reactive and non-selective oxidized electrophilic polyphenol.

5. Metabolomics of natural extracts

After two decades of reduced interest by pharmaceutical companies, natural substances are once again becoming a valuable source for new drug discovery; to date, about a third of the small molecule drugs approved in the last 40 years comes from natural products or are their derivatives [47]. This is due to the enormous potential of plants as a natural source of bioactive molecules because of their marked structural heterogeneity and their wide range of promoted beneficial effects [48].

Despite these advantages, research in this field slowed down in the 1990s because of the many technical limitations related mainly to the characterization of natural-derived bioactive compounds, which can be summarized as follows: (i) difficulty in fully and accurately characterizing the composition of extracts, (ii) possible presence of interfering species in high throughput screening (overlapping UV absorption and fluorescence profile of very similar natural constituents present in the extract under investigation), and (iii) the need to standardize the extract before any clinical trials. Moreover, numerous local flora conservation regulations are in place, hence the impossibility of obtaining high amounts of source material, which may also differ greatly from batch to batch [47]. These problems have been partly addressed in recent years mainly due to technological development and the emergence of the concept of the circular economy model, which aims at minimizing waste and resource depletion by emphasizing continuous use, recycling and reuse of by-products and waste materials. This approach could go hand in hand with the discovery of bioactive compounds as tons of waste from the agricultural process are generated each year. If thoroughly studied, these matrices could be used as potential starting point for research of new, bioactive compounds.

Although the problem of the starting material has been partially solved, characterization of the composition of these extracts remains a bottleneck. A strategic approach could be the creation of libraries of naturally occurring compounds to facilitate the application of increasingly high-performance HTS screening methods. To this end, metabolomics of natural extracts has been developed, whose main goal is the identification and characterization of multiple components. New developments in the analytical field together with computational and statistical methods, overall known as "omics" tools, have provided the unprecedented opportunity for innovation and discovery in the area of natural products [49]. Metabolomics plays a crucial role in this context by providing precise information on the composition of metabolites in natural extracts, valuable information for annotating unknown analogs and new structures [50]. This provides the basis for clarifying variations in the production of a compound of interest and optimizing

the cultivation process, if necessary. Another benefit could come from evaluating any differences in the extraction procedure, such as the yield of a classes of compounds or to help the set-up of bigger extraction scales. In addition, metabolomics could provide important inferences about the efficacy of a natural extract on a pathological model of interest, allowing investigation of the candidate target; however, such an investigation requires integration of the information gathered from the metabolomic study with that obtained from proteomics and transcriptomics to provide a more complete picture of the biological system under investigation [51].

For metabolite profiling, natural extracts are analyzed by NMR spectroscopy or high-resolution mass spectrometry (HRMS), often coupled with separation techniques aimed at resolving matrix heterogeneity, i.e., liquid chromatography or, to a lesser extent, gas chromatography. The most widely used technique, the LC-HRMS, is the most advantageous in terms of sensitivity, allowing a small volume of sample to be consumed, and enables the efficient separation of the many isomers in the extracts. On the other hand, NMR analysis is renowned for its simplicity, reproducibility, and potential to provide direct quantitative and structural information. Hybrid approaches, such as the integration of HRMS and NMR, exploit the strengths of both techniques, for example, to elucidate the structural characteristics of compounds and fractions upon proper isolation [52].

It should be pointed out that HRMS stands as the main choice for qualitative and quantitative metabolite profiling [53]. An extension of the metabolomic characterization of a natural extract by mass spectrometry is the MS imaging (MSI), a technique which adds an extra layer of information to the determination of the molecular mass of the species profiled, namely, the spatial distribution of specific compounds in the matrix, allowing in the context of natural extracts to further optimize the extraction process by selecting the best portions of the plant/fruit from which to start, or to better specify the harvest period [54].

For all applications, HRMS offers routine acquisition of accurate molecular mass data, facilitating unambiguous assignment of molecular formulae for numerous metabolites within a single extract over a dynamic range spanning several orders of magnitude.

To date, the mass spectrometry analyzers that provide the best performance in terms of resolution and sensitivity are hybrid instruments such as quadrupole time-of-flight instruments (Q-TOF), hybrid quadrupole orbitrap (Q-Orbitrap) or linear ion trap-Orbitrap (LTQ-Orbitrap). Due to the ability to operate with different ionization modes (different ionization sources), in both polarities, mass spectrometry allows investigating (almost) the entire searchable chemical space of natural products. Ion sources based on a soft ionization

technique, such as the electrospray ionization (ESI) source, can be used for more polar compounds in positive (ESI +) or negative (ESI -) polarity to cover a wider range of chemical structures, while the atmospheric pressure chemical ionization (APCI) source is used to analyze less polar metabolites. Matrix-assisted laser desorption/ionization (MALDI) sources are often used for elucidation of high-molecular-weight structures; numerous advances have been made with this source through coupling with imaging techniques [54].

However, the main challenge that persists in this field is the unambiguous identification of metabolites within bioactive extracts which involves several steps: determination of exact mass and molecular formula by querying MS databases containing information on natural products and manual check of fragmentation patterns [52]. However, it is worth noting that a comprehensive experimental tandem mass spectrometry (MS/MS) database covering all reported natural products is not currently available; in addition, the lack of standardized collision energy conditions for fragmentation in LC-MS/MS hampers the search for experimental spectra across different instrument platforms and even different laboratories; in fact, it is customary to build *in-house* databases by consulting previous literature or using isolated standard compounds. Alternatively, the recorded experimental spectra can be compared with the putative structures and corresponding predicted MS/MS spectra generated *in silico* with tools such as competitive fragmentation modeling (CFM-ID) [51].

In this context, the Global Natural Products Social (GNPS) [55], a web-based mass spectrometry ecosystem, emerges as a valuable open-access knowledge tool for organizing and sharing raw, processed or annotated fragmentation mass spectrometry (MS/MS) data. Nonetheless, the GNPS molecular networking approach has its limitations, including its varying applicability to different classes of natural products and uncertainties in structural assignments among potential candidates. Efforts are underway to address these challenges, incorporating taxonomic information into molecular networks to strengthen annotation certainty. Another valuable platform for metabolite identification is METLIN, implemented by a high-resolution MS/MS database and equipped with a fragment similarity search tool for identifying unknown compounds. Freely available software such as mzMine, Metaboanalys or XCMS2 [52] can analyze raw file from almost any vendor and help in the process of compound identification. Scores and algorithms have been developed for each data processing step to evaluate the goodness of identification, from matching the exact mass to confirming the fragmentation pattern, but it must be pointed out that these strategies for characterizing unknown natural metabolites cannot be considered unambiguous. For a correct and punctual identification a confirmation using other analytical techniques (such as NMR, semisynthesis) and a reference

standard is essential. According to Chemical Analysis Working group (CAWG) of the Metabolomics Standard Initiative (MSI) [56], the level of confidence of an identification is ranked from 1 to 4: 1 is an unambiguous identification, 2 and 3 a putative identification that can be achieved by the fragmentation pattern, retention time and assignment of a specific chemical class, and 4 an unidentified metabolite but distinguishable from other compounds in the matrix.

6. Proteomics and target identification

Discovery of therapeutically active bioactive compounds from crude extracts requires a multidisciplinary effort that starts from the appropriate choice of *in vitro* and *in vivo* assays. Historically, the so-called forward pharmacology approach has been widely adopted for the identification of bioactive compounds from natural matrices [48]. This strategy, also known as phenotypic drug discovery, relies on testing the functional activity of an entire extract by detecting phenotypic changes in the chosen biological model using suitable biological assays. Since this approach is untargeted, it only allows for the evaluation of beneficial phenotypic effects induced by stimulation with the mixture of compounds tested, so it finds application in screening bioactive extracts or fractions of such extracts to identify potential bioactive compounds contained therein; therefore, it is an approach that only allows for hypothesis about the target, but not for its precise identification, that must be confirmed by targeted assays. To this approach, a reverse strategy is also commonly used [57]. It typically starts with the identification of a promising target protein, which is then screened against libraries of well-characterized compounds using high-throughput strategies to identify a lead compound that can then be studied for functional activity *in vivo*. The latter approach is not often used in the context of natural products because of the chemical structure of the compounds that is not always compatible with high throughput approaches, mainly being fluorescent and UV-absorbing compounds. In addition, it has been recently observed that a target-based screening strategies cannot be considered as effective as the phenotypic one in screening bioactive compounds, since it fails to inform either molecular target or mechanism of action, devaluing conventional drug-discovery roadmaps [58].

6.1. Phenotypic drug discovery - pharmacological approach

Following the advanced pharmacology approach, evaluation of functional activity is often carried out using phenotypic assays, mostly based on cell-based screening technology. This approach is more suitable for natural products, as it follows a mostly medium- or high-throughput workflows, and thus smaller amounts of extracts and/or purified molecules are required. This strategy has proven valuable, particularly for describing relevant biological conditions, and takes advantage of the broad spectrum of cell-based assays available today. Engineering cell lines with fluorescence gene reporters (e.g., luciferase), introduced to measure the magnitude of a specific intracellular response of interest, is an effective strategy often used in combination with other assays that evaluate phenotypic parameters such as apoptosis, redox state, migration, differentiation, senescence, etc [59]. As anticipated, these assays are used to screen for potential bioactive compounds or crude extracts, but they do not provide information on the possible stimulated target/s; however, cell based phenotypic models can be used to study the molecular mechanism behind certain cellular signaling pathways.

To this end, recent technological progress, together with advances in omics sciences including genomics, proteomics, metabolomics, and lipidomics, has given rise to an emerging field known as systems biology. Systems biology represents an innovative and highly interdisciplinary field of scientific investigation that requires the continuous integration of data derived from the analysis of diverse molecular components. This approach enables the comprehensive exploration of molecular mechanisms behind various biological functions, without the need for pre-formulated hypotheses. It also allows us to predict how specific biological systems will respond to particular stimuli, including therapeutic interventions.

Of all the omics sciences, proteomics stands out as the most firmly established discipline contributing to these achievements. This discipline allows for the exploration of various aspects of proteins, including expression, structure, functions, interactions, and post-translational modifications, thus offering a wide range of applications in the biomedical field: e.g., (i) identification of diagnostic and (ii) prognostic biomarkers, and (iii) screening of bioactive compounds for new drug development [60]. It is essential to emphasize that the proteome of a cell or organism is extremely dynamic, evolving over time and in response to diverse external factors or stimuli; proteins can undergo post-translational modifications, move within the cell, undergo de novo synthesis, or undergo degradation. The proteome is a snapshot of the phenotype at the biochemical level, thus proteomics aims at studying which proteins are expressed and how they are expressed, to describe at a molecular level the biological system.

Proteomics encompasses both descriptive (qualitative) and quantitative approaches. Descriptive proteomics aims to identify and characterize proteins within a biological sample from a qualitative point of view, while quantitative proteomics allows for the measurement of protein levels between different experimental conditions, offering the possibility of identifying significant variations in the proteome of the chosen biological model and highlighting a potential activated or inhibited mechanism of action, or even formulating hypotheses about the target modulated by the treatment/stimulus [61]. As the latter proteomic approach is untargeted, it is worth noting that this type of analysis requires high-throughput instrumentation to ensure optimal performance in terms of resolution and sensitivity. A bottom-up analytical approach is followed, whereby peptide mixtures obtained by enzymatic hydrolysis of a protein extract (cell lysate, tissue homogenate, etc.) are sequenced by LC-HRMS analysis. Trypsin is the most commonly used enzyme because of its ability to achieve a high digestion yield, providing almost complete coverage of protein sequences. The resulting peptide mixtures are then subjected to chromatographic separation with a reversed-phase method. This procedure is aimed to resolve the sample heterogeneity and improve coverage of the proteome under investigation. The sample is then analyzed in real-time with high-resolution hybrid mass spectrometry instruments such as Q-TOFs or (Q)-Orbitraps.

For most proteomics experiments, mass spectrometry data are collected using a data-dependent acquisition (DDA) method. The mass analyzer selects the most intense peptide ions in a first stage of full mass analysis (MS1), and then they are fragmented (MS/MS) and analyzed in a second stage of tandem mass spectrometry (MS2) [62].

The most complex part of the experimental workflow is definitely data analysis, even though dedicated bioinformatics databases are available; data analysis is based on the implementation of complex algorithms designed to match theoretical information found in specific databases available online, i.e., protein sequence information of a specific proteome collected in *.fasta* format, with acquired experimental data (full mass and fragmentation spectra). Data processing aims to determine not only protein identity, but also to calculate the abundance of each gene product. These abundance values are derived from the normalization of individual peptide intensities. Regarding the quantification aspect of this technique, it is important to underline that mass spectrometry is not inherently a quantitative technique because the ionization efficiency, which determines the intensity of each ion in the mass spectrum, varies from one molecule to another due to different chemical and physical properties. Consequently, unless a reference standard is available, calculating the relative abundance of each protein to

assess changes in expression levels under different experimental conditions is the common approach [63].

For quantitative analysis there are methods that utilize isotopic labeling, such as Stable Isotope Labeling by/with Amino acids in Cell culture (SILAC), Isobaric tags for relative and absolute quantitation (iTRAQ), and Tandem Mass Tag (TMT), as well as label-free methods that do not require labeling steps.

Among the labeling approaches, the SILAC strategy uses a metabolic labeling strategy to incorporate ^{13}C - or ^{15}N -labeled "heavy" amino acids in vivo into proteins during translation. Samples from differently labeled cells, from different experimental conditions, are mixed and analyzed. During sample preparation, proteins are digested to obtain peptides containing differentially labeled amino acid/s, ensuring a mass weight shift that is detected by the instrument; comparison of the MS1-recorded intensity of the heavy peptide with the light peptide ensures relative quantification of the identified protein [64].

The TMT approach employs isobaric tags that covalently label peptides from various experimental conditions. During the mass spectrometry analysis, in particular during tandem MS experiments, these isobaric tags fragment, releasing reporter ions that are quantified based on their respective intensities. This enables comprehensive comparative analysis of protein expression levels across multiple conditions [65].

Label-free quantification (LFQ) does not require a stable isotope-containing compound to chemically bind to the protein and then label it. Unlike labeled experiments, in label-free experiments each sample is measured in a separate mass spectrometry (MS) run, dramatically increasing the machine time required. Another disadvantage of LFQ approaches is that run conditions (e.g., temperature, experimenter, column conditions) may differ between samples, so label-free experiments are more prone to errors introduced by measurement conditions than labeled experiments. On the other hand, while all labeled techniques require additional pretreatment in the wet lab, in LFQ experiments samples can be measured without any preparation, reducing potential errors during sample processing. In LFQ experiments, quantification is based on integrating the areas under the chromatographic peaks and normalizing them according to the number of peptides of the same protein [66].

With all these approaches, a statistical analysis of this data allows for the identification of proteins with significant differential expression when comparing two or more distinct experimental conditions, such as pathological phenotype vs. physiological phenotype or treated vs. untreated pathological phenotype.

For functional analysis, dedicated bioinformatics software, such as STRING [67] and Ingenuity Pathway Analysis (IPA) [68], which rely on gene ontology annotation databases, allow in-depth investigation of protein-protein interaction networks. These analyses provide detailed information about the cellular pathways that are modulated according to the differentially expressed proteins involved; in particular, (i) STRING builds protein-protein interaction networks, and (ii) Ingenuity Pathway Analysis (IPA) allows to add an extra layer of information, as it also associates the realization of the networks with the expression levels of individual proteins, allowing for the prediction of the activation/inhibition of a cellular pathway.

6.2. Target identification by proteomics approaches

Proteomics potentially enables the identification and validation of possible targets of natural products. A more conventional, older approach is based on affinity chromatography with immobilization of the ligand of interest [69]. Protein lysates are then eluted on the chromatographic column and the target is ideally identified. Since the immobilization of natural products compounds is difficult, time consuming and often source consuming, alternatives to this approach have been developed.

Other strategies that can be implemented are based on the evaluation of the response of the treated system to thermal or proteolytic stimulation. For example, the drug affinity responsive target stability (DARTS) [70] has been optimized on the concept that ligand-bound proteins show altered stability in presence of proteolytic enzymes compared to unbound targets. This analysis can be performed by investigating the isolated SDS page bands of the proteins interacting with the ligand by means of LC-MS/MS based proteomics. This approach does not require any labelling of the compound or the extracts but has some limitations regarding the identification of low abundant proteins. Another strategy is the Stability of Proteins from Rates of Oxidation (SPROX) [71] in which instead of the evaluation of the stabilization to a proteolytic treatment, it measures the levels of methionine oxidation of target proteins. The lysate is treated with an oxidizing agent (H₂O₂) with a denaturing agent (guanidine) to oxidize methionine, then a proteomic approach is deployed to analyze tryptic peptides and the methionine oxidation rate. When plotting the rate with the quantity of denaturing agent used, the protein interacting with the ligand will show larger transition shifts than the control proteins. Another approach exploiting the thermodynamic properties of a protein-ligand interaction is the SILAC pulse proteolysis (SILAC-PP) [72]. This approach combines the quantitative strategy of stable isotopes labelling in cell culture with the pulse proteolysis. In

this case the ligand of interest is added to either the heavy or light labeled lysate, these lysates are then distributed into denaturant-containing buffers and treated with a proteolytic enzyme. The samples are combined and fractionated using SDS-PAGE. A quantitative proteomics analysis identifies and quantifies the relative amounts of protein from each lysate in gel bands. The L/H ratios of proteins are analyzed to detect ligand interactions. If the compound is added to the heavy lysate, proteins unaffected by the ligand will have L/H ratios close to 1. Interacting proteins show altered resistance to proteolysis, with L/H ratios departing from 1 at intermediate denaturant concentrations. Challenging the response of the proteome to a thermal treatment in the presence of a ligand is the base of the cellular thermal shift assay (CETSA) [73] and the thermal proteome profile (TPP) [74]. In both these approaches the ligand-induced thermodynamic stabilization of the protein target is evaluated by heating the cell or the protein lysate at different temperatures and observing which protein remains in the soluble fraction of the proteome. Stronger is the interaction by the ligand, greater is the temperature-based stabilization the protein will show. Both these approaches make use of the multiplexing option offered by the TMT labelling, while the results show proteome-wide melting curves that could highlight the possible direct and indirect target of the compound of interest. Some of these approaches have been used to validate or identify the targets of isolated natural compounds but rarely have been used to assess the multiplicity of targets that a bioactive extract could have but if applicable, these approaches could speed up the target identification process.

7. References

1. Weiss, U. Inflammation. *Nature* 2008, 454, 427–427, doi:10.1038/454427a.
2. Furman, D.; Campisi, J.; Verdin, E.; Carrera-Bastos, P.; Targ, S.; Franceschi, C.; Ferrucci, L.; Gilroy, D.W.; Fasano, A.; Miller, G.W.; et al. Chronic Inflammation in the Etiology of Disease across the Life Span. *Nat Med* 2019, 25, 1822–1832, doi:10.1038/s41591-019-0675-0.
3. Gupta, S.C.; Kim, J.H.; Kannappan, R.; Reuter, S.; Dougherty, P.M.; Aggarwal, B.B. Role of Nuclear Factor- κ B-Mediated Inflammatory Pathways in Cancer-Related Symptoms and Their Regulation by Nutritional Agents. *Exp Biol Med (Maywood)* 2011, 236, 658–671, doi:10.1258/ebm.2011.011028.
4. Deng, W.; Du, H.; Liu, D.; Ma, Z. Editorial: The Role of Natural Products in Chronic Inflammation. *Front. Pharmacol.* 2022, 13, 901538, doi:10.3389/fphar.2022.901538.
5. Netea, M.G.; Balkwill, F.; Chonchol, M.; Cominelli, F.; Donath, M.Y.; Giamarellos-Bourboulis, E.J.; Golenbock, D.; Gresnigt, M.S.; Heneka, M.T.; Hoffman, H.M.; et al. A Guiding Map for Inflammation. *Nat Immunol* 2017, 18, 826–831, doi:10.1038/ni.3790.
6. Karin, M.; Yamamoto, Y.; Wang, Q.M. The IKK NF- κ B System: A Treasure Trove for Drug Development. *Nat Rev Drug Discov* 2004, 3, 17–26, doi:10.1038/nrd1279.
7. Waltenberger, B.; Atanasov, A.G.; Heiss, E.H.; Bernhard, D.; Rollinger, J.M.; Breuss, J.M.; Schuster, D.; Bauer, R.; Kopp, B.; Franz, C.; et al. Drugs from Nature Targeting Inflammation (DNTI): A Successful Austrian Interdisciplinary Network Project. *Monatsh Chem* 2016, 147, 479–491, doi:10.1007/s00706-015-1653-y.
8. Vallabhapurapu, S.; Karin, M. Regulation and Function of NF- κ B Transcription Factors in the Immune System. *Annu. Rev. Immunol.* 2009, 27, 693–733, doi:10.1146/annurev.immunol.021908.132641.
9. Gu, Y.; Wu, J. The Potential of Antioxidative and Anti-Inflammatory Peptides in Reducing the Risk of Cardiovascular Diseases. *Current Opinion in Food Science* 2016, 8, 25–32, doi:10.1016/j.cofs.2016.01.011.
10. Deng, W.; Du, H.; Liu, D.; Ma, Z. Editorial: The Role of Natural Products in Chronic Inflammation. *Front. Pharmacol.* 2022, 13, 901538, doi:10.3389/fphar.2022.901538.
11. Zhu, F.; Du, B.; Xu, B. Anti-Inflammatory Effects of Phytochemicals from Fruits, Vegetables, and Food Legumes: A Review. *Critical Reviews in Food Science and Nutrition* 2018, 58, 1260–1270, doi:10.1080/10408398.2016.1251390.

12. Azab, A.; Nassar, A.; Azab, A. Anti-Inflammatory Activity of Natural Products. *Molecules* 2016, 21, 1321, doi:10.3390/molecules21101321.
13. Venkatesha, S.H.; Acharya, B.; Moudgil, K.D. Natural Products as Source of Anti-Inflammatory Drugs. In *Inflammation - From Molecular and Cellular Mechanisms to the Clinic*; Wiley-VCH Verlag GmbH & Co. KGaA: Weinheim, Germany, 2017; pp. 1661–1690 ISBN 978-3-527-69215-6.
14. Chauhan, A.; Islam, A.U.; Prakash, H.; Singh, S. Phytochemicals Targeting NF- κ B Signaling: Potential Anti-Cancer Interventions. *Journal of Pharmaceutical Analysis* 2022, 12, 394–405, doi:10.1016/j.jpha.2021.07.002.
15. Wang, J.; Tan, X.F.; Nguyen, V.S.; Yang, P.; Zhou, J.; Gao, M.; Li, Z.; Lim, T.K.; He, Y.; Ong, C.S.; et al. A Quantitative Chemical Proteomics Approach to Profile the Specific Cellular Targets of Andrographolide, a Promising Anticancer Agent That Suppresses Tumor Metastasis. *Molecular & Cellular Proteomics* 2014, 13, 876–886, doi:10.1074/mcp.M113.029793.
16. Nie, X.; Chen, S.-R.; Wang, K.; Peng, Y.; Wang, Y.-T.; Wang, D.; Wang, Y.; Zhou, G.-C. Attenuation of Innate Immunity by Andrographolide Derivatives Through NF- κ B Signaling Pathway. *Sci Rep* 2017, 7, 4738, doi:10.1038/s41598-017-04673-x.
17. Tang, T.; Targan, S.R.; Li, Z.-S.; Xu, C.; Byers, V.S.; Sandborn, W.J. Randomised Clinical Trial: Herbal Extract HMPL-004 in Active Ulcerative Colitis - a Double-Blind Comparison with Sustained Release Mesalazine: Randomised Clinical Trial: Herbal Extract HMPL-004 for Ulcerative Colitis. *Alimentary Pharmacology & Therapeutics* 2011, 33, 194–202, doi:10.1111/j.1365-2036.2010.04515.x.
18. Chao, J.; Dai, Y.; Verpoorte, R.; Lam, W.; Cheng, Y.-C.; Pao, L.-H.; Zhang, W.; Chen, S. Major Achievements of Evidence-Based Traditional Chinese Medicine in Treating Major Diseases. *Biochemical Pharmacology* 2017, 139, 94–104, doi:10.1016/j.bcp.2017.06.123.
19. Biswas, S.K. Does the Interdependence between Oxidative Stress and Inflammation Explain the Antioxidant Paradox? *Oxidative Medicine and Cellular Longevity* 2016, 2016, 1–9, doi:10.1155/2016/5698931.
20. Ndhala, A.; Moyo, M.; Van Staden, J. Natural Antioxidants: Fascinating or Mythical Biomolecules? *Molecules* 2010, 15, 6905–6930, doi:10.3390/molecules15106905.
21. Aldini, G.; Altomare, A.; Baron, G.; Vistoli, G.; Carini, M.; Borsani, L.; Sergio, F. N-Acetylcysteine as an Antioxidant and Disulphide Breaking Agent: The Reasons Why. *Free Radical Research* 2018, 52, 751–762, doi:10.1080/10715762.2018.1468564.

22. Bellezza, I.; Giambanco, I.; Minelli, A.; Donato, R. Nrf2-Keap1 Signaling in Oxidative and Reductive Stress. *Biochimica et Biophysica Acta (BBA) - Molecular Cell Research* 2018, 1865, 721–733, doi:10.1016/j.bbamcr.2018.02.010.
23. Kobayashi, A.; Kang, M.-I.; Watai, Y.; Tong, K.I.; Shibata, T.; Uchida, K.; Yamamoto, M. Oxidative and Electrophilic Stresses Activate Nrf2 through Inhibition of Ubiquitination Activity of Keap1. *Molecular and Cellular Biology* 2006, 26, 221–229, doi:10.1128/MCB.26.1.221-229.2006.
24. Mou, Y.; Wen, S.; Li, Y.-X.; Gao, X.-X.; Zhang, X.; Jiang, Z.-Y. Recent Progress in Keap1-Nrf2 Protein-Protein Interaction Inhibitors. *European Journal of Medicinal Chemistry* 2020, 202, 112532, doi:10.1016/j.ejmech.2020.112532.
25. Hayes, J.D.; Dinkova-Kostova, A.T. The Nrf2 Regulatory Network Provides an Interface between Redox and Intermediary Metabolism. *Trends in Biochemical Sciences* 2014, 39, 199–218, doi:10.1016/j.tibs.2014.02.002.
26. Lu, M.; Ji, J.; Jiang, Z.; You, Q. The Keap1–Nrf2–ARE Pathway As a Potential Preventive and Therapeutic Target: An Update. *Medicinal Research Reviews* 2016, 36, 924–963, doi:10.1002/med.21396.
27. Bitar, M.S.; Liu, C.; Ziaei, A.; Chen, Y.; Schmedt, T.; Jurkunas, U.V. Decline in DJ-1 and Decreased Nuclear Translocation of Nrf2 in Fuchs Endothelial Corneal Dystrophy. *Invest. Ophthalmol. Vis. Sci.* 2012, 53, 5806, doi:10.1167/iops.12-10119.
28. Davies, S.S.; Zhang, L.S. Reactive Carbonyl Species Scavengers—Novel Therapeutic Approaches for Chronic Diseases. *Curr Pharmacol Rep* 2017, 3, 51–67, doi:10.1007/s40495-017-0081-6.
29. Panieri, E.; Buha, A.; Telkoparan-Akillilar, P.; Cevik, D.; Kouretas, D.; Veskoukis, A.; Skaperda, Z.; Tsatsakis, A.; Wallace, D.; Suzen, S.; et al. Potential Applications of NRF2 Modulators in Cancer Therapy. *Antioxidants* 2020, 9, 193, doi:10.3390/antiox9030193.
30. Suzuki, M.; Betsuyaku, T.; Ito, Y.; Nagai, K.; Nasuhara, Y.; Kaga, K.; Kondo, S.; Nishimura, M. Down-Regulated NF-E2-Related Factor 2 in Pulmonary Macrophages of Aged Smokers and Patients with Chronic Obstructive Pulmonary Disease. *Am J Respir Cell Mol Biol* 2008, 39, 673–682, doi:10.1165/rcmb.2007-0424OC.
31. Siewert, S.; González, I.; Santillán, L.; Lucero, R.; Ojeda, M.S.; Gimenez, M.S. Downregulation of Nrf2 and HO-1 Expression Contributes to Oxidative Stress in Type 2 Diabetes Mellitus: A Study in Juana Koslay City, San Luis, Argentina. *JDM* 2013, 03, 71–78, doi:10.4236/jdm.2013.32011.
32. Zhou, S.-F.; Wang, Y.-Y.; Zhe, H.; Yang, Y.; He, Z. Bardoxolone Methyl (CDDO-Me) as a Therapeutic Agent: An Update on Its Pharmacokinetic and Pharmacodynamic Properties. *DDDT* 2014, 2075, doi:10.2147/DDDT.S68872.

33. Rushworth, S.A.; Chen, X.-L.; Mackman, N.; Ogborne, R.M.; O'Connell, M.A. Lipopolysaccharide-Induced Heme Oxygenase-1 Expression in Human Monocytic Cells Is Mediated via Nrf2 and Protein Kinase C. *The Journal of Immunology* 2005, 175, 4408–4415, doi:10.4049/jimmunol.175.7.4408.
34. Rushworth, S.A.; Zaitseva, L.; Murray, M.Y.; Shah, N.M.; Bowles, K.M.; MacEwan, D.J. The High Nrf2 Expression in Human Acute Myeloid Leukemia Is Driven by NF- κ B and Underlies Its Chemo-Resistance. *Blood* 2012, 120, 5188–5198, doi:10.1182/blood-2012-04-422121.
35. Wardyn, J.D.; Ponsford, A.H.; Sanderson, C.M. Dissecting Molecular Cross-Talk between Nrf2 and NF- κ B Response Pathways. *Biochemical Society Transactions* 2015, 43, 621–626, doi:10.1042/BST20150014.
36. Lee, D.-F.; Kuo, H.-P.; Liu, M.; Chou, C.-K.; Xia, W.; Du, Y.; Shen, J.; Chen, C.-T.; Huo, L.; Hsu, M.-C.; et al. KEAP1 E3 Ligase-Mediated Downregulation of NF- κ B Signaling by Targeting IKK β . *Molecular Cell* 2009, 36, 131–140, doi:10.1016/j.molcel.2009.07.025.
37. Kim, J.-E.; You, D.-J.; Lee, C.; Ahn, C.; Seong, J.Y.; Hwang, J.-I. Suppression of NF- κ B Signaling by KEAP1 Regulation of IKK β Activity through Autophagic Degradation and Inhibition of Phosphorylation. *Cellular Signalling* 2010, 22, 1645–1654, doi:10.1016/j.cellsig.2010.06.004.
38. Madden, S.K.; Itzhaki, L.S. Structural and Mechanistic Insights into the Keap1-Nrf2 System as a Route to Drug Discovery. *Biochimica et Biophysica Acta (BBA) - Proteins and Proteomics* 2020, 1868, 140405, doi:10.1016/j.bbapap.2020.140405.
39. Kim, S.-W.; Lee, H.-K.; Shin, J.-H.; Lee, J.-K. Up-down Regulation of HO-1 and iNOS Gene Expressions by Ethyl Pyruvate via Recruiting P300 to Nrf2 and Depriving It from P65. *Free Radical Biology and Medicine* 2013, 65, 468–476, doi:10.1016/j.freeradbiomed.2013.07.028.
40. Shekh-Ahmad, T.; Eckel, R.; Dayalan Naidu, S.; Higgins, M.; Yamamoto, M.; Dinkova-Kostova, A.T.; Kovac, S.; Abramov, A.Y.; Walker, M.C. KEAP1 Inhibition Is Neuroprotective and Suppresses the Development of Epilepsy. *Brain* 2018, 141, 1390–1403, doi:10.1093/brain/awy071.
41. Lee, A. Omaveloxolone: First Approval. *Drugs* 2023, 83, 725–729, doi:10.1007/s40265-023-01874-9.
42. Magesh, S.; Chen, Y.; Hu, L. Small Molecule Modulators of Keap1-Nrf2-ARE Pathway as Potential Preventive and Therapeutic Agents. *Medicinal Research Reviews* 2012, 32, 687–726, doi:10.1002/med.21257.
43. Pouremamali, F.; Pouremamali, A.; Dadashpour, M.; Soozangar, N.; Jeddi, F. An Update of Nrf2 Activators and Inhibitors in Cancer Prevention/Promotion. *Cell Commun Signal* 2022, 20, 100, doi:10.1186/s12964-022-00906-3.

44. Kang, S.; Kim, W.; Jeong, S.; Lee, Y.; Nam, J.; Lee, S.; Jung, Y. Oxidized 5-Aminosalicylic Acid Activates Nrf2-HO-1 Pathway by Covalently Binding to Keap1: Implication in Anti-Inflammatory Actions of 5-Aminosalicylic Acid. *Free Radical Biology and Medicine* 2017, 108, 715–724, doi:10.1016/j.freeradbiomed.2017.04.366.
45. Qin, S.; Hou, D. Multiple Regulations of Keap1/Nrf2 System by Dietary Phytochemicals. *Molecular Nutrition Food Res* 2016, 60, 1731–1755, doi:10.1002/mnfr.201501017.
46. Serafini, M.; Peluso, I. Functional Foods for Health: The Interrelated Antioxidant and Anti-Inflammatory Role of Fruits, Vegetables, Herbs, Spices and Cocoa in Humans. *CPD* 2017, 22, 6701–6715, doi:10.2174/1381612823666161123094235.
47. Newman, D.J.; Cragg, G.M. Natural Products as Sources of New Drugs from 1981 to 2014. *J. Nat. Prod.* 2016, 79, 629–661, doi:10.1021/acs.jnatprod.5b01055.
48. Atanasov, A.G.; Waltenberger, B.; Pferschy-Wenzig, E.-M.; Linder, T.; Wawrosch, C.; Uhrin, P.; Temml, V.; Wang, L.; Schwaiger, S.; Heiss, E.H.; et al. Discovery and Resupply of Pharmacologically Active Plant-Derived Natural Products: A Review. *Biotechnology Advances* 2015, 33, 1582–1614, doi:10.1016/j.biotechadv.2015.08.001.
49. Aharoni, A.; Goodacre, R.; Fernie, A.R. Plant and Microbial Sciences as Key Drivers in the Development of Metabolomics Research. *Proc. Natl. Acad. Sci. U.S.A.* 2023, 120, e2217383120, doi:10.1073/pnas.2217383120.
50. Demarque, D.P.; Dusi, R.G.; De Sousa, F.D.M.; Grossi, S.M.; Silvério, M.R.S.; Lopes, N.P.; Espindola, L.S. Mass Spectrometry-Based Metabolomics Approach in the Isolation of Bioactive Natural Products. *Sci Rep* 2020, 10, 1051, doi:10.1038/s41598-020-58046-y.
51. the International Natural Product Sciences Taskforce; Atanasov, A.G.; Zotchev, S.B.; Dirsch, V.M.; Supuran, C.T. Natural Products in Drug Discovery: Advances and Opportunities. *Nat Rev Drug Discov* 2021, 20, 200–216, doi:10.1038/s41573-020-00114-z.
52. Wolfender, J.-L.; Nuzillard, J.-M.; Van Der Hooft, J.J.J.; Renault, J.-H.; Bertrand, S. Accelerating Metabolite Identification in Natural Product Research: Toward an Ideal Combination of Liquid Chromatography–High-Resolution Tandem Mass Spectrometry and NMR Profiling, in Silico Databases, and Chemometrics. *Anal. Chem.* 2019, 91, 704–742, doi:10.1021/acs.analchem.8b05112.
53. Wolfender, J.-L.; Marti, G.; Thomas, A.; Bertrand, S. Current Approaches and Challenges for the Metabolite Profiling of Complex Natural Extracts. *Journal of Chromatography A* 2015, 1382, 136–164, doi:10.1016/j.chroma.2014.10.091.

54. Alvarez-Rivera, G.; Ballesteros-Vivas, D.; Parada-Alfonso, F.; Ibañez, E.; Cifuentes, A. Recent Applications of High Resolution Mass Spectrometry for the Characterization of Plant Natural Products. *TrAC Trends in Analytical Chemistry* 2019, 112, 87–101, doi:10.1016/j.trac.2019.01.002.
55. Jouaneh, T.M.M.; Rosario, M.E.; Li, Y.; Leibovitz, E.; Bertin, M.J. Incorporating LC–MS/MS Analysis and the Dereplication of Natural Product Samples into an Upper-Division Undergraduate Laboratory Course. *J. Chem. Educ.* 2022, 99, 2636–2642, doi:10.1021/acs.jchemed.1c01212.
56. Sumner, L.W.; Amberg, A.; Barrett, D.; Beale, M.H.; Beger, R.; Daykin, C.A.; Fan, T.W.-M.; Fiehn, O.; Goodacre, R.; Griffin, J.L.; et al. Proposed Minimum Reporting Standards for Chemical Analysis: Chemical Analysis Working Group (CAWG) Metabolomics Standards Initiative (MSI). *Metabolomics* 2007, 3, 211–221, doi:10.1007/s11306-007-0082-2.
57. Schenone, M.; Dančík, V.; Wagner, B.K.; Clemons, P.A. Target Identification and Mechanism of Action in Chemical Biology and Drug Discovery. *Nat Chem Biol* 2013, 9, 232–240, doi:10.1038/nchembio.1199.
58. Sadri, A. Is Target-Based Drug Discovery Efficient? Discovery and “Off-Target” Mechanisms of All Drugs. *J. Med. Chem.* 2023, 66, 12651–12677, doi:10.1021/acs.jmedchem.2c01737.
59. Michelini, E.; Cevenini, L.; Mezzanotte, L.; Coppa, A.; Roda, A. Cell-Based Assays: Fuelling Drug Discovery. *Anal Bioanal Chem* 2010, 398, 227–238, doi:10.1007/s00216-010-3933-z.
60. Aslam, B.; Basit, M.; Nisar, M.A.; Khurshid, M.; Rasool, M.H. Proteomics: Technologies and Their Applications. *J Chromatogr Sci* 2017, 55, 182–196, doi:10.1093/chromsci/bmw167.
61. Ong, S.-E.; Mann, M. Mass Spectrometry–Based Proteomics Turns Quantitative. *Nat Chem Biol* 2005, 1, 252–262, doi:10.1038/nchembio736.
62. Lenčo, J.; Jadeja, S.; Naplekov, D.K.; Krokhin, O.V.; Khalikova, M.A.; Chocholouš, P.; Urban, J.; Broeckhoven, K.; Nováková, L.; Švec, F. Reversed-Phase Liquid Chromatography of Peptides for Bottom-Up Proteomics: A Tutorial. *J. Proteome Res.* 2022, 21, 2846–2892, doi:10.1021/acs.jproteome.2c00407.
63. Shuken, S.R. An Introduction to Mass Spectrometry-Based Proteomics. *J. Proteome Res.* 2023, 22, 2151–2171, doi:10.1021/acs.jproteome.2c00838.
64. Ong, S.-E.; Blagoev, B.; Kratchmarova, I.; Kristensen, D.B.; Steen, H.; Pandey, A.; Mann, M. Stable Isotope Labeling by Amino Acids in Cell Culture, SILAC, as a Simple and Accurate Approach to Expression Proteomics. *Molecular & Cellular Proteomics* 2002, 1, 376–386, doi:10.1074/mcp.M200025-MCP200.
65. Thompson, A.; Schäfer, J.; Kuhn, K.; Kienle, S.; Schwarz, J.; Schmidt, G.; Neumann, T.; Hamon, C. Tandem Mass Tags: A Novel Quantification Strategy for Comparative Analysis of Complex Protein Mixtures by MS/MS. *Anal. Chem.* 2003, 75, 1895–1904, doi:10.1021/ac0262560.

66. Cox, J.; Hein, M.Y.; Lubner, C.A.; Paron, I.; Nagaraj, N.; Mann, M. Accurate Proteome-Wide Label-Free Quantification by Delayed Normalization and Maximal Peptide Ratio Extraction, Termed MaxLFQ. *Molecular & Cellular Proteomics* 2014, 13, 2513–2526, doi:10.1074/mcp.M113.031591.
67. Szklarczyk, D.; Kirsch, R.; Koutrouli, M.; Nastou, K.; Mehryary, F.; Hachilif, R.; Gable, A.L.; Fang, T.; Doncheva, N.T.; Pyysalo, S.; et al. The STRING Database in 2023: Protein–Protein Association Networks and Functional Enrichment Analyses for Any Sequenced Genome of Interest. *Nucleic Acids Research* 2023, 51, D638–D646, doi:10.1093/nar/gkac1000.
68. Krämer, A.; Green, J.; Pollard, J.; Tugendreich, S. Causal Analysis Approaches in Ingenuity Pathway Analysis. *Bioinformatics* 2014, 30, 523–530, doi:10.1093/bioinformatics/btt703.
69. Chang, J.; Kim, Y.; Kwon, H.J. Advances in Identification and Validation of Protein Targets of Natural Products without Chemical Modification. *Nat. Prod. Rep.* 2016, 33, 719–730, doi:10.1039/C5NP00107B.
70. Lomenick, B.; Jung, G.; Wohlschlegel, J.A.; Huang, J. Target Identification Using Drug Affinity Responsive Target Stability (DARTS). *CP Chemical Biology* 2011, 3, 163–180, doi:10.1002/9780470559277.ch110180.
71. Jin, L.; Wang, D.; Gooden, D.M.; Ball, C.H.; Fitzgerald, M.C. Targeted Mass Spectrometry-Based Approach for Protein–Ligand Binding Analyses in Complex Biological Mixtures Using a Phenacyl Bromide Modification Strategy. *Anal. Chem.* 2016, 88, 10987–10993, doi:10.1021/acs.analchem.6b02658.
72. Adhikari, J.; Fitzgerald, M.C. SILAC-Pulse Proteolysis: A Mass Spectrometry-Based Method for Discovery and Cross-Validation in Proteome-Wide Studies of Ligand Binding. *J. Am. Soc. Mass Spectrom.* 2014, 25, 2073–2083, doi:10.1007/s13361-014-0992-y.
73. Prabhu, N.; Dai, L.; Nordlund, P. CETSA in Integrated Proteomics Studies of Cellular Processes. *Current Opinion in Chemical Biology* 2020, 54, 54–62, doi:10.1016/j.cbpa.2019.11.004.
74. Franken, H.; Mathieson, T.; Childs, D.; Sweetman, G.M.A.; Werner, T.; Tögel, I.; Doce, C.; Gade, S.; Bantscheff, M.; Drewes, G.; et al. Thermal Proteome Profiling for Unbiased Identification of Direct and Indirect Drug Targets Using Multiplexed Quantitative Mass Spectrometry. *Nat Protoc* 2015, 10, 1567–1593, doi:10.1038/nprot.2015.101.

Acknowledgments

The figures used for this introduction were created by me using information from the cited literature and with the help of the Biorender.com website. In particular, some of them were created by adapting “Keap1–Nrf2 Pathway”, and “NF-KB Signaling Pathway” by BioRender.com (2023). Retrieved from <https://app.biorender.com/biorender-templates>.

AIM OF THIS WORK

Considering the intimate connection between chronic inflammatory pathologies and oxidative stress, a promising approach to mitigate inflammatory states involves the activation of the NRF2 pathway to alleviate the oxidative stress burden and ultimately resolve pathological conditions. Natural extracts have garnered significant attention in both clinical and preclinical studies for their potential to resolve inflammatory states while also exhibiting antioxidant properties.

Therefore, the central aim of this research project encompasses three key objectives. The first one is to thoroughly examine the potential of fruit and vegetable extracts to act as modulators of inflammation and assess their capacity to activate the NRF2 pathway. To this purpose, R3/1 cells with NF- κ B gene reporter have been used to evaluate the dose-dependent anti-inflammatory and antioxidant effect of the extract in different conditions, for instance after challenging the cells with a pro-inflammatory stimulus such as IL-1 α and TNF- α . The effects of the extract on the NRF2 pathways have been assayed by a HEK292-ARE reporter cell lines to directly evaluate the effect on the NRF2 antioxidant pathway.

The second aim was to create an in-house database of literature-characterized metabolites for the natural extract that was taken into consideration. This comprehensive database serves as the cornerstone for subsequent targeted analyses that helped uncover the components that contribute to the extract's bioactivity. This identification was based on the combination of all the literature-based information related to retention time (RT), accurate mass and fragmentation (MS/MS) pattern. In cases where a putative identification was not possible, an untargeted approach was deployed to investigate the extract, identifying the components from the comparison of the MS spectra and MS/MS fragmentation with online databases and fragmentation prediction tools. Whenever possible, standard compounds were utilized to enhance the identification process.

The final aim of this work was to investigate the possible mechanisms of action of the selected natural extracts and assess the impact on the proteome. To address this experimental question, quantitative proteomic studies with both SILAC and Label-free approaches were deployed. Thanks to an external collaboration with the University of Messina, it was also possible to

assess the anti-inflammatory activity of a thinned young apple polyphenols extract on an animal model of DNBS induced ulcerative colitis while performing an *ex-vivo* label-free quantitative proteomic study. Making use of a recently developed mass spectrometry-based proteomic technique such as MS-Cellular Thermal Shift Assay (MS-CETSA) it was also possible to hypothesize direct protein targets of a bergamot leaves polyphenols extract while observing its influence on the proteome of a treated cell line.

In summary, this research project aims to elucidate the roles of natural extracts as modulators of inflammation and oxidative stress, assess their efficacy in pathological cell models and, by means of modern analytical Mass Spectrometry techniques, identify the active compounds responsible for their effects, along with a comprehensive understanding of their mechanisms of action.

Chapter 1

Characterization of a Red Grape skin by-product

Study 1 - Effect of extraction solvent and temperature on polyphenol profiles, antioxidant and anti-inflammatory effects of Red Grape Skin By-Product

(10.3390/molecules26185454)

1. Abstract

A fully-detailed LC-MS qualitative profiling of red grape skin, extracted with a mixture of ethanol and water (70:30 v:v) has permitted the identification of 65 compounds which can be classified into the following chemical classes: organic and phenolic acids (14 compounds), stilbenoids (1 compound), flavanols (21 compounds), flavonols (15 compounds) and anthocyanins (14 compounds). The extraction yield obtained with water at different temperatures (100 °C, 70 °C, room temperature (RT)) was then evaluated and the overall polyphenol content indicates that EtOH:H₂O solvent is the most efficient and selective for polyphenol extraction. However, by analyzing the recovery yield of each single polyphenol, we found that water extraction under heating conditions is effective (extraction yield similar or even better in respect to the binary solvent) for some polyphenolic classes, such as hydrophilic procyanidins, phenolic acids, flavonol glucosides and stilbenoids. However, according to their lipophilic character, a poor yield was found for the most lipophilic components, such as flavonol aglycones, and in general for anthocyanins. The radical scavenging activity was in accordance with the polyphenol content, and hence, much higher for the extract obtained with the binary solvent in respect to water extraction. All the tested extracts were found to have an anti-inflammatory activity in the R3/1 cell line with NF-κB reporter challenged with 0.01 μg/mL of IL-1α, in a 1 to 250 μg/mL concentration range. An intriguing result was that the EtOH:H₂O extract was found to be superimposable with that obtained using water at 100 °C despite the lower polyphenol content. Taken together, the results show the bioactive potentialities of grape skin extracts and the possibility to exploit this rich industrial waste. Water extraction carried

out by heating is an easy, low cost and environmentally friendly extraction method for some polyphenol classes and may have great potential for extracts with anti-inflammatory activities.

2. Introduction

Grapes are amongst the most cultivated fruits in the world. In Europe alone, around 3.5 million hectares are dedicated to grape cultivation with a production of almost 27 million tons of fruit [1]. It is also estimated that 14.5 million tons of grape by-products are generated annually [2]. The main component of this waste is the grape pomace, mainly composed (50–65%) of grape skin [3]. Even though it is mostly used as compost or animal fertilizer, the phenolic rich composition of the skin is what supports its use as a source of bioactive phytochemicals. It contains anthocyanins alongside various members of the flavonoid family (flavan-3-ols, flavonols and flavanones), which have shown healthy activity as antioxidant and anti-inflammatory agents [4–6]. Hence, grape skin represents a valuable source of bioactive polyphenols and would represent a valuable industrial source to satisfy the growing demand. A recent study conducted by Transparency Market Research, a global market intelligence group, has predicted a further increase in the polyphenol market owing to increasing demand and market size. This study indicates that the global demand for polyphenols in the global polyphenol market was valued at USD 761.9 million in 2020 and is expected to reach USD 969.2 million by the end of 2026, growing at a CAGR (Compound Annual Growth Rate) of 3.5% between 2021–2026 [7].

The appropriate industrial evaluation of red grape skin needs a suitable and green extraction method which should have the least experimental set-up, a low cost and have environmental and user-friendly characteristics.

Although many technological advancements in polyphenol extraction have been proposed, such as supercritical fluid extraction (SFE), ultrasound-assisted extraction (UAE), microwave assisted extraction (MAE), pressurized liquid extraction (PLE) and pressurized hot water extraction (PHWE) [8,9], the solid–liquid extraction (SLE), which simply consists of solvent application and leaching, remains the most popular. Since the structure of phenolic compounds determines their solubility in solvents of different polarity, the type of extraction solvent may have a significant impact on the yield of extraction polyphenols from plant material [10]. There are some reports concerning optimization of extraction conditions of the phenolic compound content and antioxidant activities of some plant foods, and the optimal procedure is usually different for different plant matrices and depends on the polyphenol composition [11–13]. For instance, acetone has been proven efficient in polyphenol extraction from lychee flowers

compared to methanol, water and ethanol [14]. However, another study reported water as the best solvent for polyphenol extraction from walnut green husks [15]. In general, binary solvents such as ethyl acetate, acetone, methanol and ethanol with a differing water content are used as suitable extraction solvents of polyphenols from raw material.

However, legal limitations for solvent residues and restrictions on the use of conventional organic solvents are becoming more and more rigorous, especially in the fields of food and pharmaceutical, and together with the use of flammable and costly solvents, they represent a limit for industrial extraction.

In this work, a selected red grape skin by-product was extracted using water extraction at different temperatures and the metabolomic, antioxidant and anti-inflammatory profiles compared in respect to those obtained using EtOH:H₂O 70:30 (v:v). Our aim is to fully characterize the profile and activities of the polyphenol fractions isolated by a water-based extraction of red grape skin and evaluate the temperature effect thus to understand if this easy, low-cost and environmentally friendly extraction method may prompt industrial interest. Polyphenol profiling was carried out by targeted LC-MS analyses and the antioxidant and anti-inflammatory activities of the extracts tested by *in vitro* and cell methods, respectively.

3. Material and Methods

3.1. Chemicals

6-hydroxy-2,5,7,8-tetramethyl-3,4-dihydrochromene-2-carboxylic acid (trolox), (-)-epicatechin, ethyl gallate, protocatechuic acid, Folin–Ciocalteu reagent, sodium carbonate, gallic acid, (+)-catechin, vanillin, hydrochloric acid, potassium chloride, sodium acetate, DMSO, 3-(4,5-Dimethyl-2-thiazolyl)-2,5-diphenyl-2H-tetrazolium bromide (MTT), IL1 α , ethanol, formic acid and LC-MS grade solvents were purchased from Merck KGaA, Darmstadt, Germany. Quercetin 3-galactoside and malvidin 3-glucoside were obtained from Extrasynthese (Genay CEDEX, France). LC-grade H₂O (18 M Ω cm) was prepared with a Milli-Q H₂O purification system (Millipore, Bedford, MA, USA).

3.2. Sample Preparation

Extraction from dried red grape skin derived from controlled and selected wineries in central Italy was carried out under the following conditions: 2 g of raw material in 40 mL of EtOH-H₂O 70:30 (% v/v) under magnetic stirring for 24 h at room temperature (extract A); 2 g of raw material in 40 mL of EtOH-H₂O 70:30 (% v/v) at 50 °C for one hour followed by 24 h at

room temperature under magnetic stirring (extract A50); 2 g of raw material in 40 mL of H₂O (100%) at 100 °C for one hour followed by 24 h at room temperature under magnetic stirring (extract B); 2 g of raw material in 40 mL of H₂O (100%) at 70 °C for one hour followed by 24 h at room temperature under magnetic stirring (extract C); 2 g of raw material in 40 mL of H₂O (100%) under magnetic stirring for 24 h at room temperature (extract D). Samples were then centrifuged at 5000 × g for 10 min, filtered on 0.45 µm filters and dried overnight under a vacuum. The conditions used combined the idea of a low-cost and simple method easily transferrable to industrial scale. Room temperature was selected as the low-cost condition for 24 h, since it is demonstrated that a prolonged extraction period led to the degradation of polyphenols [16]. A limited period of warming (1 h) was applied to avoid polyphenols degradation (especially anthocyanins [17]) at two different temperatures: boiling point (100 °C) and 70 °C, which is a mean of the most used temperature for water extract (60–80 °C) applied in the literature.

3.3. HPLC-HRMS Analysis

The extracts were resuspended in EtOH:H₂O (50:50, % v/v) to obtain a concentration 5×10^4 µg/mL, then diluted in H₂O/HCOOH, 100/0.1% v/v (mobile phase A) at the final concentration of 5×10^3 µg/mL and spiked with the internal standard (6-hydroxy-2,5,7,8-tetramethyl-3,4-dihydrochromene-2-carboxylic acid) at a final concentration of 5×10^{-5} M. The analyses were performed in triplicate by LC-HRMS: the mixtures were separated on a reversed-phase Agilent Zorbax SB-C18 column (150 × 2.1 mm, i.d. 3.5 µm, CPS analitica, Milan, Italy) by using a multi-step gradient of mobile phase A H₂O-HCOOH (100:0.1, v/v) and phase B CH₃CN-HCOOH (100:0.1, v/v) and analyzed by a LTQ Orbitrap XL mass spectrometer (Thermo Fisher Scientific, San Jose, CA, USA), as described by Baron et al. [18]. The spectra were acquired in negative and positive ion modes. Xcalibur 4.0 and Chromeleon Xpress 6.80 were used for instrument control and spectra analysis. A targeted data analysis was performed on the base of a database built searching in the literature for the known grape components [19–28] and the identification was carried out by using the exact mass (5 ppm of mass tolerance), the isotopic and fragmentation patterns. Quantitative analyses were assessed for epicatechin (0.11–7.26 µg/mL), quercetin 3-glucoside (0.045–2.90 µg/mL), ethyl gallate (0.019–4.95 µg/mL), protocatechuic acid (0.015–3.85 µg/mL) and malvidin 3-glucoside (0.048–12.3 µg/mL), using pure reference standards: calibration curves were built by plotting the peak area ratios of metabolite/trolox versus the nominal concentrations of the metabolite by weighted ($1/x^2$)

least-squares linear regression. Table 1 shows all the obtained linear curves and the relative limit of quantification (LOQ).

Table 1 - Calibration curve parameters for the available compounds.

	Slope	Intercept	R²	LOQ [$\mu\text{g}/\text{mL}$]
Epicatechin	0.3264	0.0287	0.9996	0.113
Quercetin 3-galactoside	0.5361	0.0139	0.9998	0.045
Ethyl gallate	0.3767	0.0194	0.9962	0.019
Protocatechuic acid	0.1417	0.0118	0.9916	0.015
Malvidin 3-glucoside	2.0151	0.3377	0.9965	0.048

3.4. Determination of Total Polyphenol Content

Determination of total polyphenol content was conducted spectrophotometrically by a slight modification of the method described by Dewanto et al. [29]. Briefly, 12.5 μL of diluted extract (1000 $\mu\text{g}/\text{mL}$) was spiked with 50 μL of water, 12.5 μL of Folin–Ciocalteu reagent and 125 μL of Na_2CO_3 (7%) in a 96-well plate. The mixture was incubated at room temperature for 90 min in the dark, then the absorbance was read at 760 nm in a spectrophotometric microplate reader (BioTek's PowerWave HT, Winooski, VT, USA). The results were then compared with a curve of gallic acid (0–1000 $\mu\text{g}/\text{mL}$) prepared with the same protocol of samples and expressed as % w/w (grams of polyphenols per one gram of starting material or dry extract).

3.5. Determination of Tannin Content

Determination of total tannin content was carried out by the vanillin assay [30] in 96-plate wells. Briefly, 150 μL of vanillin (4% solution in methanol) and 75 μL of concentrated HCl were added to 2.5 μL of diluted extract (1000 $\mu\text{g}/\text{mL}$). The mixture was mixed at room temperature for 15 min and then the absorbance measured against the blank at 500 nm using a microplate reader (BioTek's PowerWave HT, Winooski, VT, USA). The readings were compared to standards containing known amounts of (+)-catechin (0–1000 $\mu\text{g}/\text{mL}$) and prepared with the same protocol as the samples. The results were then expressed as % w/w (grams of polyphenols per one gram of starting material or dry extract).

3.6. Total Anthocyanin Content

Total anthocyanin content was evaluated as cyanidin 3-glucoside at 520 nm, using a molar absorptivity coefficient of 26,900 M⁻¹ cm⁻¹ [31]. Extracts were diluted in buffer pH 1 (0.025 M KCl solution brought to pH 1 with 37% HCl) and pH 4.5 (0.4 M CH₃COONa) and the absorbance read both at 520 nm and 700 nm in a spectrophotometric microplate reader after 15 min. Anthocyanin pigment concentration (as cyanidin 3-glucoside equivalents, µg/mL) was expressed as follows:

$$\text{Anthocyanin pigment } (\mu\text{g/mL}) = \frac{A \times MW \times DF \times 10^3}{\epsilon \times l} \quad (1)$$

where A = (A_{520nm}–A_{700nm}) pH 1.0–(A_{520nm}–A_{700nm}) pH 4.5; MW (molecular weight) = 449.38 g/mol for cyanidin-3-glucoside; DF = dilution factor; l = pathlength in cm; ε = 26,900 molar extinction coefficient, in L mol⁻¹ cm⁻¹, for cyaniding 3-glucoside; and 10³ = factor for conversion from g to mg. The results were expressed as % w/w (grams of polyphenols per one gram of starting material or dry extract).

3.7. Antioxidant Activity

The antioxidant capacity was evaluated by the DPPH radical-scavenging method [32], with a few modifications. An aliquot of 100 µL of the extract solution at different concentrations (1–25 µg/mL) was spiked with 750 µL of ethanol and 400 µL of acetate buffer (0.1 M, pH 5.5), mixed and spiked with 250 µL of DPPH ethanolic solution (0.5 × 10⁻³ M). After 90 min at room temperature and in the dark the absorbance at 515 nm was measured for each sample analyzed in triplicate with a UV reader Shimadzu UV 1900 (Shimadzu, Milano, Italia). The percentage of inhibition was calculated as expressed by Equation (3) and the results expressed as mean ± SD.

$$\frac{\text{Abs}_{\text{blank}} - \text{Abs}_{\text{sample}}}{\text{Abs}_{\text{blank}}} \times 100 \quad (2)$$

3.8. Anti-Inflammatory Activity

To assess the in vitro anti-inflammatory activity of the four different extracts, and evaluate the influence of the different extraction methods, the same cell model used by Baron et al. was deployed [18]. Extracts ranging from 1 to 250 µg/mL were incubated with R3/1 cells transduced with the NF-κB reporter gene and challenged with 0.01 µg/mL IL1α. The cell

viability of the extracts on the same cell line was evaluated for the same concentrations used in the anti-inflammatory assay by MTT assay as reported by Baron et al. [18].

4. Results and discussion

4.1. Absolute Quantification of Polyphenols, Tannins and Anthocyanins

As shown in Table 2, the % of dry extract in respect to the starting material was the highest for 100% water at 100 °C and reduced on the basis of the extraction temperature, reaching the lowest residue amount for EtOH:H₂O and EtOH:H₂O at 50 °C. By contrast, the extraction yield of polyphenols calculated in respect to the dry extract was much higher (almost 4 fold) in EtOH:H₂O in respect to water extracts. The % yield of polyphenols in respect to the starting material was at 4% for EtOH:H₂O and reduced by almost 50% in water and further reduced at 70 °C and room temperature. The data well indicate that EtOH:H₂O solvent is the most efficient and selective for polyphenol extraction, while water is able to extract not only polyphenols but also many other constituents in a temperature dependent manner as already observed by González-Centeno et al. [33]. We observed no difference between the two hydroalcoholic extracts.

Table 2 - Total polyphenol content calculated in respect to the dry extract and to the starting material.

Extract	% Dry Extract (in respect to starting material)	% Polyphenols (in respect to Dry Extract)	% Polyphenols (in respect to Starting Material)
Extract A	15.27 ± 0.38	28.23 ± 0.30	4.34 ± 0.07
Extract A50	12.50 ± 0.42	27.86 ± 0.17	4.15 ± 0.05
Extract B	35.00 ± 0.27	7.79 ± 0.10	2.77 ± 0.07
Extract C	28.81 ± 0.30	6.79 ± 0.17	1.92 ± 0.09
Extract D	21.69 ± 0.20	4.14 ± 0.07	0.83 ± 0.04

Table 3 reports the % of tannins and anthocyanins in respect to the dry extract and starting material. For EtOH:H₂O, the % in respect to the starting material was 3.28 and 0.271, respectively, an amount almost two times and one and a half times higher in respect to water at 100 °C. The extraction yield of tannins and anthocyanins reduced on the basis of the temperature for the water extracts, while for the two hydroalcoholic extracts overlapped.

Table 3 - Tannins and anthocyanins content calculated in respect to the dry extracts and to the starting material.

Extract	% Tannins <i>(in respect to Dry Extract)</i>	% Tannins <i>(in respect to Starting Material)</i>	% Anthocyanins <i>(in respect to Dry Extract)</i>	% Anthocyanins <i>(in respect to Starting Material)</i>
Extract A	21.49 ± 0.89	3.28 ± 0.14	1.78 ± 0.22	0.27 ± 0.03
Extract A50	21.52 ± 1.04	3.44 ± 0.17	1.52 ± 0.36	0.23 ± 0.06
Extract B	4.49 ± 0.32	1.57 ± 0.11	0.52 ± 0.10	0.18 ± 0.04
Extract C	3.78 ± 0.31	1.09 ± 0.09	0.45 ± 0.03	0.13 ± 0.01
Extract D	2.267 ± 0.22	0.49 ± 0.04	0.31 ± 0.06	0.07 ± 0.01

Comparing our results with previous studies [34–36] on grape skin extracts performed by SLE (Table 4), as expected we can generally observe a higher anthocyanins yield when acid is added in the extraction solvent and the temperature is lower, but their content is highly variable depending on the grape variety ([35,36]). On the other hand, tannin yield seems not to be affected by acid or temperature. Observing the results, where a higher tannins/polyphenols ratio is found, there is a lower anthocyanins/polyphenols ratio due to the different physico-chemical properties of the two classes.

Table 4 - Comparison of different SLE of grape skin extracts with relative tannins/polyphenols and anthocyanins/polyphenols ratios.

Starting Material	Extraction Solvent	Sample to Solvent Ratio	Time	Temperature	Tannins/ Polyphenols	Anthocyanins/ Polyphenols	Reference
Red grape skin without treatment	70% EtOH	2 g/40 mL	24 h	RT	0.750	0.081	Extract A
Red grape skin without treatment	H ₂ O	2 g/40 mL	1 h + 24 h	100 °C + RT	0.571	0.125	Extract B
Red grape skin without treatment	H ₂ O	2 g/40 mL	1 h + 24 h	70 °C + RT	0.500	0.133	Extract C
Red grape skin without treatment	H ₂ O	2 g/40 mL	24 h	RT	0.500	0.150	Extract D
Red grape skin without treatment	80% EtOH	500 g/500 mL	1 h	RT	-	0.136	[34]
Lyophilized powder	0.01% HCl in 80% aqueous MeOH	-	18 h	RT	0.074–0.131	1.250–5.326	[36]
Skin powder	MeOH/H ₂ O/HCl (80/20/0.1)	100 mg/8 mL	2 h	RT	0.595–1.222	0.093–0.347	[35]

4.2. Compound Identification, Absolute and Relative Content

Figure 1 shows the LC-ESI(-)-MS (Total Ion Current) profiles of the four extracts: extract A (panel A), extract B (panel B), extract C (panel C) and extract D (panel D). The comparison between the extract A and extract A50 profiles (which are almost overlapping) is reported in Figure S1 of the Supplementary Material. The peak eluting at 1.5 min and detected in all the extracts was assigned to tartaric acid (peak 1).

The TIC showing the highest number of peaks is that referred to EtOH-H₂O (panel A); eluted peaks of the extracts can be clustered into three main groups based on their RT: group (A), which includes peaks eluting between 3 and 20 min, group (B) medium lipophilic compounds, eluting between 20 and 40 min, and group (C) the most lipophilic compounds, eluting after 40 min. TICs relative to groups A, B and C are reported in Figures 2–4, respectively. The LC-ESI(+)-MS (positive ion mode) profiles are reported in Figure 5.

The comparison between the extract A and extract A50 positive profiles (which are almost overlapping) are reported in Figure S2 of the Supplementary Material. Compound identification was carried out on the basis of the accurate MS and MS/MS fragmentation and the lists of identified peaks in all the extracts are reported in Table 5 (relative to the acquisition in negative ion mode) and Table 6 (relative to the acquisition in positive ion mode). The 65 identified compounds can be classified into the following chemical classes: organic and phenolic acids (14 compounds), stilbenoids (1 compound), flavanols (21 compounds), flavonols (15 compounds) and anthocyanins (14 compounds).

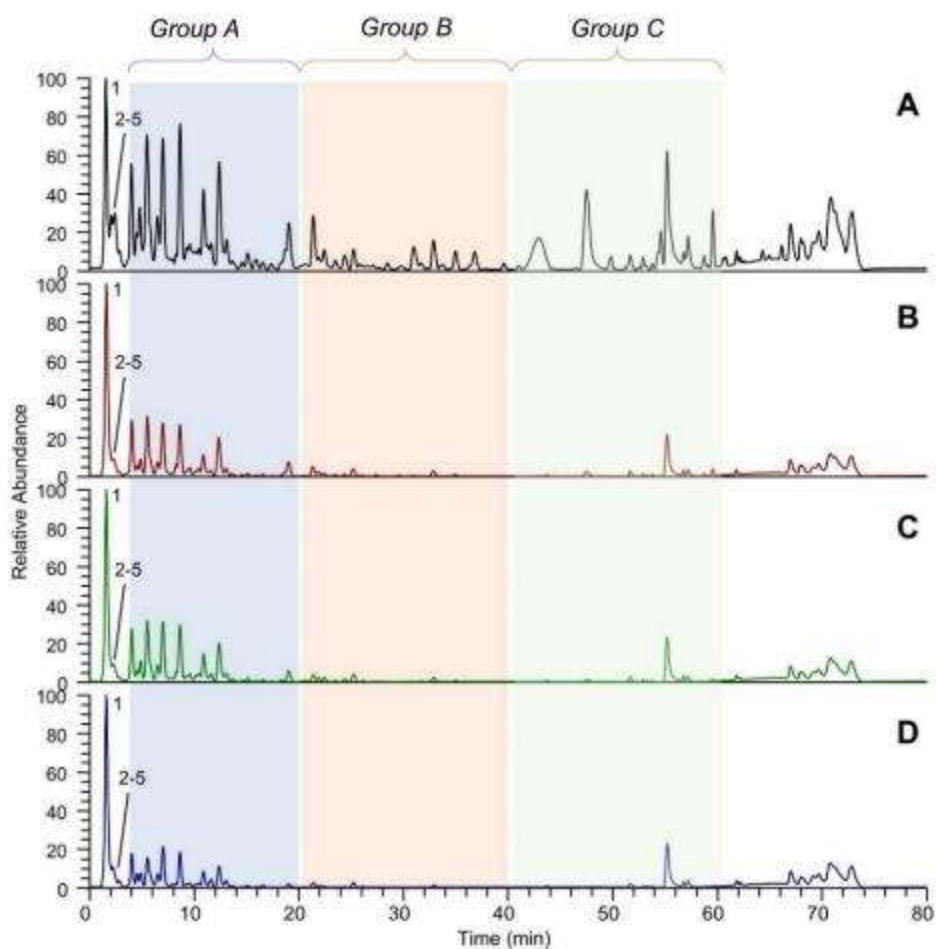


Figure 1 - LC-ESI(-)-MS total ion currents (TICs) in negative ion mode of the four extracts: (A) EtOH-H₂O 70:30 (% v/v); extract A; (B) water at 100 °C, extract B; (C) water at 70 °C extract C; (D) water at room temperature, extract D. Peaks numbered from 1 to 5 eluted within 3 min and are not included in the groups A, B and C which are magnified in Figures 2-4.

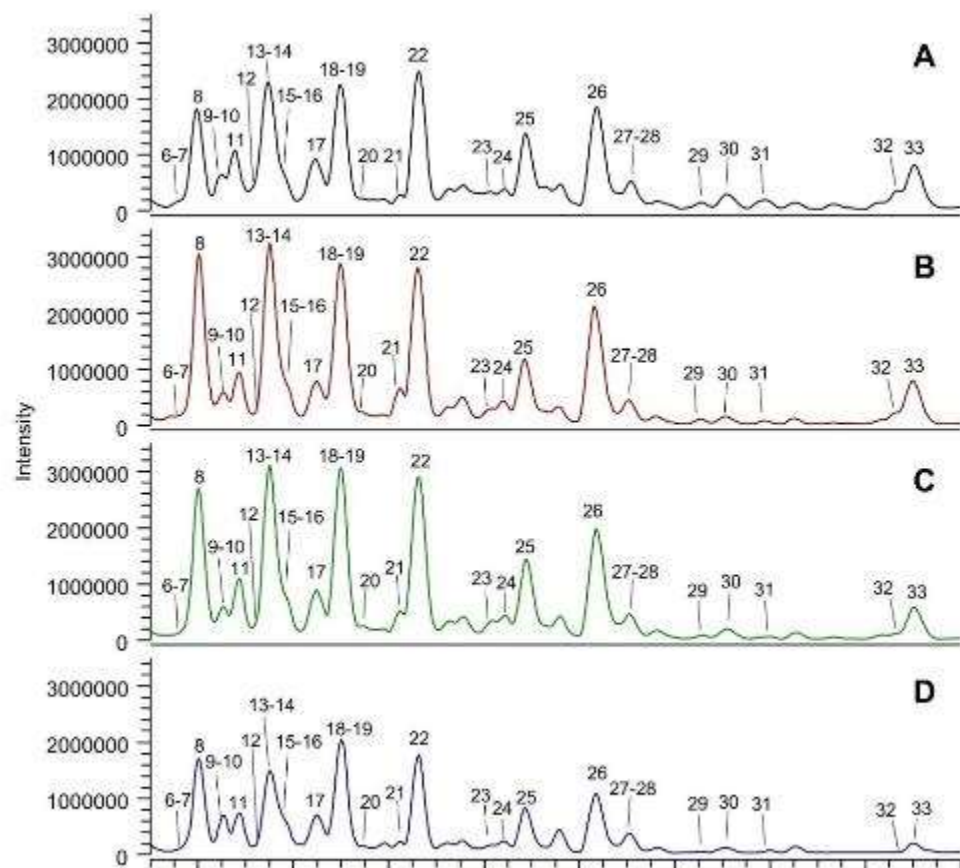


Figure 2 - Magnification (range time 20–40 min) of the LC-ESI(-)-MS total ion currents (TICs) recorded in negative ion mode of the four extracts: (A) EtOH-H₂O 70:30 (% v/v); extract A; (B) water at 100 °C, extract B; (C) water at 70 °C extract C; (D) water at room temperature, extract D. Identified peaks (group B) are numbered progressively based on the RT and their assignment is reported in Table 5.

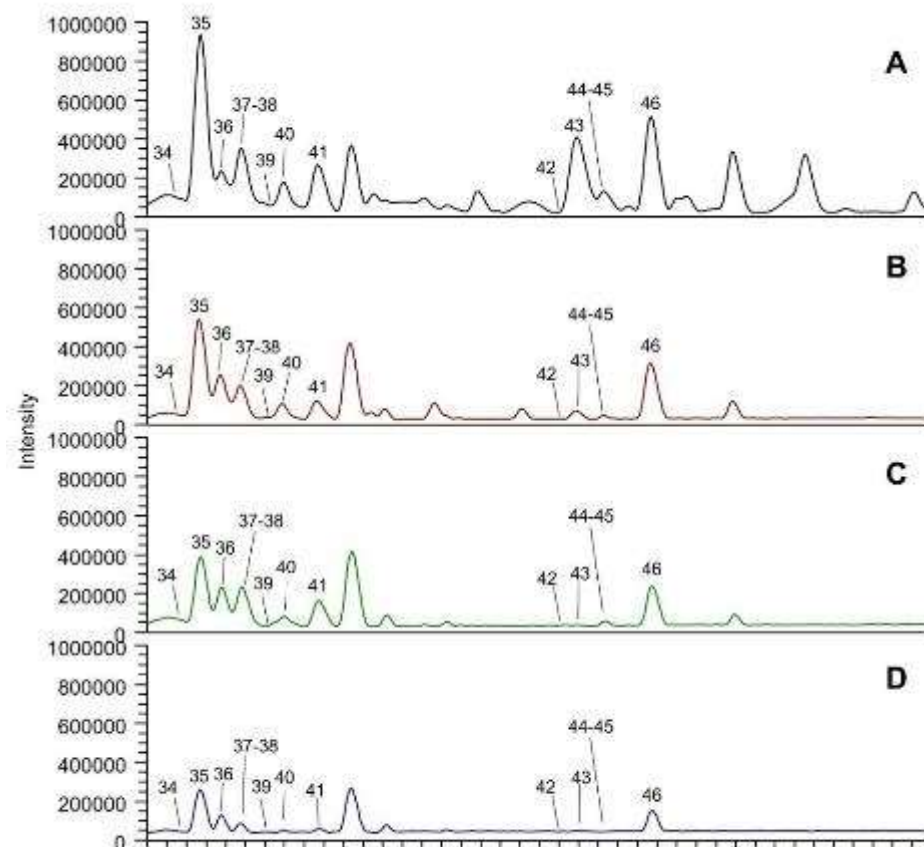


Figure 3 - Magnification (range time 3–20 min) of the LC-ESI(-)-MS total ion currents (TICs) recorded in negative ion mode of the four extracts: (A) EtOH-H₂O 70:30 (% v/v); extract A; (B) water at 100 °C, extract B; (C) water at 70 °C extract C; (D) water at room temperature, extract D. Identified peaks (group A) are numbered progressively based on the RT and their assignment is reported in Table 5.

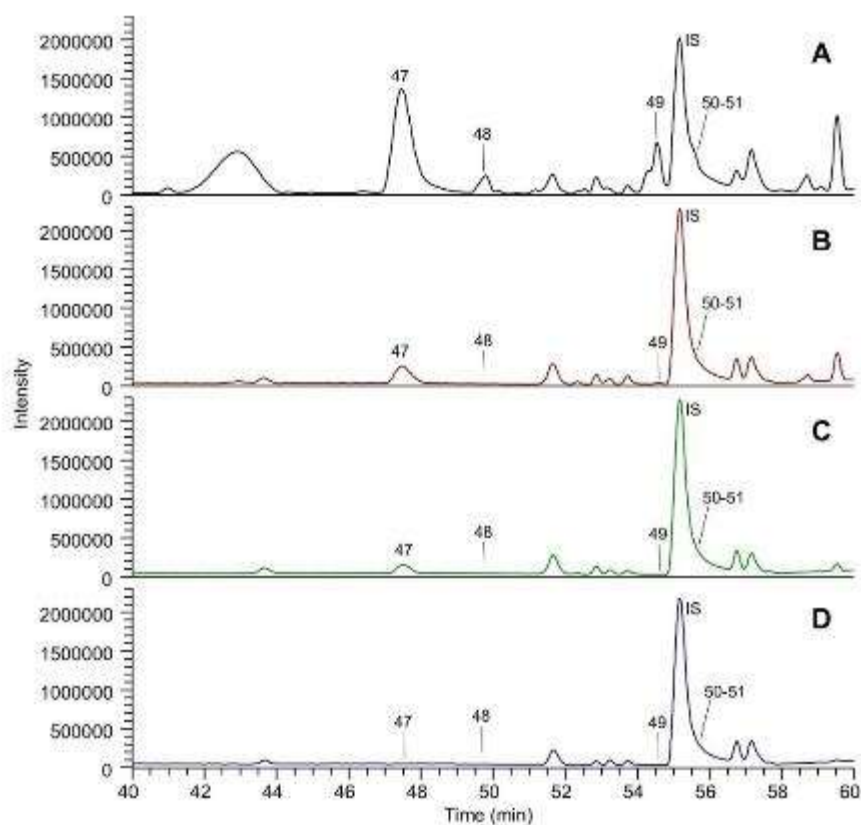


Figure 4 - Magnification (range time 40–60 min) of the LC-ESI(-)-MS total ion currents (TICs) recorded in negative ion mode of the four extracts. Identified peaks (group C) are numbered progressively based on the RT and their assignment is reported in Table 5.

Table 5 - LC-ESI(-)-MS identification (negative ion mode) of the EtOH-H₂O extract constituents. The peak numbers refer to those reported in Figures 1–4.

Group	Peak	Name	RT	m/z_{calc}	m/z_{exp}	Δppm	MS/MS
	1	Tartaric acid	1.5	149.0086	149.0093	-4.698	87–103–131
	2	Gallic acid	2.3	169.0137	169.0143	-3.550	125
	3	Galloyl glucose	2.4	331.0665	331.0664	0.362	125–169
	4	Protocatechuic acid hexoside	2.7	315.0716	315.0715	0.317	153
	5	Gallocatechin	2.9	305.0661	305.0665	-1.246	125–165–179–219–221–261–287
	6	Protocatechuic acid	3.7	153.0188	153.0195	-4.705	109
	7	Caftaric acid	3.8	311.0403	311.0404	-0.289	149–179
	8	Procyanidin B peak 1	4.0	577.1346	577.1331	2.582	289–407–425–451–559
	9	Epigallocatechin	4.3	305.0661	305.0660	0.393	125–165–179–219–221–261–287
A	10	Caffeoyl hexoside 1	4.4	341.0873	341.0869	1.026	179–221–251–281
	11	Procyanidin B peak 2	4.9	577.1346	577.1330	2.755	289–407–425–451–559
	12	Caffeoyl hexooside 2	5.2	341.0873	341.0872	0.147	179–221–251–281
	13	Procyanidin trimer peak 1	5.4	865.1980	865.1945	4.022	287–289–407–451–577–695–713–739
	14	Catechin	5.5	289.0712	289.0706	2.110	179–205–245
	15	Coutaric acid	5.8	295.0454	295.0452	0.644	163

16	Procyanidin trimer peak 2	5.8	865.1980	865.1937	4.947	287-289-407-451-577-695-713-739	
17	Procyanidin B peak3	6.5	577.1346	577.1334	2.062	289-407-425-451-559	
18	<i>p</i> -Coumaroyl hexoside 1	6.9	325.0923	325.0921	0.738	163-235-265	
19	Procyanidin B peak4	7.0	577.1346	577.1331	2.582	289-407-425-451-559	
20	Fertaric acid	7.3	325.0560	325.0560	-0.154	193	
21	<i>p</i> -Coumaroyl hexoside 2	8.3	325.0923	325.0922	0.431	163-235-265	
22	Epicatechin	8.7	289.0712	289.0708	1.418	179-205-245	
23	Vanillic acid hexoside	10.0	329.0873	329.0869	1.064	167-191-314	
24	Procyanidin trimer peak 3	10.2	865.1980	865.1937	4.947	287-289-407-451-577-695-713-739	
25	Procyanidin trimer peak 4	10.9	865.1980	865.1951	3.329	287-289-407-451-577-695-713-739	
26	Procyanidin dimer gallate	12.4	729.1431	729.1435	-0.590	287-289-407-451-559-577	
27	Ethyl gallate	13.1	197.0450	197.0456	-3.045	169	
28	Procyanidin tetramer	13.1	1153.2544	1153.2501	3.720	-	
29	Myricetin 3-galactoside	14.5	479.0826	479.0819	1.378	317	
30	Procyanidin pentamer	15.1	720.1559	720.1569	-1.389	-	
31	Procyanidin hexamer gallate	15.9	940.1956	940.1914	4.499	-	
32	Procyanidin dimer 3,3'-di-O-gallate	18.7	881.1565	881.1530	3.972	289-407-559-577-711-729	
33	Epicatechin 3-gallate	18.9	441.0822	441.0812	2.199	169-289	
B	34	Quercetin 3-glucoside	20.7	463.0877	463.0871	1.188	301
	35	Quercetin 3-glucuronide	21.3	477.0669	477.0661	1.698	301

	36	Quercetin 3-galactoside	22.1	463.0877	463.0869	1.620	301
	37	Dihydroquercetin 3-rhamnoside	22.3	449.1084	449.1077	1.514	285-303
	38	Procyanidin trimer gallate peak 1	22.4	1017.2034	1017.203	0.364	-
	39	Kaempferol 3-hexoside	23.2	447.0927	447.0919	1.856	285
	40	Laricitrin 3-galactoside	23.5	493.0982	493.0979	0.629	331
	41	Procyanidin tetramer gallate	24.4	652.1322	652.1312	1.602	-
	42	Dihydrokaempferol 3-rhamnoside	30.5	433.1135	433.1133	0.393	287-269
	43	Myricetin	30.9	317.0297	317.0296	0.442	137-151-179
	44	Resveratrol glucoside	31.4	389.1236	389.1234	0.617	227
	45	Procyanidin trimer gallate peak 2	31.6	1017.2089	1017.2042	4.620	-
	46	Syringetin 3-glucoside	32.8	507.1139	507.1130	1.696	345
	47	Quercetin	47.5	301.0348	301.0348	0.100	151-179
	48	Laricitrin	49.7	331.0454	331.0450	1.178	151-179-316
C	49	Kaempferol	54.6	285.0399	285.0400	-0.316	151
	50	Syringetin	55.4	345.0610	345.0606	1.275	315-330
	51	Isorhamnetin	55.5	315.0505	315.0503	0.571	300

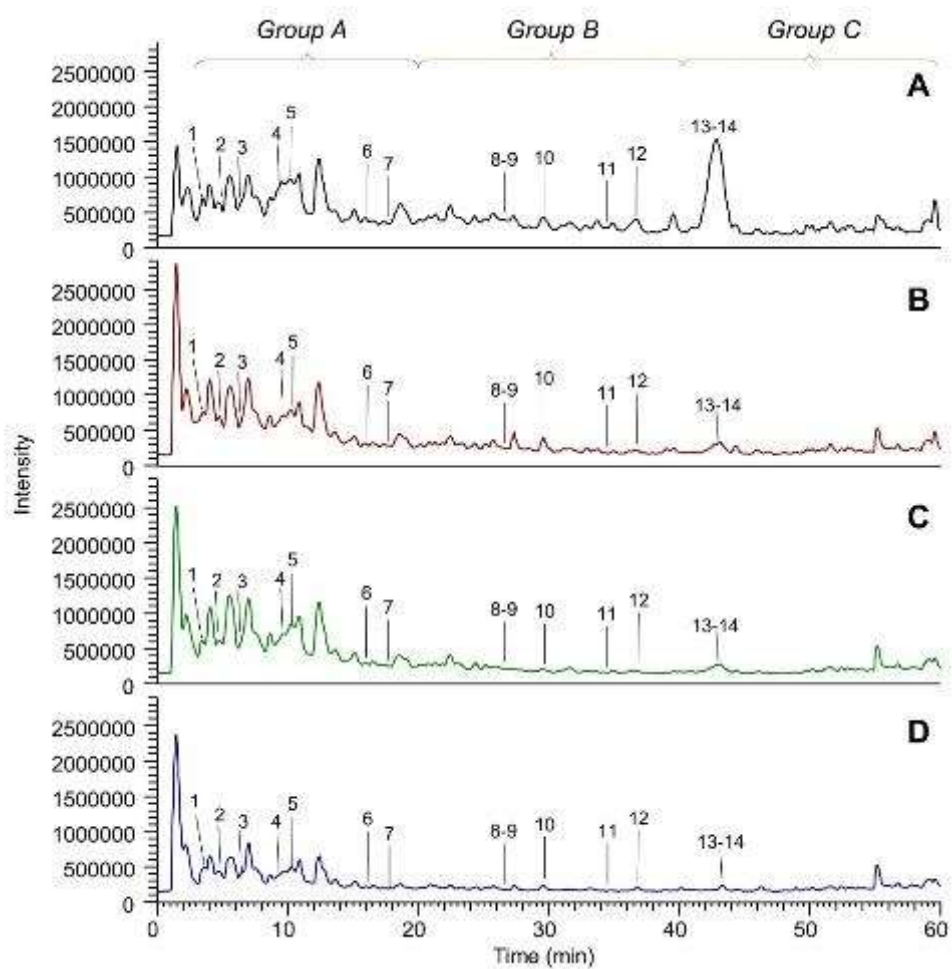


Figure 5 - LC-ESI-(+)-MS total ion currents (TICs) in positive ion mode of the four extracts. Peaks are numbered on the basis of the RT and the peak assignment is reported in Table 6.

Table 6 - LC-ESI-(+)-MS identification (positive ion mode) of the EtOH-H₂O extract constituents. The peak numbers refer to those shown in Figure 5.

Peak	Name	RT	<i>m/z</i> _{calc}	<i>m/z</i> _{exp}	Δ ppm	MS/MS
1	Delphinidin 3-glucoside	3.7	465.1033	465.1028	1.054	303
2	Cyanidin 3-glucoside	5.2	449.1084	449.1079	1.069	287
3	Petunidin 3-glucoside	6.1	479.1189	479.1179	2.171	317
4	Peonidin 3-glucoside	8.8	463.124	463.1234	1.360	301
5	Malvidin 3-glucoside	9.6	493.1346	493.1339	1.399	331
6	Vitisin A	15.9	561.1244	561.1238	1.105	399
7	Vitisin B	18.2	517.1346	517.1339	1.334	355
8	Peonidin 3-(6''-acetyl)-glucoside	26.2	505.1346	505.1340	1.168	301
9	Malvidin 3-(6''-acetyl)-glucoside	26.6	535.1452	535.1445	1.215	331
10	Delphinidin 3-(6''-coumaroyl)-glucoside	29.6	611.1401	611.1396	0.769	303
11	Malvidin 3-(6''-caffeoyl)-glucoside	34.4	655.1663	655.1661	0.275	331
12	Petunidin 3-(6''-coumaroyl)-glucoside	36.4	625.1557	625.1551	0.992	317
13	Peonidin 3-(6''-coumaroyl)-glucoside	42.7	609.1608	609.1602	0.985	301
14	Malvidin 3-(6''-coumaroyl)-glucoside	42.9	639.1714	639.1706	1.205	331

4.3. Flavanols

As expected, most of the procyanidins (18 out of 21) eluted in group A, as the most hydrophilic compounds of the extract. A total number of 21 procyanidins were identified from monomers (catechin, epicatechin, galliccatechin, epigallocatechin, epicatechin-gallate) to oligomers, such as hexamer gallate.

The relative content of procyanidins calculated for the EtOH:H₂O extract on the basis of the area of the peaks reconstituted by setting the [M-H]⁻ values as filter ion is summarized in Table 7. Dimers and the corresponding gallate esters, reaching more than 40% of the total procyanidins, represent the main species, followed by monomers (catechin, epi-catechin and gallates), more than 25%, and trimers, with a relative content of 21%, followed by oligomers such as tetramer, pentamer and hexamer.

Table 7 - Relative content of flavanols in the EtOH-H₂O extract. The % was determined by measuring the peak area of each compound in respect to the sum of the peak areas of all the identified flavanols.

Compound	Relative Content (%)
Gallocatechin	0.090 (±0.001)
Procyanidin B peak1	6.46 (±0.05)
Epigallocatechin	0.0124 (±0.0001)
Procyanidin B peak2	4.50 (±0.07)
Procyanidin trimer peak 1	3.54 (±0.04)
Catechin	8.65 (±0.14)
Procyanidin trimer peak 2	2.46 (±0.04)
Procyanidin B peak3	6.11 (±0.06)
Procyanidin B peak4	9.75 (±0.20)
Epicatechin	11.11 (±0.20)
Procyanidin trimer peak 3	1.63 (±0.03)
Procyanidin trimer peak 4	8.51 (±0.12)
Dimer gallate	15.24 (±0.18)
Tetramer	1.85 (±0.02)
Pentamer	3.07 (±0.04)
Hexamer gallate	0.359 (±0.003)
Procyanidin dimer 3,3'-di-O-gallate	2.40 (±0.02)
epicatechin 3-gallate	5.75 (±0.03)
Trimer gallate	3.37 (±0.02)
Tetramer gallate	3.54 (±0.03)
Trimer gallate	1.60 (±0.02)

Procyanidins were present in all four extracts but with a different relative abundance as shown in Table 8. The relative percentage of each extract (where i = A or A50 or B or C or D) was calculated with the following formula with the area of the peaks identified in extract A set as 100%:

$$\frac{(Area_{analyte}/Area_{IS})_{extract\ i}}{(Area_{analyte}/Area_{IS})_{extract\ A}} \times 100 \quad (1)$$

Table 8 - Relative percentage (mean \pm SD) of each flavanol in extracts A50, B, C and D calculated in respect to the content determined in extract A and set as 100%. The relative percentages were calculated by measuring the areas of the peaks reconstituted by setting the [M-H]⁻ as filter ions.

Compound	Extract A	Extract A50	Extract B	Extract C	Extract D
<i>Flavanols</i>					
Gallocatechin	100.00 (\pm 1.24)	136.82 (\pm 1.76)	255.85 (\pm 1.33)	216.64 (\pm 0.58)	20.72 (\pm 1.24)
Procyanidin B peak1	100.00 (\pm 1.01)	104.22 (\pm 0.70)	148.13 (\pm 1.72)	137.17 (\pm 1.74)	101.91 (\pm 0.56)
Epigallocatechin	100.00 (\pm 1.59)	143.61 (\pm 1.67)	627.16 (\pm 3.17)	660.25 (\pm 2.00)	95.90 (\pm 0.99)
Procyanidin B peak2	100.00 (\pm 1.30)	106.07 (\pm 0.95)	93.56 (\pm 0.92)	106.66 (\pm 0.98)	76.84 (\pm 0.88)
Procyanidin trimer peak 1	100.00 (\pm 0.93)	133.64 (\pm 1.07)	88.95 (\pm 0.72)	108.11 (\pm 1.05)	57.64 (\pm 0.74)
Catechin	100.00 (\pm 1.83)	119.26 (\pm 4.27)	127.26 (\pm 1.39)	111.38 (\pm 1.78)	66.85 (\pm 0.17)
Procyanidin trimer peak 2	100.00 (\pm 2.01)	94.01 (\pm 1.68)	118.11 (\pm 1.33)	122.07 (\pm 1.34)	105.38 (\pm 0.90)
Procyanidin B peak3	100.00 (\pm 0.79)	91.52 (\pm 0.84)	75.79 (\pm 0.73)	89.42 (\pm 0.62)	80.13 (\pm 0.30)
Procyanidin B peak4	100.00 (\pm 1.82)	108.22 (\pm 1.53)	110.40 (\pm 1.07)	122.58 (\pm 0.67)	100.44 (\pm 0.76)
Epicatechin	100.00 (\pm 1.74)	106.68 (\pm 1.32)	113.32 (\pm 1.66)	120.78 (\pm 1.67)	83.55 (\pm 0.78)
Procyanidin trimer peak 3	100.00 (\pm 1.56)	118.38 (\pm 2.82)	104.93 (\pm 1.05)	122.54 (\pm 1.20)	70.62 (\pm 1.15)
Procyanidin trimer peak 4	100.00 (\pm 1.50)	120.04 (\pm 0.71)	81.74 (\pm 0.51)	110.56 (\pm 1.02)	66.48 (\pm 0.35)
Procyanidin dimer gallate	100.00 (\pm 1.37)	93.17 (\pm 0.78)	87.56 (\pm 0.69)	81.17 (\pm 0.51)	49.09 (\pm 0.48)
Procyanidin tetramer	100.00 (\pm 1.02)	93.26 (\pm 0.34)	63.35 (\pm 0.99)	92.90 (\pm 1.43)	62.22 (\pm 0.90)
Procyanidin pentamer	100.00 (\pm 0.97)	116.02 (\pm 0.97)	51.53 (\pm 0.88)	70.97 (\pm 0.73)	52.04 (\pm 0.36)
Procyanidin hexamer gallate	100.00 (\pm 0.89)	89.62 (\pm 0.89)	63.56 (\pm 0.64)	46.22 (\pm 0.52)	47.44 (\pm 0.81)
Procyanidin dimer 3,3'-di-O-gallate	100.00 (\pm 0.93)	109.65 (\pm 0.25)	65.90 (\pm 0.59)	39.13 (\pm 0.53)	12.70 (\pm 0.07)
Epicatechin 3-gallate	100.00 (\pm 0.62)	145.58 (\pm 1.25)	102.69 (\pm 0.41)	73.58 (\pm 0.25)	29.99 (\pm 0.38)
Procyanidin trimer gallate	100.00 (\pm 0.86)	93.74 (\pm 1.81)	54.75 (\pm 0.78)	64.27 (\pm 0.93)	28.62 (\pm 0.59)
Procyanidin tetramer gallate	100.00 (\pm 1.03)	98.70 (\pm 1.09)	37.36 (\pm 0.83)	46.61 (\pm 0.65)	18.93 (\pm 0.35)
Procyanidin trimer gallate	100.00 (\pm 1.13)	117.58 (\pm 0.71)	40.41 (\pm 0.89)	38.39 (\pm 0.17)	16.19 (\pm 0.07)
MEAN	100	111	120	123	59

For some of the most hydrophilic compounds (procyanidins eluting up to 12.3 min) such as gallocatechin and epigallocatechin, the yield was much higher when the extraction process was carried out with water in respect to both EtOH:H₂O A and A50. For other hydrophilic components such as procyanidin trimer, catechin, epicatechin and some procyanidins B, the extraction yield in water was slightly but significantly higher and this in accordance with their hydrophilicity. Heating at 50 °C seems not to globally affect the yield of extraction.

The extraction yield in water solvents was found reduced for procyanidins eluting from 12 to 19 min by almost 50% and much lower when the water-based extraction was carried out without a heating step which was also found to significantly increase the extraction of the most hydrophilic components.

In Table 9 are reported the absolute concentrations ($\mu\text{g}/\text{mL}$) of epicatechin in all the extracts.

Table 9 - Epicatechin absolute concentrations ($\mu\text{g}/\text{mL}$, mean \pm SD) in the extracts.

	Extract A	Extract A50	Extract B	Extract C	Extract D
Epicatechin	3.83 (± 0.07)	4.06 (± 0.05)	4.42 (± 0.01)	4.72 (± 0.15)	3.24 (± 0.03)

4.4. Flavonols

Flavonols were identified mainly as glycosides (8 out of 15), which eluted in group B. A glucuronide derivative (quercetin 3-glucuronide) and 6 aglycones (group C, except for myricetin) were also detected.

Table 10 reports the relative abundance of flavonols in the EtOH:H₂O. Quercetin is the main flavanol, accounting for almost 40%, followed by its glucuronide (16%), syringetin 3-glucoside (11%), myricetin (9%) and kaempferol (almost 6%). The other constituents have a relative content lower than 5%.

Table 10 - Relative content of flavonols in the EtOH-H₂O extract. The % was determined by measuring the peak area of each compound in respect to the sum of the peak areas of all the identified flavonols.

Compound	Relative Content (%)
Myricetin 3-galactoside	1.82 (±0.03)
Quercetin 3-glucoside	0.675 (±0.008)
Quercetin 3-glucuronide	16.33 (±0.22)
Quercetin 3-galactoside	2.01 (±0.05)
Dihydroquercetin 3-rhamnoside	1.58 (±0.02)
Kaempferol 3-hexoside	0.662 (±0.004)
Laricitrin 3-galactoside	3.13 (±0.03)
Dihydrokaempferol 3-rhamnoside	0.299 (±0.002)
Myricetin	9.07 (±0.05)
Syringetin 3-glucoside	11.48 (±0.07)
Quercetin	39.99 (±0.21)
Laricitrin	2.54 (±0.03)
Kaempferol	5.91 (±0.13)
Syringetin	1.08 (±0.01)
Isorhamnetin	3.41 (±0.03)

Table 11 shows the relative percentage in the five extracts. For all the identified flavonols both as aglycones and glucosides, the highest extraction yield was obtained when EtOH:H₂O mixture was used as extraction solvent and the recovery yield followed the following order: extract B > extract C > extract D. By calculating the mean of %, the yield of extraction for the conjugated forms reduced to almost 66% when water was used in respect to EtOH:H₂O and further decreased for aglycones which reduced by almost 88% in extract B and 94% in extract C to reach an almost negligible yield for H₂O extraction in RT condition (0.3%). The extraction yield of EtOH:H₂O after heating is comparable to that without heating both for glycosides and aglycones.

Table 11 - Relative percentage (mean \pm SD) of each flavonol in extracts A50, B, C and D calculated in respect to the content determined in extract A and set as 100%. The relative percentages were calculated by measuring the areas of the peaks reconstituted by setting the [M-H]⁻ as filter ions.

Compound	Extract A	Extract A50	Extract B	Extract C	Extract D
<i>Flavonols</i>					
Myricetin 3-galactoside	100.00 (\pm 1.21)	115.48 (\pm 1.46)	88.27 (\pm 1.15)	66.97 (\pm 1.14)	48.93 (\pm 0.27)
Quercetin 3-glucoside	100.00 (\pm 0.93)	117.94 (\pm 1.63)	57.51 (\pm 0.65)	42.33 (\pm 0.40)	15.83 (\pm 0.43)
Quercetin 3-glucuronide	100.00 (\pm 1.64)	106.20 (\pm 1.69)	56.28 (\pm 0.33)	45.02 (\pm 0.21)	37.60 (\pm 0.23)
Quercetin 3-galactoside	100.00 (\pm 2.26)	106.01 (\pm 1.41)	75.67 (\pm 1.81)	64.18 (\pm 0.87)	34.22 (\pm 1.30)
Dihydroquercetin 3-rhamnoside	100.00 (\pm 1.10)	103.02 (\pm 1.52)	77.01 (\pm 0.56)	78.56 (\pm 0.23)	109.37 (\pm 1.19)
Kaempferol 3-hexoside	100.00 (\pm 0.69)	102.09 (\pm 0.54)	27.44 (\pm 0.50)	10.47 (\pm 0.11)	3.31 (\pm 0.07)
Laricitrin 3-galactoside	100.00 (\pm 1.20)	95.08 (\pm 1.29)	63.05 (\pm 0.97)	45.80 (\pm 1.05)	34.88 (\pm 0.24)
Dihydrokaempferol 3-rhamnoside	100.00 (\pm 0.64)	97.02 (\pm 0.34)	77.75 (\pm 1.11)	91.09 (\pm 0.63)	81.70 (\pm 1.40)
Syringetin 3-glucoside	100.00 (\pm 0.67)	104.41 (\pm 0.80)	67.60 (\pm 0.47)	53.43 (\pm 0.33)	35.36 (\pm 0.29)
<i>Mean glycosides</i>	100	101	66	55	45
Myricetin	100.00 (\pm 0.57)	88.19 (\pm 0.10)	18.06 (\pm 0.18)	9.76 (\pm 0.05)	0.115 (\pm 0.004)
Quercetin	100.00 (\pm 0.61)	89.55 (\pm 0.74)	23.07 (\pm 0.37)	13.88 (\pm 0.29)	0.560 (\pm 0.011)
Laricitrin	100.00 (\pm 1.19)	99.98 (\pm 2.74)	14.82 (\pm 0.52)	6.21 (\pm 0.06)	0.105 (\pm 0.005)
Kaempferol	100.00 (\pm 2.03)	102.49 (\pm 1.10)	7.49 (\pm 0.04)	3.61 (\pm 0.07)	0.360 (\pm 0.012)
Syringetin	100.00 (\pm 0.67)	117.56 (\pm 0.32)	5.11 (\pm 0.34)	1.61 (\pm 0.05)	0.364 (\pm 0.080)
Isorhamnetin	100.00 (\pm 0.73)	108.53 (\pm 0.69)	5.96 (\pm 0.62)	2.48 (\pm 0.04)	0.170 (\pm 0.021)
<i>Mean aglycones</i>	100	105	12	6	0.3

Table 12 reports the absolute concentrations of quercetin 3-galactoside in all the extracts.

Table 12 - Quercetin 3-galactoside absolute concentrations ($\mu\text{g/mL}$, mean \pm SD) in the extracts.

	Extract A	Extract A50	Extract B	Extract C	Extract D
Quercetin 3-galactoside	0.251 (± 0.006)	0.267 (± 0.004)	0.183 (± 0.0004)	0.152 (± 0.003)	0.069 (± 0.002)

4.5. Stilbenoids, Phenolic and Organic Acids

Only one stilbenoid was detected in all the extracts, resveratrol glucoside, whose extraction yield was similar in extracts A, A50 B and C but reduced by almost 30% in extract D. A total number of 14 organic and phenolic acids were identified, whose relative abundance in extract A is reported in Table 13. Tartaric acid represents the main organic acid, accounting for more than 40%. Taking into consideration only phenolic acids, ethyl gallate is the main species (30.2%) followed by *p*-coumaroyl-glucosides (more than 20%) gallic acid (15.4%) and galloyl glucose (14.5%).

Table 13 - Relative content of phenolic acids in the EtOH-H₂O extract. The % was determined by measuring the peak area of each compound in respect to the sum of the peak areas of all the identified phenolic acids.

Compound	Relative Content (%)
Gallic acid	15.40 (± 0.12)
Galloyl glucose	14.48 (± 0.18)
Protocatechuic acid hexoside	1.84 (± 0.01)
Protocatechuic acid	1.24 (± 0.02)
Caftaric acid	2.73 (± 0.06)
Caffeoyl hexoside 1	3.76 (± 0.04)
Caffeoyl hexoside 2	2.33 (± 0.04)
Coutaric acid	1.24 (± 0.02)
<i>p</i> -Coumaroyl glucoside 1	8.38 (± 0.13)
Fertaric acid	3.54 (± 0.04)
<i>p</i> -Coumaroyl-glucoside 2	12.3 (± 0.30)
Vanillic acid hexoside	2.48 (± 0.02)
Ethyl gallate	30.25 (± 0.34)

As shown in Table 14, some of the organic acids were extracted in a greater yield with water based solvents, such as protocatechuic acid, caftaric acid and p-coumaroyl hexoside 1, while for some others, such as galloyl glucose, protocatechuic acid hexoside, fertaric acid and ethyl gallate, the extraction yield was greater with EtOH:H₂O (both extract A and A50). The % mean calculated not considering tartaric acid was higher by almost 40% for extract B in respect to A and reduced in C and D, this latter similar to A.

Table 14 - Relative percentage (mean \pm SD) of each organic and phenolic acid in extracts A50 B, C and D calculated in respect to the content determined in extract A and set as 100%. The relative percentages were calculated by measuring the areas of the peaks reconstituted by setting the [M-H]⁻ as filter ions.

Compound	Extract A	Extract A50	Extract B	Extract C	Extract D
<i>Organic and phenolic acids</i>					
Tartaric acid	100.00 (\pm 1.85)	36.79 (\pm 0.33)	396.77 (\pm 0.67)	361.47 (\pm 0.77)	398.50 (\pm 0.51)
Gallic acid	100.00 (\pm 1.25)	105.17 (\pm 1.29)	90.84 (\pm 1.23)	93.47 (\pm 0.83)	78.66 (\pm 0.92)
Galloyl glucose	100.00 (\pm 1.77)	84.24 (\pm 0.92)	67.99 (\pm 1.04)	71.69 (\pm 1.05)	33.03 (\pm 0.05)
Protocatechuic acid hexoside	100.00 (\pm 0.59)	103.36 (\pm 0.57)	73.76 (\pm 0.84)	82.09 (\pm 0.90)	80.16 (\pm 0.94)
Protocatechuic acid	100.00 (\pm 1.16)	61.67 (\pm 0.39)	204.07 (\pm 1.01)	196.38 (\pm 1.03)	77.69 (\pm 1.26)
Caftaric acid	100.00 (\pm 1.63)	107.31 (\pm 0.48)	244.63 (\pm 2.09)	233.37 (\pm 2.38)	225.71 (\pm 0.45)
Caffeoyl hexoside 1	100.00 (\pm 0.93)	102.34 (\pm 0.69)	103.87 (\pm 1.00)	106.29 (\pm 0.65)	128.09 (\pm 0.53)
Caffeoyl hexoside 2	100.00 (\pm 0.72)	94.22 (\pm 1.10)	181.01 (\pm 0.87)	169.08 (\pm 0.98)	165.44 (\pm 0.58)
Coutaric acid	100.00 (\pm 1.62)	116.31 (\pm 2.12)	119.55 (\pm 0.83)	108.56 (\pm 0.53)	81.58 (\pm 0.71)
<i>p</i> -Coumaroyl hexoside 1	100.00 (\pm 1.11)	102.35 (\pm 0.18)	214.77 (\pm 1.03)	170.65 (\pm 1.06)	82.63 (\pm 1.19)
Fertaric acid	100.00 (\pm 0.64)	98.56 (\pm 1.42)	61.82 (\pm 0.51)	64.50 (\pm 0.45)	78.97 (\pm 0.49)
<i>p</i> -Coumaroyl hexoside 2	100.00 (\pm 1.93)	99.10 (\pm 1.09)	219.64 (\pm 1.62)	153.30 (\pm 1.56)	93.92 (\pm 1.51)
Vanillic acid hexoside	100.00 (\pm 1.10)	105.65 (\pm 0.38)	110.91 (\pm 0.75)	105.28 (\pm 0.83)	75.86 (\pm 0.76)
Ethyl gallate	100.00 (\pm 1.63)	100.00 (\pm 0.58)	87.01 (\pm 1.04)	84.00 (\pm 0.20)	82.48 (\pm 0.29)
Mean	100	94	136	126	99
<i>Stilbenoids</i>					
Resveratrol glucoside	100.00 (\pm 2.11)	98.41 (\pm 1.48)	84.71 (\pm 1.91)	104.06 (\pm 0.90)	72.66 (\pm 1.00)

Table 15 reports the absolute concentrations of protocatechuic acid and ethyl gallate in all the extracts.

Table 15 - Protocatechuic acid and ethyl gallate absolute concentrations ($\mu\text{g}/\text{mL}$, mean \pm SD) in the extracts.

	Extract A	Extract A50	Extract B	Extract C	Extract D
Protocatechuic acid	0.681 (± 0.009)	0.387 (± 0.003)	1.47 (± 0.01)	1.41 (± 0.02)	0.509 (± 0.003)
Ethyl gallate	1.71 (± 0.01)	1.72 (± 0.01)	1.48 (± 0.02)	1.43 (± 0.003)	1.40 (± 0.005)

4.6. Anthocyanins

As summarized in Table 16, two pyroanthocyanins (vitisin A and B) and twelve anthocyanins were identified: 5 glucosides, 1 caffeoyl glucoside, 2 acetyl glucosides and 4 coumaroyl glucosides. The relative content of anthocyanins in the EtOH:H₂O extract is summarized in Table 16. Malvidin coumaroyl glucoside is the most abundant component, reaching a relative content of almost 55%, followed by malvidin glucoside (14%) and malvidin acetyl glucoside (almost 8%), and petunidin coumaroyl glucoside (6.4%) while the relative content of the other compounds was lower than 5%.

Table 16 - Relative content of anthocyanins in the EtOH-H₂O extract. The % was determined by measuring the peak area of each compound in respect to the sum of the peak areas of all the identified anthocyanins.

Compound	Relative Content (%)
Delphinidin 3-glucoside	0.410 (±0.012)
Cyanidin 3-glucoside	0.252 (±0.009)
Petunidin 3-glucoside	2.01 (±0.03)
Peonidin 3-glucoside	1.52 (±0.05)
Malvidin 3-glucoside	14.22 (±0.03)
Vitisin A	0.783 (±0.014)
Vitisin B	0.267 (±0.001)
Peonidin 3-(6''-acetyl)-glucoside	0.603 (±0.003)
Malvidin 3-(6''-acetyl)-glucoside	8.33 (±0.02)
Delphinidin 3-(6''-coumaroyl)-glucoside	2.62 (±0.01)
Malvidin 3-(6''-caffeoyl)-glucoside	3.40 (±0.07)
Petunidin 3-(6''-coumaroyl)-glucoside	5.99 (±0.11)
Peonidin 3-(6''-cis-coumaroyl)-glucoside	3.98 (±0.03)
Malvidin 3-(6''-cis-coumaroyl)-glucoside	55.61 (±0.16)

Malvidin coumaroyl glucoside was the most abundant also in the water extracts but its relative content is reduced in respect to malvidin acetyl glucoside as explained by its greater polarity.

The relative percentage of the aqueous extracts in respect to EtOH:H₂O is reported in Table 17, showing that for most of the identified anthocyanins, the recovery yield followed the following order: extract A > extract A50 > extract B > extract C > extract D and the yields reduced proportionally with lipophilicity (RT). Vitisin B was an exception, since its extraction yield was greater in extracts C and D. By calculating the % mean, the anthocyanin content is almost 40% in B in respect to A, similar to C and reduced to 28% in D. Regarding the two hydroalcoholic extracts, heating reduces anthocyanins content of about 11.

Table 17 - Relative percentage (mean \pm SD) of each anthocyanin in extracts A50, B, C and D calculated in respect to the content determined in extract A and set as 100%. The relative percentages were calculated by measuring the areas of the peaks reconstituted by setting the [M-H]⁻ as filter ions.

Compound	Extract A	Extract A50	Extract B	Extract C	Extract D
<i>Anthocyanins</i>					
Delphinidin 3-glucoside	100.00 (\pm 2.17)	89.59 (\pm 1.47)	73.16 (\pm 1.40)	76.02 (\pm 0.75)	21.82 (\pm 1.50)
Cyanidin 3-glucoside	100.00 (\pm 2.77)	79.57 (\pm 0.58)	50.64 (\pm 1.06)	30.19 (\pm 1.82)	27.58 (\pm 1.14)
Petunidin 3-glucoside	100.00 (\pm 2.19)	125.80 (\pm 1.74)	36.63 (\pm 0.14)	49.68 (\pm 0.38)	36.90 (\pm 2.83)
Peonidin 3-glucoside	100.00 (\pm 2.47)	80.24 (\pm 1.58)	52.65 (\pm 0.46)	54.12 (\pm 0.18)	37.96 (\pm 0.83)
Malvidin 3-glucoside	100.00 (\pm 0.82)	79.44 (\pm 1.70)	43.50 (\pm 0.46)	56.01 (\pm 0.62)	37.24 (\pm 0.42)
Vitisin A	100.00 (\pm 1.19)	85.73 (\pm 1.42)	71.51 (\pm 1.23)	37.91 (\pm 0.66)	31.46 (\pm 1.04)
Vitisin B	100.00 (\pm 1.07)	110.02 (\pm 2.84)	68.73 (\pm 1.18)	154.26 (\pm 1.03)	156.42 (\pm 1.10)
Peonidin 3-(6''-acetyl)-glucoside	100.00 (\pm 1.05)	81.07 (\pm 1.66)	46.73 (\pm 0.76)	43.34 (\pm 0.40)	15.20 (\pm 0.53)
Malvidin 3-(6''-acetyl)-glucoside	100.00 (\pm 1.01)	78.11 (\pm 2.75)	38.63 (\pm 0.45)	45.34 (\pm 0.74)	15.69 (\pm 0.09)
Delphinidin 3-(6''-coumaroyl)-glucoside	100.00 (\pm 1.23)	75.54 (\pm 1.17)	14.38 (\pm 0.27)	11.96 (\pm 0.22)	2.06 (\pm 0.06)
Malvidin 3-(6''-caffeoyl)-glucoside	100.00 (\pm 1.24)	78.60 (\pm 2.35)	15.90 (\pm 0.16)	11.42 (\pm 0.15)	6.37 (\pm 0.11)
Petunidin 3-(6''-coumaroyl)-glucoside	100.00 (\pm 1.06)	76.09 (\pm 1.90)	13.12 (\pm 0.15)	10.21 (\pm 0.11)	1.87 (\pm 0.06)
Peonidin 3-(6''-coumaroyl)-glucoside	100.00 (\pm 1.36)	125.09 (\pm 2.97)	14.33 (\pm 0.19)	10.44 (\pm 0.14)	2.75 (\pm 0.05)
Malvidin 3-(6''-coumaroyl)-glucoside	100.00 (\pm 1.00)	80.26 (\pm 1.65)	12.20 (\pm 0.27)	12.12 (\pm 0.04)	2.54 (\pm 0.02)
Mean	100	89	39	43	28

Table 18 reports the absolute concentrations of malvidin 3-glucoside in all the extracts.

Table 18 - Malvidin 3-glucoside absolute concentrations ($\mu\text{g}/\text{mL}$, mean \pm SD) in the extracts.

	Extract A	Extract A50	Extract B	Extract C	Extract D
Malvidin 3-glucoside	4.97 (\pm 0.04)	3.93 (\pm 0.09)	2.07(\pm 0.02)	2.71 (\pm 0.03)	1.74 (\pm 0.02)

Considering the almost overlapping analytical profile of extract A and A50, the activities were evaluated for the extract A only.

4.7. DPPH Assay

The radical scavenging activity was measured by the DPPH test as reported in Table 19. By calculating the activity as IC₅₀ of the dry residue, as expected, extract A was significantly more active than water extracts, according to the polyphenol contents, which represent the main antioxidant components of the extract. The radical scavenging activity of the extracts was almost superimposable when the activity was normalized in respect to the polyphenol content demonstrating that the extracted polyphenols have a quite similar radical scavenging activity.

Table 19 - Antioxidant activity determined by the DPPH test. Values are reported as µg/mL in respect to the dry residue and to total polyphenol content.

Extract	IC ₅₀ µg/mL (dry residue)	IC ₅₀ µg/mL (polyphenols)
Extract A	7.303 ± 0.338	2.062 ± 0.095
Extract B	38.667 ± 0.790	3.013 ± 0.062
Extract C	56.673 ± 3.087	3.847 ± 0.210
Extract D	52.000 ± 2.009	2.154 ± 0.083

4.8. Anti-Inflammatory Activity

The MTT assay (Figure 6) indicates that cell viability was not affected by the four extracts at all concentrations tested and up to 250 $\mu\text{g/mL}$.

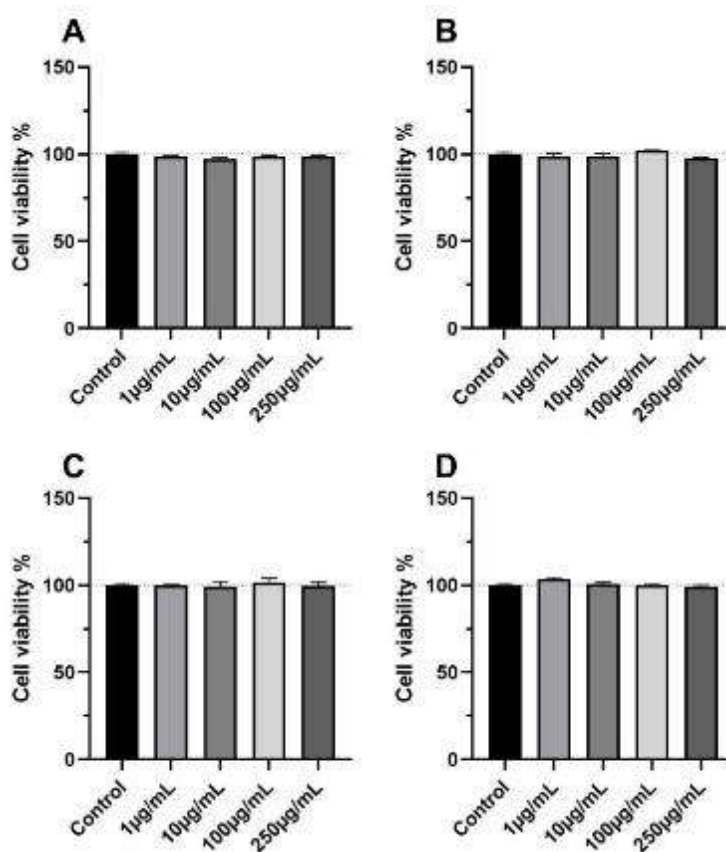


Figure 6 - Viability of R3/1 cells incubated with the four extracts in a 1 to 250 $\mu\text{g/mL}$ concentration range. Cell viability was measured by the MTT assay. All the extracts were found not to significantly change the cell viability at all the tested concentrations. The letter of the panel refers to the letter of the extract. Statistical significance was calculated by ANOVA analysis followed by Dunnett's multiple comparisons. A $p > 0.05$ was found for all the extracts. **A:** EtOH 70% RT; **B:** H₂O 100°C; **C:** H₂O 70°C; **D:** H₂O RT.

The anti-inflammatory activity was then tested by measuring the NF- κ B dependent luciferase activity induced by IL1- α stimulus. The protective effect of the four extracts is reported as % of inhibition of luciferase activity in respect to control cells (Figure 7). For all the extracts, a dose-dependent effect was observed. All the data were statistically significant ($p < 0.01$) except for the 1 and 10 $\mu\text{g/mL}$ concentrations of extract C and D and 10 $\mu\text{g/mL}$ for extract A. The anti-inflammatory activity of extract A was found superimposable to B and this latter higher than C and D. The order of anti-inflammatory potency for the water extracts was expected on the basis of the content of polyphenols which, in line of principle, could be considered as the main anti-

inflammatory components. However, the superimposable activity of A with B cannot be explained on the basis of the polyphenol content since it is more than three times higher in A in respect to B. This apparent contradiction can be explained in different ways. The first, is that the extracted polyphenols do not have the same anti-inflammatory potency and that those extracted in a similar way in A and B, such as the hydrophilic procyanidins, are the most effective anti-inflammatory components. A second explanation is that beside polyphenols, other constituents present in the water extracts but not present or present to a lesser extent in A, do have an anti-inflammatory activity which adds up to those of the polyphenols. A third explanation is that the water-soluble constituents such as macromolecules (proteins, polysaccharides) significantly influence polyphenol bio accessibility in the cells [37].

Regarding this latter aspect it could be considered that water extraction could preserve the extracellular vesicles (EVs) which are naturally loaded with polyphenols and which could facilitate the cell absorption of polyphenols [38]. Water extraction but presumably not EtOH-H₂O, would preserve the integrity of such vesicles.

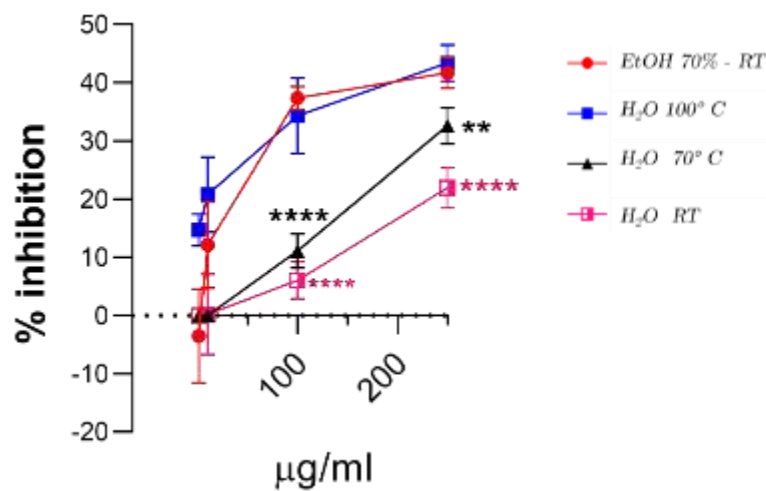


Figure 7 - Dose-dependent anti-inflammatory activity of the four extracts. Extracts ranging from 1 to 250 µg/mL were incubated with R3/1 cells transduced with the NF-κB reporter gene and challenged with 0.01 µg/mL of IL1α. Results are reported as % inhibition of luciferase signal in respect to control cells. Statistical analysis: ANOVA followed by Dunnett's multiple comparisons test in respect to the EtOH extract. The % inhibition found for each concentration was compared in respect to the control (untreated sample).

5. Conclusion

In conclusion, a fully detailed qualitative profiling of red grape skin extracted with ethanol and water mixture has permitted the identification of 65 compounds which can be classified into the following chemical classes: organic and phenolic acids (14 compounds), stilbenoids (1 compound), flavanols (21 compounds), flavonols (15 compounds) and anthocyanins (14 compounds). The extraction yield of water at different temperatures (100 °C, 70 °C, room temperature) was then evaluated and the results indicate that extraction using water under heating conditions is effective in extracting some polyphenolic classes with a good recovery in respect to EtOH based binary extraction. In particular, a good extraction yield was observed for the hydrophilic procyanidins, phenolic acids, flavonol glucoside and stilbenoid. However, according to their lipophilic character, poor absorption was observed for the most lipophilic components, such as flavonol aglycones and in general for anthocyanins. The radical scavenging activity was in accordance with the polyphenol content and hence much higher for the extract obtained with the binary solvent in respect to water extraction. All the tested extracts were found effective as anti-inflammatory compounds, and an intriguing result was that the EtOH:H₂O extract was found superimposable with that obtained using water at 100 °C. Taken together, the results indicate that water extraction carried out with heating condition is an easy, low-cost and environmentally friendly extraction method for some polyphenol classes and may have an industrial application for extracts with anti-inflammatory activity.

6. References

1. Food and Agriculture Organization of the United Nations. FAOSTAT Database; FAO: Rome, Italy, 2019.
2. Teixeira, A.; Baenas, N.; Dominguez-Perles, R.; Barros, A.; Rosa, E.; Moreno, D.A.; Garcia-Viguera, C. Natural bioactive compounds from winery by-products as health promoters: A review. *Int. J. Mol. Sci.* 2014, 15, 15638–15678, doi:10.3390/ijms150915638.
3. Dávila, I.; Robles, E.; Egüés, I.; Labidi, J.; Gullón, P. The Biorefinery Concept for the Industrial Valorization of Grape Pro-cessing By-Products. In *Handbook of Grape Processing By-Products*; Elsevier: Amsterdam, The Netherlands, 2017; pp. 29–53; ISBN 9780128112915.
4. Ali, T.; Kim, T.; Rehman, S.U.; Khan, M.S.; Amin, F.U.; Khan, M.; Ikram, M.; Kim, M.O. Natural Dietary Supplementation of Anthocyanins via PI3K/Akt/Nrf2/HO-1 Pathways Mitigate Oxidative Stress, Neurodegeneration, and Memory Impairment in a Mouse Model of Alzheimer’s Disease. *Mol. Neurobiol.* 2018, 55, 6076–6093, doi:10.1007/s12035-017-0798-6.
5. Nani, A.; Murtaza, B.; Sayed Khan, A.; Khan, N.A.; Hichami, A. Antioxidant and Anti-Inflammatory Potential of Polyphenols. *Molecules* 2021, 26, 985.
6. Kim, M.J.; Paramanatham, A.; Lee, W.S.; Yun, J.W.; Chang, S.H.; Kim, D.C.; Park, H.S.; Choi, Y.H.; Kim, G.S.; Ryu, C.H.; et al. Anthocyanins Derived from *Vitis coignetiae* Pulliat Contributes Anti-Cancer Effects by Suppressing NF- κ B Pathways in Hep3B Human Hepatocellular Carcinoma Cells and In Vivo. *Molecules* 2020, 25, 5445, doi:10.3390/molecules25225445.
7. QY Research. *Global Polyphenols Market Research Report 2020*; 2020.
8. Alara, O.R.; Abdurahman, N.H.; Ukaegbu, C.I. Extraction of phenolic compounds: A review. *Curr. Res. Food Sci.* 2021, 4, 200–214, doi:10.1016/j.crfs.2021.03.011.
9. Ameer, K.; Shahbaz, H.M.; Kwon, J.H. Green Extraction Methods for Polyphenols from Plant Matrices and Their Byproducts: A Review. *Compr. Rev. Food Sci. Food Saf.* 2017, 16, 295–315, doi:10.1111/1541-4337.12253.
10. Babbar, N.; Oberoi, H.S.; Sandhu, S.K.; Bhargav, V.K. Influence of different solvents in extraction of phenolic compounds from vegetable residues and their evaluation as natural sources of antioxidants. *J. Food Sci. Technol.* 2014, 51, 2568–2575, doi:10.1007/s13197-012-0754-4.
11. Złotek, U.; Mikulska, S.; Nagajek, M.; Świeca, M. The effect of different solvents and number of extraction steps on the polyphenol content and antioxidant capacity of basil leaves (*Ocimum basilicum* L.) extracts. *Saudi J. Biol. Sci.* 2016, 23, 628–633, doi:10.1016/j.sjbs.2015.08.002.
12. Rababah, T.M.; Banat, F.; Rababah, A.; Ereifej, K.; Yang, W. Optimization of extraction conditions of total phenolics, antioxidant activities, and anthocyanin of oregano, thyme, terebinth, and pomegranate. *J. Food Sci.* 2010, 75, 626–632, doi:10.1111/j.1750-3841.2010.01756.x.

13. Pellegrini, N.; Colombi, B.; Salvatore, S.; Brenna, O.V.; Galaverna, G.; Del Rio, D.; Bianchi, M.; Bennett, R.N.; Brighenti, F. Evaluation of antioxidant capacity of some fruit and vegetable foods: Efficiency of extraction of a sequence of solvents. *J. Sci. Food Agric.* 2007, 87, 103–111, doi:10.1002/jsfa.2682.
14. Liu, S.C.; Lin, J.T.; Wang, C.K.; Chen, H.Y.; Yang, D.J. Antioxidant properties of various solvent extracts from lychee (*Litchi chinensis* Sonn.) flowers. *Food Chem.* 2009, 114, 577–581, doi:10.1016/j.foodchem.2008.09.088.
15. Fernández-Agulló, A.; Pereira, E.; Freire, M.S.; Valentão, P.; Andrade, P.B.; González-álvarez, J.; Pereira, J.A. Influence of solvent on the antioxidant and antimicrobial properties of walnut (*Juglans regia* L.) green husk extracts. *Ind. Crops Prod.* 2013, 42, 126–132, doi:10.1016/j.indcrop.2012.05.021.
16. Casazza, A.A.; Aliakbarian, B.; Perego, P. Recovery of phenolic compounds from grape seeds: Effect of extraction time and solid-liquid ratio. *Nat. Prod. Res.* 2011, 25, 1751–1761, doi:10.1080/14786419.2010.524889.
17. Brglez Mojzer, E.; Knez Hrnčič, M.; Škerget, M.; Knez, Ž.; Bren, U. Polyphenols: Extraction Methods, Antioxidative Action, Bioavailability and Anticarcinogenic Effects. *Molecules* 2016, 21, 901, doi:10.3390/molecules21070901.
18. Baron, G.; Altomare, A.; Mol, M.; Garcia, J.L.; Correa, C.; Raucci, A.; Mancinelli, L.; Mazzotta, S.; Fumagalli, L.; Trunfio, G.; et al. Analytical profile and antioxidant and anti-inflammatory activities of the enriched polyphenol fractions isolated from bergamot fruit and leave. *Antioxidants* 2021, 10, 141, doi:10.3390/antiox10020141.
19. Colombo, R.C.; Roberto, S.R.; Nixdorf, S.L.; Pérez-Navarro, J.; Gómez-Alonso, S.; Mena-Morales, A.; García-Romero, E.; Azeredo Gonçalves, L.S.; da Cruz, M.A.; de Carvalho, D.U.; et al. Analysis of the phenolic composition and yield of 'BRS Vitoria' seedless table grape under different bunch densities using HPLC–DAD–ESI–MS/MS. *Food Res. Int.* 2020, 130, 108955, doi:10.1016/j.foodres.2019.108955.
20. Lago-Vanzela, E.S.; Da-Silva, R.; Gomes, E.; García-Romero, E.; Hermosín-Gutiérrez, I. Phenolic composition of the edible parts (flesh and skin) of Bordô grape (*Vitis labrusca*) using HPLC–DAD–ESI–MS/MS. *J. Agric. Food Chem.* 2011, 59, 13136–13146, doi:10.1021/jf203679n.
21. Manfra, M.; de Nisco, M.; Bolognese, A.; Nuzzo, V.; Sofò, A.; Scopa, A.; Santi, L.; Tenore, G.C.; Novellino, E. Anthocyanin composition and extractability in berry skin and wine of *Vitis vinifera* L. cv. Aglianico. *J. Sci. Food Agric.* 2011, 91, 2749–2755, doi:10.1002/jsfa.4517.
22. Mulinacci, N.; Santamaria, A.R.; Giaccherini, C.; Innocenti, M.; Valletta, A.; Ciolfi, G.; Pasqua, G. Anthocyanins and fla-van-3-ols from grapes and wines of *Vitis vinifera* cv. Cesanese d'Affile. *Nat. Prod. Res.* 2008, 22, 1033–1039, doi:10.1080/14786410802133845.
23. Pérez-Navarro, J.; Izquierdo-Cañas, P.M.; Mena-Morales, A.; Martínez-Gascueña, J.; Chacón-Vozmediano, J.L.; García-Romero, E.; Hermosín-Gutiérrez, I.; Gómez-Alonso, S. Phenolic compounds profile of different berry parts from novel *Vitis vinifera* L. red grape genotypes and Tempranillo using HPLC–DAD–ESI–MS/MS: A varietal differentiation tool. *Food Chem.* 2019, 295, 350–360, doi:10.1016/j.foodchem.2019.05.137.

24. Zhu, L.; Zhang, Y.; Lu, J. Phenolic contents and compositions in skins of red wine grape cultivars among various genetic backgrounds and originations. *Int. J. Mol. Sci.* 2012, 13, 3492–3510, doi:10.3390/ijms13033492.
25. Castillo-Muñoz, N.; Gómez-Alonso, S.; García-Romero, E.; Hermosín-Gutiérrez, I. Flavonol profiles of *Vitis vinifera* red grapes and their single-cultivar wines. *J. Agric. Food Chem.* 2007, 55, 992–1002, doi:10.1021/jf062800k.
26. Peixoto, C.M.; Dias, M.I.; Alves, M.J.; Calhela, R.C.; Barros, L.; Pinho, S.P.; Ferreira, I.C.F.R. Grape pomace as a source of phenolic compounds and diverse bioactive properties. *Food Chem.* 2018, 253, 132–138, doi:10.1016/j.foodchem.2018.01.163.
27. Pérez-Trujillo, J.P.; Hernández, Z.; López-Bellido, F.J.; Hermosín-Gutiérrez, I. Characteristic phenolic composition of single-cultivar red wines of the Canary Islands (Spain). *J. Agric. Food Chem.* 2011, 59, 6150–6164, doi:10.1021/jf200881s.
28. Hayasaka, Y.; Waters, E.J.; Cheynier, V.; Herderich, M.J.; Vidal, S. Characterization of proanthocyanidins in grape seeds using electrospray mass spectrometry. *Rapid Commun. Mass Spectrom.* 2003, 17, 9–16, doi:10.1002/rcm.869.
29. Dewanto, V.; Wu, X.; Adom, K.K.; Liu, R.H. Thermal Processing Enhances the Nutritional Value of Tomatoes by Increasing Total Antioxidant Activity. *J. Agric. Food Chem.* 2002, 50, 3010–3014, doi:10.1021/jf0115589.
30. Sun, B.; Ricardo-da-Silva, J.M.; Spranger, I. Critical Factors of Vanillin Assay for Catechins and Proanthocyanidins. *J. Agric. Food Chem.* 1998, 46, 4267–4274, doi:10.1021/jf980366j.
31. Di Stefano, R.; Cravero, M.C. Metodi per lo studio dei polifenoli dell'uva. *Riv. Enol. Vitic.* 1991, 44, 37–45.
32. Brand-Williams, W.; Cuvelier, M.E.; Berset, C. Use of a free radical method to evaluate antioxidant activity. *LWT-Food Sci. Technol.* 1995, 28, 25–30, doi:10.1016/S0023-6438(95)80008-5.
33. González-Centeno, M.R.; Comas-Serra, F.; Femenia, A.; Rosselló, C.; Simal, S. Effect of power ultrasound application on aqueous extraction of phenolic compounds and antioxidant capacity from grape pomace (*Vitis vinifera* L.): Experimental kinetics and modeling. *Ultrason. Sonochem.* 2015, 22, 506–514, doi:10.1016/j.ultsonch.2014.05.027.
34. Kim, J.; Oh, J.; Averilla, J.N.; Kim, H.J.; Kim, J.S.; Kim, J.S. Grape Peel Extract and Resveratrol Inhibit Wrinkle Formation in Mice Model Through Activation of Nrf2/HO-1 Signaling Pathway. *J. Food Sci.* 2019, 84, 1600–1608, doi:10.1111/1750-3841.14643.
35. Sri Harsha, P.S.C.; Gardana, C.; Simonetti, P.; Spigno, G.; Lavelli, V. Characterization of phenolics, in vitro reducing capacity and anti-glycation activity of red grape skins recovered from winemaking by-products. *Bioresour. Technol.* 2013, 140, 263–268, doi:10.1016/j.biortech.2013.04.092.

36. Doshi, P.; Adsule, P.; Banerjee, K.; Oulkar, D. Phenolic compounds, antioxidant activity and insulinotropic effect of extracts prepared from grape (*Vitis vinifera* L) byproducts. *J. Food Sci. Technol.* 2015, 52, 181–190, doi:10.1007/s13197-013-0991-1.
37. Grgić, J.; Šelo, G.; Planinić, M.; Tišma, M.; Bucić-Kojić, A. Role of the encapsulation in bioavailability of phenolic compounds. *Antioxidants* 2020, 9, 923, doi:10.3390/antiox9100923.
38. Rome, S. Biological properties of plant-derived extracellular vesicles. *Food Funct.* 2019, 10, 529–538, doi:10.1039/C8FO02295J.

7. Supplementary materials

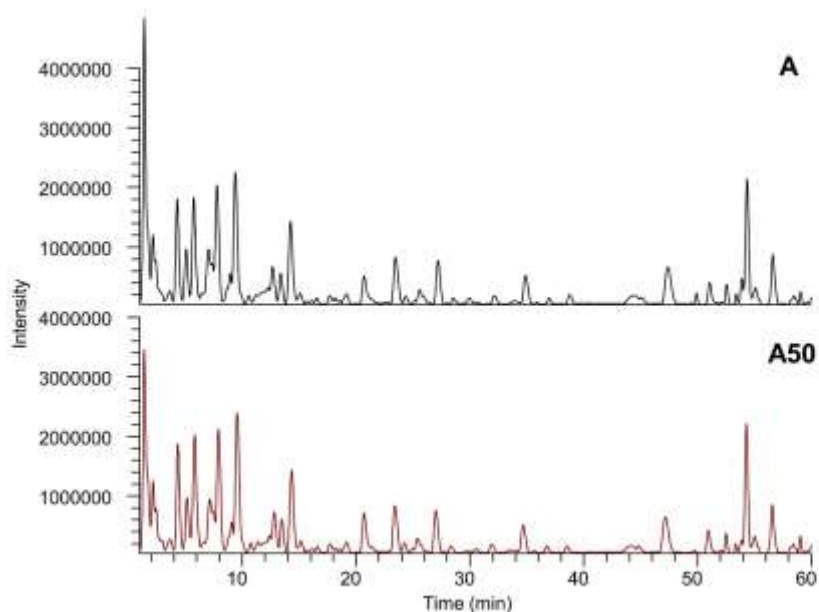


Figure S1 - LC-ESI(-)-MS total ion currents (TICs) in negative ion mode of the hydroalcoholic extracts: A) EtOH-H₂O 70:30 (% v/v) at room temperature for 24 h, extract A; A50) EtOH-H₂O 70:30 (% v/v) at 50 °C for 1 h followed by 24 h at room temperature, extract A50.

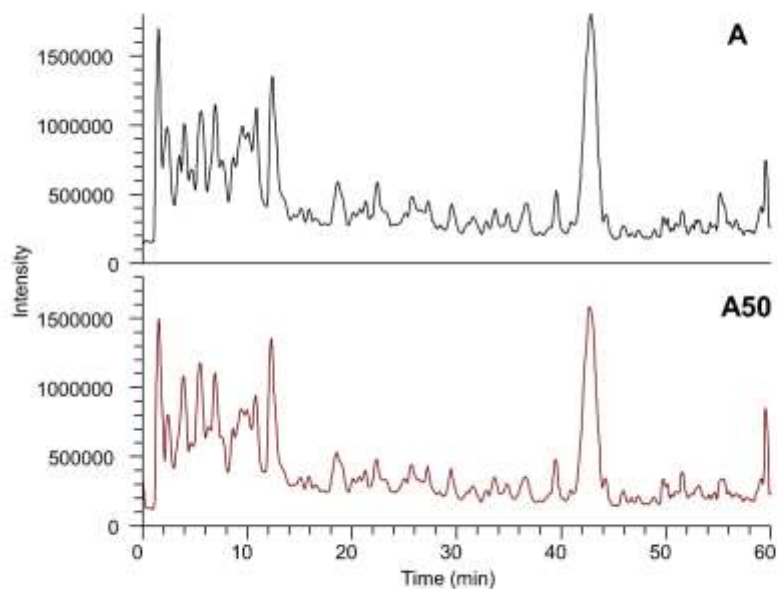


Figure S2 - LC-ESI(+)-MS total ion currents (TICs) in positive ion mode of the hydroalcoholic extracts: A) EtOH-H₂O 70:30 (% v/v) at room temperature for 24 h, extract A; A50) EtOH-H₂O 70:30 (% v/v) at 50 °C for 1 h followed by 24 h at room temperature, extract A50.

Chapter 2

Characterization of a Thinned Young Apples polyphenols extract

Study 1 - Polyphenols from Thinned Young Apples: HPLC-HRMS profile and evaluation of their antioxidant and anti-inflammatory activities by proteomic studies

(10.3390/antiox11081577)

1. Abstract

The qualitative profile of thinned apple polyphenols (TAP) fraction ($\approx 24\%$ of polyphenols) obtained by purification through absorbent resin was fully investigated by LC-HRMS in positive and negative ion mode and using ESI source. A total of 68 polyphenols were identified belonging to six different classes: flavanols, flavonols, dihydrochalcones, flavanones, flavones and organic and phenolic acids. The antioxidant and anti-inflammatory activities were then investigated in cell models with gene reporter for NRF2 and NF- κ B and by quantitative proteomic (label-free and SILAC) approaches. TAP dose-dependently activated NRF2 and in the same concentration range (10–250 $\mu\text{g}/\text{mL}$) inhibited NF- κ B nuclear translocation induced by TNF- α and IL-1 α as pro-inflammatory promoters. Proteomic studies elucidated the molecular pathways evoked by TAP treatment: activation of the NRF2 signaling pathway, which in turn up-regulates protective oxidoreductases and their nucleophilic substrates such as GSH and NADPH, the latter resulting from the up-regulation of the pentose phosphate pathway. The increase in the enzymatic antioxidant cellular activity together with the up-regulation of the heme oxygenase would explain the anti-inflammatory effect of TAP. The results suggest that thinned apples can be considered as a valuable source of apple polyphenols to be used in health care products to prevent/treat oxidative and inflammatory chronic conditions.

2. Introduction

Epidemiological studies indicate that consumption of apples and derivatives, such as apple juice, are beneficial in the treatment of some human diseases including CVD and related events, cancer and diabetes [1]. Beneficial effects have also been confirmed by intervention studies. Vallée Marcotte et al. [2] recently reviewed 20 intervention studies using apple juice, concluding that its consumption could exert some benefits on a variety of markers associated with the risk of developing chronic diseases including cardiovascular, cancer, and neurodegenerative diseases.

Recently, a regular consumption of 2–3 apples per day was associated to beneficial effects. In a randomized, controlled, crossover intervention study, in healthy subjects with mildly raised serum cholesterol concentrations, consumption of two Renetta Canada apples for eight weeks improved CVD risk factors, by reducing total and LDL cholesterol and ICAM-1 and increasing microvascular vasodilation [3]. Liddle et al. recently reported that consumption of three whole Gala apples per day for 6 weeks may be an effective strategy to mitigate inflammation in overweight and obese subjects, by reducing circulating biomarkers of inflammation and endotoxin exposure, including CRP, IL-6 and LBP and increasing the plasma antioxidant capacity [4].

Most of the documented beneficial effects of apples are attributed to the fraction of polyphenols represented by five main groups, namely, flavanols (catechins, epicatechin and procyanidins), flavonols (quercetin glycosides), phenolic acids (chlorogenic, gallic and coumaric acids), dihydrochalcones (phloretin glycosides) and anthocyanins (cyanidin) [5–7]. Apple polyphenols exert antioxidant, anti-inflammatory and lipid lowering effects as also confirmed by pre-clinical studies. In particular, isolated apple polyphenols (AP) have been proven to be effective in preventing/treating hypercholesterolemia [8,9], atherosclerosis in ApoE-deficient mice [10], colorectal cancer [11], non-alcoholic hepatitis [12], ulcerative colitis [13] and indomethacin-induced gastric damage [14].

At a molecular level, the antioxidant and anti-inflammatory activities of apple polyphenols can be partially explained by considering the role of polyphenols as activators of the NRF2 pathway [15]. NRF2 is a transcriptional factor associated with antioxidant enzymes playing a master role in redox homeostasis in cells. NRF2 and its principal negative regulator, KEAP1, play a central role in the maintenance of intracellular redox homeostasis and regulation of inflammation. NRF2 is proved to contribute to the regulation of the heme oxygenase-1 (HMOX1) axis, which is a potent anti-inflammatory target [16], and to inhibit oxidative stress by up-regulating

antioxidant enzymes and co-factors [17]. Recently, there is an increase in the research literature regarding the regulation of NRF2 signaling pathways in different aspects of inflammation such as cytokines, chemokine releasing factors, MMPs and other inflammatory mediators affecting the NF- κ B and MAPK networks to control inflammation, as recently reviewed by Saha et al. [18]. Activation of NRF2 by polyphenol compounds is mainly mediated by those compounds bearing an ortho-diphenol moiety which is oxidized to the corresponding quinone, which, being an electrophilic compound, reacts with the thiols of the KEAP1, thus releasing NRF2, which then translocates into the nucleus [19].

Hence, the phenolic enriched fraction from apples represents a valuable source of natural compounds with a beneficial effect against inflammation and oxidative stress, and they may be applied as a food supplement and/or functional ingredient for the treatment of chronic inflammatory diseases.

There is nowadays great interest in the bioactive compounds obtained from the waste products deriving from agriculture and the food industry (circular economy) [20]. Thinning young apples (around one month after blossom), which constitute a massive waste product of the apple production chain, is carried out in order to guarantee the output and to increase the quality of the harvested apples and are usually discarded in the orchard soil [21]. However, this has the negative effect of increasing the soil acidity and thus disturbing the microbial community, which in turn affects the growth of fruit trees [22]. Thinned young apples are particularly rich in polyphenols, more than 10-fold with respect to harvested apples. The total polyphenols and total antioxidant activity show a rapid decrease after 45 days from blossoming, stabilizing after 85 days, as found in the Fuji apples [23]. Recently, some papers have reported methods for purifying polyphenols from thinned apples by successive use of polyethylene and polyamide resins [24]. Moreover, studies have reported the beneficial effects of polyphenols from thinned apples which have a significant antibacterial activity and were found to be effective in inhibiting halitosis-related bacteria through damage to the cell membrane and hence should be a valuable waste material as a source of bioactive compounds [25]. Polyphenols from unripe apples were also found to exert anti-obesity activity in rats through the modulation of the fatty acid metabolism in the liver and the inhibition of the absorption of carbohydrates and fat [26]. Considering, on the one hand, the growing scientific interest in the apple and particularly in the apple polyphenol fraction as a source of bioactive compounds effective against inflammation and oxidative stress, and, on the other hand, taking into account that thinned apples are a waste product particularly rich in polyphenols, this work is aimed at fully characterizing the qualitative profile of polyphenols purified from thinned apples by a dual LC-HRMS approach

(targeted and non-targeted), and at investigating their anti-inflammatory and antioxidant activities. Cell lines with gene reporters for NRF2 and NF- κ B nuclear translocation were first used to assess the dose-dependent antioxidant and anti-inflammatory activities, and then to outline the molecular pathways involved by means of two integrated proteomic approaches, based on label-free and SILAC methodologies.

3. Material and Methods

3.1. Chemicals

Thinned Golden, Fuji, Bella del Bosco and Rosa Mantovana apples were sourced from farms located in Trentino-Alto Adige, Italy. Ultrapure water was prepared by a Mil-li-Q purification system (Millipore, Bedford, MA, USA). Protocatechuic acid, caffeic acid, p-coumaric acid, (+)-catechin, (-)-epicatechin, prunin (naringenin glucoside), phlorizin, phloretin, luteolin, cysteine (Cys), iodoacetamide (IAA), tris(2-carboxyethyl)phosphine (TCEP), tetraethylammonium bromide (TEAB), 3-(4,5-Dimethyl-2-thiazolyl)-2,5-diphenyl-2H-tetrazolium bromide (MTT), IL-1 α , TNF- α , 6-hydroxy-2,5,7,8-tetramethyl-3,4-dihydrochromene-2-carboxylic acid (Trolox), ascorbic acid, catechin, sodium carbonate, Folin-Ciocalteu reagent, ferulic acid, naringenin-7-O-glucoside, quercetin, ethanol, methanol, phlorizin dihydrate, sodium acetate, acetic acid, 2,2-diphenyl-1-picrylhydrazyl (DPPH), CDDO-Me, rosiglitazone, formic acid (FA), trifluoroacetic acid (TFA), acetonitrile (ACN) and all ultra-pure-grade (99.5%) solvents used in LC-MS analysis were obtained from Merck KGaA, Darmstadt, Germany. Kaempferol, quercetin, quercetin-3-O-rhamnoside and quercetin-3-O-galactoside were purchased from Extrasynthese (Genay Cedex, France). S-TRAP columns were provided by Protifi (Huntington, NY, USA).

3.2. Isolation of Thinned Apple Polyphenols (TAP) Fraction

A total of 500 kg of thinned Golden, Fuji, Bella del Bosco and Rosa Mantovana apples were harvested 1 month after blossoming and stored at 2 °C for 1 month. The apples were thoroughly washed in a mixer with an aqueous solution containing 0.05% citric acid and then coarsely ground in a hammer mill. A 0.1% solution of pectinase was added to the resulting mush, which was then heated in a linear tunnel at 25 °C for 20 min.

The mass was then continuously forced through a filter with pressure of 200 bar and the squeezed juice was enzymatically treated with pectinase and centrifuged until a colorless solution was obtained. The liquid was then eluted through 20 L of XAD7 absorbent resin and

washed with demineralized water until elimination of all the substances not retained by the resin. At the end of the elution with water, the retained substances (polyphenols) were eluted with 95% ethanol until all the bound components were recovered. Elution of polyphenols was checked by TLC. The hydro-alcoholic solution was concentrated under vacuum and then micronized.

3.3. Qualitative Analysis by LC-HRMS

The phytochemical profile of TAP fraction was performed by LC-HRMS as described by Baron et al. [27]. The extract was dissolved in methanol and diluted with mobile phase A to a final concentration of 2 mg/mL, added with Trolox (50 μ M, final concentration) as internal standard (IS). The mixture was separated on a RP Agilent Zorbax SB-C18 column (150 \times 2.1 mm i.d., 3.5 μ m, CPS analitica, Milan, Italy) by an Ultimate 3000 system (Dionex, Sunnyvale, CA, USA) with a multistep program (80 min) of mobile phase A (H₂O/HCOOH, 100/0.1, %v/v) and B (CH₃CN/HCOOH, 100/0.1, %v/v). An LTQ Orbitrap XL mass spectrometer (Thermo Fisher Scientific, San Jose, CA, USA) was set to perform the analysis in data-dependent scan mode and acquired the spectra in positive and negative ion mode. Full MS spectra were acquired by the FT analyzer (resolution 30,000 FWHM at m/z 400) in profile mode and in the range of m/z 120–1800. The MS/MS spectra of the 3 most intense ions exceeding 1×10^4 counts of the full MS scan were acquired by the linear ion trap (LTQ) by using a normalized collision energy (CID) of 40 eV. A database containing the known components of apples and derivatives was built for the targeted data analysis [28–44]: the putative identification was obtained by comparing the accurate mass (5 ppm mass tolerance), the isotopic pattern and the fragmentation pattern with the compounds in the database. The identity of some molecules was confirmed by means of pure standards available in our laboratory. An untargeted data analysis was performed of the most intense ions not identified in the targeted analysis, as described by Baron et al. [27].

3.4. Quantitative Analysis of Total Polyphenol Content

3.4.1. Colorimetric Analysis

The total polyphenol content was determined by the Folin–Ciocalteu colorimetric method, as reported by Baron et al. [45]; the calibration curve was built using catechin as a standard in a 1–1000 μ g/mL range.

3.4.2. HPLC Analysis

High-performance liquid chromatography (HPLC) coupled with a PDA detector was performed to evaluate the total polyphenol content. For the analysis, a methanolic solution of thinned apple polyphenols (TAP) fraction was diluted 1:4 in H₂O/HCOOH, 100/0.1, %v/v (mobile phase A) to obtain a final concentration of 1 mg/mL. The sample (injection volume, 10 µL) was analyzed in triplicate with a HPLC system (Surveyor, ThermoFinnigan Italy, Milan, Italy), equipped with a PDA detector (Surveyor, ThermoFinnigan Italy, Milan, Italy) and an RP Agilent Zorbax SB-C18 column (150 × 2.1 mm i.d., 3.5 µm, CPS analitica, Milan, Italy). The same gradient program described in Section 2.3 was used for the separation and quantification of TAP polyphenols, setting the PDA detector in a 200–600 nm range. For the quantification, five calibration curves were built using a standard for each class of polyphenols characterizing the TAP extract: catechin for flavanols (10–100 µg/mL; λ_{max} 278 nm), ferulic acid for phenolic acids (1–10 µg/mL; λ_{max} 323 nm), naringenin-7-glucoside for flavanones (10–100 µg/mL; λ_{max} 283 nm), phlorizin for dihydrochalcones (10–100 µg/mL; λ_{max} 284 nm) and quercetin for flavonols (10–100 µg/mL; λ_{max} 371 nm). Each chromatographic peak of the sample was assigned to the corresponding polyphenolic class on the basis of the UV spectrum. For the quantification, the AUC was interpolated using the calibration curve of the relative standard and the sum of the concentrations of all the compounds belonging to the same polyphenol class was calculated. The total polyphenol content was then expressed as a percentage (%), that is, mg of polyphenols present in 100 mg of extract.

3.5. Direct Radical Scavenging Activity

The antioxidant activity was evaluated with the DPPH assay. A solution of thinned apple polyphenols (TAP) fraction was prepared with H₂O:EtOH 50:50 (%v/v) to obtain final concentrations in the range 1–20 µg/mL. An aliquot of TAP extract solution (500 µL) was mixed with 1 mL of acetate buffer (pH 5.5, 100 mM) and 1 mL of EtOH. Then, 500 µL of DPPH (500 µM, ethanolic solution) was added and samples were kept in the dark for 90 min. A Shimadzu UV 1900 spectrophotometer (Shimadzu, Milan, Italy) was used for reading the absorbance at 517 nm. Trolox and ascorbic acid were used as reference antioxidant compounds. The percentage of inhibition (I%) was calculated as expressed by Equation (1) and the results are reported as mean ± SD.

$$I\% = \frac{Abs(\text{blank sample}) - Abs(\text{sample})}{Abs(\text{blank sample})} \times 100 \quad (2)$$

3.6. Cell-Based Assays

3.6.1. MTT Assay

The effect of thinned apple polyphenols (TAP) fraction on the cell viability for all the concentrations tested in the anti-inflammatory and antioxidant assays was verified by MTT assay on R3/1-NF- κ B cells and HEK293 cells in transparent 96-well plates seeded with 4000 cells/well and 10,000 cells/well, respectively. Cells were treated with different concentration of the extract (1 μ g/mL–250 μ g/mL) for 18 h in complete medium (DMEM 10% FBS, 1% penicillin/streptomycin). Subsequently, media were removed and only for R3/1-NF- κ B cell line, one wash with 100 μ L PBS occurred. Then, 100 μ L of DMEM, not supplemented with FBS and penicillin/streptomycin, was added to each well and the 4 h incubation started after the addition of 11 μ L, 5 mg/mL MTT reagent. After medium removal, cells were lysed using 100 μ L of a solution composed of DMSO, 8 mM HCl and 5% TWEEN20. The 96-well plate was shaken for 15 min in a plate shaker in the dark and the absorbance at 575 nm and 630 was measured using a plate reader (BioTek's PowerWave HT, Winooski, VT, USA). Cells incubated with DMSO (0.1%) were used as a control for 100% cell proliferation, while cells incubated with DMSO (3%) were used as a negative control.

3.6.2. NRF2 Gene Reporter Cell Model

Thinned apple polyphenols (TAP) extract was evaluated for its ability to modulate the antioxidant response mediated by NRF2 activation using NRF2/ARE Responsive Luciferase Reporter HEK293 stable cell line (Signosis, Santa Clara, CA, USA) as previously described [46]. Briefly, HEK293 cells (10,000 cells/well) were treated with the extract (concentrations between 1 and 250 μ g/mL). CDDO-Me 75 (bardoxolone methyl) 75 nM was used as a positive control [47]. After adding ONE-Glo Luciferase Assay Substrate (purchased from Promega Corporation, Madison, WI, USA) (100 μ L/well), luciferase measurement was performed with a luminometer (Wallac Victor2 1420, Perkin-Elmer Life Science, Monza, Italy). Experiments were carried out with biological and technical replicates; values are reported as mean \pm SD compared to untreated control cells. One-way ANOVA with Bonferroni's multiple comparisons test ($p < 0.05$ was considered significant) was used for the statistical analysis.

3.6.3. *NF-κB Gene Reporter Cell Model*

The in vitro anti-inflammatory activity of the TAP extract was evaluated by using a cell model previously described [27]. Briefly, R3/1 NF-κB cells (5000 cells/well) were pre-treated for 18 h with different concentrations of the extract (1–250 µg/mL) in complete medium (DMEM 10% FBS, 1% L-glutamine, 1% Penicillin/Streptomycin). Rosiglitazone 10 µM was used as a positive control [27]. Then, cells were stimulated for 6 h with 10 ng/mL IL-1α, and for 6 and 24 h with 10 ng/mL TNF-α. Luciferase measurements were performed with a luminometer (Wallac Victor2 1420, Perkin-Elmer Life Science, Monza, Italy) after adding 100 µL of ONE-Glo Luciferase Assay Substrate (purchased from Promega Corporation, Madison, WI, USA). Experiments were carried out with biological and technical replicates; values are reported as mean ± SD compared to untreated control cells. One-way ANOVA with Bonferroni's multiple comparisons test ($p < 0.05$ was considered significant) was used for the statistical analysis.

3.7. *Quantitative Proteomic Studies*

3.7.1. *SILAC Culture*

The R3/1 NF-κB reporter cell line used for SILAC experiments was cultured in DMEM for SILAC supplemented with 10% FBS, 1% pen/strep and 1% sodium pyruvate; the medium was completed by adding 0.5 mL of heavy or light L-lysine and L-arginine 1000X stock solution diluted in PBS. The final concentration of the light amino acids was 84 mg/mL for arginine and 146 mg/mL for lysine. For the heavy condition, both amino acids ($^{13}\text{C}_6$ $^{15}\text{N}_2$ lysine and $^{13}\text{C}_6$ $^{15}\text{N}_4$ arginine) were diluted in the medium up to the working concentration of 88 mg/mL and 151.3 mg/mL for the heavy arginine and lysine, respectively; this difference in concentration is due to the different molecular weights of the amino acids [48,49]. The cell line was cultivated for at least 9 passages and the incorporation rate was checked: more than 95% of all peptides are required to be labeled.

3.7.1.1. *SILAC Experimental Design*

Each condition tested was cultivated in biological triplicate, and once 70% confluence was reached in a T75 flask, the cells were treated according to the planned experimental design, as shown in Figure 1. Overall, the conditions chosen were as follows: (i) *Control (CTR)*, i.e., untreated cells; (ii) *Thinned apple polyphenols (TAP) extract treatment (CTR-TAP)*, i.e., cells that underwent a double 24 h treatment with the extract at a 200 µg/mL concentration; (iii) *Inflammation (CTR-TNF)*, condition achieved treating cells for 24 h with TNF-α 0.01 µg/mL; (iv)

Thinned apple polyphenols (TAP) extract treatment of inflamed cells (CTR-TNF-TAP), consisting of the 24 h pre-treatment with the extract at 200 µg/mL and then with TNF-α at 0.01 µg/mL for another 24 h.

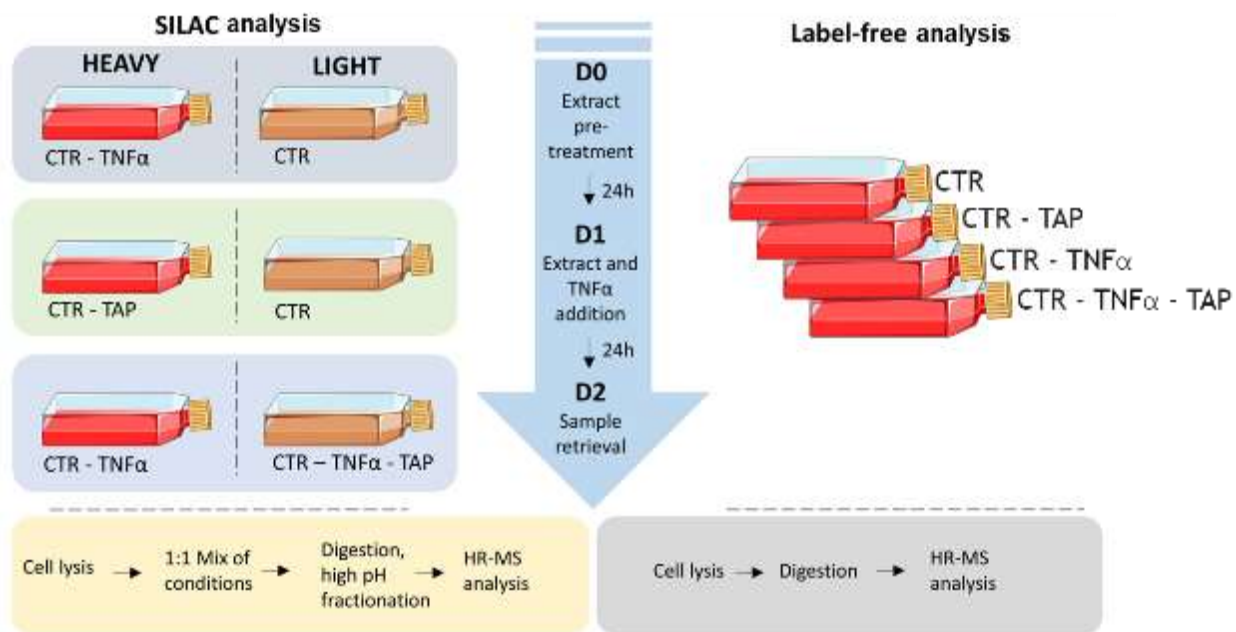


Figure 1 - Experimental design of the quantitative proteomic analysis based on the two orthogonal approaches applied, namely, SILAC (left side) and LFQ (right side), interspersed by a timeline describing the three basic treatment steps. Below is a schematic of the sample processing protocol.

The metabolic labeling strategy was planned so that all conditions are compared with each other in order to have a comprehensive and meaningful pathway modulation overview (Figure 1). All the experiments were planned to finish in the same day. After light or heavy amino acid incorporation, the flasks were washed twice with warmed PBS and the cell was detached using 2 mL of warmed trypsin incubated at 37 °C for 5 min. Cells were then recovered. After diluting the trypsin with 8 mL of complete medium, the suspension was centrifuged for 5 min at 300× g at room temperature and the pellet was then washed 5 times with 5 mL of 4 °C PBS. The cell pellets were then lysed using a suitable S-trap buffer composed of SDS 5%, TEAB 50 mM, MgCl 2 mM, one cOmplete EDTA-free protease inhibitor cocktail tablet (Sigma-Aldrich, Milan, Italy) and 100 Unit of benzonase to reduce nucleic acids content that could occlude the S-trap column. The lysates completely solubilized after 30 min of mechanic resuspension in a tube rotator at 4 °C and were spun centrifuged at 10,000× g for 15 min at 4 °C in a refrigerated centrifuge. Once the lysates were ready, the protein concentration of differentially labeled samples was assessed using the BCA kit and the conditions were mixed in a 1:1 ratio to obtain 100 µg of proteins

before any further processing. Each mixture was prepared by mixing one specific biological replicate with another at random.

3.7.1.2. *S-Trap Digestion*

Samples collected from all the prepared incubation mixtures were then processed according to the bottom-up proteomics procedure. Sample preparation begins with the solubilization of samples in 5% SDS followed by further denaturation by acidification and subsequent exposure to a high concentration of methanol. The collected incubation mixtures were then solubilized 1:1 in lysis buffer (10% SDS, 100 mM TEAB). The reduction of disulfide bridges was performed by adding 5 μ L of the reducing solution of tris(2-carboxyethyl)phosphine (c.f. 5 mM TCEP in 50 mM AMBIC) and incubating the mixtures under slow shaking in a Thermomixer for 10 min at 95 °C. Next, a volume of 5 μ L of iodoacetamide solution (c.f. 20 mM IAA in 50 mM AMBIC) was added, with the aim of alkylating the free thiol residues; incubation in this case was carried out for 45 min at room temperature in the dark. Proteins were further denatured by acidification to pH < 1 by adding a 12% phosphoric acid solution in water (1:10 relative to sample volume). The next step consisted of the sample loading: 165 μ L of the binding buffer (90% methanol, 10% TEAB 1 M) and 25 μ L of sample were simultaneously added onto the spin columns, then centrifuged at a speed of 4000 \times g for 1 min at 15 °C; this step was repeated until the protein sample was fully loaded onto the columns. After that, three washing steps by adding 150 μ L of binding buffer onto the S-TRAP columns, followed by centrifugation (1 min, 4000 \times g, 15 °C), were performed to remove all the excess of unbound sample. At this point, the proteolytic digestion step started by adding a volume of 25 μ L containing 1 μ g of trypsin (sequencing-grade trypsin, Roche) diluted in 50 mM AMBIC. Upon addition of the protease, the physical confinement within the submicron pores of the trap forces substrate and protease interaction to yield rapid digestion; therefore, protein digestion requires much shorter incubation times, i.e., 1.5 h at 47 °C under slow stirring (400 rpm). The peptide mixture was recovered by loading two different solutions; 40 μ L of elution buffer 1 (10% H₂O, 90% ACN, 0.2% FA) and 35 μ L of elution buffer 2 (60% H₂O, 40% ACN, 0.2% FA) onto the columns (elution and 1' centrifugation, 4000 \times g, 15 °C). The collected peptide mixtures were dried in the SpeedVac (Martin Christ., Osterode am Harz, Germany) at 37 °C and stored at -80 °C until analysis.

3.7.1.3. *High pH Fractionation*

The digested peptide mixtures obtained by means of the S-Trap micro-spin column digestion strategy were fractionated using the Pierce High pH Reversed-Phase Peptide

Fractionation Kit according to the manufacturer's instructions, with one additional fraction at 80% ACN.

3.7.1.4. *nLC-HRMS Orbitrap Elite Mass Spectrometer Analysis*

Tryptic peptides, resuspended in an appropriate volume (18 μL , sufficient for two technical replicates) of 0.1% TFA mobile phase, were analyzed using a Dionex Ultimate 3000 nano-LC system (Sunnyvale, CA, USA) connected to the Orbitrap Elite Mass Spectrometer (Thermo Scientific, Bremen, Germany) equipped with an ionization source, the nanospray (Thermo Scientific Inc., Milan, Italy). For each sample, 5 μL of solubilized peptides was injected in triplicate onto the Acclaim PepMap C18 column (75 $\mu\text{m} \times 25 \text{ cm}$, 100 \AA pores, Thermo Scientific, Waltham, MA, USA), "protected" by a pre-column, the Acclaim PepMap (100 $\mu\text{m} \times 2 \text{ cm}$, 100 \AA pores, Thermo Scientific, Waltham, MA, USA), thermostatically controlled at 40 $^{\circ}\text{C}$. The chromatographic method used a binary pump system (LC/NC pumps) and started from sample loading onto the pre-column (3 min) using the loading pump with a flow rate of 5 $\mu\text{L}/\text{min}$ of mobile phase consisting of 99% buffer A_{LC}, 0.1% TFA/1% buffer B_{LC} and 0.1% FA in ACN. After the loading valve switching, peptide separation was performed by the Nano Column Pump (NC_{pump}) with a 117 min linear gradient (0.3 $\mu\text{L}/\text{min}$) of buffer B_{NC_{pump}} (0.1% FA in ACN) from 1% to 40%, and a further 8 min of linear gradient from 40% to 95% (Buffer B_{NC_{pump}}). Then, 5 min at 95% of buffer B_{NC_{pump}} to rinse the column followed the separative gradient, and the last 7 min served to re-equilibrate the column to initial conditions. The total run time was 144 min. A washout injection with pure acetonitrile (5 μL) was performed between sample injections. The nanospray ionization source was set as follows: positive ion mode, spray voltage at 1.7 kV; capillary temperature at 220 $^{\circ}\text{C}$, capillary voltage at 35 V; tube lens offset at 120 V. The orbitrap mass spectrometer operating in data-dependent acquisition (DDA) mode was set to acquire full MS spectra in "profile" mode over a scan range of 250–1500 m/z , with the AGC target at 5×10^5 , and resolution power at 120,000 (FWHM at 400 m/z). Tandem mass spectra were instead acquired by the linear ion trap (LTQ), set to automatically fragment in CID mode the ten most intense ions for each full MS spectra (over 1×10^4 counts) under the following conditions: centroid mode, normal mode, isolation width of the precursor ion of 2.5 m/z , AGC target 1×10^4 and normalized collision energy of 35 eV. Dynamic exclusion was enabled (exclusion dynamics for 45 s for those ions observed 2 times in 10 s). Charge state screening and monoisotopic precursor selection were enabled, and singly charged and unassigned charged ions were not fragmented. Xcalibur software (version 3.0.63, Thermo Scientific Inc., Milan, Italy) was used to control the mass spectrometer.

3.7.2. LFQ Analysis

For the LFQ (Label-Free Quantitative Proteomics) experiment, the same cell line (R3/1 NF- κ B reporter cell line) was cultivated in biological triplicate in T-25 flasks and the same experimental conditions were tested for SILAC ((i) Control, CTR; (ii) Thinned apple extract treatment (CTR-TAP); (iii) Inflammation (CTR-TNF); (iv) Thinned apple extract treatment of inflamed cells (CTR-TNF-TAP), as shown in Figure 1). Except for the labeling strategy, the lysate preparation procedure is the same, as is the proteolytic digestion performed exploiting the potential of the S-Trap Micro Spin Column Digestion Protocol.

3.7.2.1. nLC-HRMS Orbitrap Fusion Tribrid Mass Spectrometer Analysis

Tryptic peptides were analyzed using a Dionex Ultimate 3000 nano-LC system (Sunnyvale, CA, USA) connected to an Orbitrap Fusion Tribrid Mass Spectrometer (Thermo Scientific, Bremen, Germany) equipped with a nano-electrospray ion source according to the procedure previously described [50].

3.8. Data Analysis

For both the SILAC and label-free analysis, the instrumental raw files were processed by MaxQuant software v.1.6.6.0 set on *Rattus_Norvegicus* database (Uniprot taxonomy ID: 10116) against the Andromeda search engine. Protein quantification using SILAC (3 biological \times 2 technical replicates for each condition) was based on the ratio of peptides' peak intensities in the mass spectrum reflecting the relative protein abundance, while for the label-free approach (3 biological \times 3 technical replicates for each condition), the quantification was based on LFQ intensity. In both analyses, trypsin was specified as proteolytic enzyme, cleaving after lysine and arginine except when followed by proline, and up to two missed cleavages were allowed along with match between run option. The precursor ion tolerance was set to 5 ppm while the fragment tolerance was set to 0.5 Da. Carbamidomethylation of cysteine was defined as fixed modification, while oxidation of methionine and acetylation at the protein N-terminus were specified as variable modifications. For the SILAC experiment, only the multiplicity of the labels was set to 2, and Arg10 and Lys8 were selected as heavy aminoacidic residues. Interpretation of the results was performed using Perseus (v.1.6.1.43, Max Plank Institute of Biochemistry, Germany). For the SILAC analysis, the normalized ratio count was selected, transformed in \log_2 , filtered for minimum of 3 valid values and then a one sample t-test was performed with Benjamini–Hochberg FDR for truncation with a threshold of 0.05. LFQ analysis was validated by applying a two-sample t-test of the \log_2 LFQ intensities. The network protein

analyses related to significantly altered proteins were carried out by means of Cytoscape v.3.9.1 and the ingenuity pathways analysis (IPA) (QIAGEN Aarhus Prismet, Denmark, September 2021) licensed software based on the Gene Ontology database. All statistical analyses of the inflammatory assays were conducted using GraphPad prism 8. The Venn diagrams with proportional areas were obtained using the bioVenn package for R [51].

3.8.1. Cytoscape Analysis

The protein–protein interaction network of the up-regulated proteins (\log_2 Fold-Change > 0.5) and down-regulated proteins (\log_2 Fold-Change < -0.5) was obtained by importing a list of Protein IDs into Cytoscape v.3.9.1 (<http://cytoscape.org>, accessed on 15 February 2022). We used the embedded STRING interaction database (<http://apps.cytoscape.org/apps/stringApp>) with a default confidence cut-off score of 0.4. *Rattus Norvegicus* was selected as a reference database with GO, KEGG, PFAM, WikiPathways, Reactome and InterPro cluster terms selected as functional annotations for the enrichment analyses.

3.8.2. Ingenuity Pathways Analysis (IPA)

The core analyses performed by IPA, using the differentially expressed proteins in the uploaded dataset, assess signaling pathways, molecular interaction network and biological functions that can likely be perturbed. The overall activation/inhibition states of canonical pathways are predicted through a z-score algorithm. This z-score is used to statistically compare the uploaded dataset with the pathway patterns. The pathways are colored to indicate their activation z-scores: orange predicts a gain of function, and blue a loss of function. The pathway is activated when molecules' causal relationships with each other (i.e., activation edge and the inhibition edge between the molecules based on literature findings) generate an activity pattern for the molecules and the endpoint functions in the pathway.

4. Results and discussion

4.1. Qualitative Profile of Polyphenols Determined by Targeted LC-HRMS Analysis

The qualitative profile of polyphenol components of TAP was firstly evaluated by a targeted and untargeted metabolomic approach by HPLC-HRMS in negative and positive ion mode. Figure 2 shows the chromatograms of the extract as total ion current (TIC) recorded in negative (A) and positive (B) ion mode where the identified peaks are numbered progressively (co-eluting peaks share the same number), according to the elution order. The peak of the internal standard (Trolox) is indicated by "IS". A total of 68 compounds were identified, 68 of which are polyphenols, 52 by the targeted approach and 16 by the untargeted approach.

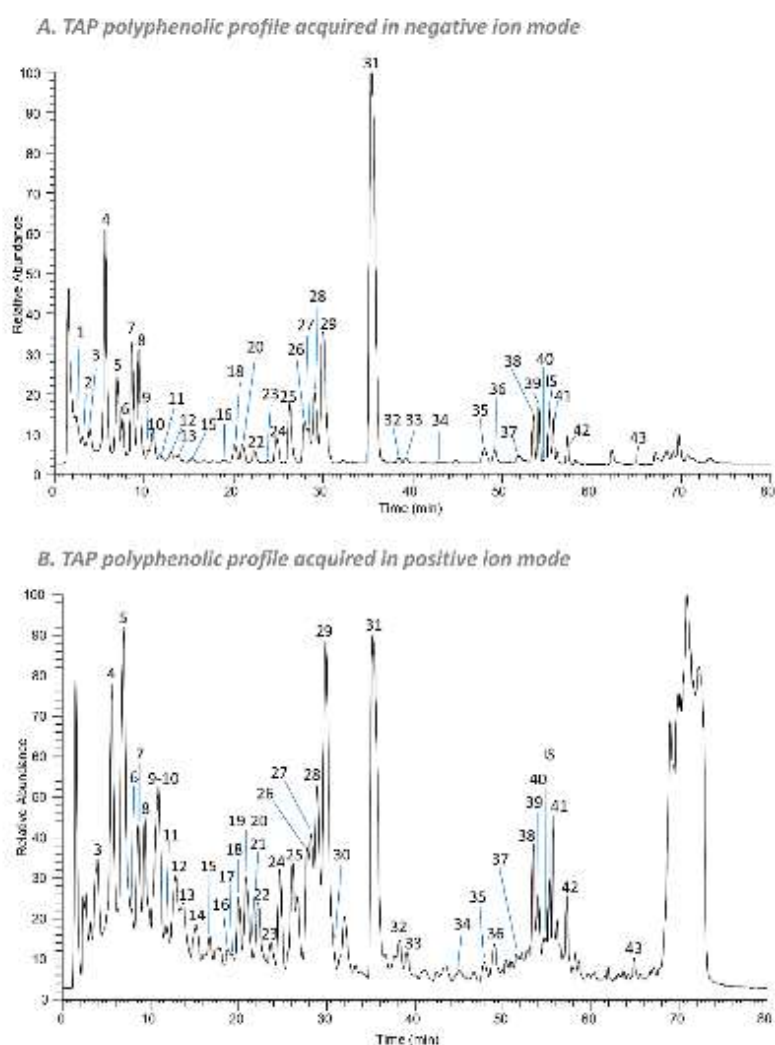


Figure 2 - Total ion currents (TICs) of PAT fraction acquired in (A) negative ion mode and (B) positive ion mode.

Identified peaks are numbered progressively, according to the elution order, and their identity or putative identity is shown in Table S1 of the Supplementary Materials with the experimental mass, MS/MS fragments and identification method. IS: internal standard.

The 52 compounds identified or putatively identified with the targeted analysis are listed in Table S1 of the Supplementary Materials; for each identified compound, the relative peak number (Figure 2), the retention time (RT), the experimental mass (as $[M-H]^-$, $[M+H]^+$, $[M+2H]^{2+}$ or $[M+Na]^+$), the mass accuracy (Δ ppm), MS/MS fragments and identification method are reported. Thirty-nine compounds were detected in both polarities, seven in negative ion mode and six in positive ion mode. Among the 52 components, 20 are phenolic and organic acids, 11 are flavanols, 10 are flavonols, 5 are flavanones, 4 are dihydrochalcones, 1 is a flavone (luteolin) and 1 is a triterpenoid (euscaphic acid). Thirteen compounds were confirmed by means of in-house available pure standards: three phenolic acids, protocatechuic acid, caffeic acid and p-coumaric acid; two flavanols, catechin and epicatechin; two flavanones, naringenin glucoside and naringin; four flavonols, quercetin-3-O-galactoside, quercetin-3-O-rhamnoside, quercetin and kaempferol; two dihydrochalcones, phlorizin and phloretin; one flavone, luteolin. For the compounds for which the standard was not available (39 molecules), a putative identification was carried out by matching the accurate mass, the isotopic pattern and the fragmentation pattern with data reported in the literature. Among phenolic acids, the glucoside forms of protocatechuic, ferulic, caffeic and coumaric acids, and also quinic acid esters of caffeic and coumaric acids were identified. Flavanols are represented in the monomeric forms (catechin and epicatechin) up to the nonamer oligomer, detected as $[M+2H]^{2+}$. Naringenin and eriodictyol derivatives (and aglycones) were the flavanones identified in the extract. The untargeted analysis allowed the putative identification of 16 compounds (Table S2 of Supplementary Materials): nine flavonols, three phenolic acids, one flavanone, one dihydrochalcone and two lipids. As an example, 3-(benzoyloxy)-2-hydroxypropyl glucopyranosiduronic acid (compound 11) was tentatively annotated, firstly by calculating the possible molecular formula with the QualBrowser tool of Xcalibur (mass tolerance of 5 ppm and using C, H, O, N, S as possible atoms). The resulting formulae were searched in databases and in the literature and we found a match with 3-(benzoyloxy)-2-hydroxypropyl glucopyranosiduronic acid ($C_{16}H_{20}O_{10}$, 0.037 ppm, in negative ion mode) [52]. The MS/MS spectrum was also compared: the main fragment was at m/z 249 in negative ion mode deriving from the loss of benzoic acid (-122 Da). Glycosides of quercetin, methoxyquercetin (patuletin, detected with the untargeted approach) and kaempferol are the most representative flavonols identified, but they were also present as aglycones, and a coumaroylglucoside derivative of quercetin was annotated with the untargeted approach. Methoxyquercetin (patuletin, compound 36) was putatively identified through HMDB database: the molecular formula $C_{16}H_{12}O_8$ (0.107 ppm in negative ion mode; 1.862 ppm in positive ion mode) and MS/MS

fragments at m/z 285, 209 and 181 (in negative ion mode) matched with those found in the database, and in addition, we detected an additional fragment at m/z 316, corresponding to the loss of a methyl group (-15 Da). We detected also five patuletin derivatives: three hexoside isomers (compounds 20, 22 and 23) at 20.8, 22.5 and 23.8 min, tentatively annotated with PubChem; one patuletin pentoside derivative (compound 27), tentatively identified through the matching of the molecular formula ($C_{21}H_{20}O_{12}$, -0.179 ppm and -1.591 ppm in negative and positive ion mode, respectively); and characteristic fragments of patuletin aglycone at m/z 331 and 316 due to a neutral loss of -132 Da, corresponding to a pentoside moiety and a subsequent loss of a methyl moiety. Similarly, patuletin rhamnoside (compound 29) was annotated through the molecular formula ($C_{22}H_{22}O_{12}$, 0.161 ppm and -2.066 ppm in negative and positive ion mode, respectively) and the MS/MS fragments (at m/z 331 and 316) deriving from the neutral loss of a rhamnoside moiety (-146 Da) and a subsequent loss of a methyl (-15 Da). Patuletin is a methoxy derivative of quercetin which, among the bioactivities reported in the literature, was found effective in the reduction of serum TNF- α in a rodent model of adjuvant-induced arthritis [53]. CFM-ID online software gave for compound 38 eriodictyol 7-(6-trans-p-coumaroylglucoside) as the best match, using the compound identification tool which compares the molecular ion (mass tolerance of 5 ppm) and the MS/MS fragments to data present in online databases. Coumaroyl glucosides seems to show a higher antioxidant effect with respect to the relative glucoside derivative as reported by Li X. et al. [54]: in TAP extract, we found eriodictyol 7-(6-trans-p-coumaroylglucoside) and quercetin 3-(3-p-coumaroylglucoside) (putatively identified with HMDB). The phloretin derivatives typically identified in apples were also found, with a new putative annotation (through HMDB) of hydroxyphloretin glucoside (peak 25) detected with the untargeted approach. The untargeted approach also revealed two lipids (peaks 41 and 42), annotated as (10E,15Z)-9,12,13-trihydroxy-10,15-octadecadienoic acid and trihydroxy-octadecenoic acid.

4.2. Quantitative Analyses (Total Polyphenols and HPLC)

The total polyphenol content was determined both by spectrophotometry and HPLC analysis as reported in the Methods section. Overall, the results derived by these two methods are superimposable, being 24.14 ± 1.58 and 27.97 ± 0.68 mg/100 mg, as determined by the Folin–Ciocalteu colorimetric test and HPLC analysis, respectively. By considering the values reported by Sun et al., who found that the total extractable phenolic content from fresh apples is between 110 and 357 mg/100 g [55], we can say that the preparation of the TAP extract resulted in a significant increase in the recovery yield of the polyphenolic fraction.

4.3. Direct Radical Scavenging Activity (DPPH)

The direct radical scavenging activity was evaluated by the DPPH assay and the results are reported in Table 1 and expressed as IC₅₀. The lower the value obtained, the higher the direct radical scavenging activity. The TAP extract was found to exert a significant radical scavenging activity, which was found to be significantly higher than the reference compounds when expressed on the basis of the polyphenol content as determined by HPLC.

Table 1 - Direct radical scavenging activity of TAP extract, TAP expressed on the basis of polyphenol content, Trolox, and ascorbic acid. Results are reported as mean ± standard deviation.

<i>Sample</i>	Radical Scavenging Activity	
	IC₅₀ µg/mL (Mean ± SD)	
<i>TAP</i>	11.4 ± 1.1	
<i>TAP (expressed on polyphenol content)</i>	3.2 ± 0.3	
<i>Trolox</i>	5.0 ± 0.3	
<i>Ascorbic acid</i>	3.9 ± 0.05	

4.4. NRF2 Activation and Anti-Inflammatory Activity

We first tested the effect of TAP on cell viability using the MTT assay up to a concentration of 250 µg/mL. Cell viability was found to be higher than 95% at all the tested doses (data not shown). Figure 3 reports the dose-dependent effect of TAP on NRF2 activation after 6 and 18 h of incubation in a concentration range between 1 and 250 µg/mL. After 6 h, the effect started to be significant at a concentration of 50 µg/mL and induced a 2.3-fold increase at a 250 µg/mL concentration. The fold increase was higher after an incubation time of 18 h to reach more than a 5-fold increase at the highest tested dose.

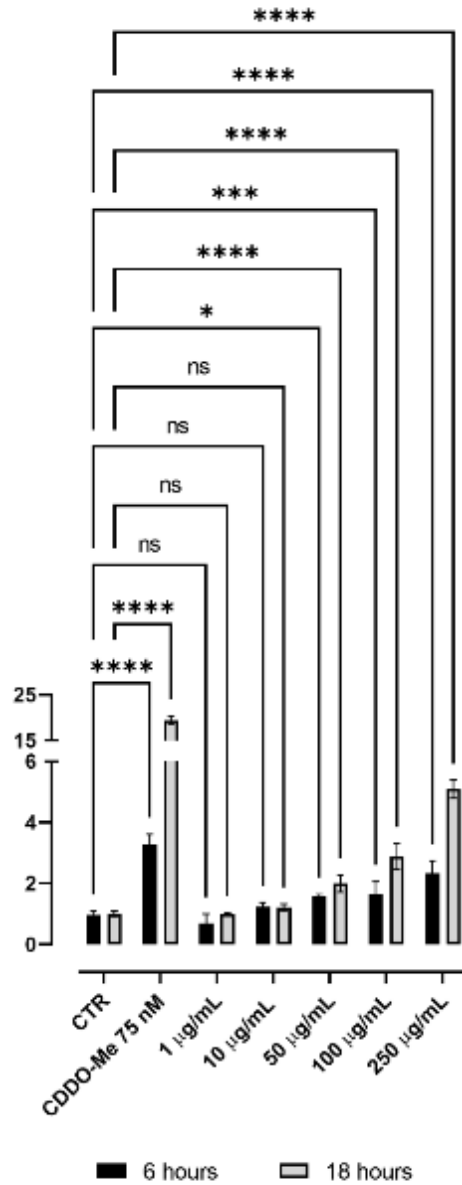


Figure 3 - Dose-dependent effect of TAP on NRF2 nuclear translocation. NRF2 activation was tested using NRF2/ARE Responsive Luciferase Reporter HEK293 stable cell line incubated for 6 and 18 h with TAP in a concentration range between 1 and 250 µg/mL. CDDO-Me 75 nM was used as a positive control. Statistical analysis was calculated by two-way ANOVA with Dunnett's multiple comparison test, with individual variances computed for each comparison (* $p < 0.05$, ** $p < 0.005$, *** $p < 0.001$, **** $p < 0.0001$).

The anti-inflammatory activity of TAP extract was then tested in the same concentration range (1–250 µg/mL) using R3/1 NF-κB cells and two different inflammatory inducers: TNF-α and IL-1α. The results are summarized in Figure 4. (A) shows the NF-κB-dependent luciferase activity in cells incubated in the absence (black columns) and presence (gray columns) of IL-1α and treated with TAP. Results are reported as luciferase fold increase with respect to untreated cells. IL-1α induced more than a 5-fold increase in NF-κB-induced luciferase, which was dose-

dependently reduced by TAP incubation. Luciferase activity as not affected by TAP in the absence of IL-1 α . TAP was then tested using TNF- α as a stimulus (Figure 4B), and in this condition, it was found to dose-dependently reduce the NF- κ B-dependent luciferase activity after both 6 and 24 h of incubation. The TAP anti-inflammatory activity was greater when IL-1 α was used as an inflammatory stimulus with respect to TNF- α .

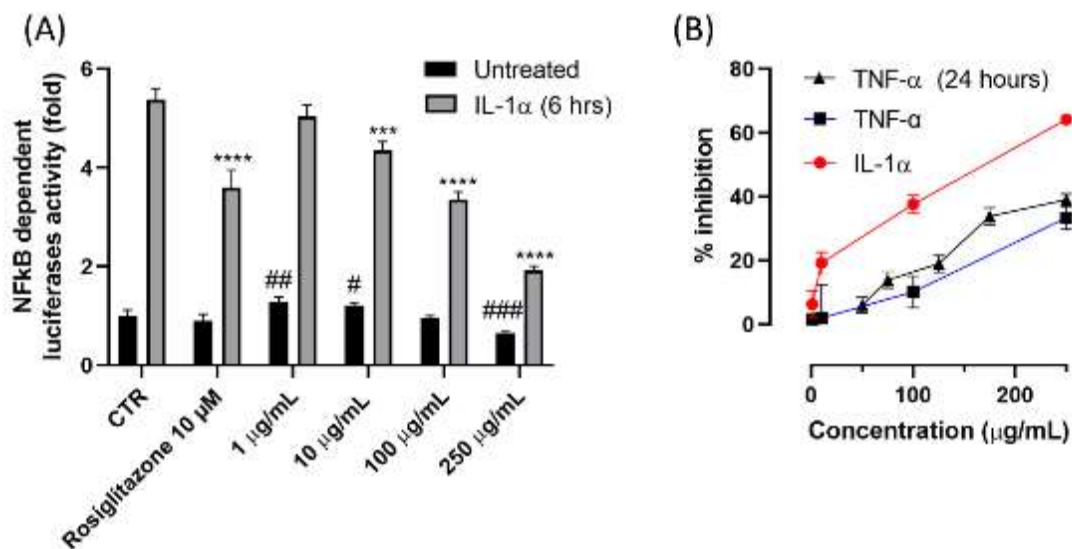


Figure 4 - Dose-dependent anti-inflammatory activity of TAP. Activity was tested in R3/1 with the luciferase gene reported for NF- κ B nuclear translocation. **(A)** The NF- κ B-dependent luciferase activity in cells incubated in the absence (black columns) and presence (gray columns) of IL-1 α and treated with TAP in a 1–250 μ g/mL concentration range. Rosiglitazone 10 μ M was used as a positive control. **(B)** The dose-dependent effect of TAP on the NF- κ B-dependent luciferase activity of cells challenged for 6 h with IL1- α , and for 6 and 24 h with TNF- α (* p < 0.05, ** p < 0.005, *** p < 0.001, **** p < 0.0001—# p < 0.05, ## p < 0.005, ### p < 0.001, #### p < 0.0001).

4.5. Quantitative Proteomic Studies

The effect of TAP on the proteome of control cells and cells stimulated with TNF- α was then studied by using two different quantitative proteomic approaches, SILAC and label-free, and the following four different experimental groups: control cells, cells stimulated with TNF- α , and cells incubated in the absence and presence of TAP.

4.5.1. SILAC Proteomic Studies

Figure 5 shows the volcano plots obtained from the three comparative analyses: (i) cells incubated in the absence (CTR) and presence of TAP (CTR-TAP), (ii) cells incubated in the absence (CTR) and presence of TNF- α (CTR-TNF); (iii) cells stimulated with TNF- α and incubated in the absence (CTR-TNF) and presence of TAP (CTR-TNF-TAP). The analyses were conducted through two orthogonal proteomic approaches, SILAC and the label-free method.

(cont'd) the differential proteome expression for the inflamed cells treated with TAP extract. In each volcano plot, the most representative proteins identified in the various analyses are labeled in red if up-regulated (p value < 0.05 , \log_2 Fold-change > 0.5), in blue if down-regulated (p value < 0.05 , \log_2 Fold-change < -0.5) and in black when they do not fall into the two aforementioned conditions. A more comprehensive analysis of the \log_2 Fold-change values is available in Table 2.

The first experimental comparison analysis permits the evaluation of the general effect of TAP on the cell proteome in homeostatic conditions. From the SILAC experiment, 24 and 14 proteins were found to be up- and down-regulated, respectively, while 1235 were found to be unchanged. Ingenuity pathway analysis identified two main up-regulated pathways: the nuclear factor, erythroid-derived 2 signaling pathway with a z-Score of +2.9 (Figure 6A), and the pentose phosphate pathway with a z-Score of +2.0 (Figure 6B).

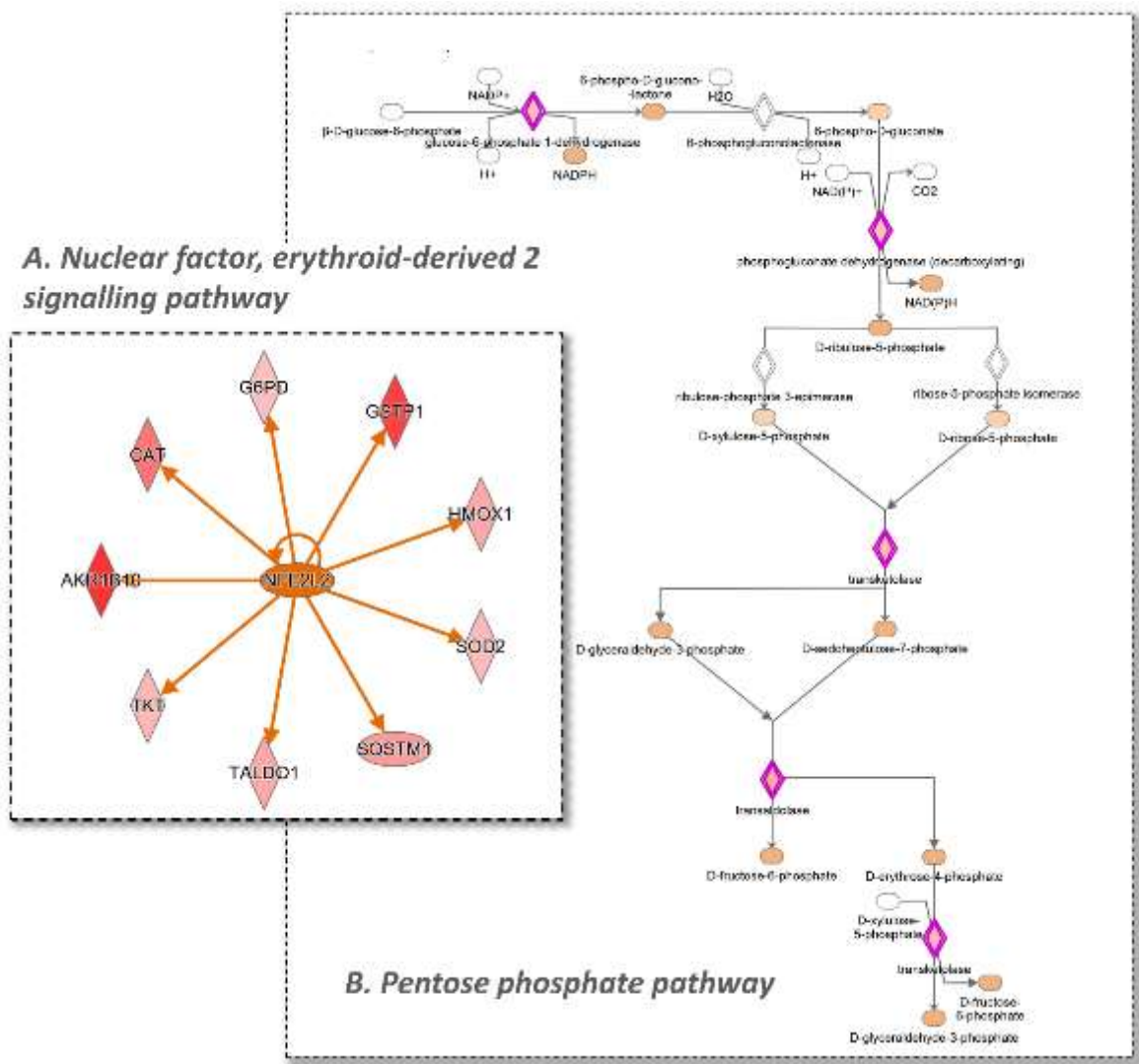


Figure 6 - IPA analysis of the effect of the extract on the cell proteome. (A) illustrates that the differentially regulated proteins in the analysis are consistent with an NRF2 activation.

(cont'd.) (B) illustrates the Pentose Phosphate Pathway; in red are the proteins that were found to be up-regulated by TAP, resulting in an increment in the NADPH pool in the cell. Color legend: red represents the increased genes, green the decreased (not present in the figure). The intensity of the color is related to the intensity of up- or down-regulation. The orange line leads to activation and a blue line (not present in the figure) leads to inactivation. The yellow line indicates findings that are not consistent with the proteomics results obtained.

In particular, the up-regulated enzymes involved in the first pathway include HMOX1, CAT, GSTP1, AKR(1-7), NQO1 and SQSTM1, while for the second one, TKT, PGD, G6PDX and TALDO1 are identified. In addition to these proteins, PTGR1 and BLVRB were also found to be up-regulated, as reported in the volcano plots (Figure 5). PTGR1 is an NADPH-dependent oxidoreductase which is found to be induced by NRF2 activators [56] and directly regulated by NRF2 [57]. BLVRB is found to be an NRF2 target gene and together with HMOX is critical in the heme metabolism [58]. (Figure 11A).

The volcano plot relative to the second experimental comparison analysis (CTR-TNF vs. CTR, Figure 5C,D) mainly identifies two overexpressed proteins involved in inflammation, NF-KB2 and SOD2. As expected, the ingenuity pathway analysis identifies, with a z-Score of 1.8, the TNF- α as up-stream regulator (data not shown).

The volcano plot displaying the third comparison analysis (CTR-TNF-TAP vs. CTR-TNF, Figure 5E,F) reports that TAP treatment down-regulates the two proteins over-expressed in the inflammatory conditions (NF-KB2 and SOD2), while the two main pathways up-regulated by the TPA treatment were confirmed to be the NRF2 and the pentose phosphate pathway.

Finally, protein-protein interaction network analysis using the Cytoscape interface in STRING confirmed the modulation of a protein set involved in the biological processes/pathways already highlighted in IPA, as a result of TAP treatment (Figure 7A,B). Assigned GO annotations lead firstly to confirmation of the activation of the NRF2 and pentose phosphate pathways and the involvement of several oxidoreductive enzymes as well as of proteins involved in the metabolism of glutathione (GSH). It should be taken into account that STRING-Cytoscape network analysis does not distinguish between up- and down-regulated proteins but only considers significant expression modulation.

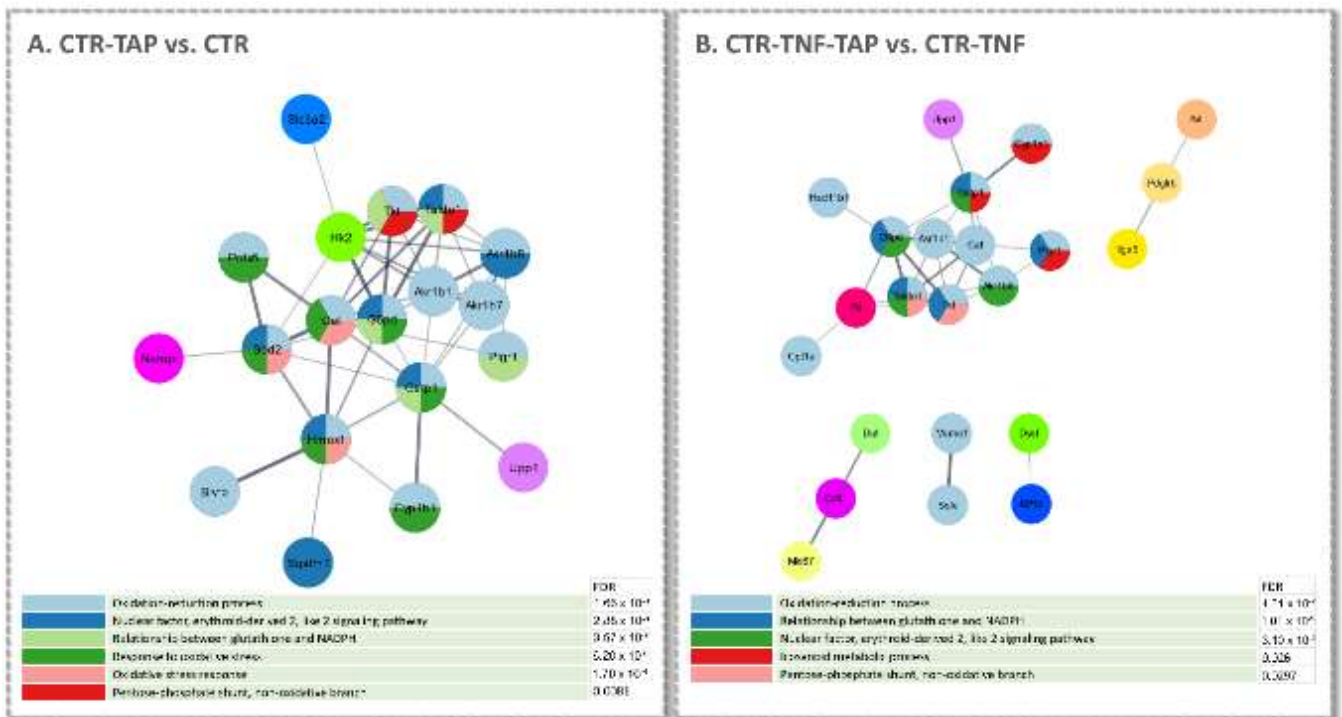


Figure 7 - Cytoscape and STRING analysis of the up-regulated gene products determined by SILAC. The panels illustrate the protein-protein interaction networks obtained by STRING in the CTR-TAP vs. CTR (A) and CTR-TNF-TAP vs. CTR (B) conditions. The color/s of each node (gene product) reflect/s the functional enrichment analysis performed; the color code describing the enriched biological processes with the corresponding FDR value is shown below each network. In both analyses, the singlets were left out.

4.5.2. Label-free quantitative proteomic studies.

The label-free quantitative proteomic study, through the use of a Fusion MS analyzer, identified a larger number of proteins with respect to those identified by the SILAC approach, which was based on an LTQ Orbitrap system. In particular, LFQ identified 2340 more proteins than SILAC in the CTR-TNF vs. CTR mixture, 2412 more in the CTR-TAP vs. CTR mixture and 2259 more in the CTR-TNF-TAP vs. CTR-TNF mixture. As shown by the volcano plots relative to the three experimental conditions' comparison, depicted in Figure 5 (lower panels), besides a larger number of identified proteins, the LFQ approach also permitted the identification of more up- and down-regulated proteins in all three conditions. Details about the comparison of the number of up- and down-regulated proteins identified by the two approaches in the three experimental groups are shown by Venn diagrams in Figure 8.

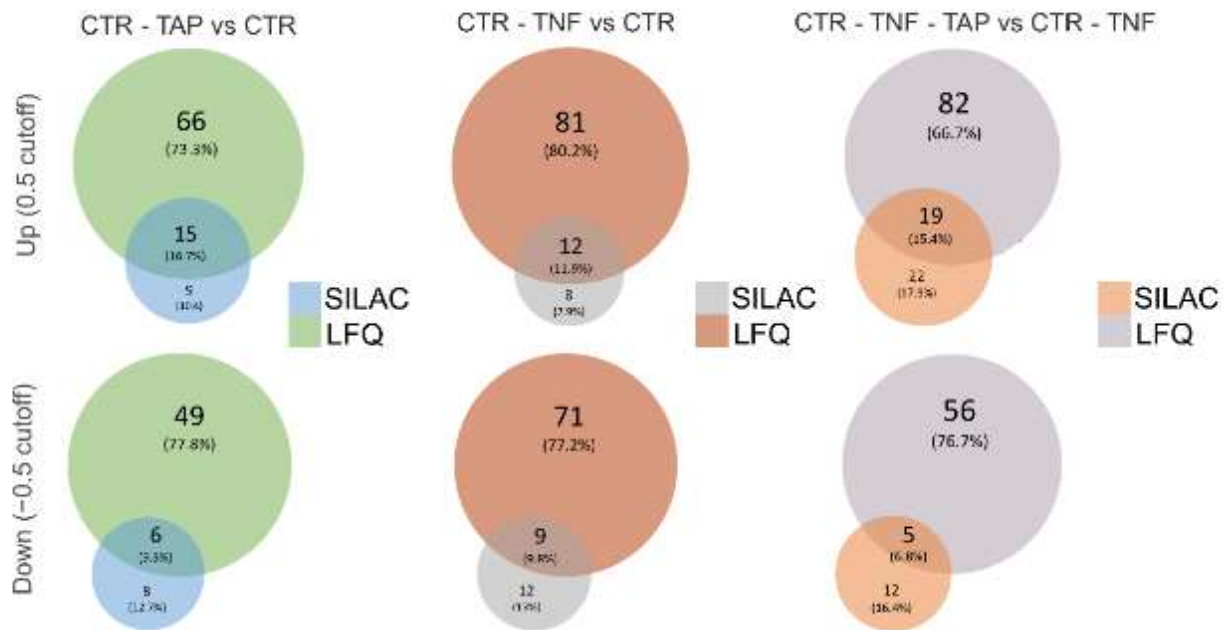


Figure 8 - Venn diagrams showing technical differences in terms of the number of significantly (log ratio cutoff \pm 0.5) up- (first line diagrams) and down-regulated (second line diagrams) proteins identified by the two approaches in the three comparison analyses (CTR-TAP vs. CTR; CTR-TNF vs. CTR; CTR-TNF-TAP vs. CTR-TNF). Additionally, the percentage distribution of identifications in the two approaches and the percentage of common assignments are shown for each diagram.

Pathway analysis (IPA) of the LFQ results, besides confirming the results achieved by the SILAC approach, identified further regulated pathways. As shown in Figure 9, a better description of the NF- κ B activation was observed because two upstream regulators were found to be compatible with the overexpressed proteins, AKT (protein kinase B, Figure 9B) and IKBKB (inhibitor of nuclear factor kappa-B kinase subunit beta, Figure 9C). AKT regulates the transcriptional activity of NF- κ B by inducing phosphorylation and the subsequent degradation of the inhibitor of κ B (I κ B). IKBKB phosphorylates the inhibitor in the inhibitor/NF- κ B complex, causing dissociation of the inhibitor and activation of NF- κ B. As a result, the number of proteins identified in the TNF- α pathway significantly increases. Besides AKT and IKBKB, another obvious upstream regulator is reported in Figure 9A, the TNF pathway, which simply confirms the effectiveness of the method used to induce inflammation.

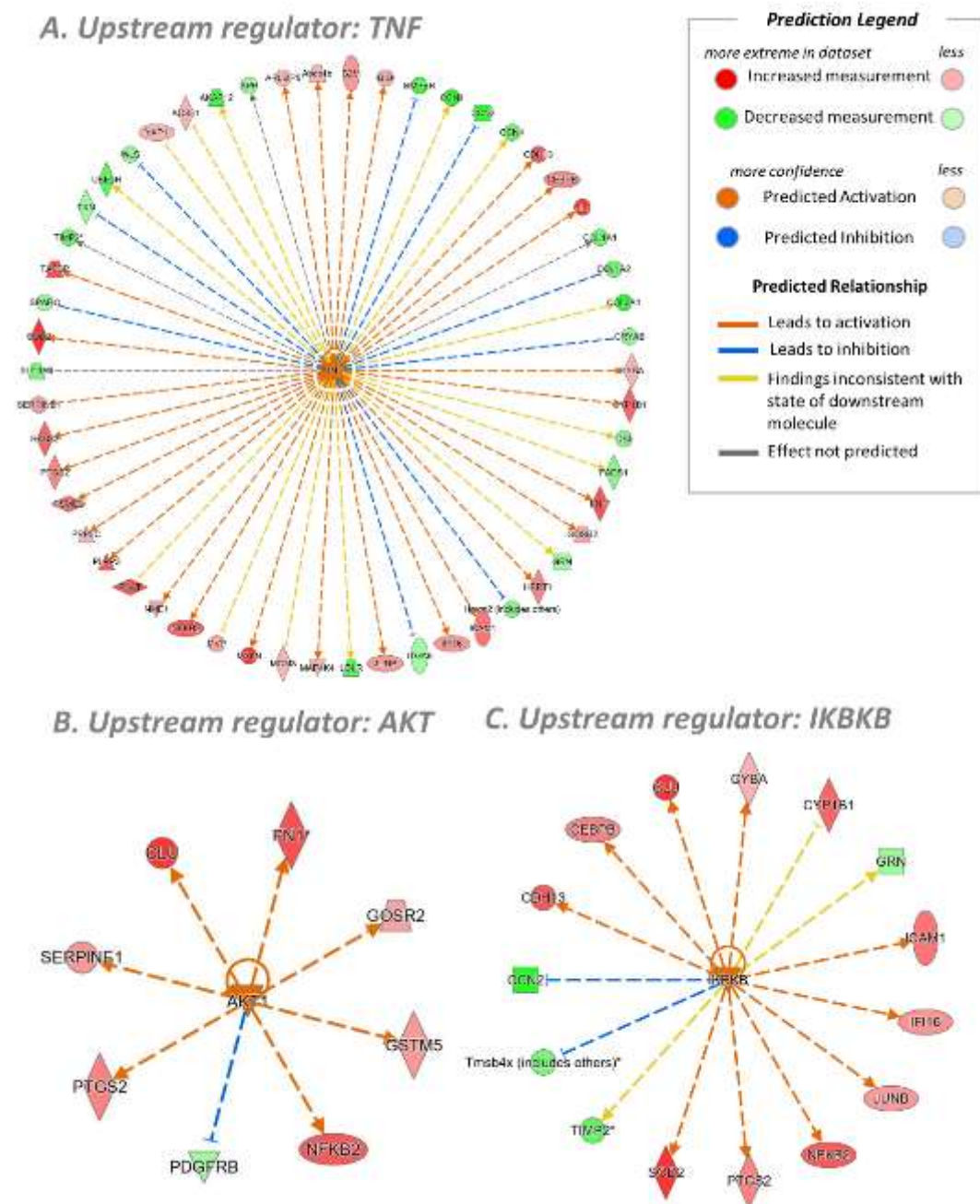


Figure 9 - Upstream regulators determined in the CTR-TNF vs. CTR condition by IPA analysis (LFQ). (A) The wheel of proteins involved in the TNF α stimuli. (B,C) The wheels of proteins associated with AKT and IKKB as upstream regulators. Above is the prediction legend (IPA) essential for understanding networks. *multiple isoforms.

Regarding the CTR-TAP vs. CTR comparison, the activation of the NRF2 pathway by TAP, as already evidenced by the SILAC approach, was confirmed and the number of proteins involved in the signaling was greatly extended. Furthermore, TAP treatment was associated with a reduction in ferroptosis, apoptosis and oxidative stress (data not shown).

5. Discussion

Epidemiological and intervention studies indicate that consumption of apples and derivatives, such as apple juice, exert beneficial effects relating to some human diseases including CVD and related events, e.g., cancer and diabetes. Some of the health effects, and in particular, the antioxidant and anti-inflammatory activities, have been attributed to the polyphenol fraction, as also confirmed by preclinical studies. Hence, there is a growing interest in the use of apple polyphenols as health care products, as well as on their production with green methods. Apple polyphenols are contained in large quantities in thinned apples which represent a large waste material of the apple chain. Based on these premises, the aim of the present study was to evaluate thinned apples as a source for the isolation of bioactive apple polyphenols, effective as anti-inflammatory and antioxidant compounds to be used in health care products. To reach this goal, we first set up a scalable procedure for polyphenol isolation from thinned apple. The polyphenol content of the purified fraction obtained by absorption resin accounted for 24%, as determined by colorimetric analysis, and almost 28% by HPLC, indicating the suitability of the isolation process. The isolated polyphenols were then fully identified by a targeted and untargeted LC-HRMS approach which is, to our knowledge, the first qualitative profile of polyphenols from thinned apples.

The targeted and untargeted metabolomics approaches allowed us to identify a total of 68 polyphenols belonging to the six polyphenolic classes. Moreover, 16 compounds were found in the TAP fraction, though not yet reported in apple or derivatives. All the characteristic polyphenols identified in harvested apples as reported in the most recent literature were identified.

The biological evaluation of the extract followed the qualitative characterization; TAP was first evaluated in two cell models in order to evaluate the antioxidant and anti-inflammatory properties of the extract, the two main activities ascribed to apple polyphenols as reported by the most recent literature. The antioxidant activity was firstly studied by the DPPH assay, which demonstrated a greater radical scavenging activity of the polyphenol fraction with respect to reference compounds, i.e., Trolox and ascorbic acid. For several years, the *in vivo* antioxidant activity of plant polyphenols has been explained by considering their direct radical scavenging activity towards ROS and carbon centered radicals. However, as pointed out by Forman and Ursini [59], kinetic constraints indicate that *in vivo* scavenging of radicals is ineffective in antioxidant defense (except for vitamin E towards peroxy radicals). Instead, enzymatic removal of non-radical electrophiles, such as hydroperoxides, in two-electron redox reactions,

is the major antioxidant mechanism. Based on this overview, the major mechanism of action for nutritional antioxidants, and in particular, for plant polyphenols such as those contained in TAP, is the paradoxical oxidative activation of the NRF2 (NF-E2-related factor 2) signaling pathway, which maintains protective oxidoreductases and their nucleophilic substrates. As stated by Ursini, the maintenance of the “Nucleophilic Tone” by a mechanism called “Para-Hormesis” provides a means for regulating physiological non-toxic concentrations of the non-radical oxidant electrophiles that boost antioxidant enzymes, damage removal and repair systems (for proteins, lipids and DNA) at the optimal levels consistent with good health [59]. Hence, based on this new vision of the antioxidant activity of natural antioxidants, as a next step, we tested the ability of TAP to act as an indirect antioxidant by activating the NRF2 pathway.

Results well indicate that TAP dose-dependently activates the NRF2 pathway, as determined by measuring the activity of luciferase, which is the product of the gene reporter activated by the nuclear binding of NRF2. Activation of NRF2 by TAP can be firstly ascribed to the polyphenol compounds bearing an ortho-diphenol moiety which is oxidized to the corresponding quinone, which, being an electrophilic compound, reacts with the thiols of KEAP1, thus releasing NRF2, which then translocates into the nucleus. TAP contains a set of polyphenols containing the catechol moiety, including derivatives of caffeic acid, and quercetin. TAP also contains phenols or methoxy derivatives, such as derivatives of coumaric acid, phloretin and naringenin, which can also be NRF2 activators, but in this case, metabolic activation is required to form a di-phenol moiety. In particular, the metabolic activation of phenols requires the insertion of a hydroxyl group in ortho or para position mediated by the cytochrome enzymes, as found for resveratrol [60], while a CYP mediated O-demethylation activates methoxy derivatives, as reported for silybin [61]. Such metabolic reactions usually occur in the liver tissue and hence are unlikely to occur in the cell model used in the in vitro assay. Hence, we presume that the potency of NRF2 activation is underestimated and that presumably it is potentiated in vivo by metabolic activation occurring in the organism, as well as by the microbiota in the gastrointestinal tract. NRF2 activation paralleled the dose-dependent anti-inflammatory activity, as demonstrated in the tested cell model (luciferase gene reporter for NF- κ B nuclear translocation), and using two different pro-inflammatory agents, IL1- α and TNF- α . A strict inter-dependence between oxidative stress and inflammation and between the two transcriptional factors involved, NF- κ B and NRF2, is well established [62,63]. When oxidative stress appears as a primary disorder, inflammation develops as a secondary disorder and further enhances oxidative stress. On the other hand, inflammation as a primary disorder can induce oxidative stress as a secondary

disorder, which can further enhance inflammation [64]. Based on this evidence, a well-established strategy to block the inflammatory chronic condition consists of inhibiting oxidative stress, and in turn, the best approach to inhibit oxidative stress is to activate the nucleophilic tone by inducing NRF2 nuclear translocation. Hence, the anti-inflammatory activity of TAP can be first of all ascribed to the NRF2-2-dependent antioxidant effect. To gain a deeper insight into this mechanism, and in particular, to confirm the activation of antioxidant enzymes and to search for other enzymes involved in the anti-inflammatory activity, a proteomic investigation was then carried out. Quantitative proteomic studies were carried out using the cell line with the gene reporter for NF- κ B, used for the anti-inflammatory activity evaluation, and TNF- α as an inflammatory inducer. Two orthogonal proteomic approaches were applied, namely, a label-free method, using a Fusion MS analyzer, and a stable isotope in vivo labeling method, i.e., SILAC, coupled to a LTQ Orbitrap system. In general, the label-free approach identified many more proteins with respect to SILAC and was revealed to be more efficient in the identification of up- and down-regulated pathways. These differences could be easily explained by considering the intrinsic potential in terms of sensitivity and resolution characteristics of the mass analyzers used for each of the experiments.

Besides the different performances, the two approaches identified the same modulated pathways, although with a different number of proteins, making the results more robust, as confirmed by two orthogonal approaches. This very interesting technical aspect is particularly evident in the following table (Table 2), which shows the experimentally calculated fold-change values for each key protein identified, whose expression is significantly modulated in the comparative analysis between the tested conditions.

Table 2 - Key proteins identified by quantitative proteomics analysis; fold-change values calculated by each of the experimental approaches used are reported by gene product. The fold-change values are classified according to (cont'd) the comparative analysis of the conditions tested. ND indicates a not-detected protein identification with the corresponding proteomic approach. The value 0 indicates a fold-change not significantly different from zero. Each fold-change set, reported per gene product and per proteomic approach, is colored on a green (minimum value) to light orange (maximum value) color scale according to the conditional formatting function of excel. The gene products involved in the nuclear factor erythroid-derived 2 signaling pathway are highlighted in light violet and those involved in the pentose phosphate pathway in light blue.

<i>Gene Name</i>	<i>CTR-TNF vs. CTR</i>		<i>CTR-TAP vs. CTR</i>		<i>CTR-TNF-TAP vs. CTR-TNF</i>	
	<i>LFQ</i>	<i>SILAC</i>	<i>LFQ</i>	<i>SILAC</i>	<i>LFQ</i>	<i>SILAC</i>
Akr1b1	0	0	0.4508	0.5497	0.5960	0.6343
Akr1b3	0	ND	0.4508	ND	0.5960	ND
Akr1b7	0	0	1.2905	1.7506	1.4273	ND
Akr1b8	0	0	1.4440	1.7608	1.5898	2.1034
Blvrb	-0.3809	-0.2301	0	0.5764	0.7862	0.4835
Cat	0	0	1.0800	1.1262	1.0148	1.2222
G6pdx	0	0	0.5651	0.5211	0.7523	0.5877
Gsta3	0	ND	1.2664	ND	0.9136	ND
Gstp1	-0.3949	-0.1888	0.9105	1.5843	1.2616	1.7841
Hmox1	-0.2424	-0.1233	0.8703	0.7048	0.6607	0.4045
Nfkb2	1.1143	1.3995	0	ND	0	-0.2200
Nqo1	0	ND	1.7907	ND	1.6534	ND
Pgd	0	0.1012	0.5913	0.4975	0.6452	0.5666
Por	-0.0862	ND	0.0429	ND	0.3405	0.1561
Prdx1	0	0	0.2915	0.2540	0.4062	0.2665
Prdx5	0	0.1132	0.4444	0.5167	0.6037	0.3645
Ptgr1	0	0	0.9705	1.2600	0.9978	1.2999
Sqstm1	-0.3753	-0.6061	0.4559	0.8246	0.4579	1.3186
Taldo1	0	ND	0.5603	0.7171	0.9184	0.8525
**Tkt	-0.1891	0	0.4719	0.5824	0.4815	0.5555
Txn1	-0.5145	0	0	0.2655	0.4939	0.2589
Sod2	1.6735	1.8043	0.7816	0.5633	0.6954	0.1391

The first relevant observation emerging from the comparison of the calculated fold-change values in the different conditions tested is the apparent shift in the expression of some of the proteins involved in the NRF2 and pentose phosphate pathways. A fitting example could be the HMOX1 expression modulation, having a negative fold-change (LFQ: -0.2424, SILAC: -0.1233) in the first comparison, meaning that inflammation causes its down-regulation, and showing a significant up-regulation when the cells are treated with TAP extract, in both conditions. Targeting a more comprehensive biological significance, rather than investigating individual key proteins, the global effect of TAP treatment in physiological conditions (CTR), to identify the set of genes whose expression is variably modulated by treatment, was evaluated. As expected, many up-regulated genes involved in the NRF2 pathway activation were detected, particularly antioxidant enzymes, or those directly involved in the detoxification of peroxides and in two-electron redox reactions, e.g., SOD, CAT, GXP and redox proteins such as thioredoxins. Furthermore, a set of enzymes required for the synthesis of GSH and NADPH, co-factors for the enzymes involved in the antioxidant and redox regulation, were also identified. GCLC, GSTA3 and GSTP were the identified up-regulated enzymes involved in the GSH synthesis and metabolism while the enzymes belonging to the oxidative pentose-phosphate pathway are those up-regulated for NADPH synthesis, such as malic enzyme-1 (ME-1), isocitrate dehydrogenase-1 (IDH1), glucose-6-phosphate dehydrogenase (G6PDX) and 6-phosphogluconate dehydrogenase (PGD).

The crucial finding is that TAP treatment over-expresses the inducible isoform of heme oxygenase (HMOX1), a well-established immunomodulator [65–67]; it has been proven that the induction of HMOX1 protects against the cytotoxicity caused by oxidative stress and apoptotic cell death, making HMOX1 an appealing target for the treatment of several chronic inflammatory diseases, including osteoporosis [68], cancer [69], acute kidney injury [70], retinal pigment epithelium degeneration [71] and Parkinson's disease [56,67].

In physiological conditions, HMOX1 is involved in rate-limiting heme degradation using NADPH-cytochrome P450 reductase (POR) and oxygen to generate linear tetrapyrrole biliverdin (further converted into linear tetrapyrrole bilirubin by the enzyme biliverdin reductase, BLVRB), ferrous iron (Fe²⁺) and carbon monoxide (CO) (Figure 11A). The enzymatic heme-degradation by-products are known to be the main cause of the beneficial protective effects promoted by HMOX1; bilirubin, in particular, is one of the most potent antioxidant and is particularly effective in protecting against lipid peroxidation.

HMOX1 can be up-regulated in response to numerous different stress stimuli, including various pro-oxidant and pro-inflammatory mediators; most of them do not interact directly with the transcription factors, but activate them via intermediate signaling pathways. HMOX1 expression is largely under the control of NRF2, a well-known binder of the ARE (antioxidant response element), aimed at promoting many antioxidant genes, including HMOX1. Under homeostatic conditions, NRF2 is bound to Kelch-like ECH-associated protein 1 (KEAP1), ubiquitylated and targeted by the proteasome for degradation (Figure 11B); meanwhile, BACH1 binds to ARE and inhibits gene transcription. An increased level of reactive oxygen species (ROS) during cell stress implies a concomitant KEAP1-NRF2 dissociation due to their reactivity against thiols in KEAP1; in turn, NRF2 translocates to the nucleus and binds the ARE to promote transcription of HMOX1 (Figure 11C). Basically, NRF2, KEAP1 and BACH1 constitute an intricate feedback system enabling cells to respond to oxidative stress ending at the up-regulation of HMOX1.

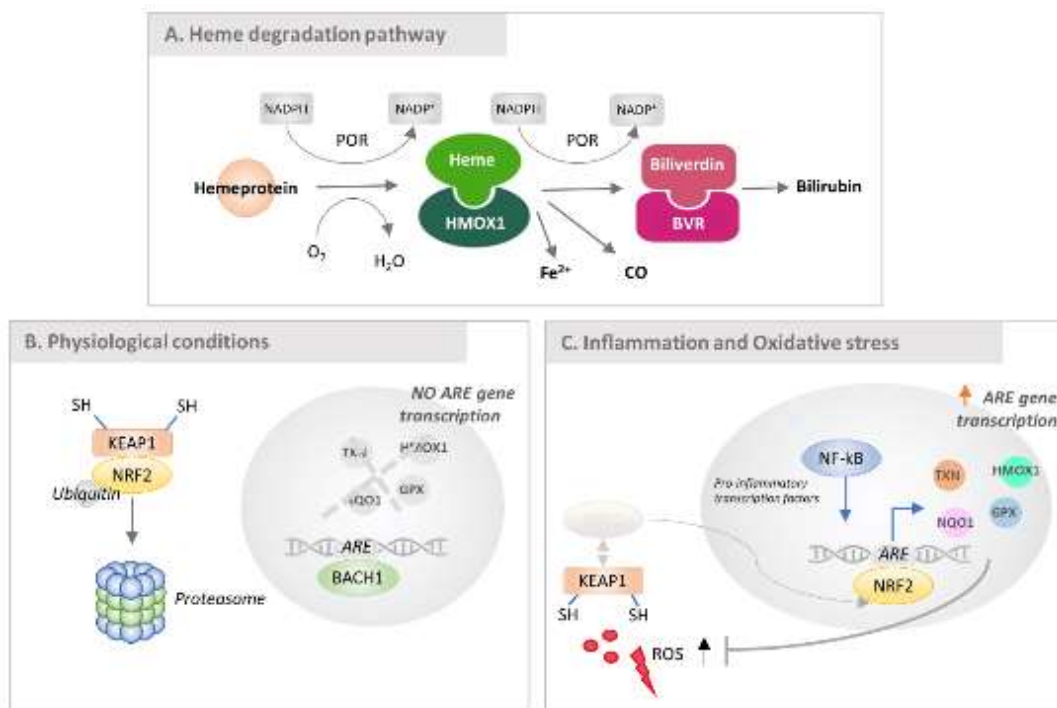


Figure 11 - Signaling pathways in which HMOX1 is involved. (A) Heme degradation pathway promoted by HMOX1 occurring in the cytosol of the cell. Heme degradation occurs in the cytosol by the enzyme HMOX1; the reaction involves cytochrome P450 reductase, NADPH as cofactor and O₂, leading to the production of NADP⁺, and an equimolar amount of biliverdin, carbon monoxide and iron (Fe²⁺). Specifically, biliverdin can be further converted to bilirubin by the enzyme biliverdin reductase (BVR). (B) Regulation of HMOX1 expression under homeostatic conditions. NRF2 is bound to KEAP1, ubiquitinated and targeted for proteasomal degradation. BACH1 binds the antioxidant response element (ARE) at the promoter of HMOX1, inhibiting transcription of the gene. (C) Regulation of HMOX1 expression during inflammation and oxidative stress. Increased intracellular

(cont'd) heme levels lead BACH1 to dissociate from ARE, and reactive oxygen species (ROS), interacting with cysteine residues on KEAP1, cause dissociation from NRF2, which in turn migrates into the nucleus, binds ARE and promotes transcription of HMOX1 (adapted from [67]).

The pathway activation in this study is supported not only by the significant modulation of HMOX1 but also by the up-regulation of BLVRB and POR (NAPH-Cytochrome P450 reductase), which, although not significantly up-regulated (fold-change: 0.340528912, p-value n.s.), exactly matches the trend of the other associated gene products. In addition, activation of the pentose phosphate pathway leads to a plausible increase in circulating NADPH, a cofactor of both POR and BLVRB (Table 2).

The phenotypic effect described here, in terms of protein expression induced by TAP treatment, is completely concordant when comparing CTR-TNF-TAP to CTR-TNF conditions. The protective effect manifested, such as the triggering of the two pathways of interest, is perhaps even more evident looking at the volcano plots shown in Figure 5A,B: AKR1B1, AKR1B8, BLVRB, CAT, G6PDX, GSTP1, HMOX1, PGD, PTGR1, SQSTM1, TALDO1 and TKT (listed alphabetically) switch to a fold-change value indicating significant up-regulation, explaining the anti-inflammatory activity overall.

Besides the up-regulated set of NRF2-dependent pathways, another key point is the regulation of TAP towards the increased content of NF- κ B in cells exposed to TNF- α with respect to control (Figure 5C,D), and the overexpression of a set of proteins which are known to be overexpressed by the TNF-signaling. Hence, NF- κ B, in the cell model used, besides being activated and translocated at the nuclear level, as evidenced by the gene reporter, is also overexpressed, thus sustaining the inflammatory process. As stated above, TAP treatment of the inflamed cells not only inhibits NF- κ B activation but also its overexpression: NF- κ B2, together with SOD2, returns to homeostatic conditions, even if the fold-change was not significantly different from zero (Figure 5E,F). An interesting aspect to stress is that NF- κ B, together with AP-1 (Figure 11C), can also bind the HMOX1 promoter to enhance its expression; indeed, some instances of HMOX1 up-regulation in vitro have been shown to be dependent on or correlated with NF- κ B or AP-1 expression [72].

6. Conclusions

In conclusion, thinned apples represent a valuable source of apple polyphenols whose qualitative profile was fully elucidated by targeted and untargeted metabolomic approaches. The anti-inflammatory and antioxidant activities of TPA were first evaluated by cell-based assays using engineered cells with gene reporters for NRF2 and NF- κ B nuclear translocation. Quantitative proteomic studies were then used to deeply investigate the molecular mechanisms involved in the proven biological activity. Two different proteomic approaches, i.e., label-free and SILAC, both confirmed TAP ability in improving the antioxidant cellular defense, by activating the NRF2 signaling pathway which up-regulates protective oxidoreductases and their nucleophilic substrates. A clear increase in enzymatic antioxidants together with the up-regulation of the heme-oxygenase explain the anti-inflammatory effect of TAP. Taken together, these results suggest that thinned apples can be effectively considered a valuable source of apple polyphenols to be used in health care products to prevent/treat oxidative and inflammatory chronic conditions.

7. References

1. Boyer, J.; Liu, R. Apple phytochemicals and their health benefits. *Nutr. J.* 2004, 3, 5. <https://doi.org/10.1186/1475-2891-3-5>.
2. Vallée Marcotte, B.; Verheyde, M.; Pomerleau, S.; Doyen, A.; Couillard, C. Health benefits of apple juice consumption: A review of interventional trials on humans. *Nutrients* 2022, 14, 821. <https://doi.org/10.3390/nu14040821>.
3. Koutsos, A.; Riccadonna, S.; Ulaszewska, M.; Franceschi, P.; Trošt, K.; Galvin, A.; Braune, T.; Fava, F.; Perenzoni, D.; Mattivi, F.; et al. Two apples a day lower serum cholesterol and improve cardiometabolic biomarkers in mildly hypercholesterolemic adults: A randomized, controlled, crossover trial. *Am. J. Clin. Nutr.* 2019, 111, 307–318. <https://doi.org/10.1093/ajcn/nqz282>.
4. Liddle, D.; Lin, X.; Cox, L.; Ward, E.; Ansari, R.; Wright, A.; Robinson, L. Daily apple consumption reduces plasma and peripheral blood mononuclear cell–secreted inflammatory biomarkers in adults with overweight and obesity: A 6-week randomized, controlled, parallel-arm trial. *Am. J. Clin. Nutr.* 2021, 114, 752–763. <https://doi.org/10.1093/ajcn/nqab094>.
5. Łata, B.; Trampczynska, A.; Paczesna, J. Cultivar variation in apple peel and whole fruit phenolic composition. *Sci. Hortic.* 2009, 121, 176–181. <https://doi.org/10.1016/j.scienta.2009.01.038>.
6. Patocka, J.; Bhardwaj, K.; Klimova, B.; Nepovimova, E.; Wu, Q.; Landi, M.; Kuca, K.; Valis, M.; Wu, W. *Malus domestica*: A Review on nutritional features, chemical composition, traditional and medicinal value. *Plants* 2020, 9, 1408. <https://doi.org/10.3390/plants9111408>.
7. Wojdyło, A.; Oszmiański, J.; Laskowski, P. Polyphenolic compounds and antioxidant activity of new and old apple varieties. *J. Agric. Food Chem.* 2008, 56, 6520–6530. <https://doi.org/10.1021/jf800510j>.
8. Aprikian, O.; Busserolles, J.; Manach, C.; Mazur, A.; Morand, C.; Davicco, M.-J.; Besson, C.; Rayssiguier, Y.; Rémésy, C.; Demigné, C. Lyophilized apple counteracts the development of hypercholesterolemia, oxidative stress, and renal dysfunction in obese zucker rats. *J. Nutr.* 2002, 132, 1969–1976. <https://doi.org/10.1093/jn/132.7.1969>.
9. Sekhon-Loodu, S.; Catalli, A.; Kulka, M.; Wang, Y.; Shahidi, F.; Rupasinghe, H. Apple flavonols and N-3 polyunsaturated fatty acid–rich fish oil lowers blood c-reactive protein in rats with hypercholesterolemia and acute inflammation. *Nutr. Res.* 2014, 34, 535–543. <https://doi.org/10.1016/j.nutres.2014.05.002>.
10. Soleti, R.; Trenteseaux, C.; Fizanne, L.; Coué, M.; Hilairret, G.; Kasbi-Chadli, F.; Mallegol, P.; Chaigneau, J.; Boursier, J.; Krempf, M.; et al. Apple supplementation improves hemodynamic parameter and attenuates atherosclerosis in high-fat diet-fed apolipoprotein e-knockout mice. *Biomedicines* 2020, 8, 495. <https://doi.org/10.3390/biomedicines8110495>.
11. Marzo, F.; Milagro, F.; Barrenetxe, J.; Díaz, M.; Martínez, J. Azoxymethane-induced colorectal cancer mice treated with a polyphenol-rich apple extract show less neoplastic lesions and signs of cachexia. *Foods* 2021, 10, 863. <https://doi.org/10.3390/foods10040863>.

12. Skinner, R.; Warren, D.; Naveed, M.; Agarwal, G.; Benedito, V.; Tou, J. Apple pomace improves liver and adipose inflammatory and antioxidant status in young female rats consuming a western diet. *J. Funct. Foods* 2019, 61, 103471. <https://doi.org/10.1016/j.jff.2019.103471>.
13. Yeganeh, P.; Leahy, J.; Spahis, S.; Patey, N.; Desjardins, Y.; Roy, D.; Delvin, E.; Garofalo, C.; Leduc-Gaudet, J.-P.; St-Pierre, D.; et al. Apple peel polyphenols reduce mitochondrial dysfunction in mice with dss-induced ulcerative colitis. *J. Nutr. Biochem.* 2018, 57, 56–66. <https://doi.org/10.1016/j.jnutbio.2018.03.008>.
14. Lee, Y.-C.; Cheng, C.-W.; Lee, H.-J.; Chu, H.-C. Apple polyphenol suppresses indomethacin-induced gastric damage in experimental animals by lowering oxidative stress status and modulating the MAPK signaling pathway. *J. Med. Food* 2017, 20, 1113–1120. <https://doi.org/10.1089/jmf.2017.3951>.
15. Sharma, S.; Rana, S.; Patial, V.; Gupta, M.; Bhushan, S.; Padwad, Y.S. Antioxidant and hepatoprotective effect of polyphenols from apple pomace extract via apoptosis inhibition and Nrf2 activation in mice. *Hum. Exp. Toxicol.* 2016, 35, 1264–1275. <https://doi.org/10.1177/0960327115627689>.
16. Ryter, S. Heme Oxygenase-1: An anti-inflammatory effector in cardiovascular, lung, and related metabolic disorders. *Antioxidants* 2022, 11, 555. <https://doi.org/10.3390/antiox11030555>.
17. Tonelli, C.; Chio, I.; Tuveson, D. Transcriptional regulation by Nrf2. *Antioxid. Redox Signal.* 2018, 29, 1727–1745. <https://doi.org/10.1089/ars.2017.7342>.
18. Saha, S.; Buttari, B.; Panieri, E.; Profumo, E.; Saso, L. An overview of Nrf2 signaling pathway and its role in inflammation. *Molecules* 2020, 25, 5474. <https://doi.org/10.3390/molecules25225474>.
19. Dinkova-Kostova, A.; Wang, X. Induction of the Keap1/Nrf2/ARE pathway by oxidizable diphenols. *Chem. Biol. Interact.* 2011, 192, 101–106. <https://doi.org/10.1016/j.cbi.2010.09.010>.
20. Osorio, Lady; Flórez-López, E.; Grande-Tovar, C. The potential of selected agri-food loss and waste to contribute to a circular economy: Applications in the food, cosmetic and pharmaceutical industries. *Molecules* 2021, 26, 515. <https://doi.org/10.3390/molecules26020515>.
21. Abdhul, K.; Ganesh, M.; Shanmughapriya, S.; Kanagavel, M.; Anbarasu, K.; Natarajaseenivasan, K. Antioxidant activity of exopolysaccharide from probiotic strain enterococcus faecium (BDU7) from Ngari. *Int. J. Biol. Macromol.* 2014, 70, 450–454. <https://doi.org/10.1016/j.ijbiomac.2014.07.026>.
22. Mazzola, M. Elucidation of the microbial complex having a causal role in the development of apple replant disease in washington. *Phytopathology* 1998, 88, 930–938. <https://doi.org/10.1094/PHTO.1998.88.9.930>.
23. Zheng, H.-Z.; Kim, Y.-I.; Chung, S.-K. A profile of physicochemical and antioxidant changes during fruit growth for the utilisation of unripe apples. *Food Chem.* 2012, 131, 106–110. <https://doi.org/10.1016/j.foodchem.2011.08.038>.
24. Sun, L.; Liu, D.; Sun, J.; Yang, X.; Fu, M.; Guo, Y. Simultaneous separation and purification of chlorogenic acid, epicatechin, hyperoside and phlorizin from thinned young qinguan apples by successive use of polyethylene and polyamide resins. *Food Chem.* 2017, 230, 362–371. <https://doi.org/10.1016/j.foodchem.2017.03.065>.

25. Liu, T.; Shen, H.; Wang, F.; Zhou, X.; Zhao, P.; Yang, Y.; Guo, Y. Thinned-young apple polyphenols inhibit halitosis-related bacteria through damage to the cell membrane. *Front. Microbiol.* 2022, 12, 745100. <https://doi.org/10.3389/fmicb.2021.745100>.
26. Azuma, T.; Osada, K.; Aikura, E.; Imasaka, H.; Handa, M. Anti-obesity effect of dietary polyphenols from unripe apple in rats. *Nippon Shokuhin Kagaku Kogaku Kaishi* 2013, 60, 184–192.
27. Baron, G.; Altomare, A.; Mol, M.; Garcia, J.; Correa, C.; Raucci, A.; Mancinelli, L.; Mazzotta, S.; Fumagalli, L.; Trunfio, G.; et al. Analytical profile and antioxidant and anti-inflammatory activities of the enriched polyphenol fractions isolated from bergamot fruit and leave. *Antioxidants* 2021, 10, 141. <https://doi.org/10.3390/antiox10020141>.
28. Wojdyło, A.; Oszmiański, J. Antioxidant activity modulated by polyphenol contents in apple and leaves during fruit development and ripening. *Antioxidants* 2020, 9, 567. <https://doi.org/10.3390/antiox9070567>.
29. López, V.; Les, F.; Mevi, S.; Nkuimi Wandjou, J.G.; Cásedas, G.; Caprioli, G.; Maggi, F. Phytochemicals and enzyme inhibitory capacities of the methanolic extracts from the italian apple cultivar mela rosa dei monti sibillini. *Pharmaceuticals* 2020, 13, 127. <https://doi.org/10.3390/ph13060127>.
30. Fernandes, P.; Ferreira, S.; Bastos, R.; Ferreira, I.; Cruz, M.; Pinto, A.; Coelho, E.; Passos, C.; Coimbra, M.; Cardoso, S.; et al. Apple pomace extract as a sustainable food ingredient. *Antioxidants* 2019, 8, 189. <https://doi.org/10.3390/antiox8060189>.
31. Sánchez-Rabaneda, F.; Jáuregui, O.; Lamuela-Raventós, R.; Viladomat, F.; Bastida, J.; Codina, C. Qualitative analysis of phenolic compounds in apple pomace using liquid chromatography coupled to mass spectrometry in tandem mode. *Rapid Commun. Mass Spectrom.* 2004, 18, 553–563. <https://doi.org/10.1002/rcm.1370>.
32. Mcdougall, Gordon.; Foito, A.; Dobson, G.; Austin, C.; Sungurtas, J.; Su, S.; Wang, L.; Feng, C.; Li, S.; Wang, L.; et al. Glutathionyl-S-Chlorogenic acid is present in fruit of vaccinium species, potato tubers and apple juice. *Food Chem.* 2020, 330, 127227. <https://doi.org/10.1016/j.foodchem.2020.127227>.
33. da Silva, L.; Souza, M.; Sumere, B.; Silva, L.; da Cunha, D.; Barbero, G.; Bezerra, R.; Rostagno, M. Simultaneous extraction and separation of bioactive compounds from apple pomace using pressurized liquids coupled on-line with solid-phase extraction. *Food Chem.* 2020, 318, 126450. <https://doi.org/10.1016/j.foodchem.2020.126450>.
34. Bars-Cortina, D.; Macià, A.; Iglesias, I.; Garanto, X.; Badiella, L.; Motilva, M.-J. Seasonal variability of the phytochemical composition of new red-fleshed apple varieties compared with traditional and new white-fleshed varieies. *J. Agric. Food Chem.* 2018, 66, 10011–10025. <https://doi.org/10.1021/acs.jafc.8b03950>.
35. Groth, S.; Budke, C.; Neugart, S.; Ackermann, S.; Kappenstein, F.-S.; Daum, D.; Rohn, S. Influence of a selenium biofortification on antioxidant properties and phenolic compounds of apples (*Malus Domestica*). *Antioxidants* 2020, 9, 187. <https://doi.org/10.3390/antiox9020187>.

36. Gorjanović, S.; Micić, D.; Pastor, F.; Tosti, T.; Kalušević, A.; Ristić, S.; Zlatanović, S. Evaluation of apple pomace flour obtained industrially by dehydration as a source of biomolecules with antioxidant, antidiabetic and antiobesity effects. *Antioxidants* 2020, 9, 413. <https://doi.org/10.3390/antiox9050413>.
37. Hollands, W.J.; Voorspoels, S.; Jacobs, G.; Aaby, K.; Meisland, A.; Garcia-Villalba, R.; Tomas-Barberan, F.; Piskula, M.K.; Mawson, D.; Vovk, I.; et al. Development, validation and evaluation of an analytical method for the determination of monomeric and oligomeric procyanidins in apple extracts. *J. Chromatogr. A* 2017, 1495, 46–56. <https://doi.org/10.1016/j.chroma.2017.03.030>.
38. Lee, J.; Chan, B.; Mitchell, A. Identification/Quantification of free and bound phenolic acids in peel and pulp of apples (*Malus Domestica*) using High Resolution Mass Spectrometry (HRMS). *Food Chem.* 2017, 215, 301–310. <https://doi.org/10.1016/j.foodchem.2016.07.166>.
39. Wen, C.; Wang, D.; Li, X.; Huang, T.; Huang, C.; Hu, K. Targeted isolation and identification of bioactive compounds lowering cholesterol in the crude extracts of crabapples Using UPLC-DAD-MS-SPE/NMR based on pharmacology-guided PLS-DA. *J. Pharm. Biomed. Anal.* 2018, 150, 144–151. <https://doi.org/10.1016/j.jpba.2017.11.061>.
40. Bestwick, C.; Scobbie, L.; Milne, L.; Duncan, G.; Cantlay, L.; Russell, W. Fruit-based beverages contain a wide range of phytochemicals and intervention targets should account for the individual compounds present and their availability. *Foods* 2020, 9, 891. <https://doi.org/10.3390/foods9070891>.
41. Sut, S.; Zengin, G.; Maggi, F.; Malagoli, M.; Dall'acqua, S. Triterpene acid and phenolics from ancient apples of friuli venezia giulia as nutraceutical ingredients: Lc-ms study and in vitro activities. *Molecules* 2019, 24, 1109. <https://doi.org/10.3390/molecules24061109>.
42. Yousefi-Manesh, H.; Dehpour, A.; Ansari-Nasab, S.; Hemmati, S.; Sadeghi, M.; Shahraki, R.; Shirooie, S.; Nabavi, S.; Nkuimi Wandjou, J.; Sut, S.; et al. Hepatoprotective effects of standardized extracts from an ancient Italian apple variety (*Mela Rosa Dei Monti Sibillini*) against carbon tetrachloride (CCl₄)-Induced hepatotoxicity in Rats. *Molecules* 2020, 25, 1816. <https://doi.org/10.3390/molecules25081816>.
43. Liang, X.; Zhu, T.; Yang, S.; Li, X.; Song, B.; Wang, Y.; Lin, Q.; Cao, J. Analysis of phenolic components and related biological activities of 35 apple (*Malus Pumila* Mill.) cultivars. *Molecules* 2020, 25, 4153. <https://doi.org/10.3390/molecules25184153>.
44. Kim, I.; Ku, K.-H.; Jeong, M.-C.; Kwon, S.-I.; Lee, J. metabolite profiling and antioxidant activity of 10 new early- to mid-season apple cultivars and 14 traditional cultivars. *Antioxidants* 2020, 9, 443. <https://doi.org/10.3390/antiox9050443>.
45. Baron, G.; Ferrario, G.; Marinello, C.; Carini, M.; Morazzoni, P.; Aldini, G. Effect of extraction solvent and temperature on polyphenol profiles, antioxidant and anti-inflammatory effects of red grape skin by-product. *Molecules* 2021, 26, 5454. <https://doi.org/10.3390/molecules26185454>.
46. Della Vedova, L.; Ferrario, G.; Gado, F.; Altomare, A.; Carini, M.; Morazzoni, P.; Aldini, G.; Baron, G. Liquid chromatography–high-resolution mass spectrometry (LC-HRMS) profiling of commercial enocianina and evaluation of their antioxidant and anti-inflammatory activity. *Antioxidants* 2022, 11, 1187. <https://doi.org/10.3390/antiox11061187>.

47. Wen, X.; Thorne, G.; Hu, L.; Joy, M.S.; Aleksunes, L.M. Activation of NRF2 signaling in HEK293 Cells by a first-in-class direct KEAP1-NRF2 inhibitor. *J. Biochem. Mol. Toxicol.* 2015, 29, 261–6. <https://doi.org/10.1002/jbt.21693>.
48. Ong, S.-E.; Mann, M. A practical recipe for stable isotope labeling by amino acids in cell culture (SILAC). *Nat. Protoc.* 2006, 1, 2650–2660. <https://doi.org/10.1038/nprot.2006.427>.
49. Deng, J.; Erdjument-Bromage, H.; Neubert, T. Quantitative comparison of proteomes using SILAC. *Curr. Protoc. Protein Sci.* 2018, 95, e74. <https://doi.org/10.1002/cpps.74>.
50. Aiello, G.; Rescigno, F.; Meloni, M.; Baron, G.; Aldini, G.; Carini, M.; D'amato, A. Oxidative stress modulation by carnosine in scaffold free human dermis spheroids model: A proteomic study. *Int. J. Mol. Sci.* 2022, 23, 1468. <https://doi.org/10.3390/ijms23031468>.
51. Hulsen, T. BioVenn—An r and python package for the comparison and visualization of biological lists using area-proportional venn diagrams. *Data Sci.* 2021, 4, 51–61. <https://doi.org/10.3233/ds-210032>.
52. Wang, Y.; Vorsa, N.; Harrington, P.; Chen, P. Nontargeted metabolomic study on variation of phenolics in different cranberry cultivars using UPLC-IM-HRMS. *J. Agric. Food Chem.* 2018, 66, 12206–12216. <https://doi.org/10.1021/acs.jafc.8b05029>.
53. Jabeen, A.; Mesaik, M.A.; Simjee, S.U.; Lubna; Bano, S.; Faizi, S. Anti-TNF- α and anti-arthritis effect of patuletin: A rare flavonoid from *Tagetes patula*. *Int. Immunopharmacol.* 2016, 36, 232–240. <https://doi.org/10.1016/j.intimp.2016.04.034>.
54. Li, X.; Tian, Y.; Wang, T.; Lin, Q.; Feng, X.; Jiang, Q.; Liu, Y.; Chen, D. Role of the p-coumaroyl moiety in the antioxidant and cytoprotective effects of flavonoid glycosides: Comparison of astragaloside and tiliroside. *Molecules* 2017, 22, 1165. <https://doi.org/10.3390/molecules22071165>.
55. Sun, L.; Guo, Y.; Fu, C.; Li, J.; Li, Z. Simultaneous separation and purification of total polyphenols, chlorogenic acid and phlorizin from thinned young apples. *Food Chem.* 2013, 136, 1022–1029. <https://doi.org/10.1016/j.foodchem.2012.09.036>.
56. Wang, Y.; Gao, L.; Chen, J.; Li, Q.; Huo, L.; Wang, Y.; Wang, H.; Du, J. Pharmacological modulation of Nrf2/HO-1 signaling pathway as a therapeutic target of parkinson's disease. *Front. Pharmacol.* 2021, 12, 757161. <https://doi.org/10.3389/fphar.2021.757161>.
57. Sánchez-Rodríguez, R.; Torres-Mena, J.E.; Quintanar-Jurado, V.; Chagoya-Hazas, V.; Rojas del Castillo, E.; del Pozo Yauner, L.; Villa-Treviño, S.; Pérez-Carreón, J.I. Ptgr1 expression is regulated by NRF2 in rat hepatocarcinogenesis and promotes cell proliferation and resistance to oxidative stress. *Free Radic. Biol. Med.* 2017, 102, 87–99. <https://doi.org/10.1016/j.freeradbiomed.2016.11.027>.
58. Kerins, M.; Ooi, A. The roles of NRF2 in modulating cellular iron homeostasis. *Antioxid. Redox Signal.* 2018, 29, 1756–1773. <https://doi.org/10.1089/ars.2017.7176>.
59. Forman, H.; Davies, K.; Ursini, F. How do nutritional antioxidants really work: Nucleophilic tone and para-hormesis versus free radical scavenging in vivo. *Free Radic. Biol. Med.* 2014, 66, 24–35. <https://doi.org/10.1016/j.freeradbiomed.2013.05.045>.

60. Potter, G.; Patterson, L.; Wanogho, E.; Perry, P.; Butler, P.; Ijaz, T.; Ruparelia, K.; Lamb, J.; Farmer, P.; Stanley, L.; et al. The cancer preventative agent resveratrol is converted to the anticancer agent piceatannol by the cytochrome P450 enzyme CYP1B1. *Br. J. Cancer* 2002, 86, 774–778. <https://doi.org/10.1038/sj.bjc.6600197>.
61. Xie, Y.; Zhang, D.; Zhang, J.; Yuan, J. Metabolism, transport and drug–drug interactions of silymarin. *Molecules* 2019, 24, 3693. <https://doi.org/10.3390/molecules24203693>.
62. Wardyn, J.; Ponsford, A.; Sanderson, C. Dissecting molecular cross-talk between Nrf2 and NF-KB response pathways. *Biochem. Soc. Trans.* 2015, 43, 621–626. <https://doi.org/10.1042/bst20150014>.
63. Ahmed, S.; Luo, L.; Namani, A.; Wang, X.; Tang, X. Nrf2 Signaling pathway: Pivotal roles in inflammation. *Biochim. Biophys. Acta. Mol. Basis. Dis.* 2017, 1863, 585–597. <https://doi.org/10.1016/j.bbadis.2016.11.005>.
64. Biswas, S.K. Does the interdependence between oxidative stress and inflammation explain the antioxidant paradox? *Oxid. Med. Cell. Longev.* 2016, 2016, 7432797. doi:doi.org/10.1155/2016/5698931.
65. Lee, T.-S.; Chau, L.-Y. Heme Oxygenase-1 mediates the anti-inflammatory effect of interleukin-10 in mice. *Nat. Med.* 2002, 8, 240–246. <https://doi.org/10.1038/nm0302-240>.
66. Vijayan, V.; Wagener, F.; Immenschuh, S. The macrophage heme-heme Oxygenase-1 system and its role in inflammation. *Biochem. Pharmacol.* 2018, 153, 159–167. <https://doi.org/10.1016/j.bcp.2018.02.010>.
67. Campbell, N.; Fitzgerald, H.; Dunne, A. Regulation of inflammation by the antioxidant haem oxygenase 1. *Nat. Rev. Immunol.* 2021, 21, 411–425. <https://doi.org/10.1038/s41577-020-00491-x>.
68. Che, J.; Yang, J.; Zhao, B.; Shang, P. HO-1: A new potential therapeutic target to combat osteoporosis. *Eur. J. Pharmacol.* 2021, 906, 174219. <https://doi.org/10.1016/j.ejphar.2021.174219>.
69. Chau, L.-Y. Heme Oxygenase-1: Emerging target of cancer therapy. *J. Biomed. Sci.* 2015, 22, 22. <https://doi.org/10.1186/s12929-015-0128-0>.
70. Bolisetty, S.; Zarjou, A.; Agarwal, A. Heme Oxygenase 1 as a therapeutic target in acute kidney injury. *Am. J. Kidney Dis.* 2017, 69, 531–545. <https://doi.org/10.1053/j.ajkd.2016.10.037>.
71. Tang, Z.; Ju, Y.; Dai, X.; Ni, N.; Liu, Y.; Zhang, D.; Gao, H.; Sun, H.; Zhang, J.; Gu, P. HO-1-Mediated ferroptosis as a target for protection against retinal pigment epithelium degeneration. *Redox Biol.* 2021, 43, 101971. <https://doi.org/10.1016/j.redox.2021.101971>.
72. Alam, J.; Cook, J. How many transcription factors does it take to turn on the heme Oxygenase-1 gene? *Am. J. Respir. Cell Mol. Biol.* 2007, 36, 166–174. <https://doi.org/10.1165/rcmb.2006-0340tr>.

8. Supplementary materials

Table S1 - Compounds identified by LC -HRMS in negative and positive ion modes with the targeted method ordered on the basis of the retention time.

Peak	Compound name	RT	[M-H] ⁻ _{exp}	Δ ppm	MS/MS	[M+H] ⁺ _{exp}	Δ ppm	MS/MS
<i>Organic and phenolic acids</i>								
1	Citric acid	2.3	191.01979	0.606	173	-		
2	Protocatechuic acid glucoside	2.7	315.07196	0.286	153-109	-		
3	Caffeoylquinic acid isomer 1	3.5	353.08673	0.006	135-179-191	-		
3	Protocatechuic acid	3.7	153.01971	0.962	109	-		
3	Glutathionyl chlorogenic acid	3.8	658.15118	-0.641	529-466-385- 272-193-191	660.16360	-3.211	642-585-531- 264
3	Caffeoyl glucoside isomer 1	3.8	341.08752	0.238	179-251	-		
3	Caffeoyl glucoside isomer 2	4.3	341.08716	0.133	179-251-281	343.10120	-3.323	-
4	Coumaroylquinic acid isomer 1	5.2	337.09229	0.147	119-163-191	339.10730	-0.383	147
4	Caffeoyl glucoside isomer 3	5.2	341.08660	-0.032	179-251-281	343.10110	-3.614	-
4	Caffeoylquinic acid isomer 2	5.7	353.08649	-0.062	135-179-191	355.10245	-1.239	163
5	<i>p</i> -Coumaric acid- <i>O</i> -glucoside isomer 1	6.0	325.09265	0.264	119-163	-		
5	<i>p</i> -Coumaric acid- <i>O</i> -glucoside isomer 2	6.9	325.09265	0.264	119-163-145	327.10760	1.253	-
6	Caffeic acid	7.6	179.03577	1.052	135	181.04961	-2.541	163
6	Ferulic acid- <i>O</i> -glucoside isomer 1	7.8	355.10263	0.077	193-235	357.11800	2.324	-
7	<i>p</i> -Coumaric acid- <i>O</i> -glucoside isomer 3	8.3	325.09216	0.113	119-163	327.10750	0.948	309-165-147
8	Ferulic acid- <i>O</i> -glucoside isomer 2	9.1	355.10278	0.119	295-265-235-193	357.11790	2.044	339-177
8	Coumaroylquinic acid isomer 2	9.4	337.09229	0.147	163-173	339.10720	-0.678	147
9	Ferulic acid- <i>O</i> -glucoside isomer 3	10.8	355.10284	0.136	295-265-235-193	357.11810	2.604	339-177
12	<i>p</i> -Coumaric Acid	13.1	163.04041	0.882	119	165.05453	-3.756	147
28	Dicaffeoylquinic acid	29.3	515.11853	0.025	179-191-353	517.13320	0.251	-

Flavanols								
4	Catechin	5.4	289.07153	0.299	245-205-271-179 5	291.08636	-1.649	273-165-151- 139-123
5	Procyanidin B2	6.9	577.13354	-0.088	289-407-425- 451-559	579.14850	-2.987	427-409-291
7	Epicatechin	8.7	289.07144	0.268	245-205-179	291.08643	-1.409	273-165-151- 139-123
10	Procyanidin trimer	11.0	865.19183	-0.648	449-577-695	867.21295	-0.773	715-577-289
12	Procyanidin tetramer	12.9	1153.25208	-0.758	577-739-1135	1155.27502	-1.723	-
13	Procyanidin trimer	13.8	865.19556	-0.217	407-577-695			
14	Procyanidin pentamer	15.1	-			1443.33911	-0.887	-
14	Procyanidin hexamer	15.1	-			866.20331 [M+2H] ²⁺	-4.237	-
17	Procyanidin heptamer	19.0	-			1010.23633 [M+2H] ²⁺	-2.323	-
19	Procyanidin octamer	20.4	-			1154.26868 [M+2H] ²⁺	-1.455	-
21	Procyanidin nonamer	21.5	-			1298.29871 [M+2H] ²⁺	-2.582	-
Flavanones								
15	Naringenin glucoside (prunin)	17.0	433.11041	-0.580	271	435.12848	-1.425	-
18	Eriodictyol-hexoside	20.1	449.10785	0.003	287	451.12317	-1.884	289
30	Naringin (Naringenin 7-O- neohesperidoside)	30.7	-			581.18567	-2.306	435-273
34	Eriodictyol	42.9	287.05579	0.270	151-135	289.07101	-0.657	-
38	Naringenin	53.1	271.06076	0.243	151-177	273.07584	-1.611	-
Flavonols								
16	Kaempferol-glucoside	18.9	447.09161	-0.129	285	449.10751	-1.915	287
20	Quercetin-3-O-glucoside	21.0	463.08673	-0.080	301	465.10236	-1.978	303
22	Quercetin-3-O-galactoside	22.5	463.08694	-0.035	301	465.10211	-2.516	303
24	Quercetin pentoside isomer 1	24.8	433.07687	0.079	301	435.09180	-2.114	303
26	Quercetin pentoside isomer 2	28.0	433.07675	0.051	301	435.09171	-2.321	303

28	Quercetin pentoside isomer 3	29.0	433.07715	0.143	301	435.09186	-1.977	303
29	Quercetin-3-O-rhamnoside	29.8	447.09262	0.097	301	449.10730	-2.382	303
35	Quercetin	48.0	301.03476	0.159	151-179-232-273	303.04999	-1.551	285-257-229-165-153-137
40	Kaempferol	54.7	285.04013	0.268	155	287.05511	-1.533	-
40	Isorhamnetin	54.7	315.05054	0.194	300	317.06567	-1.388	302
<i>Dihydrochalcones</i>								
27	Phloretin-O-xyloglucoside isomer 1	28.8	567.17010	-0.128	273-167	569.18561	-2.460	437-419-275
29	Phloretin-O-xyloglucoside isomer 2	30.0	567.17072	-0.019	273-167	569.18579	-2.143	437-275
31	Phlorizin	35.0	435.12845	-0.152	273	437.14401	-1.693	275
39	Phloretin	54.1	273.07593	0.066	167	275.09190	-0.109	169-149-127-107
<i>Flavones</i>								
36	Luteolin	49.1	285.04013	0.268	151-175-199-217-241	287.05527	-0.975	269-245-153
<i>Triterpenoids</i>								
44	Euscaphic acid	65.0	487.34171	-0.127	-	489.35681	-2.370	471-453-443-425-407

Table S2 - Compounds putatively identified by LC -HRMS in negative and positive ion modes with the untargeted method ordered on the basis of the retention time.

Peak	Compound name	RT	[M-H] ⁻ _{exp}	Δ ppm	MS/MS	[M+H] ⁺ _{exp}	Δ ppm	MS/MS	Identificati on strategy
<i>Organic and phenolic acids</i>									
11	3-(benzoyloxy)-2-hydroxypropyl glucopyranosiduronic acid	11.8	371.09741	0.037	249-121	373.11310	0.509	-	[68]
13	Sinapoyl hexoside	13.9	385.11290	-0.006	267-249				[69]
37	3-[2,4,5-trihydroxy-3-(3-methylbut-2-en-1-yl) phenyl] propanoic acid	51.8	265.10748	0.163	247-221-203-177-151-87	267.12290	0.824	249-221	[27]
<i>Dihydrochalcones</i>									
25	Hydroxyphloretin glucoside	26.2	451.12428	0.176	433-313-289	453.13900	-0.265	435-291-235-165	FooDB
<i>Flavonols</i>									
20	Patuletin hexoside isomer 1	20.8	493.09738	-0.058	316-331	495.11260	-1.414	333	PubChem
22	Patuletin hexoside isomer 2	22.5	493.09698	-0.139	316-331	495.11270	-1.212	333	PubChem
23	Patuletin hexoside isomer 3	23.8	493.09747	-0.040	316-331	495.11240	-1.818	333	PubChem
27	Patuletin pentoside	28.4	463.08682	-0.179	331-316-209-181	465.10200	-1.591	333	Patuletin fragment and loss of a pentoside (-132 Da)
29	Patuletin rhamnoside	30.0	477.10352	0.161	316-331	479.11740	-2.066	333	Patuletin fragment and loss of a rhamnoside (-146 Da)
32	Isorhamnetin rhamnoside	38.5	461.10745	-0.084	315-300	463.12300	-1.015	317	Isorhamnetin fragment and loss of a rhamnoside (-146 Da)

33	Kaempferol rhamnoside	39.1	431.09695	- 0.075	285	433.1128 0	-0.254	287	Kaempferol fragment and loss of a rhamnoside (-146 Da)
36	Methoxyquercetin (patuletin)	49.3	331.04520	0.107	316-209	333.0611 0	1.862	318	HMDB
37	Quercetin 3-(3- <i>p</i> - coumaroylglucoside)	52.1	609.12440	0.085	301	611.1389 0	-0.998	303	HMDB
Flavanones									
38	Eriodictyol 7-(6- <i>trans-p</i> - coumaroylglucoside)	53.5	595.14441	- 0.034	287-307-459- 449	597.1594 0	-1.423	579-331- 289	CFM-ID
Lipids									
42	(10E,15Z)-9,12,13- Trihydroxy-10,15- octadecadienoic acid	55.7	327.21707	0.146	171-229-291- 211	351.2141 4 [M+Na] ⁺	-1.680	333-315- 235	mzCloud
43	Trihydroxy-octadecenoic acid	57.2	329.23251	0.082	293-229-211- 183-171	353.2296 4 [M+Na] ⁺	-2.095	335-317- 235	mzCloud

Study 2 - Thinned apple polyphenols alleviate inflammation in a mouse model of DNBS-induced colitis: label-free quantitative proteomics studies.

1. Abstract

Ulcerative colitis (UC), one of the major inflammatory bowel diseases (IBDs), is a complex and multifactorial disease whose incidence rate has significantly increased in recent decades. Current available drug therapies, including Nonsteroidal anti-inflammatory drugs (NSAIDs) and corticosteroids, partially relieve the symptoms but are associated with nonnegligible side effects. Hence, the search for new therapeutic strategies that counteract inflammation with reduced side effects is still a medical need. Since oxidative stress and inflammation contribute to tissue damage during colitis, the administration of natural compounds with antioxidant and anti-inflammatory activity represents a promising treatment for UC. We recently identified thinned apples (TA), a waste-product of the apple production chain, as a valuable source of polyphenols (TAP) acting as anti-inflammatory and antioxidant agents in a cell model of inflammation. The aim of the present work is to evaluate the therapeutic potential of TAP in a mouse model of DNBS induced colitis. Using state of the art label-free proteomic techniques (LFQ) we performed *ex vivo* studies to describe at the molecular level the pathological phenotype and the proteins modulated following treatment with the TAP extract. Overall, proteomics studies allowed the identification of 5400 proteins and delineated the molecular pathways evoked by TAP treatment. This approach confirmed the usefulness of the chosen method to induce a pathological state, characterized by immune cells infiltration and showed an overall state of inflammation and oxidative stress. On the other hand, TAP treatment highlighted: (i) activation of antioxidant-acting mechanisms; (ii) reversal of mechanisms overexpressed/activated in the presence of DNBS, with particular reference to mechanisms of ferroptosis and heme-toxicity; (iii) inhibition of the immune response; (iv) reduced ulcerative condition with a consequent downregulation of proteins involved in the coagulation, inflammation and angiogenesis processes. These results suggest that TAP can be considered a valuable source of polyphenols for health care products to prevent/treat oxidative and inflammatory chronic conditions in UC; moreover, TA represent an innovative source for the industrial production of bioactive extract.

2. Introduction

Inflammatory bowel disease (IBD) is a term used to refer to a pathological condition characterized by chronic inflammation of the gastrointestinal (GI) tract. Ulcerative colitis (UC), one of the main IBDs, which specifically affects the colon, is a complex, multifactorial disorder whose incidence rate has increased significantly in recent decades [1]; related symptoms greatly impact patients' quality of life, alternating between periods of remission and periods of exacerbation. Although the etiology is still unclear, the most accepted hypothesis involves defects in tight junctions leading to altered intestinal permeability, and thus resulting in increased entry of antigens into the luminal space contributing to intestinal inflammation.

Currently available drug therapies represent symptomatic treatments, with the goal of keeping the patient in a state of remission to avoid flare-ups. Aminosalicylates and corticosteroids, although they succeed in partially relieving the symptoms of the disease and are associated with nonnegligible side effects, to date are considered the first line of treatment for UC. Recently, biologics are being used to treat people with moderate to severe ulcerative colitis, mainly monoclonal antibodies directed against specific mediators of inflammation, such as TNF-alpha (Infliximab). Despite their proven efficacy, the prescription of biologics treatment is limited by the strict criteria for patient eligibility established by AIFA due to high manufacturing costs. Hence the interest in finding new therapeutic strategies that counteract intestinal inflammation as effectively but with reduced side effects, which remains a medical need. Since oxidative stress and inflammation contribute to UC tissue damage, the use of natural compounds with antioxidant and anti-inflammatory activity has recently been proposed as a treatment for IBDs [2].

Natural extracts, mostly from readily available plants or, even, from agro-food waste materials, have been considered a valuable source of bioactive molecules for centuries and have been recently widely re-evaluated by the pharmaceutical industry, especially considering that polyphenols have been shown to be effective for gut health in both animal models and humans [3,4].

Specifically, it has been reported that certain phytoconstituents are able to target two closely related systems within the cell, namely the NRF2/ARE and NF- κ B pathways [5,6]. While NRF2/ARE pathway, as a central defense mechanism against oxidative stress, controls the expression of many antioxidant genes in the nucleus (antioxidants response elements, ARE), thus playing a crucial role in the treatment of ulcerative colitis [7], NF- κ B is the main effector

pathway involved in inflammation; its activation is markedly induced in patients with IBD and, by promoting the expression of various pro-inflammatory genes, NF- κ B strongly influences the course of mucosal inflammation [8].

Apples, for instance, are a rich source of phytochemicals, particularly polyphenols, which can act as NRF2 inducers due to their chemical structure; special attention should be paid to the 1,2-diphenols present in apples and their derivative products (e.g. quercetin and its glycosides, procyanidins and their monomers catechin and epicatechin, and chlorogenic acid), which when oxidized to their more reactive quinone form could interact with cysteine residues of the KEAP1 regulatory protein, promoting detachment from NRF2, free to translocate into the nucleus and activate transcription of ARE genes. Contextually, increasing experimental evidence suggests the possibility of controlling and reducing a state of inflammation through the activity of apple phytochemicals capable of inhibiting the NF- κ B pathway [9]. Overall, the efficacy of apple polyphenols in inhibiting microbial dysbiosis, chronic inflammation, and modulating intestinal permeability suggests potential use as dietary supplements to improve gut health.

In this regard, thinned apples, can be considered an interesting source of polyphenols due to their anti-inflammatory and antioxidant potential, as demonstrated by the work previously illustrated in this thesis' chapter. The crucial results gathered from the *in vitro* studies laid a solid background for subsequent *ex-vivo* studies aimed at evaluating the therapeutic potential of orally administered thinned apple polyphenolic extract (TAP) in an animal model of UC (DNBS-induced UC). Besides macroscopic and microscopic assessment of the extent of tissue damage (on explanted colon) upon TAP treatment, using state-of-the-art techniques in the field of proteomics, functional studies were performed to describe at the molecular level the distinctive biological processes of the pathological phenotype, as well as to understand the molecular pathways evoked by TAP extract to effectively limit the inflammatory state.

Even though there is general knowledge of the potential targets of these compounds, omics approaches could better illustrate the biological impact of the extract and identify the most relevant phytochemical compounds. Combining the use of these advanced analytical strategies with a circular economy concept to valorize industrial waste products could reduce the impact of cultivation on waste production, minimizing disposal problems while obtaining a potential source of bioactive compounds. This work specifically could help in promoting the use of thinned apples as a valuable source of apple polyphenols to be used in health care products to prevent/treat oxidative and inflammatory chronic conditions.

3. Material and Methods

3.1. Reagents

Purified and sterilized bi-distilled water with the Milli-Q system (Millipore, Bedford, MA, USA) was used to prepare the *buffers* or for other applications that required it. The following reagents were used for tissue homogenisation: SDS (sodium dodecyl sulphate), supplied by Bio-Rad (Hercules, CA, USA), NaCl (sodium chloride) and MgCl₂ (magnesium chloride), from Fluka Chemical (Ronkonkoma, New York), TEAB (triethylammonium bromide) and *Benzonase Nuclease*, purchased from Sigma-Aldrich (Milan, Italy) and, finally, cOmplete protease inhibitor *cocktail*, purchased from Roche Diagnostics GmbH (Mannheim, Germany). For the quantification of protein samples, a BCA assay was performed according to the manufacturer's protocol (Thermo Fisher Scientific™, USA). For the proteolytic digestion of protein extracts, solutions containing TCEP (tris(2-carboxyethyl) phosphine), IAA (iodoacetamide) and AMBIC (ammonium bicarbonate) supplied by the company Sigma-Aldrich (Milan, Italy) were prepared; other reagents used during proteolytic digestion are: H₃PO₄ (phosphoric acid, Fluka Chemical™, Ronkonkoma, New York), MeOH (methanol, Sigma-Aldrich™) and TEAB (see above), while *trypsin (sequencing-grade trypsin, Roche)* was chosen as the proteolytic enzyme. The ultrapure formic acid (FA) and acetonitrile (ACN) used in the LC-MS analysis were supplied by Sigma-Aldrich (Milan, Italy). The thinned apple polyphenols extract (TAP) whose anti-inflammatory activity was requested for possible future commercialization was supplied by the company Plantex Research Srl (Milan, Italy), with whom a scientific collaboration is ongoing.

3.2. Animal model

3.2.1. General characteristics

Male CD1 mice (25 g; Envigo, Milan, Italy) were housed in a well-ordered locality (room 22 ± 1 °C 12-h dark/light cycles) with ordinary rodent chow and water. Messina University Review Board for the animal care endorsed the research. All animal experiments agree with the new Italian regulations (D.Lgs 2014/26), EU regulations (EU Directive 2010/63).

3.2.2. Induction of colitis, treatment with TAP and colon sampling

Colitis was provoked in mice by an intrarectally injection of DNBS. Briefly, isoflurane anesthetized mice. DNBS (4 mg in 100 µl of 50% ethanol per mouse) was instilled into the rectum within a catheter introduced 4.5 cm proximally to the anus. Thereafter, the animals

were kept for 15 min in a Trendelenburg position to avoid reflux. On day 4 after DNBS injection, the animals were weighed and sacrificed, the abdomen opened by a midline cut. The colon was removed and freed from surrounding tissues, opened along the antimesenteric border, washed, weighed and processed for histological and biochemical studies. During sacrifice, the colon length (starting above the anus to the top of the cecum), was measured in cm.

3.3. Experimental design

Animals were randomly divided into several groups (n=6 for each group) (figure 1):

1. Sham + vehicle group: vehicle alone (100 ul of 50% ethanol) was administered intrarectally in control (sham) instead of DNBS and treated orally with saline by oral gavage for 4 days.
2. DNBS + vehicle group: mice were subjected to DNBS administration described as above, and saline was administered by oral gavage every 24 h, for 4 days, starting from 1 h after the administration of DNBS.
3. DNBS + TAP (10 mg/kg) group: mice were subjected to DNBS administration described as above, and Meline (10 mg/kg) was administered by oral gavage every 24 h, for 4 days starting from 1 h after the administration of DNBS.

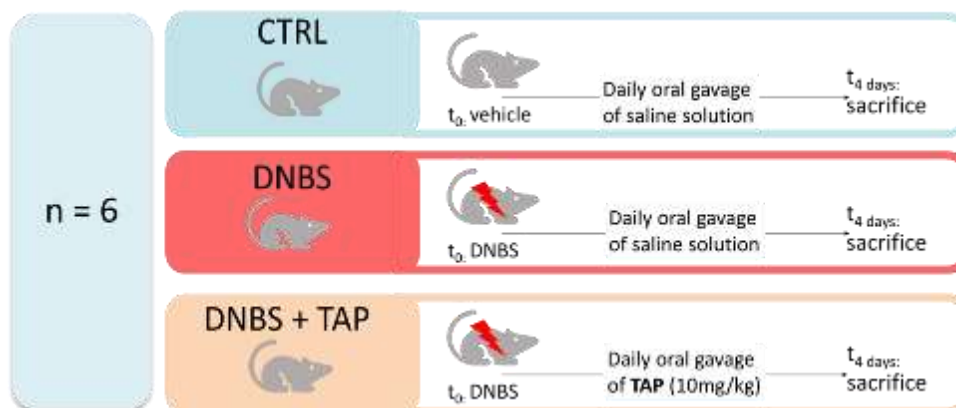


Figure 12 - Animal treatment scheme.

3.4. Assessment of tissue damage

3.4.1. Evaluation of colon damage

After its removal, the total colon was softly washed with saline, opened by a longitudinal incision, and examined under a microscope. Macroscopic damage score was

evaluated and scored by two independent observers. 0, no injury; 1, limited hyperemia without ulcers; 2, linear ulcers and no important inflammation; 3, linear ulcers with one site of inflammation; 4, two or more sites of inflammation with ulceration covering > 1 cm along the length of the colon; and 5–8, additional one point for each centimeter of ulceration beyond an initial 2 cm.

3.4.2. *Histological examination*

For histological analysis, tissues were collected, fixed in 10% of buffered formalin phosphate, embedded in paraffin sectioned and subjected to haematoxylin and eosin staining. The degree of histological damage of the colon sections was scored semiquantitatively from 0 to 4 as described. In particular, (0, no indication of inflammation; 1, very little level of inflammation; 2, little level of leucocytes infiltration; 3, elevated level of leucocytes infiltration, elevated vascular density, colon wall thickening; 4, loss of goblet cells, transmural infiltration elevated vascular density and colon wall thickening). Five H&E stained sections from each mouse were scored in a blinded fashion, using a Leica DM6 microscope (Leica Microsystems SpA, Milan, Italy) associated with Leica LAS X Navigator software (Leica Microsystems SpA, Milan, Italy).

3.4.3. *Myeloperoxidase assay*

Neutrophil infiltration in the colon was monitored by measuring tissue myeloperoxidase (MPO) activity using a spectrophotometric assay with tetramethylbenzidine as substrate. At the specified time following the intracolonic injection of DNBS, colon tissues were obtained and weighed. Each piece of tissue was homogenized in a solution containing 0.5% hexa-decyl-trimethyl-ammonium bromide dissolved in 10 mM potassium phosphate buffer pH 7 and centrifuged for 30 min at 20,000 g at 4 C. An aliquot of the supernatant was then allowed to react with a solution of 1.6 mM tetramethylbenzidine and 0.1 mM H₂O₂. The rate of change in absorbance was measured spectrophotometrically at 650 nm. MPO activity was defined as the quantity of enzyme degrading 1 mmol of peroxide per min at 37 C° and was expressed in U/g wet tissue.

3.5. Label-Free Quantitative Proteomics (LFQ)

Figure 2 shows the schematic representation of the experimental workflow optimized for the quantitative proteomic study.

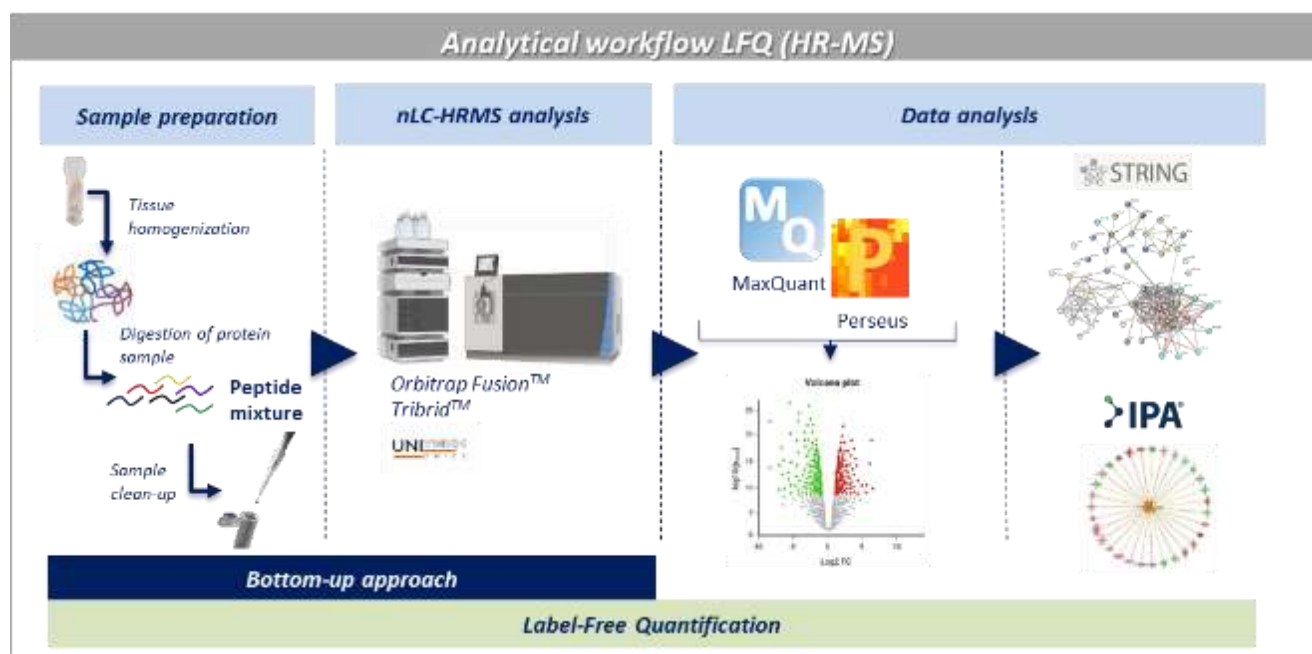


Figure 13 - Schematic representation of the experimental set-up.

3.5.1. Tissue homogenization

The process of tissue homogenization requires an appropriate harsh lysis buffer, suitable for dissolving difficult-to-solubilize proteins and compatible with S-Trap devices, which are later used for protein digestion: SDS 5%, TEAB 50 mM, NaCl 50 mM, MgCl₂ 5 mM, *Benzonase Nuclease* 500 U/mL, of *cOmplete cocktail* (1 tablet/10 mL). A high energy benchtop homogenizer (BeadBug microtube homogenizer) compatible with low working temperatures (4°C) was used to promote a rapid tissue disruption through constant high velocity impact from the hardened micro-beads chosen specifically for colon samples, namely Zirconium Bead 1.5 mm. Once the weight of the tissue portions collected for each sample was noted, they were transferred into beads pre-filled homogenizer tubes, together with a volume of 500 µl of *lysis buffer* (about 10% w/v). Four cycles of shaking/homogenization were conducted at 4000 rpm for two minutes each; if significant tissue residues were evident, an additional volume of 100 µl of lysis buffer was added and two cycles of homogenization were performed under the same conditions. Samples were then centrifuged at 10,000 rpm for 10 minutes at 4°C, and the

supernatant from each sample transferred into a new Eppendorf and stored at -80°C until the next sample processing step.

3.5.2. *Sample Preparation - Proteolytic digestion using spin-column S-TRAP*

Protein concentration was assessed for each sample using the BCA kit (provided by Sigma-Aldrich) according to the manufacturer instructions, and 30 µg of protein extract were processed through tryptic digestion using the S-Trap spin-columns (Protifi, Huntington, New York, USA). These are disposable spin columns packed with a resin that guarantees (i) excellent enzyme hydrolysis yield as it physically confines the proteins into the pores of the resin, thus forcing the interaction of the enzyme with their well-exposed cleavage sites, and (ii) removal of reagents or impurities from the digestion process (clean-up process). The collected peptic mixtures obtained according to the procedure reported in the Chapter 2 – Study 1 of this thesis were then dried under vacuum in the SpeedVac (Eppendorf s.r.l.) at a working temperature of 37°C, and stored at -80°C until analysis.

3.5.3. *nLC-HRMS analysis: Orbitrap Fusion Tribrid Mass Spectrometer*

The nLC-HRMS (*nano Liquid Chromatography-High Resolution Mass Spectrometry*) method, finely optimized and widely used in our laboratories, involves the use of an analytical platform consisting of a Dionex Ultimate 3000 nano-LC chromatograph (Sunnyvale, California, USA), coupled to the OrbitrapFusion Tribrid high-resolution mass spectrometer (Thermo Scientific, Bremen, Germany). Each sample was analyzed as reported in Chapter 2 – Study 1 of this thesis, three times (3 technical replicates), and between each run, stationary phase washes were carried out by injecting 100% ACN to prevent the so-called carry-over.

3.6. **Data Analysis**

3.6.1. *Max Quant and Perseus*

The acquired experimental data were analyzed by means of MaxQuant v.1.6.0 (Max Planck Institute of Biochemistry, Germany), a bioinformatics software designed for quantitative proteomics studies. The Andromeda search engine, implemented within the software itself, allows identification of proteins by searching a database, namely that of *Mus musculus* (Taxonomy ID: 10090). Only unique and razor peptides were considered for quantification, employing the MaxLFQ algorithm (version 1.6.2.3, Max Planck Institute of Biochemistry, Martinsried, Germany). To guarantee accurate identification and quantification of the protein

mixtures under investigation, some input information related to the sample preparation method had to be provided to the software: the type of protease used (trypsin) and the maximum number of missed cleavages (two) allowed were specified, as well as activating the match-between-run option, useful for increasing the number of identified peptides and thus the coverage of the proteome in question. A tolerance limit of 5 ppm was set for the identification of precursor ions, consistent with the performance of high-resolution instruments. Finally, chemical modifications of some amino acid residues due to sample processing were included in the input: carbamidomethylation of the thiol groups of cysteines as a fixed/static modification; particularly frequent variable modifications were, however, oxidation of methionine and acetylation at the N-terminus of the protein. For statistical analyses the Perseus software was used (version 1.6.1. 43; Max Planck Institute of Biochemistry, Martinsried, Germany). LFQ intensities values were first converted to a base-two logarithmic scale and then filtered for significance (Benjamini-Hochberg corrected two-sample t-test with a threshold value of 0.05 False Discovery Rate - FDR). Three comparison matrices were then constructed for calculating \log_2 Fold-Change values (or difference or ratio). As a method of visualizing the results, graphical representations known as Volcano Plots were used. The information about significantly up- and down-regulated proteins was then used to study the modulated pathways in the different experimental groups; a functional investigation was then conducted using two dedicated bioinformatics software: STRING v.1.7.0 and Ingenuity Pathways Analysis (IPA) (QIAGEN Aarhus Prismet, Denmark, September 2021).

3.6.2. *STRING*

STRING is an easy-to-use, open-access software built on a database that collects and integrates all information related to known and/or predicted protein-protein interactions in silico. The ultimate goal is to build protein-protein interaction networks, consisting of interactions that can be direct (physical) or indirect (functional). In the former case, there is a physical contact between two proteins, a biochemical interaction, while in the latter case, the proteins may not even interact physically, but participate jointly in the same biological function (a catabolic process, a pathway for the synthesis of a certain substance, etc.). For each experimental condition tested, two macro-networks of interaction were built by setting STRING on the *Mus musculus* database, with the default value of 0.4 as the confidence level (cut-off): one concerning the significantly over-expressed proteins, with a \log_2 Fold-Change > 0.50, and a second network comprising the significantly down-regulated proteins, associated with a \log_2 Fold-Change < -0.50. It should be emphasized that the STRING algorithm does not allow us to

produce any quantitative assessment, so this is simply a matter of grouping the significantly down-modulated proteins into functional subnetworks to begin to highlight the cellular pathways involved in the experimental condition we are studying.

3.6.3. *Ingenuity Pathway Analysis (IPA)*

Ingenuity Pathway Analysis (IPA) is a bioinformatics software designed for the functional interpretation of data produced by quantitative proteomics studies. It relies on the use of the Gene Ontology (GO) Knowledge base and complex computational algorithms based on network analysis to predict how up-regulated and down-regulated protein interactions, in a given experimental model, synergistically affect specific cellular pathways by activating or inhibiting them. Each *in silico* generated activation/inhibition hypothesis is associated with score values indicative of the goodness of prediction, namely the Z (Z-SCORE): a Z-SCORE value ≥ 2.00 indicates a significant prediction of activation/induction of a specific pathway, while Z-SCORE ≤ -2.00 indicates significant inactivation/inhibition. This information is represented graphically according to a specific color code used to indicate how the modulation of a specific gene set may affect the outcome of a specific cellular pathway: based on the up (red)/down (green) regulation of specific gene products involved in a given network, it will be potentially activated (red-orange) or inhibited (blue). As input, the operator had to build a complex matrix that includes, for each experimental condition, the \log_2 Fold-Change values of significantly up-regulated and down-regulated proteins (\log_2 Fold-Change ≥ 0.50 and ≤ -0.50), and the corresponding p-values ≤ 0.05 . In conclusion, unlike STRING, IPA provides a more realistic view of the phenotypic pattern under investigation because the hypotheses generated are weighted according to the magnitude and direction of change in the expression of a protein or set of them.

4. Results and Discussion

4.1. *Assessment of the animal's state of health*

The evidence collected from macroscopic and histological evaluations indicates an overall enhancement in the health status of the animal after TAP administration, commencing with the assessment of the animal's body weight variation (Figure 3, Panel B). Pathological damage induced by DNBS promotes a reduction in body weight, while in the TAP-treated group, a reversal of this trend is observed, with a modest increase in body weight on day 4, albeit less pronounced than the control group. Photographic documentation in Figure 3 reveals no histological alterations in the control colon (Figure 3, Panel A, and histological scores in Panel D). The control colon also exhibits a lower thickness compared to the other two experimental groups. Its coloration does not suggest the presence of hemorrhagic states or ongoing angiogenic processes, characteristic of chronic inflammatory conditions. In contrast, the organs of mice treated exclusively with DNBS exhibit a noticeable change in color (Figure 3, Panel A), shifting towards a reddish hue, indicating an excessive presence of blood. The surface is smoother, and the irregularities caused by the colon's pockets are barely discernible. Furthermore, examination of the longitudinal section (Figure 3, Panel A, lower portion) reveals a clear and evident presence of an ulcerative and necrotic zone near the rectum. The colon derived from animals subjected to TAP treatment exhibits characteristics intermediate between the control condition and the pathological phenotype. As evident from the longitudinal section (Figure 3, Panel A, lower portion), the ulcerative zone is less visible, and the coloration indicates a reduction in blood flow to the tissues, comparable to a reduction of the inflamed state.

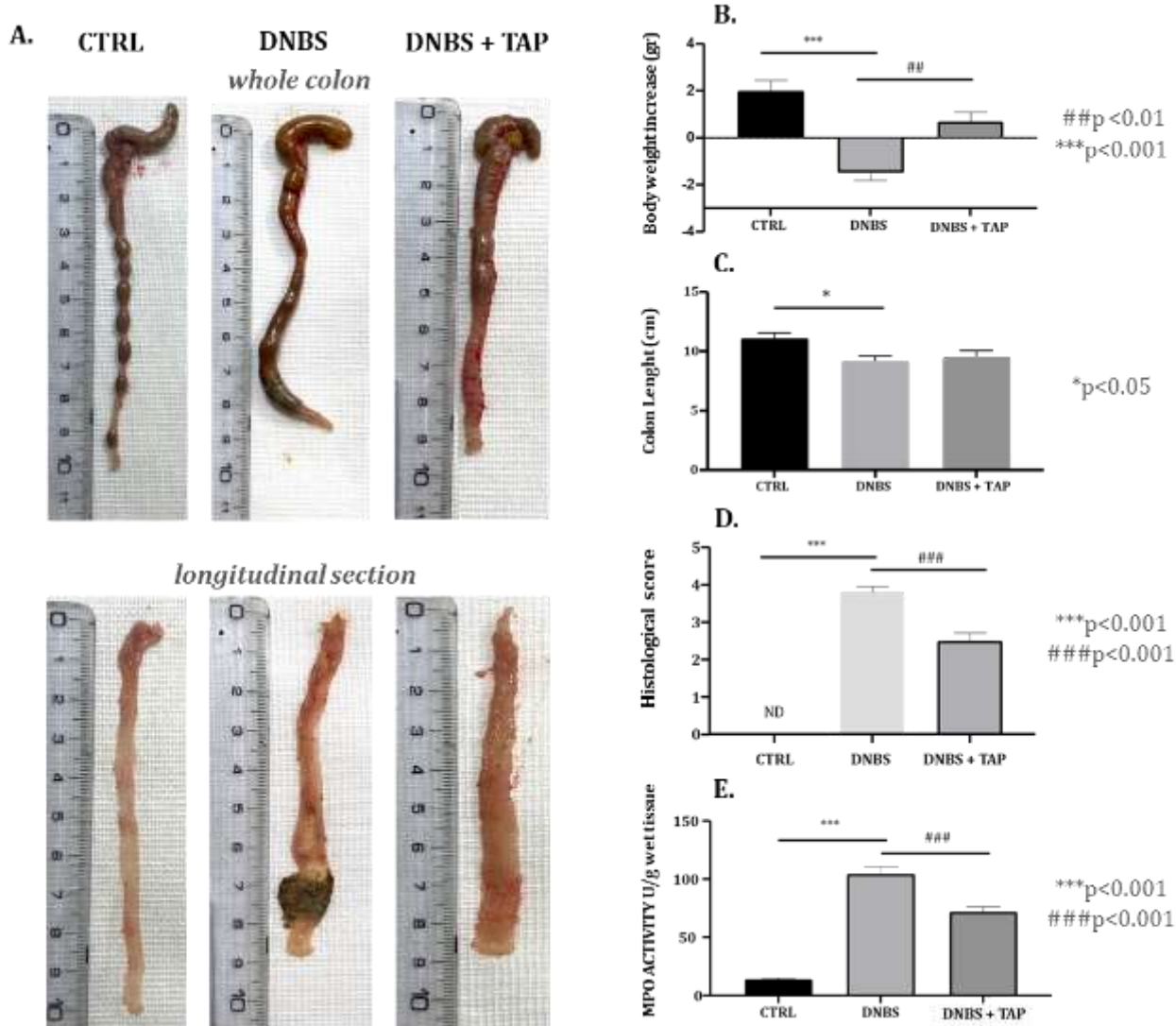


Figure 14 - A) Photographic documentation of three colons representative of the experimental groups: from left to right, CTRL, DNBS and DNBS + TAP respectively. Above are the images of intact colons, immediately after removal and cleaning of surrounding tissue, while the bottom part shows the longitudinal sections. **B)** Graphical representation of the average body weight variation values recorded for animals in the CTRL, DNBS and DNBS +TAP experimental groups. **C)** Representation of mean colon length value for animals belonging to the CTRL, DNBS and DNBS+ TAP experimental groups. **D)** Representation of data concerning the mean score assigned for the macroscopic assessment of DNBS-induced damage reported by animals belonging to CTRL, DNBS and DNBS + TAP experimental groups. **E)** Comparison of average U/g_{wet} tissue values indicative of myeloperoxidase activity calculated on tissue portions (CTRL, DNBS and DNBS_TAP) according to the method reported by Mullane et al. [10].

4.1.1. Evaluation of the activation of the immune response (myeloperoxidase assay)

The myeloperoxidase assay (expressed in neutrophils) provides a quantitative measure of the degree of immune response activation because the extent of this enzyme's activation is proportional to the recruitment of neutrophils, immune system agents. The results (Figure 3, Panel E) illustrate that in a control condition, there is a low residual activity of neutrophils, which increases significantly following the initiation of inflammation, as inferred from the increase in MPO activity value recorded for the DNBS experimental group. TAP administration again reduces enzyme activity, these results are aligned with the hypothesis that the anti-inflammatory activity of apple polyphenols is related to a downsizing of the immune response, an effect attributable to a partial improvement in the inflammatory state.

4.2. Quantitative proteomics (LFQ)

4.2.1. Data elaboration and overall analysis

Three comparison matrices were built, each analyzing differences in the expression of individual gene products (\log_2 Fold-Change or $\log_2 FC$) in two experimental conditions. The first matrix compares the quantitative protein profiles between DNBS-treated animals and untreated animals (control, CTRL), describing the cellular pathways significantly modulated upon DNBS-promoted pro-inflammatory stimulus. The second matrix compares DNBS_TAP vs. DNBS, showing the modulation of the protein profile following the administration of the TAP extract to mice exposed to the pro-inflammatory stimulus (DNBS). The third matrix compares DNBS_TAP and CTRL conditions to confirm the activation/inhibition of cellular pathways susceptible to the anti-inflammatory activity of the extract.

A total of 5451 proteins were identified (table 1), and the up- and down regulation of proteins was considered statistically significant when $\log_2 FC > 0.50$ and $\log_2 FC < -0.50$, respectively.

The reproducibility of the biological replicates (six animals *per* experimental group) and of the technical replicates (three independent analyses for each biological replicate) was assessed by means of the calculation of *Pearson's* linear correlation coefficient by comparing all nLC-HRMS analyses; for this study, the correlation coefficients calculated exceed the threshold value of 0.90, indicating an adequate linear correlation (zoom of the multi-scatter plot in Figure S1 (Supplementary Material)).

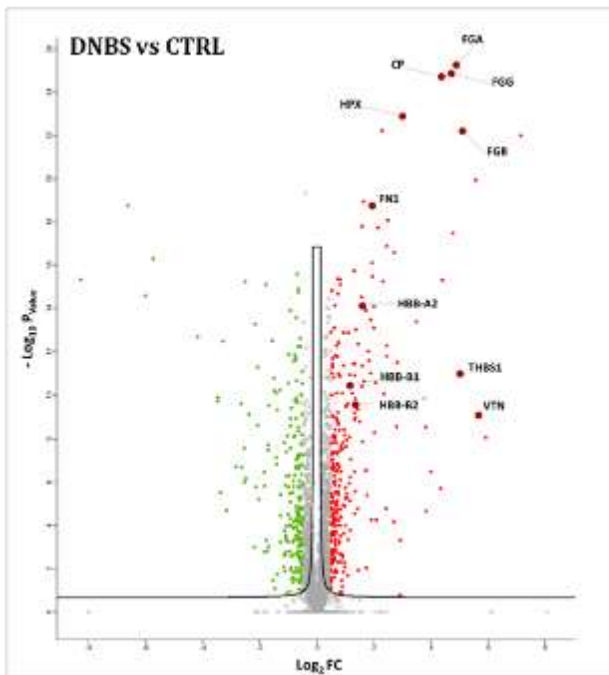
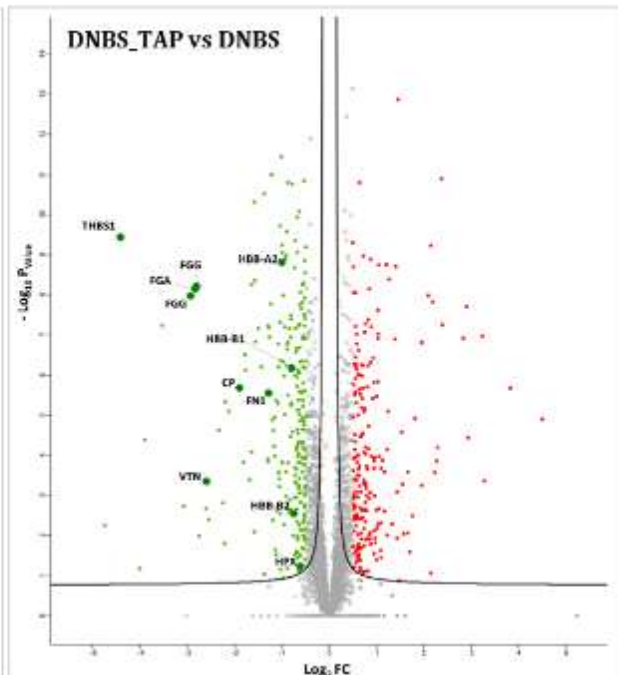
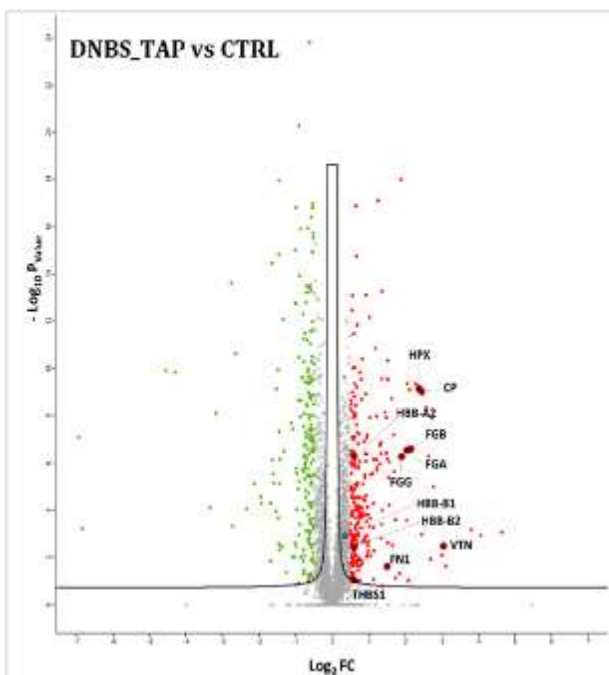
Table 3 - Technical parameters of identification and quantification. For each comparison matrix, the number of identified proteins, the number of significantly quantified proteins and the number of significantly modulated proteins, both in terms of up-regulation ($\log_2 FC > 0.50$) and down-regulation ($\log_2 FC < -0.50$), are reported.

	N° of identified proteins	Number of protein significantly modulated	
		N° of proteins with $\log_2 FC > 0.50$ (sign. Upreg.)	N° of proteins with $\log_2 FC < -0.50$ (sign. downreg.)
<i>DNBS vs CTRL</i>	5451	273	222
<i>DNBS_TAP vs DNBS</i>	5451	212	250
<i>DNBS_TAP vs CTRL</i>	5451	261	202

Figure 4 shows the graphical representation of the distribution of $\log_2 FC$ values versus log p value (Volcano Plots), where significantly up-regulated gene products are highlighted in red and significantly down-regulated ones in green. In the figure, some of the protein species involved in the molecular mechanisms relevant to the experimental model of ulcerative colitis were selected and highlighted, as those proteins were indicative for the anti-inflammatory activity promoted by the extract as below discussed.

Panel A of Figure 4 shows the Volcano Plot relative to the DNBS vs CTRL comparison matrix which highlights the up-regulation of a number of proteins involved in the inflammatory mechanism. The same protein species were highlighted in the Volcano plot relating to the DNBS_TAP vs DNBS comparison (Figure 4, panel B) which show a reversed trend, i.e. a marked down-regulation of the selected gene products, demonstrating an overall anti-inflammatory effect of the polyphenolic extract (DNBS_TAP).

Finally, Panel C of Figure 4 shows the Volcano Plot relative to DNBS_TAP vs CTRL comparison matrix, where the extent of up-regulation of inflammatory proteins is less than observed in the DNBS vs CTRL as comparison.

A.**B.****C.****Legend**

- **HPX:** Hemopexin
- **CP:** Ceruloplasmin
- **FGA:** Fibrinogen α chain
- **FGB:** Fibrinogen β chain
- **FGG:** Fibrinogen γ chain
- **HBB-A2:** Hemoglobin α 2 chain
- **HBB-B1:** Hemoglobin β 2 chain
- **HBB-B2:** Hemoglobin β 2 chain
- **VTN:** Vitronectin
- **FN1:** Fibronectin
- **THBS1:** Thrombospondin-1

Figure 15 - Volcano Plots derived from the LFQ analyses of experimental observation 1, DNBS vs CTRL (A), experimental observation 2, DNBS_TAP vs DNBS (B), experimental observation 3 (C), DNBS_TAP vs CTRL.

4.2.2. *Functional analysis*

The main functional evidence is described below and is divided into two different sections:

- (i) identification of the multi-protein complexes involved in the onset of the UC phenotype (DNBS vs. CTRL);
- (ii) description of the molecular mechanisms underlying the anti-inflammatory activity promoted by the polyphenolic extract TAP.

4.2.3. *Identification of multi-protein complexes involved in the onset of the UC phenotype (DNBS vs. CTRL)*

STRING analysis generated protein-protein interaction networks from proteins significantly modulated (up/down-regulated) following the pro-inflammatory stimulus of DNBS (comparison matrix DNBS vs. CTRL). This analysis allows us to sub-cluster the set of differently expressed proteins according to their potential functional relationships.

The network of significantly up-regulated proteins ($\log_2 FC > 0.50$) is depicted in Figure 5, and provides a list of the most representative molecular mechanisms (sub-networks) responsible for the onset of inflammation in the colon; in particular, specific protein sub-networks involved in the following mechanisms are highlighted: activation of the immune system, induction of oxidative stress and protection mechanism against it and against heme-toxicity, initiation of ferroptosis, activation of wound healing processes and reduction of the thickness of the mucus layer of the intestinal wall. In the following paragraphs the detailed molecular mechanisms involved in each-sub-network are reported.

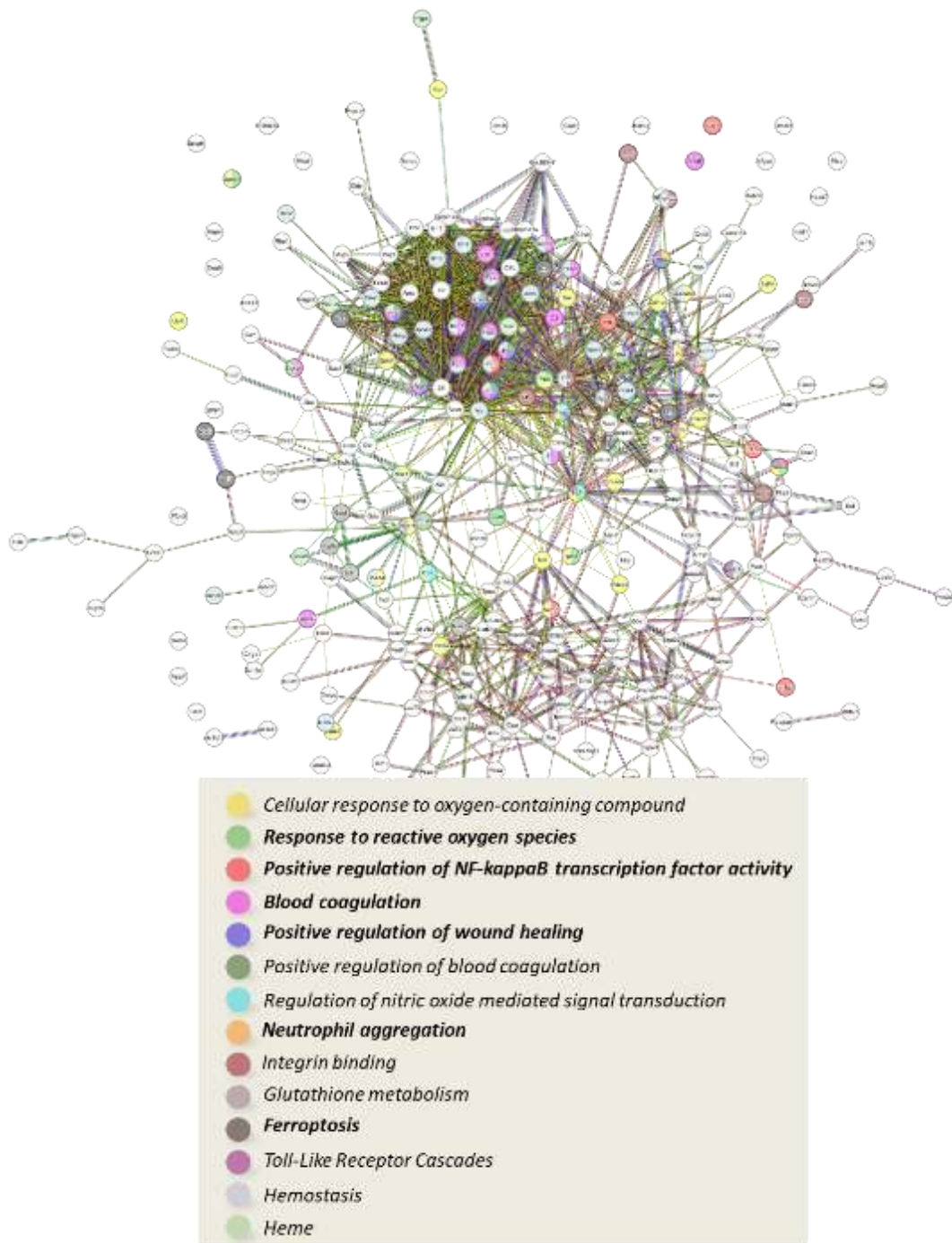


Figure 16 - Graphical representation of the network of interactions (network) between proteins that are significantly up-regulated following a pro-inflammatory stimulus (DNBS); below is a list of the most representative biological processes and cellular mechanisms, highlighted by STRING enrichment based on known (direct and/or indirect) interactions between protein species.

4.2.3.1. *Activation of the immune system*

In addition to inducing direct chemical damage, DNBS acts as a haptene, stimulating the immune response as clearly profiled by quantitative proteomics. In particular, STRING analysis (Figure 5) revealed the modulation of sub-networks linked to activation of the immune system, including a set of proteins that share the molecular function of integrin binding (*Integrin binding, strength 0.79, FDR 0.0012*). Integrins are trans-membrane glycoproteins that mediate leucocyte adhesion to the basal epithelium [11] and, by facilitating their interaction with the basement membrane, promote extravasation of immune cells to the anatomical site of damage, such as that associated with DNBS [12].

IPA software also provides useful information which evidences the involvement of the immune response in the development of the chronic inflammation state of IBDs. One example is the macrophage activation pathway, as supported by the subset of up/down-regulated genes in figure 6. It is known that, once differentiated *in situ*, macrophages phagocytose and destroy pathogens and remnants of damaged tissue, in addition to secreting several intermediates of the inflammatory process, including TNF α and IL-23, which contribute to the pathogenesis of IBD [13].

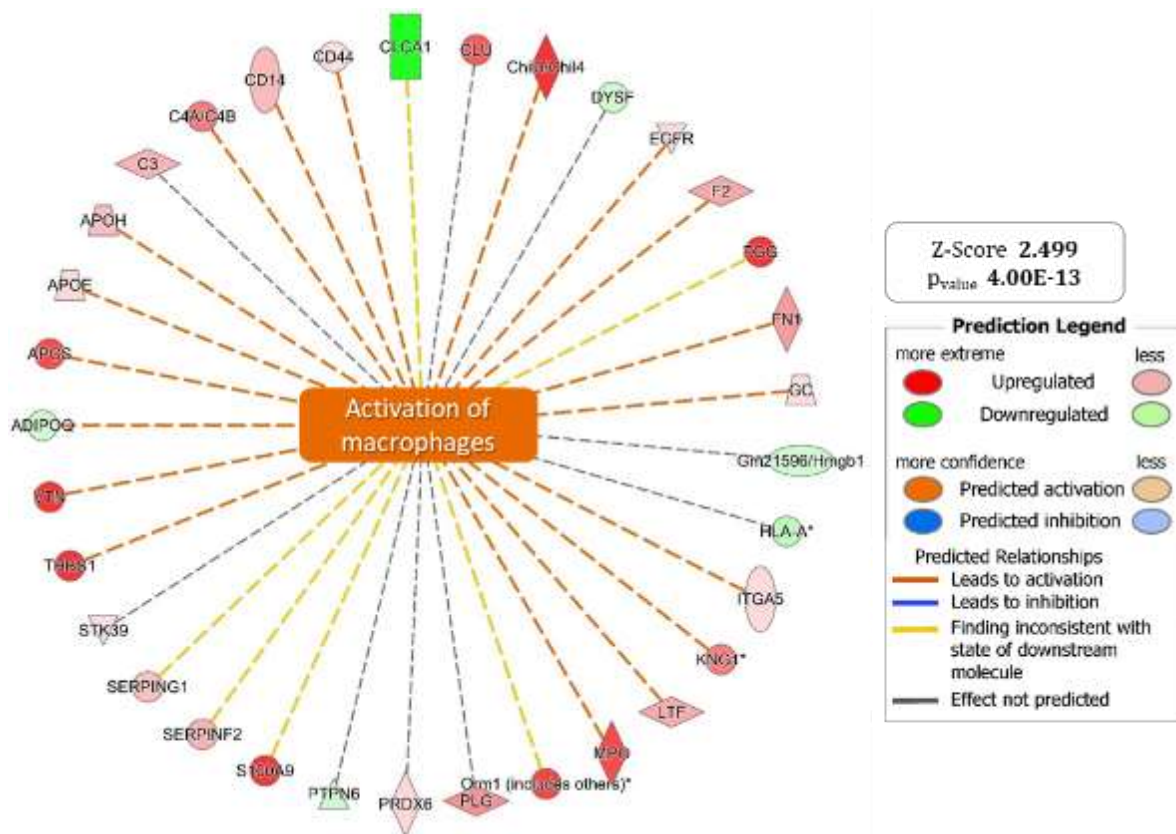


Figure 17 - Graphical representation of the 'Activation of macrophages' pathway for which IPA predicts significant activation with a Z-SCORE value of 2.499. The set of up (red) and down (green) regulated genes supporting the generated hypothesis are shown at the ends of the wheel graph.

IPA analysis also predicts the activation of the "*acute phase signaling*" pathway in DNBS samples (data not shown), supported by further predictions of increased levels of interleukin-6 (Figure S2-A) and of interleukin-1 (Figure S2-C) together with increased expression levels of its receptor IL-6R (Figure S2-B) and the prediction of activation of all associated biological processes; this latter information is consistent with the high volume of evidence reported in the literature supporting the involvement of interleukin IL-6 in the inflammatory processes characteristic of the inflammatory profile of UC.

The increase in neutrophil levels is a typical reaction of the body, which occurs to eliminate a microorganism or foreign substance by releasing various mediators of the inflammatory response. In this regard, IPA predicted an increase in neutrophils (activation of the '*Neutrophil quantity*' network) (figure S3). The hypothesis is that the recruitment of neutrophils is initiated by the chemical injury induced by DNBS, as a form of immune defense.

Confirming the above, through the "upstream regulator" tool in IPA, which aims at identifying the cascade of "upstream" transcriptional regulators that can explain the gene expression changes observed in a "downstream" dataset (overexpression of EGFR, FN1, S100A9 and S100A8), an increase in the levels and activation of the transcription factor NF- κ B (Nuclear factor kappa B) was suggested, although it could not be detected in MS (Figure S2-D). Once activated, NF- κ B regulates, either directly or by cooperating with other transcription factors, numerous cellular processes vital to inflammation and immune response. Prolonged activation of NF- κ B has been demonstrated in many chronic inflammatory diseases, including IBD [14].

4.2.3.2. *Oxidative stress and defense mechanisms*

Starting from the *network* of significantly *up-regulated* proteins following exposure to DNBS (DNBS vs. CTRL), it was possible to isolate subnetworks implicated in oxidative stress. Up-regulated proteins include the myeloperoxidase (MPO), a heme-containing peroxidase expressed mainly in neutrophils, which catalyzes the formation of reactive oxygen intermediates, including hypochlorous acid (HOCl); its overexpression well correlates with the increase of neutrophil level, as above described, and with the data on MPO activity reported in figure 3-panel E. An additional example is given by the upregulation of calprotectin, the heterodimer of the proteins S100A8 and S100A9, which is a ligand of the toll-like receptor 4 (TLR4) and of the receptor for advanced glycation end products (RAGE) [15], which generates oxidative stress via activation of NADPH oxidase [16]. Calprotectin overexpression is concordant with colon inflammation, and, in humans, its quantitative assessment in feces is a useful marker of inflammation in UC [17]. STRING analysis also highlights several metabolic pathways involved in the elimination of excess reactive oxygen and nitrogen species (ROS and RNS), which are responsible for the oxidative damage including (i) *Hydrogen peroxide catabolic process* (*strength* 2.64, FDR 0.000085) and (ii) *Response to oxidative stress* (*strength* 1.54, FDR 0.00017), both with antioxidant functions (Table S1 – Subnetwork A).

Among the catabolic pathways activated to counteract the excessive production of ROS is the well-defined protein cluster involved in glutathione metabolic processes (Table S1 – Subnetwork B) [18]; the cluster includes glutathione peroxidase 3 (GPX3), microsomal glutathione S-transferase 1 (MGST1) and gamma-glutamyl transferase 5 (GGT5), which in the DNBS vs. CTRL comparison matrix have *log₂ FC* values of 0.53, 0.57 and 0.54 respectively.

4.2.3.3. Onset of heme-mediated toxicity mechanism

Colonic bleeding, and thus an *in situ* increase in hemoglobin was found in DNBS compared to CTRL, as determined by the $\log_2 FC$ values calculated for hemoglobin β chain 1 (hemoglobin β chain 1), hemoglobin β chain 2 (hemoglobin β chain 2) and hemoglobin α chain 1 (hemoglobin α chain 1), of 1.57, 1.35 and 1.59, respectively.

Besides hemoglobin increase, STRING analysis highlighted further molecular mechanisms related to the ulcer and bleeding process, in particular those involving the tissue response to an altered iron homeostasis (heme-mediated toxicity). A significant up-regulation of hemopexin, HPX ($\log_2 FC$ of 2.98), a multi-domain protein with the highest affinity among plasma proteins for the heme group, the prosthetic constituent of hemoglobin and other proteins such as myoglobin [19], was found in DNBS compared to CTRL. The heme group, at high levels, is toxic, since it causes, through spontaneous auto-oxidation, an excessive production of ROS species. Hemopexin (HPX) has detoxifying capacity, because it is able to bind to the prosthetic group and sequester it (scavenging activity); besides HPX, a significant increase of haptoglobin was also found in DNBS, a protein which binds with high affinity free hemoglobin and whose complex is then removed by the reticuloendothelial system.

Figure 7 shows the distribution of hemopexin and haptoglobin LFQ intensity values recorded for each animal in the reference experimental condition (DNBS vs. CTRL). The figure also reports the effect of TAP treatment which is described in the following section.

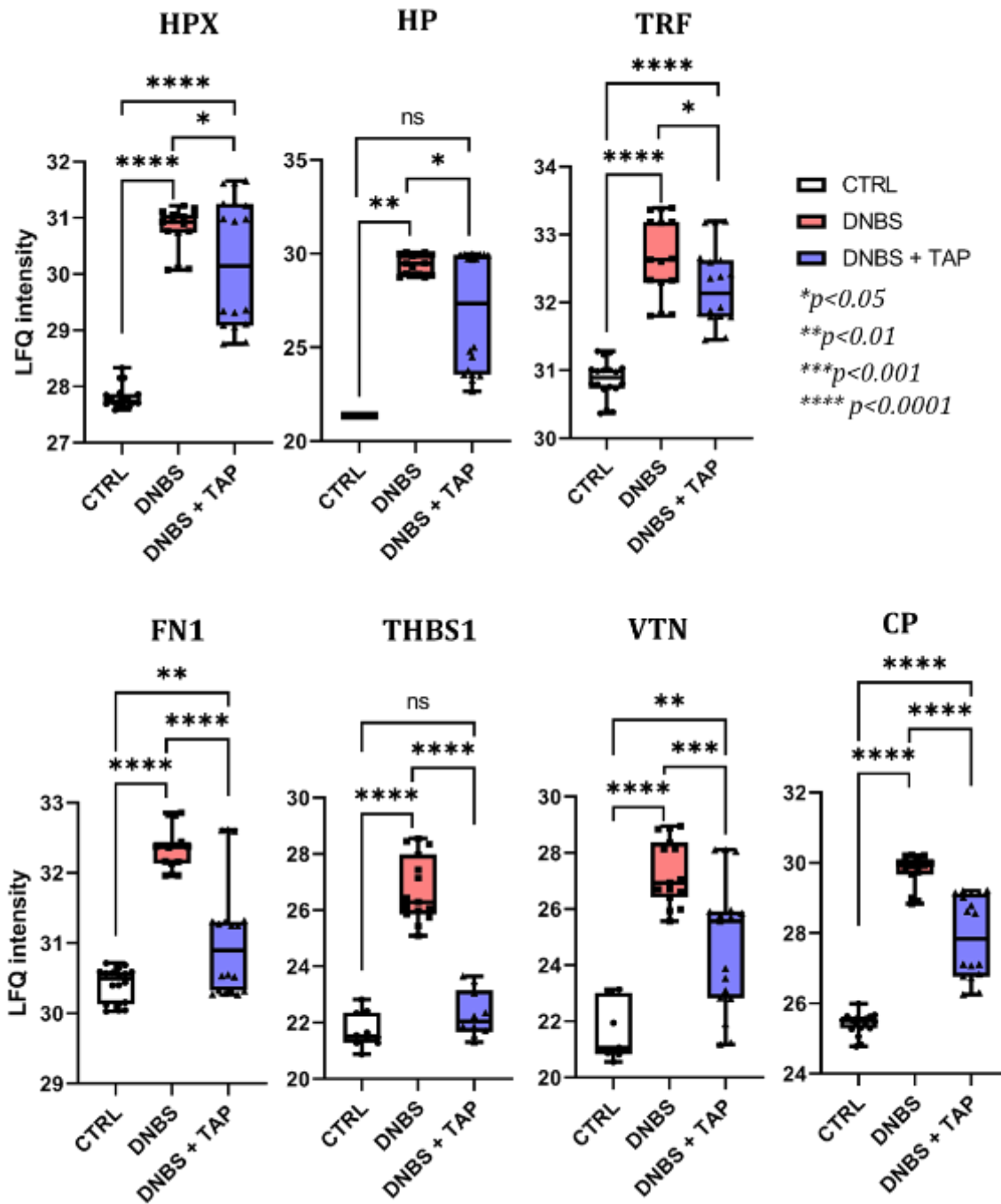


Figure 18 - Graphical representation of the distribution of LFQ intensity values recorded for hemopexin (HPX), haptoglobin (HP), transferrin (TRF), fibronectin (FN1), thrombospondin (THBS1), vitronectin (VTN) and ceruloplasmin (CP). In all the experimental conditions (CTRL, DNBS, DNBS + TAP).

For both proteins, the LFQ intensity values were significantly higher in the DNBS experimental condition than in the control condition; specifically the \log_2 FC values in the DNBS vs. CTRL matrix were 2.98 for hemopexin and 8.05 for haptoglobin. Hemopexin and haptoglobin are not the only significantly regulated proteins involved in the defense processes against heme-mediated toxicity: levels of ceruloplasmin (CP), vitronectin (VTN), fibronectin (FN), transferrin (TRF) and thrombospondin (THBS1) are significantly higher in the DNBS condition (figure 7). Overall, from the data obtained, it is evident that DNBS, by causing ulceration and bleeding of tissues, leads to an increase in hemoglobin, resulting in heme-related toxicity [20]; this condition recalls all those detoxification processes involving proteins such as HPX, VTN, CP and FN, which shares a common membership to the hemopexin superfamily, known to collaborate in the adhesion of leukocytes to epithelia and the inhibition of the immune system and coagulation, and thus become biomarkers of the ulcerative inflammatory state.

4.2.3.4. *Activation of ferroptosis*

STRING analysis also revealed a sub-set of up-regulated proteins involved in the cellular pathway of ferroptosis (*strength* 2.74, FDR 1.95E-14). Among the proteins involved in ferroptosis (Table S1 – Subnetwork C), in addition to transferrin (TRF, \log_2 FC 1.80), ceruloplasmin (CP, \log_2 FC 1.55) and ferritin 1 heavy chain (FTH1, \log_2 FC 1.74), already mentioned in the iron homeostasis path (*Iron homeostasis*, *strength* 2.72, FDR 0.0015), the presence of gene products such as ACSL3 (\log_2 FC 1.12) and ACSL4 (\log_2 FC 0.90), the Acid-CoA ligase to long-chain fatty acids 3 and 4 (Long-Chain-Fatty-Acid--CoA Ligase 3 and Long-Chain-Fatty-Acid--CoA Ligase 4), respectively, was noted; these proteins, in addition to being involved in the fatty acid biosynthesis pathway (*Fatty acid biosynthesis*, *strength* 2.59, FDR 0.0014), are crucial for ferroptosis since this kind of non-apoptotic cell death is triggered by the accumulation of membrane lipid peroxides due to iron overload [21].

4.2.3.5. *Activating wound healing*

In response to ulcers and hemorrhages induced by DNBS, a significant activation of all those cellular mechanisms of coagulation and wound healing was observed. Functional analysis (STRING) (figure 5) highlighted in the DNBS vs. CTRL comparison matrix, the over-expression of several proteins involved in the wound healing process with a particular reference to hemostasis (*Hemostasis*, *strength* 0.74, FDR 4.16E-13 / *Blood coagulation, fibrin colt formation*, *strength* 1.77, FDR 2.05E-0.5), inflammation and re-epithelialization/angiogenesis. As an example, Table S1 – Subnetwork D shows the sub-network representing the proteins involved

in the processes of the re-epithelialization and angiogenesis (*Regulation of endothelial cells chemotaxis* - strength 2.21, FDR 0.00014; *Angiogenesis* - strength 1.38, FDR 1.79 E-05; *Wound healing, spreading of cells* - strength 1.95, FDR 0.0153). In particular, the involvement of coagulation factor III (tissue factor III, F3), collagen type IV α 2 chain (COL4a2) and thrombospondin 1 (THBS1), which are the constituents of connective and endothelial tissue and growth factors involved in wound healing with the task of revascularizing the new tissue and providing the needed sustenance for the new cells [22], was highlighted.

According to these initial considerations, the analysis conducted in IPA indicates a downstream inhibition/inactivation of bleeding processes ('bleeding') with a Z-SCORE of -1.837 (Figure 8) which should be interpreted as an effect derived from the activation of all gene products essential for promoting healing in response to induced tissue damage.

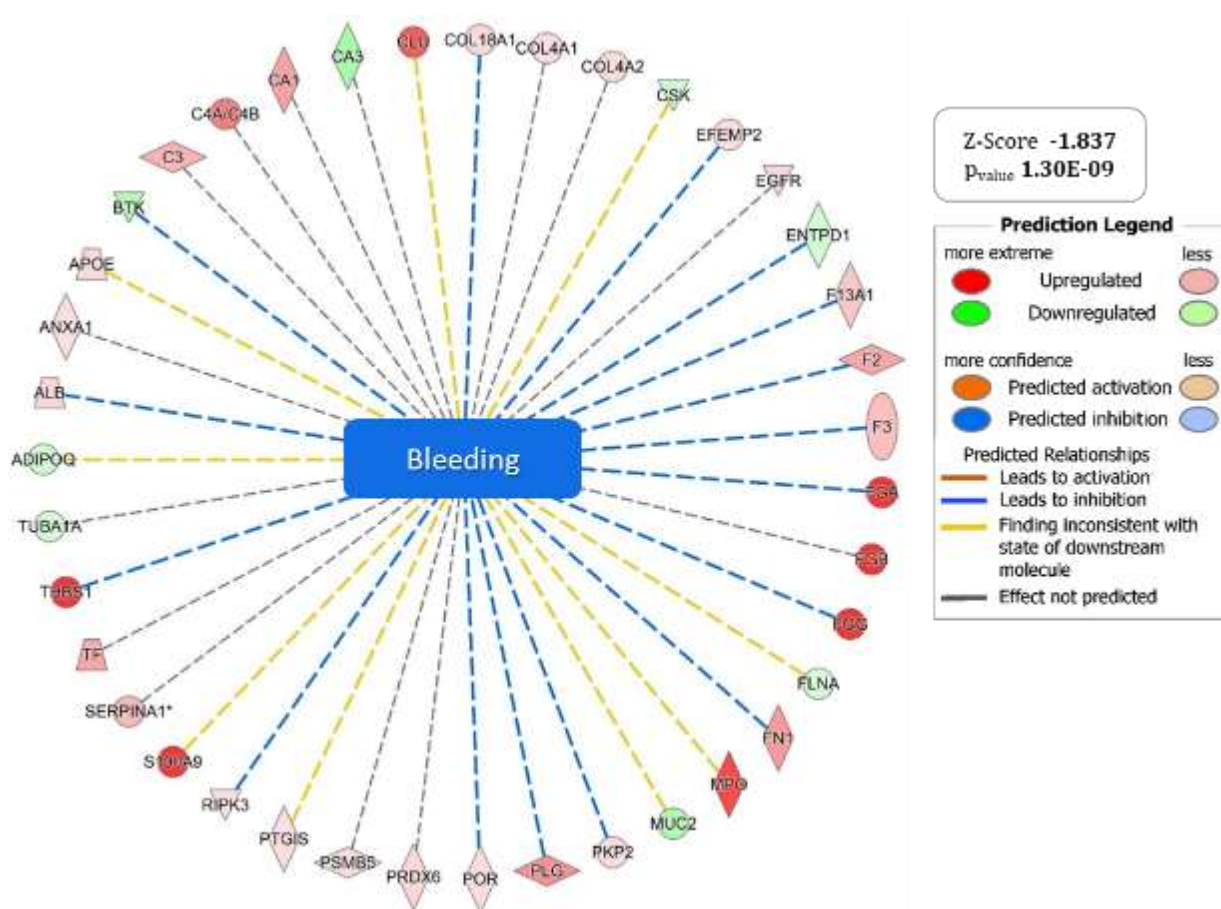


Figure 19 - Graphical representation of the 'Bleeding' pathway for which IPA predicts significant inhibition with a Z-SCORE value of -1.837. The set of up (red) and down (green) regulated genes supporting the generated hypothesis are shown at the ends of the wheel graph.

4.2.3.6. *Decreased thickness of the mucus layer of the intestinal wall*

A reduced expression of the MUC2 gene product, one of the mucus-secreting proteins, was observed in the DNBS vs CTRL comparison matrix dataset ($\log_2 FC$ equal to -0.99). Mucins are glycoproteins produced by epithelial cells and secreted to form the mucus that provides a physiological barrier. Reduction in the thickness of the mucosa covering the epithelium of the organ, which serves to protect it from external damage, certainly contributes to the onset of colon tissue damage.

4.2.3.7. *Response to the inflammatory state*

In DNBS-treated animals, IPA predicted an inhibitory effect to the inflammatory process (Z-SCORE -1.698), as an adaptive mechanism in response to the inflammatory process

itself. The set of genes up- (red) and down-regulated (green) supporting the generated hypothesis are reported in the supplementary information (Figure S4).

4.2.4. Description of the molecular mechanisms responsible for the anti-inflammatory activity (in prevention) promoted by the polyphenolic extract TAP.

Once the molecular mechanisms underlying the induction of colonic inflammation following intrarectal injection of DNBS were elucidated, the focus shifted to evaluating the molecular mechanisms explaining the efficacy of TAP extract administered via oral gavage in reducing DNBS-induced tissue damage. Quantitative proteomics found that TAP reverted the activated pathways.

4.2.4.1. TAP-mediated reversal of mechanisms activated by DNBS

Of particular interest was the functional investigation of significantly down-regulated proteins in rats exposed to DNBS and treated with the TAP extract (comparison matrix DNBS_TAP vs. DNBS), whose network of interactions extracted with the STRING software is shown in Figure 9.

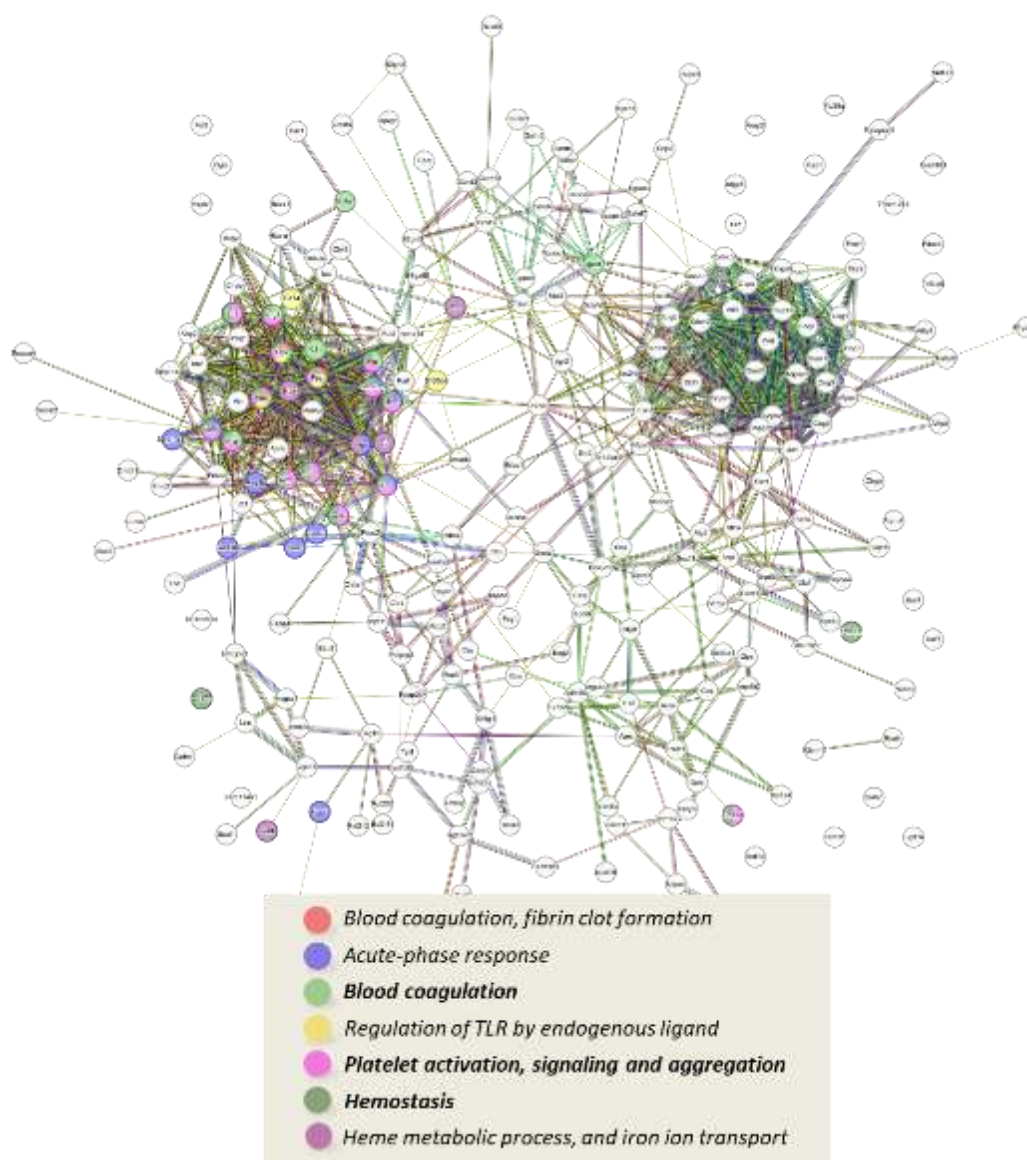


Figure 20 - Representation of the network of interactions (network) between significantly down-regulated proteins in the DNBS_TAP vs DNBS comparison matrix; below is a list of the most representative biological processes and cellular mechanisms for the study, highlighted by means of the STRING enrichment function on the basis of known (direct and/or indirect) interactions between the protein species.

Overall, the activation of the different molecular mechanisms revealed by the functional analysis of the up-regulated proteins in the DNBS vs. CTRL comparison matrix were found inactivated by the TAP treatment (DNBS_TAP vs. DNBS), indicating a reversal in the modulation of the gene products affected by the chemical damage induced by DNBS.

This is the case, for example, for proteins involved in the mechanisms of heme-mediated toxicity; haptoglobin and hemopexin, up-regulated in the experimental DNBS condition as a response to ulcer formation and hemorrhage, showed a significantly lower mean LFQ value

following TAP treatment (Figure 7). We can therefore assume that TAP treatment effectively counteracts the ulceration and hemolysis process.

Confirming this statement, Table 2 shows the $\log_2 FC$ values calculated for hemopexin and the identified hemoglobin subunits (HBB1, HBB2, HBA2) in the three comparison matrices produced for this study. The trend is absolutely superimposable for all target proteins: the induction of inflammation results in an *up-regulation* compared to the physiological condition (DNBS vs. CTRL) while treatment with the extract significantly reduces the levels of these proteins compared to the pathological model (DNBS_TAP vs. DNBS).

Table 4 - Panel of $\log_2 FC$ values extrapolated from the three comparison matrices for some of the proteins involved in the mechanisms of heme-mediated toxicity and wound healing mechanisms. Red color indicates up-regulation, green down-regulation. The intensity of the color is proportional to the magnitude of the change.

			DNBS vs. CTRL	DNBS_TAP vs. DNBS	DNBS_TAP vs. CTRL
			$\log_2 FC$	$\log_2 FC$	$\log_2 FC$
<i>Heme mediated toxicity</i>	HP	<i>Haptoglobin</i>	8.050	-2.559	5.490
	HPX	<i>Hemopexin</i>	2.989	-0.623	2.366
	HBB1	<i>Hemoglobin beta chain 1</i>	1.157	-0.802	0.356
	HBB2	<i>Hemoglobin beta chain 2</i>	1.355	-0.761	0.594
	HBA1	<i>Hemoglobin alpha chain 1</i>	1.598	-1.009	0.589
<i>Wound healing mechanisms</i>	F13A1	<i>Coagulation factor 13</i>	1.160	-0.446	0.714
	F2	<i>Coagulation factor II, thrombin</i>	1.819	-0.346	1.473
	F3	<i>Coagulation factor III, tissue factor</i>	1.325	-0.448	0.877
	FGA	<i>Fibrinogen alpha chain</i>	4.877	-2.849	2.028
	FGB	<i>Fibrinogen beta chain</i>	5.093	-2.953	2.140
	FGG	<i>Fibrinogen gamma chain</i>	4.711	-2.818	1.892
	PLG	<i>Plasminogen</i>	2.316	-1.004	1.312

The induction of vitronectin, fibronectin and thrombospondin is also reversed in the TAP-treated animals, as shown in Figure 7, which shows the distribution of the LFQ intensities values of each protein investigated; the trend is entirely superimposable: the pro-inflammatory stimulus produces significant up-regulation (DNBS), which is reduced equally significantly following TAP treatment (DNBS_TAP), although the levels do not reach the physiological state (CTRL). For protein species involved in wound healing, overall, there is a decrease in expression

levels as reduced tissue ulceration corresponds to a reduced need for the body to respond to the wound by activating all the molecular mechanisms involved in healing, i.e. the processes of coagulation, inflammation and angiogenesis. Table 2 shows the panel of $\log_2 FC$ values extrapolated from the three comparison matrices for some of the most interesting gene products involved in wound healing including coagulation factors I and II and the α -chain, β -chain and γ -chain constituents of fibrinogen.

IPA analyses also provide results that confirm the reversal of certain processes involved in the pathogenesis of ulcerative colitis. From the interpretation of the data reported in the DNBS_TAP vs. DNBS comparison matrix, two protein clusters deserve particular attention for their consistency with the experimental model. The first cluster includes the protein species involved in the immune response of neutrophils, illustrated in Figure S5, whose inhibition is consistent with a reduced immune system cell recruitment due to the anti-inflammatory activity promoted by TAP.

The second cluster concerns the 'Acute phase signaling' pathway, for which the IPA hypothesized an activation in the DNBS vs. CTRL comparison matrix, and a significant inhibition (Z-SCORE -2.00) following treatment with the extract (DNBS_TAP vs. DNBS), confirming the reduced activation of the immune system's first line of defense by the organism (figure 10). The network also highlights a hypothesis of inhibition of NF- κ B and IL-6, whose roles in the development of chronic intestinal inflammation has already been addressed.

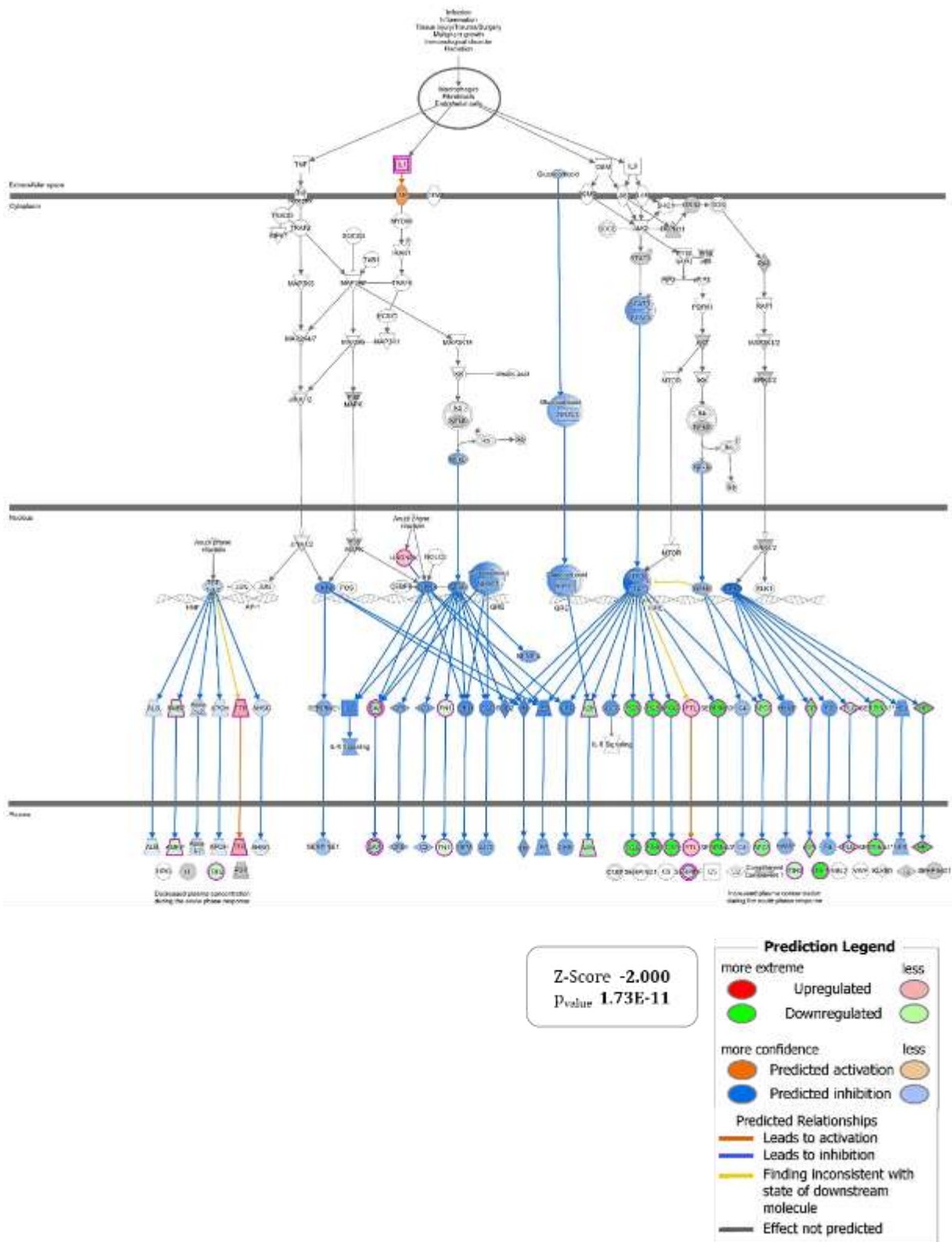


Figure 21 - Graphical representation of the 'Acute phase signaling' pathway for which IPA predicts significant inhibition with a Z-SCORE value of -1.698. The set of genes up (red) and down (green) regulated to support the hypothesis generated are shown at the ends of the wheel graph.

Furthermore, from the interpretation of the $\log_2 FC$ values reported in the DNBS_TAP vs. DNBS comparison matrix, it was possible to hypothesize the inhibition of the mechanism linked to the NOS2 (Nitric oxide synthase 2) protein thanks to the upstream regulator function available in IPA. The latter represents the inducible form of nitric oxide (NO) synthases, expressed only in response to certain stimuli, such as LPS (lipopolysaccharide) or IFN- γ (interferon γ)[23].

As can also be observed from the $\log_2 FC$ value reported in the DNBS vs. CTRL comparison matrix (Table 3), the onset of inflammation is associated with a substantial increase in NOS2 levels, (Z-SCORE 3.63; p -value 2.64E-09). Nitric oxide exerts antimicrobial activity against various species, but also plays a role in the progression of inflammation [21], especially at the vascular level, where it acts as a vasodilator to allow oedema development and extravasation of immune system cells [25]. Nitric oxide also interacts with ROS species produced by macrophages in response to increased oxidative stress. The macrophages themselves can express the NOS2 protein, so that the reaction between NO and ROS is favored, leading to the formation of RNS (Reactive Nitrogen Species). The action of nitric oxide, if produced in controlled quantities, could be crucial in various pathological conditions. In contrast, the administration of TAP drastically reduced NOS2 levels (Z-SCORE -2.52; p -value 4.22E-09), indicating, first of all, a lower production of nitric oxide, but also suggesting an improvement in the animals' status, which even seemed to return to NOS2 expression values tending towards the physiological condition (DNBS_TAP vs. CTRL).

Table 5 - Panel of Z-SCORE values extrapolated for NOS2 from the analysis of the three comparison matrices in IPA. A red color indicates activation, green inhibition. The intensity of the color is proportional to the magnitude of the effect.

		DNBS vs. CTRL		DNBS_TAP vs. DNBS		DNBS_TAP vs. CTRL	
<i>Upstream Regulators</i>		Z Score	pvalue	Z Score	pvalue	Z Score	pvalue
NOS2		3.63	2.64E-09	-2.52	4.22E-09	2.20	5.08E-09

4.2.4.2. TAP induces an antioxidant response.

Analysis of the down-regulated proteins by TAP treatment together with the morphological and histological scores well confirm the ability of TAP to reverse the tissue damaging effect induced by DNBS. Moreover, proteomic data well indicate that the damaging effect of DNBS is primarily due to the onset and propagation of an inflammatory/oxidant condition, leading to ulcers, bleeding and mucus thinning. TAP was found to inactivate all the damaging events induced by DNBS, by blocking the onset and progression of the inflammatory process. The open question is the molecular mechanism through which TAP inhibits the DNBS-induced inflammatory process. Oxidative stress and inflammatory response are strictly connected to each-other. When oxidative stress appears as a primary disorder, inflammation develops as a secondary disorder and further enhances oxidative stress. On the other hand, inflammation as a primary disorder can induce oxidative stress as a secondary disorder, which can further enhance inflammation [26]. Based on this evidence, a well-established strategy to block the inflammatory chronic condition consists of inhibiting oxidative stress, and the best approach to inhibit oxidative stress is to activate the nucleophilic tone and the antioxidant defense, by inducing NRF2 nuclear translocation. In previous *in vitro* cellular studies, we found that TAP activates NRF2, as demonstrated by quantitative proteomic studies and cell-based assay (cell model engineered with the gene reporter for nuclear translocation of NRF2), and in turn exerts anti-inflammatory activity in a dose-dependent manner, as demonstrated in cells (cell model engineered with the reporter gene for nuclear translocation of NF- κ B) using two different pro-inflammatory agents, IL1- α and TNF- α [27]. The anti-inflammatory and antioxidant actions of thinned apple polyphenol (TAP) extract was then observed in an *in vivo* model of paw edema. TAP extract reduced paw histological changes, neutrophil infiltration, mast cell degranulation, and oxidative stress. Additionally, the oral administration of TAP extract decreased thermal and mechanical hyperalgesia, along with a reduction in spinal microglia and the markers of nociception [28].

The antioxidant activity of TAP through an NRF2 activation mechanism was confirmed in this *in vivo* model as below described. Treatment with TAP extract promotes an antioxidant response through the induction of a set of detoxifying/antioxidant enzymes including: SOD1 and SOD3, catalyzing the conversion of superoxide anions to elemental oxygen and hydrogen peroxide, thus providing a significant contribution in counteracting free radical damage; glutathione peroxidase 1 (GPX1), an enzyme belonging to the class of oxidoreductases that uses reduced glutathione (GSH) as a cofactor to reduce hydrogen peroxide to water; NAD(P)H

dehydrogenase (quinone 1)-NQO1, an oxidoreductase aimed at removing quinones through an NAD(P)H(10)-mediated detoxification reaction is upregulated and it is restored to a physiological level [29] and peroxiredoxin 6 (PRDX6) which belongs to the 'non-selenic peroxidase' family. The relative content of the enzymes under the three experimental conditions is shown in Figure 11.

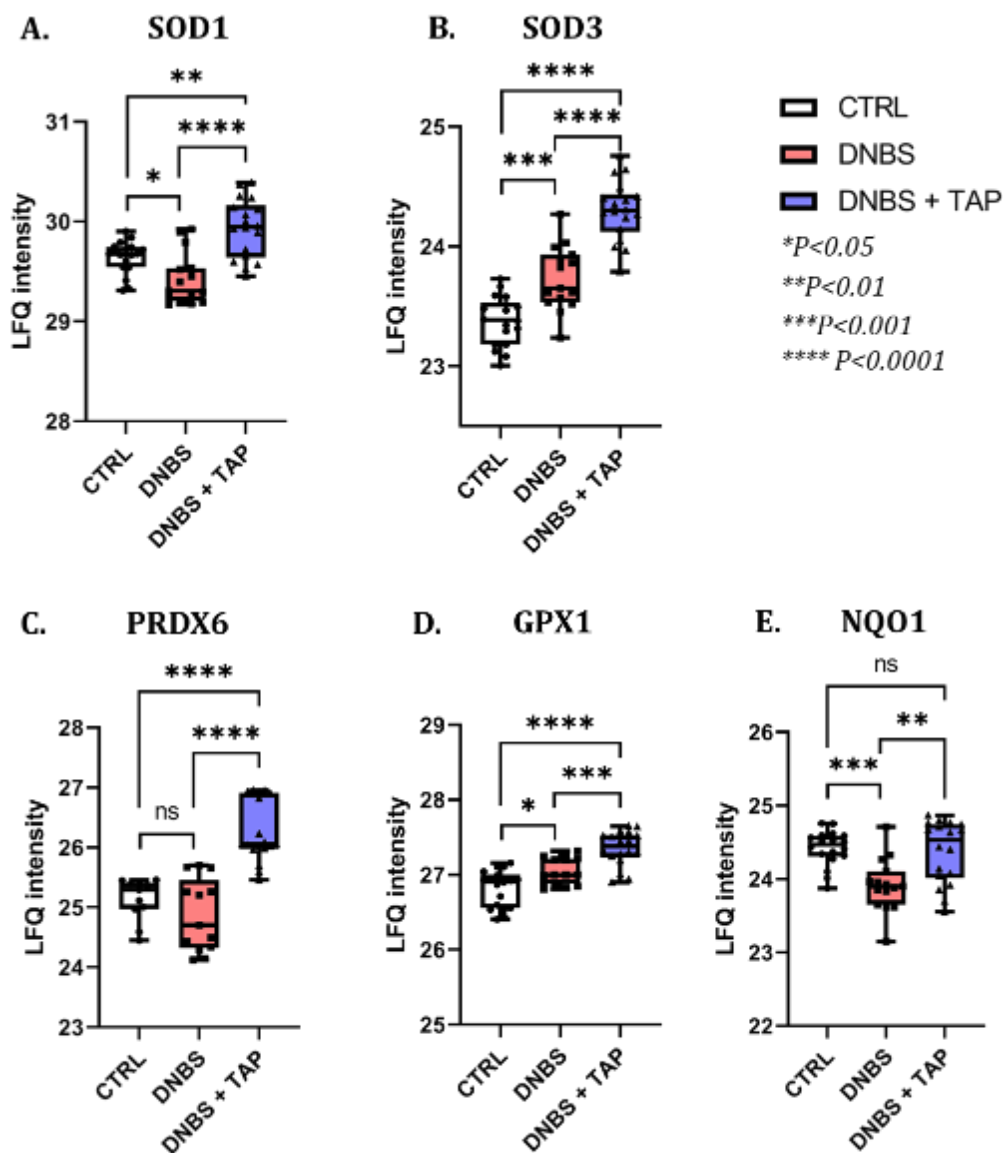


Figure 22 - Graphical representation of the distribution of LFQ intensity values recorded for Superoxide dismutase 1 and 3 (SOD1, SOD3), glutathione peroxidase 1 (GPX1), NAD(P)H dehydrogenase (quinone 1) (NQO1), and peroxiredoxin 6 (PRDX6) in all the experimental conditions (CTRL, DNBS, DNBS + TAP).

5. Conclusions

It is interesting to note that SOD1 was down-regulated in the DNBS group while SOD3 was up-regulated. Previous studies have shown that SOD3, but not SOD1 (or SOD2), is regulated through NRF2 [30] and this result would explain the expression of SOD3 in DNBS treated animals, a sign of activation of the first line of defense against oxidative stress/inflammation through the KEAP1-NRF2 signaling pathway; on the contrary, SOD1 was not activated but even reduced. The relative contents of peroxiredoxin 6 (PRDX6) and NQO1 in DNBS treated animals were not stimulated by the pro-inflammatory stimulus; It was found that TAP not only increases the regulation of antioxidant enzymes not influenced by the inflammatory state, such as SOD1, PRDX6 and NQO1, but also the further expression of those activated by the inflammatory condition induced by DNBS, i.e. SOD3 and GPX1. Thus, TAP on the one hand further enhances NRF2-dependent enzymes and on the other hand activates, probably through NRF2-independent mechanisms, some other antioxidant enzymes that are not regulated by the inflammatory/oxidative state by the adaptive response. One possible way in which TAP can activate NRF2 is through the presence of compounds which have an ortho-diphenol moiety. These compounds act as electrophilic binder of the thiol group of KEAP1 when activated as quinones and such an activation is mediated by iron and peroxides which are activated in inflammatory condition such as that induced by DNBS. Among the most significant *sub-networks*, protein *clusters* involved in the neutralization of toxic products for the cell (*Cellular detoxification*, *strength* 1.04, FDR 0.00083) are well recognized, which are essential for restoring the redox balance in inflamed tissue (*Antioxidant activity*, *strength* 2.5, FDR 1.28 E-09) (Table S2 – Subnetwork E). In conclusion, the described functional proteomics study has outlined the following molecular mechanisms modulated by treatment with TAP: an activation of antioxidant mechanisms related to an NRF2 stimulation, the reversal of mechanisms activated in the presence of DNBS, with particular reference to heme-toxicity mechanisms and also the reduction of the immune response induced in the pathological model. Ultimately, this study highlighted the therapeutic potential of thinned apple polyphenolic extract (TAP) for the use in the treatment of inflammatory and oxidative stress-related conditions such as ulcerative colitis.

6. References

1. Crocetti, E.; Bergamaschi, W.; Russo, A.G. Population-Based Incidence and Prevalence of Inflammatory Bowel Diseases in Milan (Northern Italy), and Estimates for Italy. *European Journal of Gastroenterology & Hepatology* 2021, 33, e383–e389, doi:10.1097/MEG.0000000000002107.
2. Impellizzeri, D.; Fusco, R.; Genovese, T.; Cordaro, M.; D'Amico, R.; Trovato Salinaro, A.; Ontario, M.L.; Modafferi, S.; Cuzzocrea, S.; Di Paola, R.; et al. Coriolus Versicolor Downregulates TLR4/NF- κ B Signaling Cascade in Dinitrobenzenesulfonic Acid-Treated Mice: A Possible Mechanism for the Anti-Colitis Effect. *Antioxidants* 2022, 11, 406, doi:10.3390/antiox11020406.
3. Shapiro, H.; Singer, P.; Halpern, Z.; Bruck, R. Polyphenols in the Treatment of Inflammatory Bowel Disease and Acute Pancreatitis. *Gut* 2007, 56, 426–436, doi:10.1136/gut.2006.094599.
4. Tang, T.; Targan, S.R.; Li, Z.-S.; Xu, C.; Byers, V.S.; Sandborn, W.J. Randomised Clinical Trial: Herbal Extract HMPL-004 in Active Ulcerative Colitis - a Double-Blind Comparison with Sustained Release Mesalazine: Randomised Clinical Trial: Herbal Extract HMPL-004 for Ulcerative Colitis. *Alimentary Pharmacology & Therapeutics* 2011, 33, 194–202, doi:10.1111/j.1365-2036.2010.04515.x.
5. Tanigawa, S.; Fujii, M.; Hou, D. Action of Nrf2 and Keap1 in ARE-Mediated NQO1 Expression by Quercetin. *Free Radical Biology and Medicine* 2007, 42, 1690–1703, doi:10.1016/j.freeradbiomed.2007.02.017.
6. Qin, S.; Hou, D. Multiple Regulations of Keap1/Nrf2 System by Dietary Phytochemicals. *Molecular Nutrition Food Res* 2016, 60, 1731–1755, doi:10.1002/mnfr.201501017.
7. Li, B.; Wang, Y.; Jiang, X.; Du, H.; Shi, Y.; Xiu, M.; Liu, Y.; He, J. Natural Products Targeting Nrf2/ARE Signaling Pathway in the Treatment of Inflammatory Bowel Disease. *Biomedicine & Pharmacotherapy* 2023, 164, 114950, doi:10.1016/j.biopha.2023.114950.
8. Atreya, I.; Atreya, R.; Neurath, M.F. NF- κ B in Inflammatory Bowel Disease. *Journal of Internal Medicine* 2008, 263, 591–596, doi:10.1111/j.1365-2796.2008.01953.x.
9. Gado, F.; Ferrario, G.; Della Vedova, L.; Zoanni, B.; Altomare, A.; Carini, M.; Aldini, G.; D'Amato, A.; Baron, G. Targeting Nrf2 and NF- κ B Signaling Pathways in Cancer Prevention: The Role of Apple Phytochemicals. *Molecules* 2023, 28, 1356, doi:10.3390/molecules28031356.
10. Mullane, K.M.; Kraemer, R.; Smith, B. Myeloperoxidase Activity as a Quantitative Assessment of Neutrophil Infiltration into Ischemic Myocardium. *Journal of Pharmacological Methods* 1985, 14, 157–167, doi:10.1016/0160-5402(85)90029-4.
11. Campbell, I.D.; Humphries, M.J. Integrin Structure, Activation, and Interactions. *Cold Spring Harbor Perspectives in Biology* 2011, 3, a004994–a004994, doi:10.1101/cshperspect.a004994.
12. De Franceschi, N.; Hamidi, H.; Alanko, J.; Sahgal, P.; Ivaska, J. Integrin Traffic – the Update. *Journal of Cell Science* 2015, jcs.161653, doi:10.1242/jcs.161653.

13. Na, Y.R.; Stakenborg, M.; Seok, S.H.; Matteoli, G. Macrophages in Intestinal Inflammation and Resolution: A Potential Therapeutic Target in IBD. *Nat Rev Gastroenterol Hepatol* 2019, 16, 531–543, doi:10.1038/s41575-019-0172-4.
14. Oeckinghaus, A.; Ghosh, S. The NF- B Family of Transcription Factors and Its Regulation. *Cold Spring Harbor Perspectives in Biology* 2009, 1, a000034–a000034, doi:10.1101/cshperspect.a000034.
15. Rochette, L.; Dogon, G.; Rigal, E.; Zeller, M.; Cottin, Y.; Vergely, C. Involvement of Oxidative Stress in Protective Cardiac Functions of Calprotectin. *Cells* 2022, 11, 1226, doi:10.3390/cells11071226.
16. Daffu, G.; del Pozo, C.H.; O’Shea, K.M.; Ananthakrishnan, R.; Ramasamy, R.; Schmidt, A.M. Radical Roles for RAGE in the Pathogenesis of Oxidative Stress in Cardiovascular Diseases and Beyond. *Int J Mol Sci* 2013, 14, 19891–19910, doi:10.3390/ijms141019891.
17. Gheibi, N.; Ghorbani, M.; Shariatifar, H.; Farasat, A. In Silico Assessment of Human Calprotectin Subunits (S100A8/A9) in Presence of Sodium and Calcium Ions Using Molecular Dynamics Simulation Approach. *PLoS ONE* 2019, 14, e0224095, doi:10.1371/journal.pone.0224095.
18. Diaz-Vivancos, P.; De Simone, A.; Kiddle, G.; Foyer, C.H. Glutathione – Linking Cell Proliferation to Oxidative Stress. *Free Radical Biology and Medicine* 2015, 89, 1154–1164, doi:10.1016/j.freeradbiomed.2015.09.023.
19. Piccard, H.; Van Den Steen, P.E.; Opdenakker, G. Hemopexin Domains as Multifunctional Liganding Modules in Matrix Metalloproteinases and Other Proteins. *Journal of Leukocyte Biology* 2007, 81, 870–892, doi:10.1189/jlb.1006629.
20. Montecinos, L.; Eskew, J.D.; Smith, A. What Is Next in This “Age” of Heme-Driven Pathology and Protection by Hemopexin? An Update and Links with Iron. *Pharmaceuticals* 2019, 12, 144, doi:10.3390/ph12040144.
21. Yang, Y.; Zhu, T.; Wang, X.; Xiong, F.; Hu, Z.; Qiao, X.; Yuan, X.; Wang, D. ACSL3 and ACSL4, Distinct Roles in Ferroptosis and Cancers. *Cancers* 2022, 14, 5896, doi:10.3390/cancers14235896.
22. Kyriakides, T.R.; MacLauchlan, S. The Role of Thrombospondins in Wound Healing, Ischemia, and the Foreign Body Reaction. *J. Cell Commun. Signal.* 2009, 3, 215–225, doi:10.1007/s12079-009-0077-z.
23. Mannick, J.B.; Asano, K.; Izumi, K.; Kieff, E.; Stamler, J.S. Nitric Oxide Produced by Human B Lymphocytes Inhibits Apoptosis and Epstein-Barr Virus Reactivation. *Cell* 1994, 79, 1137–1146, doi:10.1016/0092-8674(94)90005-1.
24. Bogdan, C. Nitric Oxide Synthase in Innate and Adaptive Immunity: An Update. *Trends in Immunology* 2015, 36, 161–178, doi:10.1016/j.it.2015.01.003.
25. Félétou, M.; Köhler, R.; Vanhoutte, P.M. Nitric Oxide: Orchestrator of Endothelium-Dependent Responses. *Annals of Medicine* 2012, 44, 694–716, doi:10.3109/07853890.2011.585658.
26. Biswas, S.K. Does the Interdependence between Oxidative Stress and Inflammation Explain the Antioxidant Paradox? *Oxidative Medicine and Cellular Longevity* 2016, 2016, 1–9, doi:10.1155/2016/5698931.

27. Ferrario, G.; Baron, G.; Gado, F.; Della Vedova, L.; Bombardelli, E.; Carini, M.; D'Amato, A.; Aldini, G.; Altomare, A. Polyphenols from Thinned Young Apples: HPLC-HRMS Profile and Evaluation of Their Anti-Oxidant and Anti-Inflammatory Activities by Proteomic Studies. *Antioxidants* 2022, 11, 1577, doi:10.3390/antiox11081577.
28. Interdonato, L.; Ferrario, G.; Cordaro, M.; D'Amico, R.; Siracusa, R.; Fusco, R.; Impellizzeri, D.; Cuzzocrea, S.; Aldini, G.; Di Paola, R. Targeting Nrf2 and NF- κ B Signaling Pathways in Inflammatory Pain: The Role of Polyphenols from Thinned Apples. *Molecules* 2023, 28, 5376, doi:10.3390/molecules28145376.
29. Torrente, L.; Prieto-Farigua, N.; Falzone, A.; Elkins, C.M.; Boothman, D.A.; Haura, E.B.; DeNicola, G.M. Inhibition of TXNRD or SOD1 Overcomes NRF2-Mediated Resistance to β -Lapachone. *Redox Biology* 2020, 30, 101440, doi:10.1016/j.redox.2020.101440.
30. Singh, B.; Bhat, H.K. Superoxide Dismutase 3 Is Induced by Antioxidants, Inhibits Oxidative DNA Damage and Is Associated with Inhibition of Estrogen-Induced Breast Cancer. *Carcinogenesis* 2012, 33, 2601–2610, doi:10.1093/carcin/bgs300.

7. Supplementary materials

Figure S1. Evaluation of the linear correlation of LFQ intensity values between biological and technical replicates by calculating Pearson's linear correlation coefficient.

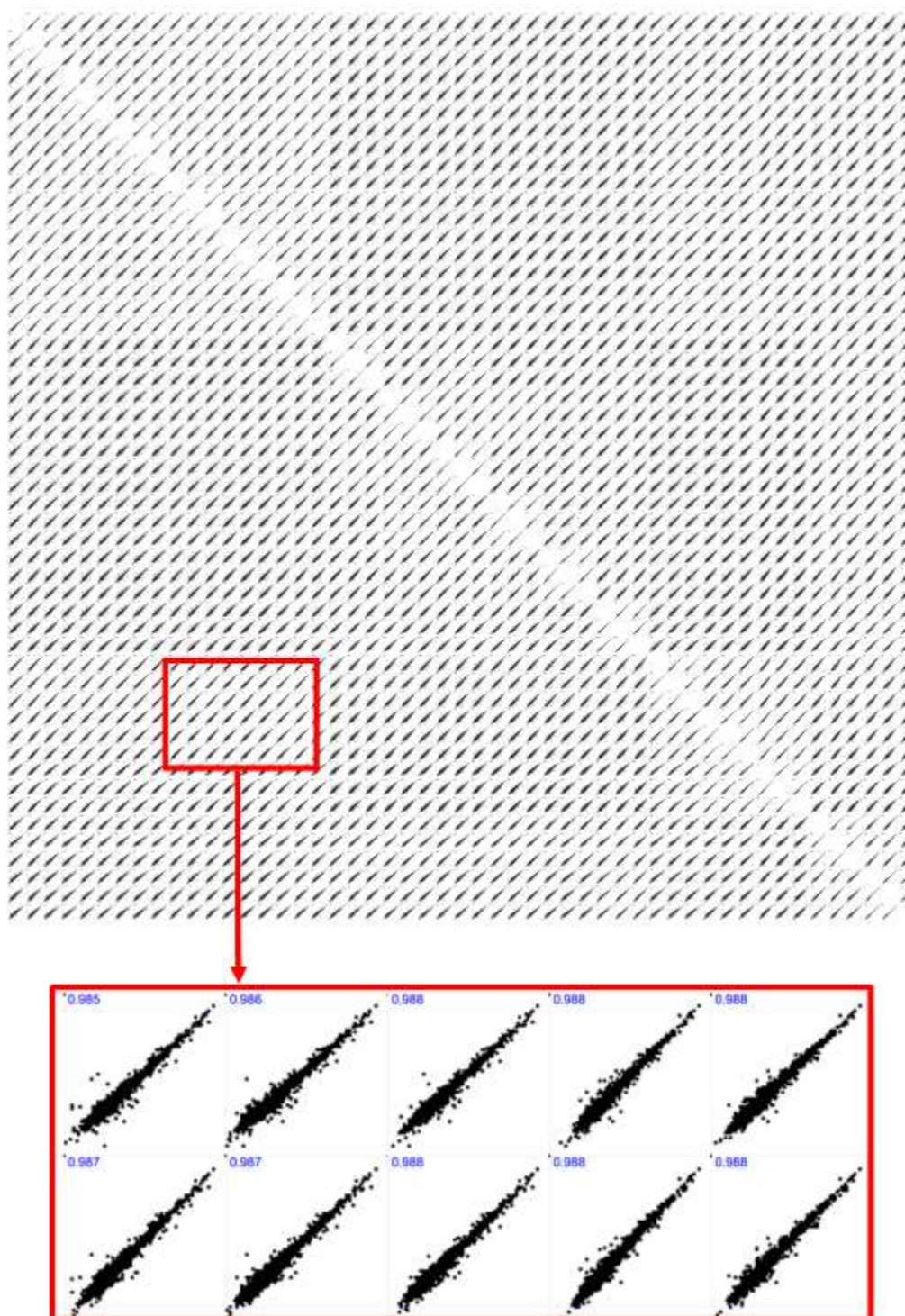


Figure S2. Graphical representation of the subset of proteins that, based on their modulation (up/down-regulation), support the activation hypothesis of IL-6 (A) and its receptor IL-6R (B) in the DNBS vs. CTRL comparison matrix. In panel C of the subset of proteins that support the hypothesis of IL-1 activation, while in panel D of NFkB pathway.

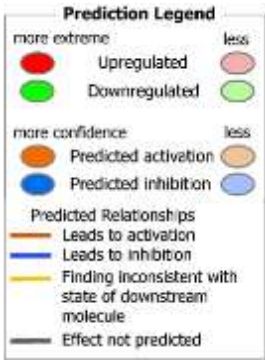
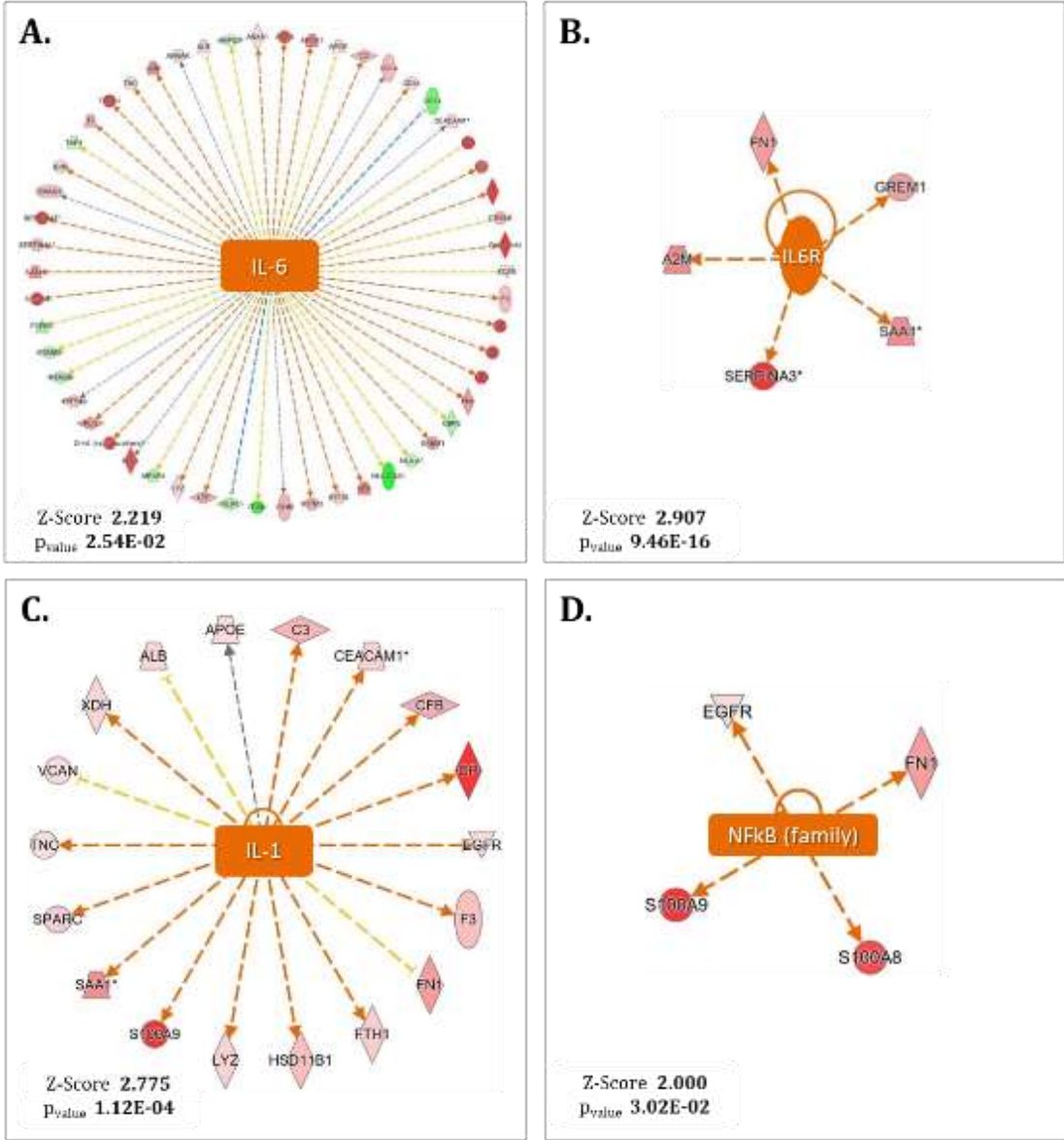


Figure S3. Graphical representation of the 'Quantity of neutrophils' pathway for which IPA predicts significant activation with a Z- SCORE value of 2.476. The set of genes up (red) and down (green) regulated to support the generated hypothesis are shown at the ends of the wheel graph.

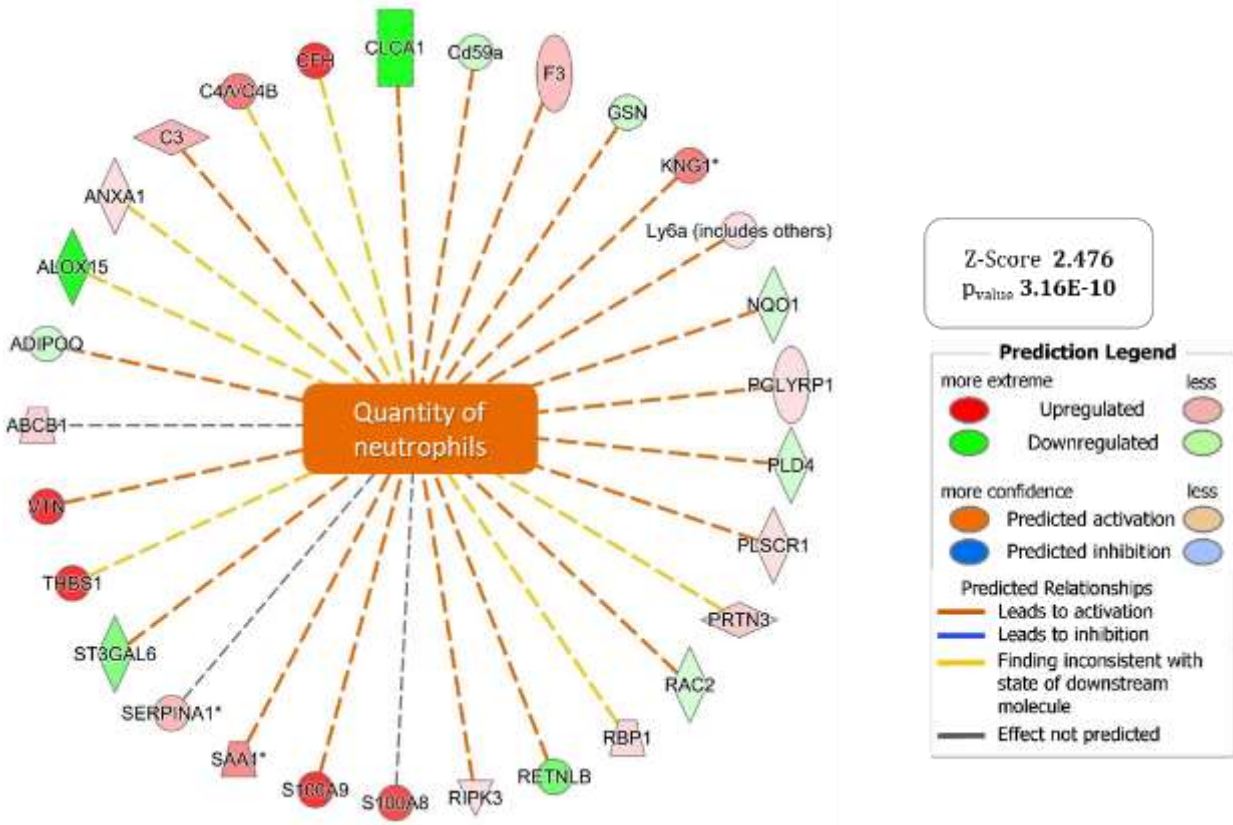


Table S1. List of sub-networks of significantly up-regulated proteins (DNBS vs. CTRL comparison matrix), united by their involvement in specific biological processes; below the list of protein involved is the color code that associates each gene product with the GO (gene ontology annotation) used for functional enrichment.

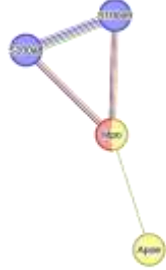

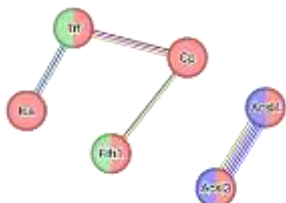
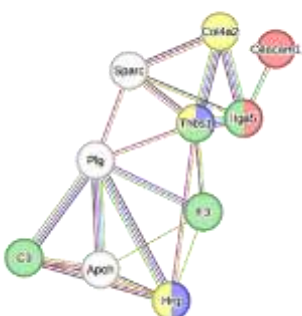
Subnetwork A				
	Protein name	Gene name	-Log pvalue	Ratio DNBS vs CTRL
	Apolipoprotein E	Apoe	6.532	0.725
	Myeloperoxidase	Mpo	4.652	3.832
	Protein S100-A8	S100a8	8.524	3.819
	Protein S100-A9	S100a9	8.049	5.929
Color code: Response to oxidative stress Hydrogen peroxide catabolic process Toll-like receptor 4 binding				
Subnetwork B				
	Protein name	Gene name	-Log pvalue	Ratio DNBS vs CTRL
	Gamma-glutamyl-transferase 5	Ggt5	9.999	0.540
	Glutathione S-transferase kappa 1	Gstk1	7.993	0.644
	Glutathione peroxidase 3	Gpx3	7.285	0.539
	Microsomal glutathione S-transferase 1	Mgst1	5.326	0.570
	High mobility group nucleosome-binding domain-containing protein 5	Hmgn5	2.834	0.621
	Dipeptidase 1	Dpep1	3.591	0.544
Color code: Glutathione catabolic process Glutathione metabolic process Glutathione peroxidase activity Glutathione transferase activity				
Subnetwork C				
	Protein name	Gene name	-Log pvalue	Ratio DNBS vs CTRL
	Serotransferrin	Trf	12.033	1.799
	Inhibitor of carbonic anhydrase	Ica	8.269	2.028
	Ferritin heavy chain	Fth1	9.508	1.038
	Ceruloplasmin	Cp	24.744	4.352
	Long chain fatty acid CoA ligase 3	Acs13	12.898	0.947
Long chain fatty acid CoA ligase 4	Acs14	4.554	0.683	
Color code: Ferroptosis Fatty acid biosynthesis Iron homeostasis				
Subnetwork D				
	Protein name	Gene name	-Log pvalue	Ratio DNBS vs CTRL
	Collagen alpha 2 IV chain	Col4a2	8.942	0.707
	Carcinoembryonic antigen-related cell adhesion molecule 1	Ceacam1	3.692	0.653
	Thrombospondin-1	Thbs1	11.008	5.016
	Integrin alpha 5	Itga5	9.219	0.737
	SPARC	Sparc	7.938	1.043
	Plasminogen	Plg	15.263	2.315
	Beta 2 glycoprotein 1	Apoh	10.913	1.326
	Tissue factor	F3	6.476	1.324
	Histidine rich glycoprotein	Hrg	15.330	4.413
	Complement C3	C3	14.564	1.572
Color code: Regulation of endothelial cell chemotaxis Wound healing, spreading of cells Positive regulation of angiogenesis Angiogenesis				

Figure S4. Graphical representation of the 'Inflammation of organ' pathway for which IPA predicts significant inhibition with a Z-SCORE value of -1.698. The set of genes up (red) and down (green) regulated to support the generated hypothesis are shown at the ends of the wheel graph.

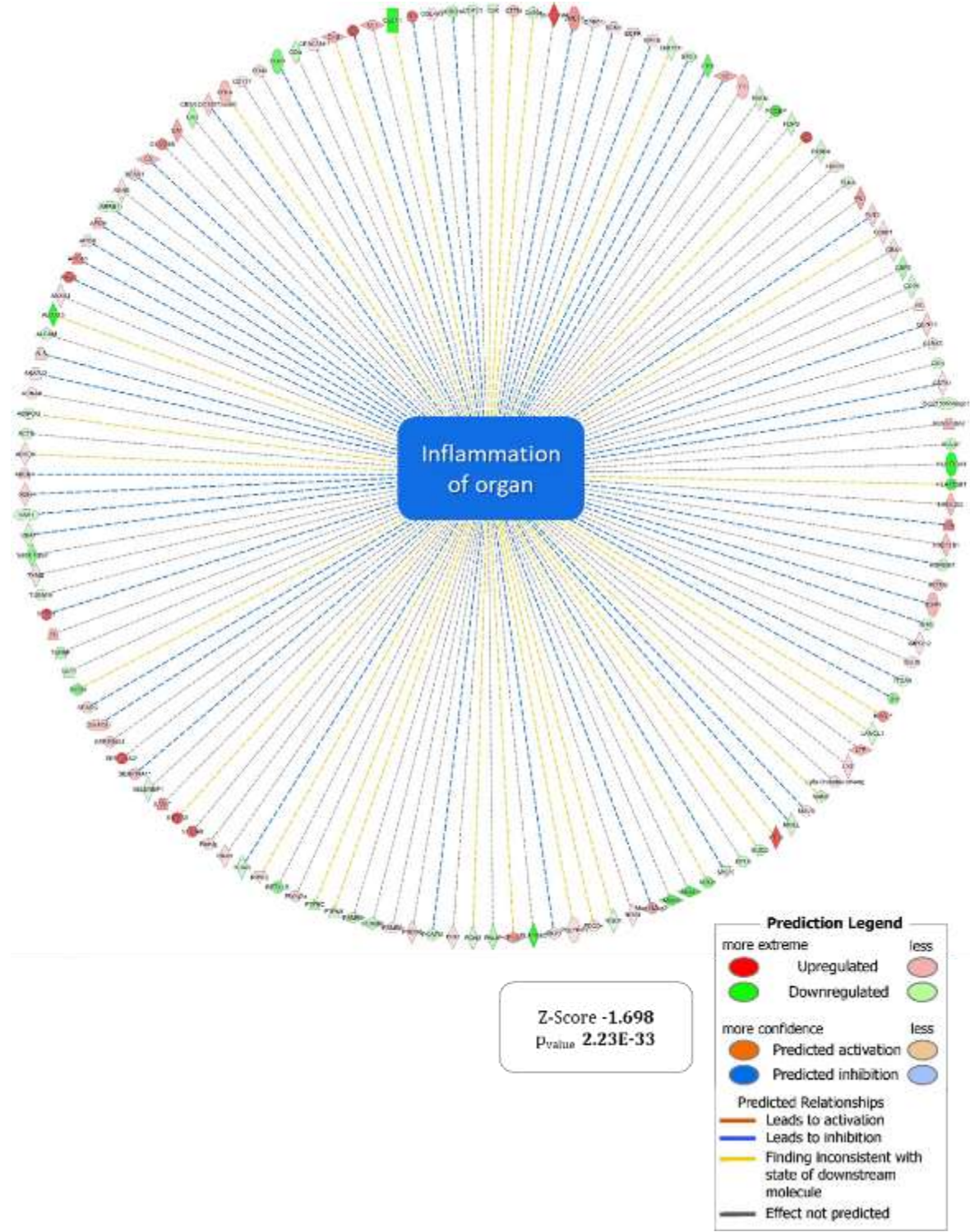


Figure S5. Graphical representation of the 'Immune response of neutrophils' pathway for which IPA predicts significant inhibition with a Z-SCORE value of -2.142. The set of genes up (red) and down (green) regulated to support the generated hypothesis are shown at the ends of the wheel graph.

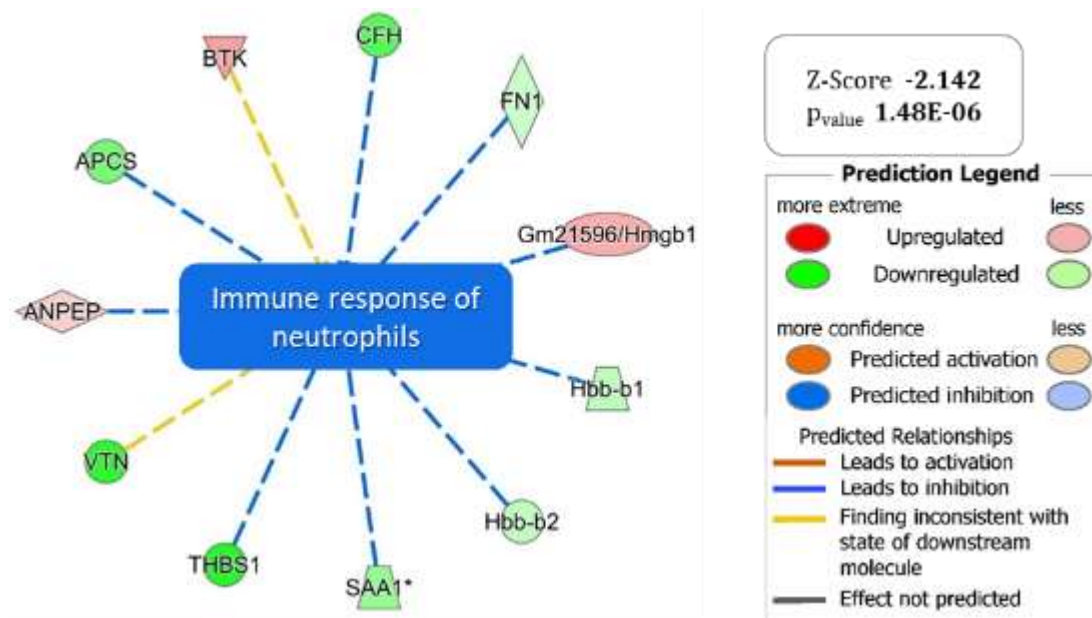


Table S2. List of sub-networks of significantly up-regulated proteins (DNBS_TAP vs. DNBS comparison matrix), united by their involvement in specific biological processes; below the list of protein involved is the color code that associates each gene product with the GO (gene ontology annotation) used for functional enrichment.

Subnetwork E				
	Protein name	Gene name	-Log pvalue	Ratio DNBS_TAP vs DNBS
	Peroxiredoxin-6	Prdx6	6.886	1.394
	Superoxide dismutase 3	Sod3	6.262	0.565
	Superoxide dismutase 1	Sod1	4.952	0.510
	Neutrophil cytosol factor 1	Ncf1	2.421	0.609
	Cytochrome b-245 heavy chain	Cybb	3.088	0.575
	Color code: Reactive oxygen species metabolic process Wound Cellular response to chemical stimulus Antioxidant activity Oxidoreductases activity Oxidative stress response			

Discovery of biological targets of natural extracts

Study 1 - Understanding the biological target of a Polyphenol-Enriched Bergamot Extract: insights from a MS-CETSA proteomic analysis

1. Introduction

Natural extracts of proven biological activity are composed of numerous potential ligands for pharmacologically interesting targets. Specifically, bergamot phytochemicals have been proven to possess promising beneficial effects in lowering triglycerides levels and attenuating pro-inflammatory stimuli in different pre-clinical studies [1,2]. However, there is a significant gap in our understanding concerning the primary and direct targets of these compounds. Metabolomic studies discovered that some of the phytochemicals of these extracts are characterized by a 3-hydroxy-3-methyl-glutaryl (HMG) moiety. These compounds, mainly flavones present in the polyphenolic fraction of the extract, have been hypothesized to interact with the HMG-CoA reductase enzyme and be responsible for some of the bioactivity of the extract. Commercially available kits that can potentially be used for the validation of this hypothesis are associated with an UV readout of the enzyme's co-factor, making them susceptible to the presence of UV-responsive components of the extract. This perspective is also centered on only a single possible target, whilst the presence of multiple phytochemicals could suggest at least a synergistic effect or the potential of multiple targets. To shed a light in this direction, we employed a mass spectrometry-based proteomic technique known as MS-CETSA (Cellular Thermal Shift Assay) both using an Isothermal Dose Response approach (ITDR) and an in-cell approach. The CETSA approach [3] is a biophysical technique to study the interaction and the binding between ligand and protein of interest. It is based on monitoring the melting curve of proteins which can be altered by the interaction with exogenous ligands, other proteins or metabolites. When a drug is added to a cell system, the mass spectrometry-based CETSA

approach not only collects the more conventional information, such as drug metabolism, detoxification, and drug-induced stress responses, but also allows additional unconventional information to be gathered, such as direct drug binders and immediate downstream effectors, overall helping in investigating the impact that a specific drug (or an extract) has on the proteome.

2. Material and methods

2.1. Cell culture

Liver HepG2 cell line were obtained from ATCC and cultured in MEM with L-glutamine (Gibco) supplemented with 10% FBS (Gibco) and 1% Sodium Pyruvate (Gibco). Cells were maintained at 37°C in a humidified atmosphere containing 5% CO₂.

2.2. Isothermal Dose Response (ITDR) treatment

For ITDR treatment, HepG2 lysate was obtained as following: cells obtained from 3 biological replicates were washed with HBSS -CaCl₂ -MgCl₂ (Gibco) and detached by treatment with TrypLE select 1X (Gibco) at 37°C. The cells were recovered with HBSS -CaCl₂ -MgCl₂, centrifuged at 300xg for 5 minutes and then washed again with HBSS -CaCl₂ -MgCl₂, after another centrifugation cells were resuspended in HBSS +CaCl₂ +MgCl₂ supplied with Halt protease inhibitor 1X (Thermo Scientific). Cells were then lysed with 3 cycles of freeze and thaw in liquid nitrogen, centrifuged at 4°C for 20 minutes at 20.000 x g to remove any insoluble particulate. Protein concentration was determined with BCA kit (Thermo Fischer) according to the manufacturer's instructions. Where necessary, lysate concentration was normalized at 5 mg/mL with HBSS +CaCl₂ +MgCl₂ for each biological replicate.

For the lysate treatment, bergamot leaves extract (previously characterized by Baron et al. [4]) was solubilized in DMSO at 180mg/mL so that when added to the protein lysate, the final DMSO concentration was 1%. The extract's concentrations were: 0 (1% DMSO as control), 0.07, 0.2, 0.6 and 1.8 mg/mL. Prior to the experiment, a pilot test was conducted to observe if the pH of the lysate was not perturbed by the addition of the extract. The extract was incubated for 3 minutes and then the samples were heated at three different temperatures: 37, 52 and 59°C for 3 minutes. Each temperature had 5 concentration and 3 biological replicates. After the heating step, the samples were once again lysed by 3 cycles of freeze and thaw and centrifuged at 20.000 x g for 20 minutes at 4°C. After the centrifugation, 80% of the liquid was recovered to make sure that no contamination from insoluble particulate was possible and the sample stored at -

80°C prior to protein quantification. Due to the presence of the extracts in the lysate, protein quantification of the soluble fraction was conducted using a Bradford (BioRad) method to avoid interferences related to the reduction of Cu²⁺ ion in the BCA reagents by the pythocomponents.

2.3. In-cell treatment

For this experiment, HepG2 cells were plated so that after 24 hours around 10 million cells were treated with different concentrations of extract and for different time point. Each condition had 3 biological replicates. Cells were treated with 200µg/mL of extract for 1h, 0.1% DMSO for 1 hour, 400µl/mL for 1 hour and then DMSO 0.1% for 8 h and 200µg/mL extract for 8 h. After the treated time, cells were detached as described above and resuspended in 1 mL. Around 1 million HepG2 cells (100µl), from each biological replicate and condition, were heated at 6 different temperatures: 37, 47, 50, 52, 54 and 57°C for 3 minutes. One set of samples from each biological replicates and condition was centrifuged ad 20.000 x g for 20 minutes and the pellet was processed in parallel as a quality control sample, without any heating step. The heated samples were freeze and thawed in liquid nitrogen and then centrifuged as described above. Protein concentration was determined using BCA.

2.4. MS-samples preparation

Once the protein concentration from all samples (ITDR and in-cell) was determined. 10µg of protein was used for MS sample preparation. The sample was dried and resuspended at 1 µg/µl in TEAB 50mM. Protein reduction started with the addition of 5 mM TCEP (Thermo Scientific) at 65°C for 30 minutes, alkylation was done using CAA (Sigma Aldrich) at 15mM room temperature for 30 minutes. Digestion was carried out with LysC (Wako Chemicals) 1:50 at 37°C for 2 hours followed by SOLu-trypsin (Sigma Aldrich) 1:50 overnight at 37°C. After checking the effectiveness of the digestion, samples were pooled and labelled with Isobaric Tandem Mass Tag (TMTpro 16 plex- Thermo Fisher Scientific) in a 1:6 ratio at 37°C for 3 h. Samples were checked for labelling (>95% TMT-labelled PSMs) before being quenched with 5% hydroxylamine (Thermo Fisher Scientific). Each TMT set contained all the experimental conditions and the biological replicates for one temperature and one channel per set was used as a carrier. Pooled samples were dried using a SpeedVac vacuum concentrator (Thermo Scientific) and desalted using an Oasis HLB 1cc (10mg) extraction cartridge (Waters) according to the manufacturer's protocol. Offline pre-fractionation of the samples was performed by high pH reverse-phase liquid chromatography using the (Shimadzu, Nexera LC-40). The column used was a Xbridge Peptide BEH C18, 300 Å, 3.5 µm, 2.1 mm x 250 mm column (Waters), with

a gradient of 3% to 80% ACN over 100 min, the fractions were concatenated into 12 fractions and dried using a SpeedVac vacuum concentrator.

2.5. LC-MS

The digested, labeled, and dried peptide sample fractions were resuspended in 0.1% FA (LC-MS grade, 533002, Merck) in H₂O (LC-MS grade, 115333 Merck). Online chromatography was performed using Dionex UltiMate 3000 UPLC system coupled to a Q-Exactive mass spectrometer (Thermo Scientific). Each fraction was separated on a 50 cm x 75 μm (ID) EASY-Spray analytical column (Thermo Scientific) in a gradient of programmed mixture of solvent A (0.1% formic acid in H₂O) and solvent B (99.9% acetonitrile, 0.1% formic acid) over 120min. MS data were acquired using a top 12 data-dependent acquisition method. Full scan MS spectra were acquired in the range of 375-1500 m/z at a resolution of 60,000 and AGC target of 3 x 10⁶; Top 12 data dependent-MS2 with a resolution of 60,000 and AGC target 3 x 10⁶ with isolation window at 1.2 m/z.

2.6. Protein identification and quantification

Data analysis was carried out starting with protein identification that was performed by Proteome Discoverer 2.1 software (Thermo Scientific), using Mascot 2.6.0 (Matrix Science) and Sequest HT (Thermo Scientific) search engines to search against reviewed human Uniprot database (downloaded on 23 Jul 2018, including 9606 sequence entries). MS precursor mass tolerance was set at 20ppm, fragment mass tolerance 0.05 Da, and maximum missed cleavage sites of 2. Dynamic modifications searched for Oxidation (M), Deamidation (NQ), and Acetyl N-terminal protein. Static modifications: Carbamidomethyl (C) and TMT16plex (K and peptide N terminus). Only the spectrum peaks with signal to- noise ratio (S/N) > 4 were chosen for searches. For statistical analysis, the false discovery rate (FDR) was set to 1% at both PSM and protein group levels. For quantification, only the unique and razor peptides were used for protein assignment and abundance quantification. Isotopic correction of the reporter ions in each TMT channel was performed according to the product sheet.

2.7. Quantitative data analysis, protein-protein interaction and enrichment analysis

Once the analysis with Proteome Discoverer was concluded, the quantified protein abundances were imported into Rstudio (<https://posit.co/download/rstudio-desktop/>) to be analysed within the R environment (<http://www.R-project.org/>). Data analysis (Data cleaning, normalisation, and calculations of protein abundance and thermal stability differences) was

performed using the in-house developed mineCETSApackage [5]. For the ITDR dataset we required that the sigmoidal curve fitting (R² value) should be greater than 0.8. A minimum of 1.3-fold change in the last three dose-points compared to the vehicle control should be exceeded in order for a protein to be considered a hit. Furthermore, hit calling requires a thermal shift at 52°C and at 59°C with a stable abundance signal at 37°C. For in-cell data the criteria were similar with proteins that should be quantified by at least 2 peptide spectrum matches (PSMs) while the log₂ fold change cut-off was set > 0.2. When the hit list was obtained, the list of Uniprot IDs were imported into Cytoscape v.3.10.0 (<http://cytoscape.org>). Using the embedded STRING interaction database (<http://apps.cytoscape.org/apps/stringApp>), a default confidence cut-off score of 0.4 was applied to retrieve the network. Each node represents one hit protein and edges symbolize protein-protein interactions. Functional enrichment was obtained through STRING Functional enrichment analysis.

3. Results and discussion

3.1. MS-CETSA Isothermal Dose Response (ITDR) results

To our knowledge, there are no similar works in literature applying this technique to complex mixtures of natural extracts. As a first step to investigate if a thermal shift is observable in these conditions, and with this type of mixture of compounds, we incubated a lysate of HepG2 cells with different doses of the bergamot extract (all with 1% final DMSO) as follow: 0 mg/mL (1% DMSO); 0.07 mg/mL; 0.2 mg/mL; 0.6 mg/mL; 1.8 mg/mL.

The extract was incubated briefly for 3 minutes with 50µl of cell lysate obtained by freeze and thaw in HBSS containing a protease inhibitor cocktail (protein concentration 5 mg/mL). Each set of 5 concentrations, named “condition” from now on, was prepared in biological triplicates; each group of three replicates (same “condition”) was heated at a selected temperature (37°C, 52°C and 59°C), meaning that each temperature had a total of 15 samples composed by three biological replicates for each condition, each made up of 5 concentrations. An illustration of the workflow is shown in figure 1.

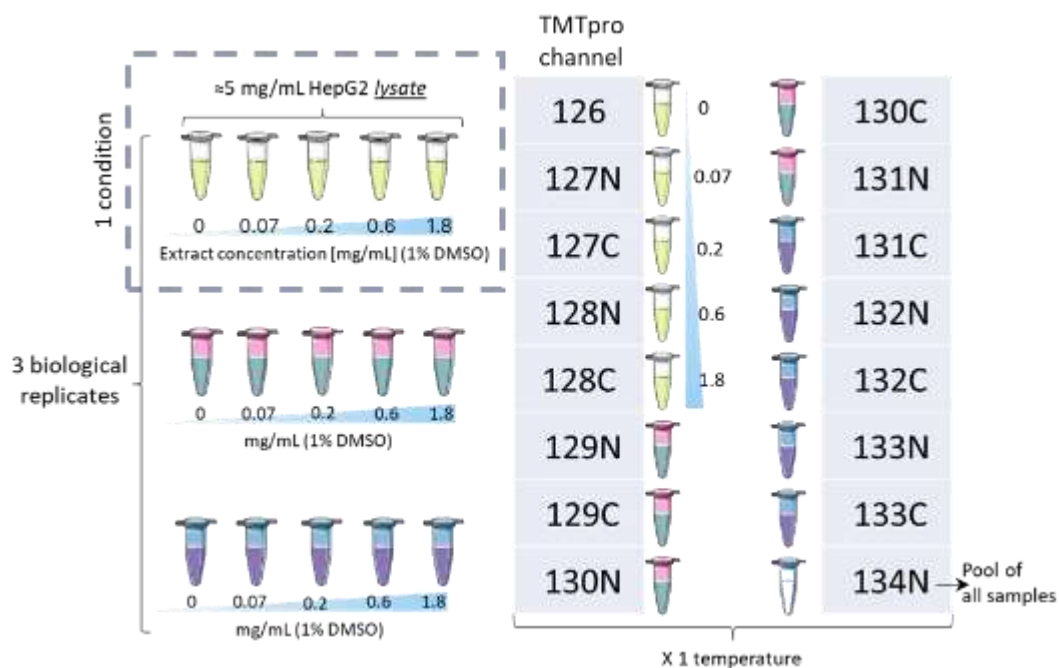


Figure 1 – Experimental set-up for the MS-CETSA ITDR approach.

From this initial approach, the proteins identified were respectively 4271 at 37°C, 3498 at 52°C and 3494 at 59°C; HMG CoA reductase was not identified nor was reported as a potential hit in this experiment. Taking into consideration a possible selection of hits (illustrated in Figure 2), some of them could be responsible for the biological activity of the extract. Adenosine kinase (ADK--Figure 2 panel A) has been identified as an enzyme with pro-obesogenic activity, exerted through its ability to promote DNA methylation and related suppression of PPAR α pathway genes; briefly, this process led to an increased fat deposition and decreased fatty acid oxidation [6].

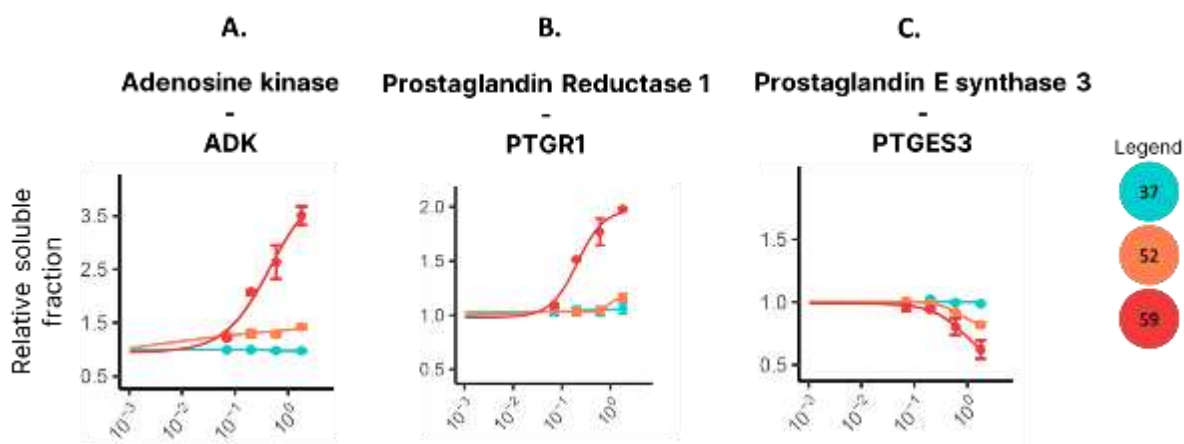


Figure 2 - Graphs of the relative soluble fraction for stabilized proteins by the bergamot extract.

In light of this background, the potential interaction of such extract components with ADK, with the possibility of inhibiting it, could be investigated further. The other two hits protein are involved in the metabolism of prostaglandins; prostaglandin reductase 1 (PTGR1 – Figure 15 panel B) has been identified as a potential target for cancer therapy [7] and indomethacin, a nonsteroidal anti-inflammatory drug, has been evaluated as an inhibitor of this enzyme. Major interest is associated with the main substrate of this enzyme: 15-keto-PGE2 [8], which is an endogenous activator of PPAR γ [9] and it has also been reported to bind NRF2 [10], improving the antioxidant state of the cell and improving the fatty acid metabolism. In addition, diet-induced obese mice have drastically reduced 15-keto-PGE2 levels compared to lean mice. Administration of 15-keto-PGE2 markedly improved insulin sensitivity and prevented diet-induced obesity [11]. A potential inhibition of this enzyme, with altered metabolism of its substrate, could explain some of the benefits associated with the extract. It is still unclear whether this stabilization could be related to an inhibition or to the recognition of potential substrate present in the extract, so that further evaluation is still needed. The last hit presented is the Prostaglandin E synthase 3 (PTGES3 - Figure 15 panel C), also known as p23, a co-chaperone for HSP90; some natural products such as the limonoid gedunin showed inhibitory activity towards p23, destabilizing the interaction with HSP90 and decreasing inflammation and inducing apoptosis in cancer cells [12].

3.2. MS- CETSA *in-cell* treatment results

To further confirm the solidity of these finding, and to investigate the target engagement in a cell model, the same extract was used in *in-cell* model of CETSA in which the heating step was performed on intact cells. This is possible thanks to the CETSA ability to observe alterations in the thermal characteristics of whole cells, allowing it to identify real-time variations in the states of protein interactions. More in detail, 10 million HepG2 cells were treated with different concentration of the extract at different timepoints:

- 200 $\mu\text{g}/\text{mL}$ for 1 h – the short incubation time was used to identify possible direct hits of the phytochemicals;
- 400 $\mu\text{g}/\text{mL}$ for 1 h;
- 200 $\mu\text{g} /\text{mL}$ for 8h – a longer incubation period to assess eventual hits that could come from the induced alteration of the proteome by the extract;
- DMSO 0.1% 1 and 8h – conditions used as controls.

Each treatment was performed in biological triplicate while the heating step was performed with 6 heating temperatures (37, 47, 50, 52, 54, 57°C). Each temperature was applied to around 1 million cells.

For each temperature, the number of proteins identified after clean up and used for the analysis are illustrated in table 1 below.

Table 1 - Number of ids of the proteins used for the analysis obtained after the clean up step

	Temperature [°C]	ids
Data composition after <i>clean up</i>	37	4916
	47	4291
	50	3781
	52	3665
	54	3276
	57	3005
	<i>QP</i>	<i>5504</i>

Results from the *in-cell* approach confirmed the two hits PTGR1 and PTGES3 (Figure 3 – panel A and B) with the first protein shifting as early as after 1 hour of treatment with the extract, with a potential of being a direct hit of the extract. The same destabilization behavior for PTGES3 observed in the ITDR approach is also present in this experiment but only after 8h of treatment. ADK does not show any shift, as presumably the compounds potentially responsible for the stabilization highlighted by ITDR approach may not be absorbed by the cells used for this approach. Once again, no shift has been observed for the HMG-CoA reductase as it was not identified in the proteomics experiment.

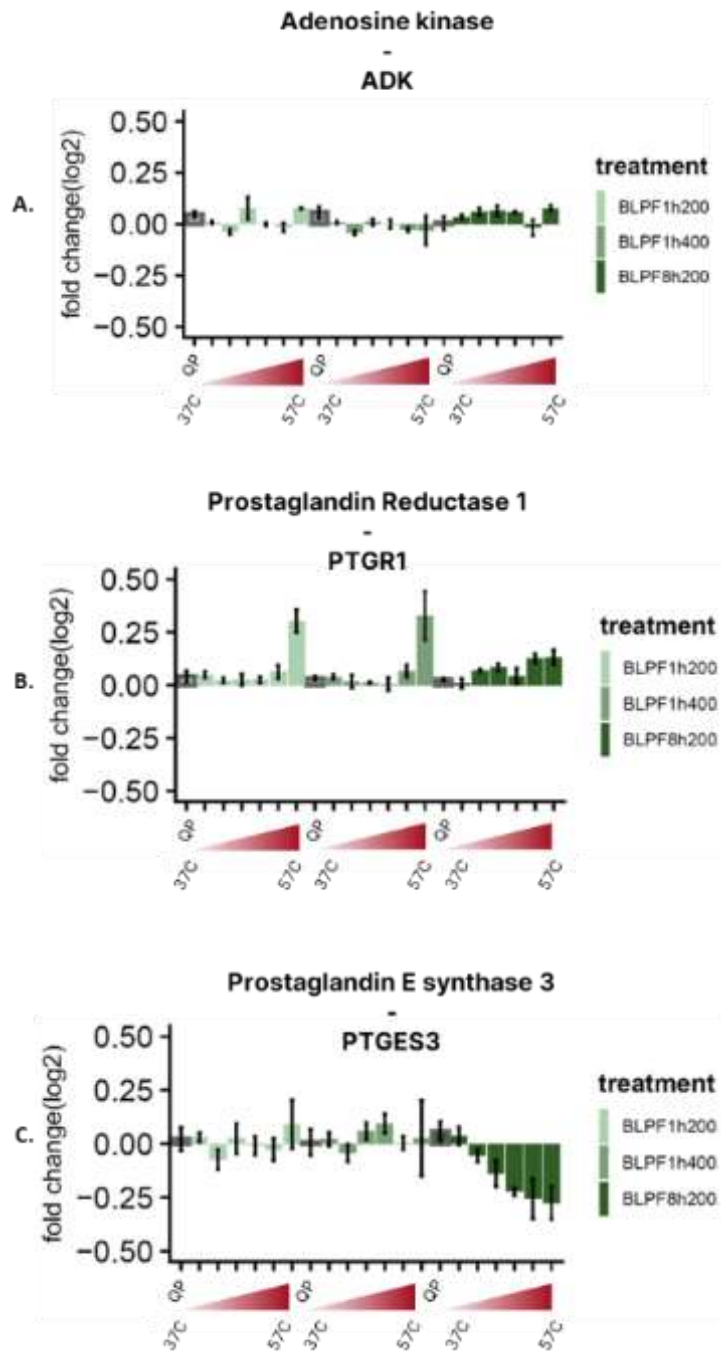


Figure 3 - Graphs illustrating the stabilization of the previously identified hits in the ITDR approach. On the y axis the log₂ fold change obtained by comparing the TMT tag intensity of each temperature with the 37°C one. On the x axis the different conditions.

Other than the previously identified hits, the significantly shifting proteins in some of the experimental conditions were analyzed using string interface in cytoscape software, and the following protein-protein interaction network graph was obtained (Figure 4).

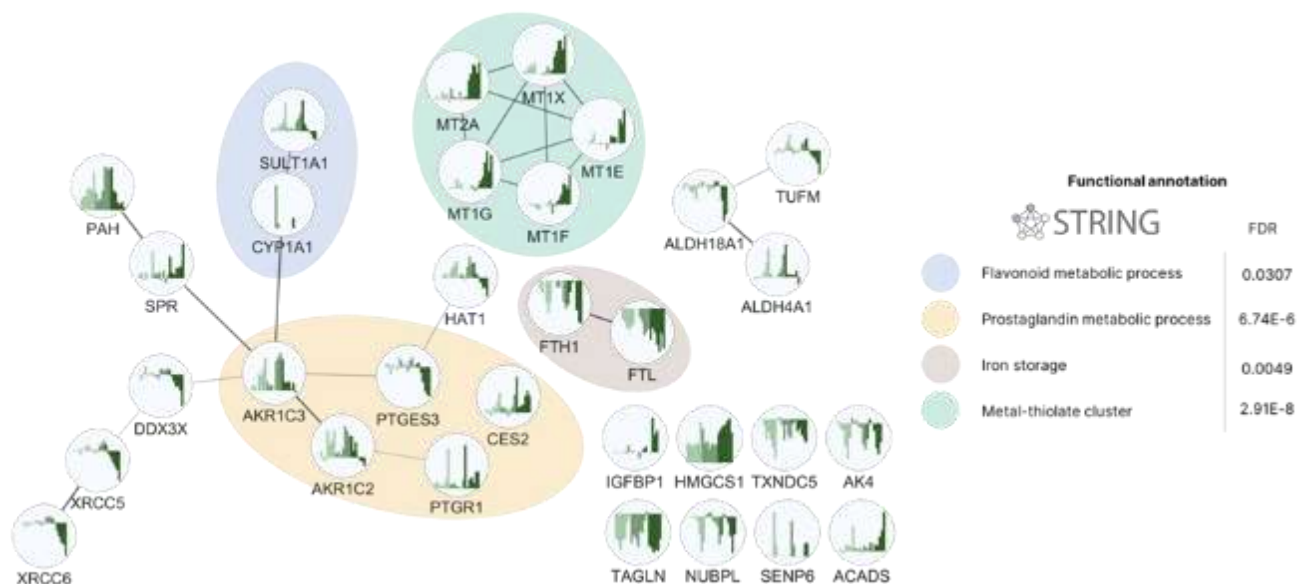


Figure 4 - Functional annotation for the major hit proteins identified in the in-cell approach.

This analysis highlighted and confirmed the impact that polyphenols have on the “redox proteome”. In fact, a potential alteration of the oxidoreductive system in the cell could explain the metallothioneins (MTs) family stabilization as illustrated in figure 4 by the cluster “metal-thiolate cluster”. A potential interaction between the cysteines in these proteins and the reactive moieties present in various polyphenols could alter the stability and cause a thermal shift. It is reported [13] that MTs’ cysteines can undergo reversible redox reactions with concomitant release and binding of zinc, thereby coupling redox and zinc metabolism. In line with this concept, we noted that SPR (sepiapterin reductase) and HAT1 (histone deacetylase) proteins, previously identified as modulated by variations in the cellular redox state in another CETSA experiment [14], are likewise observed undergoing shifts in our study. Changes in the redox state of the cofactors of some proteins is also known to potentially affect the proteins and yielding a CETSA signal [14]. This could be the case for the ferritin heavy and light chain (FTH1, FTL) and the possibility of a reaction (reduction, chelation) between intracellular iron and the absorbed polyphenols in the cell that could cause a destabilization. Other than that, the functional analysis performed in this experiment highlighted an enrichment in protein correlated to the prostaglandin metabolic process, solidifying the possible interaction of the extract with this metabolic pathway.

4. Conclusions

Recently it has been discussed that the target-based approach, one of the cornerstone of the reverse pharmacology approach, has not improved the drug discovery process, with the majority of the new drugs approved coming from a forward approach, based on phenotypic screening. A great number of natural extracts are used and observed to be active in numerous of these screening and are associated with the ability to improve a pathological condition in clinical and preclinical studies. One of the major shortcomings with this research approach is the identification of potential target(s) of these extracts, identify the impact on the organism. The use of proteomic studies, helped in the understanding of the downstream effects of these phytochemicals but are being used recently to scout the direct binding targets and effects of these compounds. The coupling of the mass spectrometry-based proteomics approach to the cellular thermal shift (CETSA) principle and advantages, can be taken in consideration for this task and this experiment observed the potential deployment of this technique in the definition of the potential effect of a bergamot leaves extract.

Taking in account the results obtained, it may be possible that one of the major impacts on the proteome is related to the chelating and redox activity of the polyphenols present in the extract; in fact, some of the most interesting information obtained from this CETSA experiment is attributable to a subset of proteins that are particularly susceptible to redox changes, with the possibility of a direct alteration of the redox state. This is supported by the identification of SPR and HAT1 proteins as being modulated by bergamot extract, as these proteins have been previously shown to be sensitive to changes in the cellular redox state. In addition, by means of an ITDR approach, we discovered that incubation with bergamot extract results in melting temperature shifts of proteins in a dose-dependent manner, with two potential hits identified with PTGR1 and PTGES3 that have also been identified as potential hit in the *in-cell* approach. These proteins are involved in the metabolism of prostaglandins, which play a role in a variety of cellular processes, including inflammation, immunity, and metabolism. These proteins are now being evaluated by orthogonal techniques to better understand the type of interaction the extract has. Overall, coupling this approach with the classical target discovery techniques could improve and streamline the discovery of new targets of different extracts by reducing the time of analysis and the possible hit list of the extract. Once the protein/s is/are identified, targeted validation studies can be deployed to understand the validity of the approach and eventually identifying newer compounds and more specific mechanism of action.

References

1. Della Vedova, L.; Gado, F.; Vieira, T.A.; Grandini, N.A.; Palácio, T.L.N.; Siqueira, J.S.; Carini, M.; Bombardelli, E.; Correa, C.R.; Aldini, G.; et al. Chemical, Nutritional and Biological Evaluation of a Sustainable and Scalable Complex of Phytochemicals from Bergamot By-Products. *Molecules* 2023, 28, 2964, doi:10.3390/molecules28072964.
2. Siqueira, J.S.; Nakandakare-Maia, E.T.; Vieira, T.A.; Palacio, T.L.N.; Grandini, N.A.; Belin, M.A.F.; Nai, G.A.; Moreto, F.; Altomare, A.; Baron, G.; et al. Effect of Bergamot Leaves (*Citrus Bergamia*) in the Crosstalk between Adipose Tissue and Liver of Diet-Induced Obese Rats. *Livers* 2023, 3, 258–270, doi:10.3390/livers3020017.
3. Prabhu, N.; Dai, L.; Nordlund, P. CETSA in Integrated Proteomics Studies of Cellular Processes. *Current Opinion in Chemical Biology* 2020, 54, 54–62, doi:10.1016/j.cbpa.2019.11.004.
4. Baron, G.; Altomare, A.; Mol, M.; Garcia, J.L.; Correa, C.; Raucci, A.; Mancinelli, L.; Mazzotta, S.; Fumagalli, L.; Trunfio, G.; et al. Analytical Profile and Antioxidant and Anti-Inflammatory Activities of the Enriched Polyphenol Fractions Isolated from Bergamot Fruit and Leave. *Antioxidants* 2021, 10, 141, doi:10.3390/antiox10020141.
5. Dai, L.; Zhao, T.; Bisteau, X.; Sun, W.; Prabhu, N.; Lim, Y.T.; Sobota, R.M.; Kaldis, P.; Nordlund, P. Modulation of Protein-Interaction States through the Cell Cycle. *Cell* 2018, 173, 1481-1494.e13, doi:10.1016/j.cell.2018.03.065.
6. Li, H.; Zheng, J.; Xu, Q.; Yang, Y.; Zhou, J.; Guo, X.; Cai, Y.; Cai, J.J.; Xie, L.; Awika, J.; et al. Hepatocyte Adenosine Kinase Promotes Excessive Fat Deposition and Liver Inflammation. *Gastroenterology* 2023, 164, 134–146, doi:10.1053/j.gastro.2022.09.027.
7. Wang, X.; Yin, G.; Zhang, W.; Song, K.; Zhang, L.; Guo, Z. Prostaglandin Reductase 1 as a Potential Therapeutic Target for Cancer Therapy. *Front. Pharmacol.* 2021, 12, 717730, doi:10.3389/fphar.2021.717730.
8. Mesa, J.; Alsina, C.; Oppermann, U.; Parés, X.; Farrés, J.; Porté, S. Human Prostaglandin Reductase 1 (PGR1): Substrate Specificity, Inhibitor Analysis and Site-Directed Mutagenesis. *Chemico-Biological Interactions* 2015, 234, 105–113, doi:10.1016/j.cbi.2015.01.021.
9. Shiraki, T.; Kamiya, N.; Shiki, S.; Kodama, T.S.; Kakizuka, A.; Jingami, H. α,β -Unsaturated Ketone Is a Core Moiety of Natural Ligands for Covalent Binding to Peroxisome Proliferator-Activated Receptor γ . *Journal of Biological Chemistry* 2005, 280, 14145–14153, doi:10.1074/jbc.M500901200.
10. Lee, J.-E.; Zhong, X.; Lee, J.-Y.; Surh, Y.-J.; Na, H.-K. 15-Keto Prostaglandin E2 Induces Heme Oxygenase-1 Expression through Activation of Nrf2 in Human Colon Epithelial CCD 841 CoN Cells. *Archives of Biochemistry and Biophysics* 2020, 679, 108162, doi:10.1016/j.abb.2019.108162.
11. Tseng, Y.-H.; Chuang, L.-M.; Chang, Y.-C.; Hsieh, M.-L.; Tsou, L.; Chen, S.-Y.; Ke, Y.-Y.; Hung, M.-S.; Hee, S.-W.; Lee, H.-L.; et al. Increasing Endogenous PPAR γ Ligands Improves Insulin Sensitivity and Protects against Diet-Induced Obesity without Side Effects of Thiazolidinediones; In Review, 2021;

12. Braga, T.M.; Rocha, L.; Chung, T.Y.; Oliveira, R.F.; Pinho, C.; Oliveira, A.I.; Morgado, J.; Cruz, A. Biological Activities of Gedunin—A Limonoid from the Meliaceae Family. *Molecules* 2020, 25, 493, doi:10.3390/molecules25030493.
13. Maret, W. Metallothionein Redox Biology in the Cytoprotective and Cytotoxic Functions of Zinc. *Experimental Gerontology* 2008, 43, 363–369, doi:10.1016/j.exger.2007.11.005.
14. Sun, W.; Dai, L.; Yu, H.; Puspita, B.; Zhao, T.; Li, F.; Tan, J.L.; Lim, Y.T.; Chen, M.W.; Sobota, R.M.; et al. Monitoring Structural Modulation of Redox-Sensitive Proteins in Cells with MS-CETSA. *Redox Biology* 2019, 24, 101168, doi:10.1016/j.redox.2019.101168.

GENERAL CONCLUSIONS

The predicted increase in the market share of polyphenol in the coming years, together with the high role of importance given to the concept of linear economy by the European Union, pose interesting research challenges that can be answered by the application of rigorous mass spectrometric approaches. Improved analytical techniques, along with the use of high-resolution mass spectrometers, could help the discovery of new active compounds isolated from complex natural matrices. During my studies I have approached this problem from different angles. With a more industrial-oriented work involving the evaluation of different extraction conditions for a red grape skin by-product, I evaluated the possibility of a greener extraction protocol for the retrieval of anti-inflammatory components. The successful extraction was accompanied by an unpredicted superimposable activity of the 100°C water-based extract and the 70% EtOH extract. Greener extraction method can and should be considered for the retrieval of bioactive components from waste by-products.

Other than that, a mass spectrometry-based analytical platform was used to investigate the major components of a thinned apple polyphenols enriched extract and, in parallel, the biological activity was evaluated in *in vitro* models of inflammation and NRF2 activation. The activation of this pathway was then confirmed by quantitative proteomics studies, highlighting the metabolic reprogramming induced by these extracts that target this pathway. This evidence confirmed our initial hypothesis that an inflammatory status could be tackled by targeting the oxidative stress that is generated by this pathological condition. The potential bioactivity of the extract was also evaluated in an animal model of ulcerative colitis, an inflammatory-based disease. Following extract treatment, we observed improved pathological phenotype and inflammatory state, along with the activation of the antioxidant defenses by means of NRF2 stimulation, confirming the potentiality of this extract on inflammatory-based pathologies.

In parallel with this project, given the pre-clinical and clinical studies addressing the efficacy of a bergamot extract enriched in polyphenols, I used a quantitative proteomics approach based on the thermal stabilization assay (i.e. MS-CETSA) to evaluate the potential of this technique in the streamlining of the target identification process of natural extracts. Given the complex nature of the extract, this approach could be considered a partial success, as it confirmed

already known hypotheses about the redox impact of polyphenols, while providing concrete results. The validation and confirmation arising from this analytical workflow is still expensive and time-consuming, but nonetheless can be considered a step forward.

SCIENTIFIC CONTRIBUTIONS

PAPERS

1. Interdonato L, Ferrario G, Cordaro M, D'Amico R, Siracusa R, Fusco R, Impellizzeri D, Cuzzocrea S, Aldini G, Di Paola R. ***Targeting Nrf2 and NF- κ B Signaling Pathways in Inflammatory Pain: The Role of Polyphenols from Thinned Apples.*** *Molecules*. 2023; 28(14):5376. <https://doi.org/10.3390/molecules28145376>
2. Gado F, Ferrario G, Della Vedova L, Zoanni B, Altomare A, Carini M, Aldini G, D'Amato A, Baron G. ***Targeting Nrf2 and NF- κ B Signaling Pathways in Cancer Prevention: The Role of Apple Phytochemicals.*** *Molecules*. 2023; 28(3):1356. <https://doi.org/10.3390/molecules28031356>
3. Ferrario G, Baron G, Gado F, Della Vedova L, Bombardelli E, Carini M, D'Amato A, Aldini G and Altomare A. ***Polyphenols from thinned young apples: HPLC-HRMS profile and evaluation of their anti-oxidant and anti-inflammatory activities by proteomic studies*** *Antioxidants* 2022, 11, 1577. <https://doi.org/10.3390/antiox11081577>
4. Della Vedova L, Ferrario G, Gado F, Altomare A, Carini M, Morazzoni P, Aldini G and Baron G ***Liquid Chromatography--High- Resolution Mass Spectrometry (LC-HRMS) Profiling of Commercial Enocianina and Evaluation of Their Antioxidant and Anti-Inflammatory Activity.*** *Antioxidants*. 2022; 11(6): 1187 <https://doi.org/10.3390/antiox11061187>
5. Baron G, Ferrario G, Marinello C, Carini M, Morazzoni P, Aldini G. ***Effect of Extraction Solvent and Temperature on Polyphenol Profiles, Antioxidant and Anti-Inflammatory Effects of Red Grape Skin By-Product.*** *Molecules*. 2021; 26(18):5454. <https://doi.org/10.3390/molecules26185454>

6. Altomare A., Baron G., Cambiaghi G., Ferrario G., Zoanni B, Della Vedova L, D'Alessandro S, Parapini S, Vittorio S, Vistoli G, Riso P, Carini M, Delbue S and Aldini G. ***Screening of Mpro protease (SARS-CoV-2) covalent inhibitors from an anthocyanin-rich blueberry extract using an OMICS-based analytical platform (HRMS) – submitted manuscript***
7. Ferrario, G.; Impellizzeri, D.; Baron, G.; Bombardelli, E.; Carini, M.; Di Paola, R., Aldini, G. and Altomare, A. ***Thinned apple polyphenols alleviate inflammation in a mouse model of DNBS-induced colitis: label-free quantitative proteomics studies – manuscript in preparation for submission***
8. Ferrario, G., Ramos, A, Nordlund, P., Aldini, G ***Understanding the biological target of a Polyphenol-Enriched Bergamot Extract: insights from MS-CETSA proteomic analysis – manuscript in preparation***

POSTERS

Understanding the biological targets of a Polyphenol-Enriched Bergamot Extract: insights from MS-CETSA proteomic analysis

Ferrario G[^], Ramos A, Nordlund P and Aldini G (RDPA - September 2023)

[^]presenting author

Synthesis and Structure-Activity Relationship Study of 1,3,4-Oxadiazole Substituted 3-Br-Isoxazolines as Potent Anti-Trypanosomal Agents

Corfu I A, Luelmo S, Santarem N, Sheraz G, Ferrario G, Aldini G, Altomare A, Cordeiro-da-Silva A, Tamborini L, Conti P, Borsari C[^]. (NMMC - September 2023)

[^]presenting author

Polyphenols from thinned young apples: LC-HRMS profile, *in-vitro* evaluation of anti-oxidant and anti-inflammatory activities by proteomic studies

Ferrario G[^], Baron G, Gado F, Della Vedova L, Bombardelli E, Carini M, D'Amato A, Aldini G and Altomare A (MSBM – July 2022)

[^]presenting author

HR-MS Characterization of commercial enocianina with antioxidant and anti-inflammatory activity in in-vitro models

Della Vedova L[^], Ferrario G, Carini M, Gado F, Morazzoni P, Aldini G and Baron G. (IMSS 2022)

[^]presenting author

HR-MS Characterisation Of Red Grapes Pomace Extract With Anti-Inflammatory Activity In Vitro

Ferrario G[^], Giovanna B, Cristina M, Altomare A, Carini M, Morazzoni P and Aldini G (RDPA - September 2021)

[^]presenting author

Characterization of the polyphenolic profile of unripe apple extract by metabolomics and evaluation of its anti-inflammatory activity

Baron G[^], Ferrario G, Altomare A, Marinello C, Carini M, D'Amato A, Trunfio G, Tucci L, Malara D, Mollace V, Bombardelli E and Aldini G.

(RDPA - September 2021)

[^]presenting author

ORAL PRESENTATION:

Exploring the anti-inflammatory and antioxidant effects of thinned young apple polyphenols: evidence from in vitro and ex vivo proteomic studies

Ferrario Giulio

(SSPA - September 2023)

M^{pro} protease (SARS-CoV-2) covalent inhibitors identification from an anthocyanin-rich blueberry extract using an OMICS-based analytical platform

Altomare A[^], Baron G, Ferrario G, Zoanni B, Della Vedova L, D'Alessandro S, Parapini S, Vittorio S, Vistoli G, Carini M, Delbue S and Aldini G.

(RDPA - September 2023)

[^]presenting author

Thinned apple polyphenols alleviate inflammation in a mouse model of dnbs-induced colitis: label-free quantitative proteomics studies

Altomare A[^], Ferrario G, Baron G, Di Paola R, Bombardelli E, Impellizzeri D and Aldini G.

(NMMC - September 2023)

[^]presenting author

Liquid Chromatography-High Resolution Mass Spectrometry (LC-HRMS) Profiling of Commercial Enocianina and Evaluation of Their Antioxidant and Anti-Inflammatory Activity

Della Vedova L, Ferrario G, Gado F, Altomare A, Carini M, Morazzoni P, Aldini G and Baron G[^].

(MASSA – June 2022)

[^]presenting author